

Computational testing of patient-specific gait features
and pelvic motion effects on the risk of edge contact
in total hip replacements



Ksenija Vasiljeva

School of Mechanical Engineering
University of Leeds

*A thesis submitted for the degree of
Doctor of Philosophy*

May, 2019

The candidate confirms that the work submitted is her own and that appropriate credit has been given where reference has been made to the work of others.

This copy has been supplied on the understanding that it is copyright material and that no quotation from the thesis may be published without proper acknowledgement.

©2019 The University of Leeds and Ksenija Vasiljeva

The right of Ksenija Vasiljeva to be identified as Author of this work has been asserted by her in accordance with the Copyright, Designs and Patents Act 1988.

Acknowledgements

I would like to take this opportunity to express my sincere gratitude to my supervisor Alison Jones for the invaluable and continuous guidance, as well as the support provided throughout the PhD and thesis writing.

I would like to thank Mazen Al-Hajjar for his help and encouragement. I would also like to thank my industrial supervisors from DePuy Synthes, Ian Flatters and Jonathan Thompson. It was a pleasure to work with all the great people across University of Leeds. And I would like to say special thanks to Ruth, Faezeh, Ama, Philippa, Gavin, Rob, Amisha and Phil.

I would like to thank Phil Hyde for recognising my strengths and encouraging me to pursue the PhD.

Thank you to all of my family and close friends for giving me moral support throughout this journey. I am especially grateful to my grandparents Valentina and Alexander Oseledjko, who inspired me to become an engineer; to my brother Grigory and to my amazing friends Valerie, Alina, Anna and Anait.



I am forever grateful to my small family Rodion and Daisy, for being there for me through the ups and downs, and for their endless love and support.

I would like to dedicate this thesis to my mother, Olga, for inspiring me to pursue my dreams and giving her all to support me. Thank you mum.

Abstract

Although total hip replacement (THR) surgery is considered one of the most successful orthopaedic interventions, failures which require revision still occur. One of the known contributors to the failure of THR is edge contact, where the acetabular cup and the femoral head remain concentric but contact falls partially on the cup's rim. Failures associated with edge contact include rim damage, osteolysis and cup dissociation due to altered *in vivo* loading and torques. The current structural and tribological pre-clinical testing protocols fail to capture the spread of pelvic movement and joint contact force directions, which can be seen in a patient-specific analysis. Therefore these tests cannot always predict the success of the THR while *in vivo*.

The broad aim of the PhD project presented in this thesis was to bridge the gap between pre-clinical testing and biomechanical THR studies with a focus on risk of edge contact. The effect of pelvic motion exclusion (common in *in vitro* studies) on the risk of edge contact was assessed from patient-specific perspective.

In this work a computational approach was used to achieve the aim. The data for the analysis was gained from previous experimental biomechanical studies, including a conventional force platform and motions marker study, an instrumented implant study and a dual video-fluoroscopy study. The developed computational algorithms identified the relative position of THR bearing components based on the motions of femur and pelvis. The results of two central studies within this PhD showed that the exclusion of pelvic motions substantially affects the risk of edge contact. However, the effect of pelvic motions on the risk of edge contact was shown to be patient-specific. It was found that pelvic sagittal tilt, coronal obliquity and internal-external rotation all contribute to the overall effect of pelvic motions on the risk of edge contact. In addition, the studies within this project revealed that static orientations of the acetabular cup during standing are not representative of the orientation during dynamic activities. The use of

dual video-fluoroscopy techniques were shown to have potential to eliminate uncertainty in variability between static acetabular cup orientation and while THR is in motion.

The work presented in this thesis, showed the importance of considering the dynamic activity effects on the success of THR device, which potentially applies to other artificial joints. The methods used can be applied to both pre-clinical testing and preoperative planning, as well as postoperative THR success management. Further studies on larger and more diverse patient cohorts are required to estimate, and in some cases predict, the patient-specific characteristics which affect the risk of edge contact *in vivo*.

Contents

Acknowledgements	i
Abstract	ii
List of Figures	x
List of Tables	xvii
List of Abbreviations	xix
1 Introduction and Literature Review	1
1.1 Introduction	1
1.1.1 Motivation for the project	3
1.1.2 Aim of the project	4
1.2 Literature review introduction	5
1.3 Natural hip joint and surrounding structures	6
1.3.1 Anatomy and functionality	6
1.4 Aspects of total hip arthroplasty	16
1.4.1 Contact mechanics principles affecting total hip replacement bearing performance	20
1.4.2 Standard pre-clinical testing	25
1.5 Dynamic <i>in vivo</i> alignment of total hip replacement	27
1.5.1 <i>In vivo</i> organisation of total hip replacement	27

1.5.2	Head-to-rim contact and implant damage	31
1.6	Biomechanical motion analysis background and considerations	39
1.6.1	Reference systems used for gait analysis	39
1.6.2	Kinematic analysis	41
1.6.3	Kinetic analysis	44
1.6.4	Temporal and spatial parameters	45
1.6.5	Muscle activity	45
1.7	Natural hip joint gait biomechanics	46
1.7.1	Kinematic analysis	47
1.7.2	Kinetic analysis	50
1.7.3	Temporal and spatial parameters	52
1.8	Artificial hip joint gait biomechanics	53
1.8.1	Comparison of THR patient biomechanics to a healthy control group	53
1.8.2	Comparison of operated hip biomechanics to opposite non-operated hip	57
1.9	Previous computational studies on total hip replacement biomechanics	61
1.9.1	Variation in computational methodologies	62
1.9.2	Previous studies on total hip replacement contact mechanics . .	64
1.10	Literature review summary	69
2	Development of the computational tool to determine the location of contact between total hip replacement bearings	72
2.1	Overview of the analytical proximity tool purpose, function and output .	73
2.2	Description of the required input type and format for the proximity tool	77
2.3	The detailed description of the datasets used in the <i>proximity tool</i> development and input selection	78
2.3.1	HIP98 dataset format and input assumptions description	78

2.3.2	LBRC format and input assumptions description	79
2.4	Description of the coordinate systems defined in datasets used for tool development	81
2.4.1	HIP98 dataset laboratory, image and pelvic coordinate system definition	81
2.4.2	LBRC coordinate systems	82
2.5	Overview of the approach taken in the analytical tool development . . .	84
2.6	Detailed description of actions taken prior and during proximity tool execution	87
2.6.1	Global coordinate system set-up	87
2.6.2	Detailed description of the centre proximity angle and edge proximity angle algorithm	87
2.6.3	Detailed description of finite element model for estimation of contact force and contact area relationship	90
2.6.4	Detailed description of the algorithm used for the positioning of the acetabular cup within the <i>proximity tool</i> environment	96
2.6.5	Detailed description of the data-specific algorithms used in the proximity tool for the addition of the pelvic motions into the simulation	101
2.6.6	Orientation of the contact along the acetabular cup rim	109
2.7	Proximity tool testing for one patient from each dataset	111
2.7.1	Case 1: HIP98 patient	111
2.7.2	Case 2: LBRC patient	113
2.7.3	Case 1a: HIP98 patient, two motions	114
2.7.4	Initial patient-specific analysis	114
2.8	Summary of proximity tool development and usage	116
2.8.1	Tool capabilities and study achievements	116
2.8.2	Limitations and considerations of the tool	116
2.8.3	Upcomming studies and future uses of the tool	117

3	The investigation into risk of edge contact with patient and activity variability	119
3.1	Introduction	119
3.2	Patients and general methods	120
3.2.1	Patient selection and description	120
3.2.2	Cup positioning reference table development	122
3.2.3	Study set-up and considerations	124
3.3	Risk of edge contact for patients across all activities	125
3.3.1	Method	125
3.3.2	Results	127
3.3.3	Conclusions and observations	143
3.4	Effect of pelvic motions onto the risk of edge contact	144
3.4.1	Method	144
3.4.2	Results	146
3.4.3	Conclusions	155
3.5	Comparison to Paul cycle of edge contact risk and location of potential rim damage location	156
3.5.1	Method	156
3.5.2	Results	159
3.5.3	Conclusions	168
3.6	Overall conclusions and summary	169
3.6.1	Main findings	169
3.6.2	Discussion on the findings	170
3.6.3	Summary	173
4	Analysis of unilateral total hip replacement patients' gait and motion profiles	174
4.1	Introduction	174

4.2	Patients and Methods	175
4.2.1	Patient demographics and selection	175
4.2.2	Study set-up and considerations	181
4.2.3	Sub-studies description and analysis.	181
4.3	Results	190
4.3.1	The effect of pelvic motions compared to simulations with no pelvic motion inclusion	194
4.3.2	The contribution of each pelvic motion to the overall effect of pelvic motions	196
4.3.3	The contribution of static pelvic orientation to the overall effect of inclusion of pelvic motions	198
4.3.4	Centre proximity angle and patient-specific demographics and gait characteristics correlation	201
4.3.5	Maximum edge proximity angles: stance regions comparison and location along the cup rim.	204
4.4	Conclusions and summary	207
4.4.1	Main findings	207
4.4.2	Discussion on the findings	209
4.4.3	Limitations and future work	212
4.5	Summary	213
5	Techniques for pelvic dynamic orientation analysis using video-fluoroscopy : a case study.	214
5.1	Introduction	214
5.2	Measurement method development	215
5.2.1	Input data and processing	215
5.2.2	Reference systems and relevant considerations	219
5.2.3	Measurement definition and methods	223
5.3	Case Study Results	225

5.4	Discussion	227
6	Final discussion and conclusions	229
6.1	Main findings and achievements	230
6.2	Discussion on the findings and achievements	232
6.2.1	Effect of patient-specific gait features	232
6.2.2	Patient-specific functional cup orientation	234
6.2.3	Importance of inpatient and interpatient variation in THR success prediction	236
6.3	Challenges, limitations and future work	237
6.4	Final conclusion	239
	References	240

Appendices

List of Figures

1.1	Schematics of the anatomical planes and anatomical terms of directions.	5
1.2	The anatomy of the right hip in the coronal plane, cross-section of the hip joint is shown exposing internal structures of the joint.	6
1.3	Anatomy of the natural hip joint's acetabular component in the sagittal plane.	9
1.4	Left: left hip, coronal, acetabular inclination angle of the acetabulum measured between acetabular rims and teardrop line.	11
1.6	Two-dimensional projection of pelvis representing sagittal radiograph. .	13
1.7	Left: left hip, coronal, femoral neck-to-shaft angle, measured between femoral shaft and femoral neck centre lines.	13
1.8	Modern modular total hip replacement. This design features acetabular shell and liner, femoral head and stem.	17
1.9	Example <i>in vitro</i> testing loading and motion profiles by (Ali et al., 2016) for THR in vitro wear testing.	26
1.10	Factors influencing the risk of sub-optimal dynamic joint organisation occurrence, excluding gait biomechanics.	27
1.11	Left hip schematics of radiographic measurements a) cup inclination angle α measurement in coronal plane b) cup version angle β measurement in the transverse plane.	29
1.12	Left hip coronal plane, possible modes of dynamic alignment of THR <i>in vivo</i> . c denotes radial clearance. a) Ideal conditions, when the cup and head are well-positioned and concentric; the contact area (in red) falls between head and cup, the separation between centres is negligible - clearance. b) Edge contact, when the cup's and the head's position deviates from ideal and theoretical contact area shifts partially outside of the cup; head and cup remain concentric and separation between centres is negligible - clearance. c) Edge loading, when the cup's centre translates away from head's centre, and the stripe-like contact area falls between the head and cup rim only. The separation between head and cup centres is significant – higher than clearance.	32
1.13	The figure shows the cracked rim cross-section of cross-linked polyethylene THR liner.	32
1.14	Left: BIOLOX® Forte with stripe wear indicated in purple, revised after 2.6 years in vivo due to pain.	36

1.15	BILOX®Forte liner with severe ceramic wear indicated in purple, and deposited titanium metal material, as a result of dislocation (Lusty et al., 2007)	38
1.16	Joint coordinate system and segment coordinate systems at the hip joint defined by ISB (Wu et al., 2002).	40
1.17	Possible movements of the femur at the hip in regard to the right side. Angles for specified movements are measured in following planes, starting from left, coronal, sagittal, transverse.	42
1.18	Possible rotations of the pelvis in coronal, sagittal and transverse planes.	43
1.19	The schematic of the gait cycle, during normal walking. LH - left hip, RH - right hip.	46
1.20	The motions of the natural hip joint, left: sagittal plane; centre: coronal plane; right: transverse plane. Vertical axis represents degrees, where +ve are flexion, adduction and internal rotation angles (Kadaba et al., 1990).	48
1.21	The motions of the pelvis, left: sagittal plane; centre: coronal plane; right: transverse plane. Vertical axis represents degrees (Kadaba et al., 1990). .	49
1.22	Figure adapted from Paul (1966), representing joint contact force at the right hip. F_{SI} for superior-inferior force, F_{ML} for medial-lateral force, F_{AP} for anterior-posterior force. The contact forces are averaged for healthy patients.	51
1.23	Figure adapted from Paul (1966), representing joint contact force at the right hip. F_{SI} for superior-inferior force, F_{ML} for medial-lateral force, F_{AP} for anterior-posterior force. The contact forces are averaged for healthy patients.	63
2.1	Illustration of the proximity tool's output, where THR is presented in cross-section and with global coordinate system marked.	75
2.2	Sample output of the proximity tool where orange curve is for centre proximity angle and blue for edge proximity angle.	76
2.3	Definition of the laboratory coordinate system for HIP98 dataset in relation to the patient lower body in frontal and sagittal planes marked as Z_L and Y_L and X_L	81
2.4	Definition of the laboratory coordinate system for LBRC dataset in relation to pelvis in the frontal plane.	82
2.5	Rotation direction definitions for LBRC dataset in relation to the right and left side acetabular cups.	83
2.6	Flow chart describes the actions executed in the proximity tool during the simulation both with and without pelvic motion addition.	84

2.7	Flow chart describes the actions executed in the proximity tool during the simulation both with and without pelvic motion addition.	86
2.8	Simplified 2D schematics of the acetabular cup, where H is the height of the theoretical contact area, α is the angle between edge of the theoretical contact and joint contact force vector.	88
2.9	Acetabular cup cross-section, X-Z plane, of the generalised total hip replacement model used to find the contact force and contact area relationship.	91
2.10	Output of the finite element simulation, contact force versus contact area marked in black.	92
2.11	Mesh convergence results for the element size between 2mm and 0.4mm for maximum and minimum contact area values.	94
2.12	Sensitivity study for radial clearance between THR bearings, for 32mm ceramic-on-polyethylene combination.	96
2.13	The initial position of the acetabular cup within the proximity tool environment.	97
2.14	Cup positioned within the proximity tool environment using inclination and version angles. Where, X axis is medial-lateral axis and Y is anterior-posterior axis.	99
2.15	Custom profiles, sine waves, to test the dynamic pelvic coordinate system rotation order and iteration count	102
2.16	Rotation test with variable step iterations per each angle.	103
2.17	Patient 001 (LBRC) two-dimensional angle profiles for pelvic motion through the gait cycle.	105
2.18	Rotation test with variable step iterations per each angle for patient 001 from LBRC dataset.	106
2.19	2D sample vector expression in relation to two different 2D coordinate systems.	108
2.20	The schematic of acetabular cup with the contact force path through the arbitrary activity cycle.	109
2.21	Schematics of acetabular cup implanted on the right side. I, II, III, IV regions marked for assessment of rim damage location.	110
2.22	Case 1 and Case 1a, patient HSR (HIP98) output of the proximity tool for three simulation scenarios.	112
2.23	Case 2, patient 001 (LBRC) output of the proximity tool for two simulation scenarios.	113

3.1	Magnitudes of resultant contact force for all nine activities for each HIP98 patient. The contact force profiles are averaged out from trials per activity per patient, where available multiple trials are available.	122
3.2	Cup orientation schematics for creation of reference table, which combined two-dimensional inclination and version angles, and rotation which has to be applied to get the desired version angle.	123
3.3	Example of output for sub-study 1 of HIP98 data analysis. The Figure presents a graph for edge proximity angles and resultant contact force magnitude during one activity cycle for one patient.	126
3.4	Edge proximity angles and resultant contact force magnitude for locomotor activities for patient HSR	129
3.5	Edge proximity angles and resultant contact force magnitude for non-locomotor activities for patient HSR	130
3.6	Risk of edge contact for patient HSR. Maximum edge proximity angles in red, average edge proximity angles in grey.	131
3.7	Edge proximity angles and resultant contact force magnitude for locomotor activities for patient PFL	134
3.8	Edge proximity angles and resultant contact force magnitude for non-locomotor activities for patient PFL	135
3.9	Risk of edge contact for patient PFL. Maximum edge proximity angles in red, mean edge proximity angles in grey.	136
3.10	Edge proximity angles and resultant contact force magnitude for locomotor activities for patient KWR	138
3.11	Edge proximity angles and resultant contact force magnitude for non-locomotor activities for patient KWR	139
3.12	Risk of edge contact for patient KWR. Maximum edge proximity angles in red, mean edge proximity angles in grey.	140
3.13	Edge proximity angles and resultant contact force magnitude for locomotor activities for patient IBL	141
3.14	Edge proximity angles and resultant contact force magnitude for non-locomotor activities for patient IBL	142
3.15	Risk of edge contact for patient IBL. Maximum edge proximity angles in red, mean edge proximity angles in grey.	142
3.16	Example of output for sub-study 2 of HIP98 data analysis. A plot of centre proximity angles where pelvic motions included and excluded during one activity cycle for one patient.	145

3.17	Walking with self-selected speed centre proximity angles for pelvic motions included and excluded cases for patients HSR, PFL, KWR.	149
3.18	Walking fast centre proximity angles for pelvic motions included and excluded cases for patients HSR, PFL, KWR.	152
3.19	Standing activity centre proximity angles for pelvic motions included and excluded cases for patients HSR, PFL, KWR.	154
3.20	<i>Paul Cycle</i> contact force gait profile (Paul, 1966).	156
3.21	Example of output for sub-study 3 of HIP98 data analysis. The figure presents a plot for centre and edge proximity angles.	157
3.22	Example of output for sub-study 3 of HIP98 data analysis. The figure presents acetabular cup opening and the location of maximum contact along the rim for pelvic motions included case.	158
3.23	Centre and edge proximity angles for (a) <i>Paul Cycle</i> , (b) - (e) for HIP98 patients during walking with self-selected speed. Sub-figure (f) - legend.	160
3.24	Location of the maximum proximity angles for heel-strike to mid-stance (left), mid-stance to toe-off (middle) and swing phase (right) for Paul Cycle .	161
3.25	Location of the maximum proximity angles for heel-strike to mid-stance (1), mid-stance to toe-off (2) and swing phase (3) across all patients for walking with self-selected speed (normally)	162
3.26	Location of the maximum proximity angles for heel-strike to mid-stance (1), mid-stance to toe-off (2) and swing phase (3) across all patients for walking with faster speed.	163
3.27	Location of the maximum proximity angles for heel-strike to mid-stance (1), mid-stance to toe-off (2) and swing phase (3) across all patients for walking with slower speed.	163
3.28	Location of the maximum proximity angles for heel-strike to mid-stance (1), mid-stance to toe-off (2) and swing phase (3) across all patients for stair ascent	164
3.29	Location of the maximum proximity angles for heel-strike to mid-stance (1), mid-stance to toe-off (2) and swing phase (3) across all patients for stair descend	165
3.30	Location of the maximum proximity angles for maximum proximity angle occurrence across all patients for raising from the chair	166
3.31	Location of the maximum proximity angles for maximum proximity angle occurrence across all patients for sitting down on the chair	166
3.32	Location of the maximum proximity angles for maximum proximity angle occurrence across all patients for bending knees	167

3.33	Location of the maximum proximity angles for maximum proximity angle occurrence across all patients for standing on two-one-two legs	167
4.1	Patient 073 pelvic dynamic and static angles.	177
4.2	Patients pelvic dynamic walking (a) and static pelvic tilt (b).	178
4.3	Patients pelvic dynamic walking (a) and static pelvic obliquity (b).	179
4.4	Patients pelvic dynamic walking (a) and static pelvic internal-external rotation (b).	180
4.5	The example of static pelvic orientations, dynamic pelvic orientations and modified pelvic motion orientations for patient 073.	185
4.6	The schematics of the cup orientation within the pelvis for cases where patient-specific pelvic tilt was included (left) and excluded (excluded) from proximity tool simulations.	186
4.7	Results for centre and edge proximity angles visualised with the confidence bands for patients who's edge contact risk was not affected by pelvic motion inclusion	192
4.8	Results for centre and edge proximity angles visualised with the confidence bands for female patients who's edge contact risk was affected by pelvic motion inclusion	193
4.9	Results for centre and edge proximity angles visualised with the confidence bands for patients who's edge contact risk was not affected by pelvic motion inclusion	194
4.10	Patient 052 centre proximity angles, separate motions and motion their pairs.	197
4.11	Results for pelvic motions included, excluded and pelvic dynamic motions included (static excluded)	200
4.12	Maximum edge proximity angles for two regions during stance phase for the <i>in vivo</i> condition, pelvic motions included. Region 1 for heel-strike to mid-stance, and region 2 for mid-stance to toe-off.	205
4.13	Average edge proximity angles for two regions during stance phase for the <i>in vivo</i> condition, pelvic motions included. Region 1 for heel-strike to mid-stance, and region 2 for mid-stance to toe-off.	205
5.1	Algorithm check for dynamic pelvic orientation. When acetabular cup and femoral head don't align the algorithm is not working, when acetabular cup and femoral head align the algorithm is working properly.	218
5.2	The schematic of laboratory space taken parallel to the ceiling.	219

5.3	Pelvic plane definition according to Grood and Suntay (Wu et al., 2002), defined by PSIS mid-point and two ASIS landmarks.	221
5.4	Definition of local pelvic coordinate system (Wu et al., 2002) in red, and global coordinate system in blue, where <i>AP</i> is anterior-posterior, <i>ML</i> - medial-lateral and <i>SI</i> - superior-inferior axes.	222
5.5	The pelvic coronal plane defined by ASIS landmarks and global transverse plane orthogonal to pelvic coronal plane.	222
5.6	View from pelvic sagittal plane and measurement of	223
5.7	The pelvic coronal plane for projection of the acetabular cup rim	225
5.8	The results for the sagittal pelvic tilt angles measured in pelvic sagittal plane, where blue, red and black lines represent stand-to-sit, supine and walking respectively.	226
5.9	The results for the inclination angles measured in pelvic coronal plane	226
A.1	RMSE ° values, between pelvic motions included and excluded, versus pelvic sagittal tilt, for region 1.	i
A.2	RMSE ° values, between pelvic motions included and excluded, versus pelvic sagittal tilt , for region 2.	i
A.3	RMSE ° values, between pelvic motions included and excluded, versus pelvic coronal obliquity, for region 1.	i
A.4	RMSE ° values, between pelvic motions included and excluded, versus pelvic coronal obliquity, for region 2.	i
A.5	RMSE ° values, between pelvic motions included and excluded, versus pelvic internal-external rotation, for region 1.	i
A.6	RMSE ° values, between pelvic motions included and excluded, versus pelvic internal-external rotation, for region 2.	i

List of Tables

1.1	Full ROMs' for gait kinematic angles identified by two studies Kadaba et al. (1990) and Bennett et al. (2008). The ROM is from +ve and -ve	47
1.2	The list of the computational studies on THR performance, including contact mechanics and tribology.	62
2.1	Rotation direction definitions in relation to the acetabular cup. The definitions apply independently of the hip side	83
2.2	Mesh convergence test results for element sizes 2mm, 1mm and 0.5mm.	94
2.4	Contact area and contact force variation and uncertainty depending on radial clearance value.	96
3.1	Detailed patient demographics and cup orientation information for HIP98 dataset. Number of trials for each activity is displayed next to activity name.	121
3.2	The proximity result comparison between different patients and activities. PA - angle measured in degrees [$^{\circ}$], for maximum edge proximity angle. In square brackets, A.C. is for gait cycle instance of the maximum proximity. F_p - contact force of maximum proximity angles, F_{max} - maximum contact force during activity cycle. * symbolises edge contact occurrence.	127
3.3	Centre proximity results comparison between different patients and activities with pelvic motion included/excluded.	147
4.1	Patients demographics and walking speed.	176
4.2	Cases for each sub-study. The outputs were separated into, CP - centre proximity angle profiles, EP - edge proximity angles and none.	182
4.3	RMSE values for pelvic motions included versus excluded	195
4.4	Pelvic motion or combination, that contributes to overall pelvic motion effect for each patient.	198
4.5	Linear regression analysis results between RMSE values and pelvic sagittal tilt maximum, minimum, range and mean.	201

4.6	The linear regression analysis results between RMSE values and pelvic coronal obliquity maximum, minimum, range and mean. The positive slope direction - positive linear correlation, negative slope direction - negative linear correlation, negative adjusted R^2 - correlation is too complex to be described by linear regression, R^2 - the closer to 1 the stronger the correlation.	202
4.7	The linear regression analysis results between RMSE values and pelvic internal-external rotation maximum, minimum, range and mean. The positive slope direction - positive linear correlation, negative slope direction - negative linear correlation, negative adjusted R^2 - correlation is too complex to be described by linear regression, R^2 - the closer to 1 the stronger the correlation.	203
4.8	Potential of edge contact clock-wise orientation along the rim.	207
5.1	Pre-processed data provided by COB, including format and application.	217
A.1	Reference table developed for HIP98 cup orientation in proximity tool. .	ii

List of Abbreviations

AA - abduction-adduction
AP - anterior-posterior
ASIS - anterior superior iliac spine
BMI - body mass index
CAD - computer-aided design
COB - Centre of Orthopaedic Biomechanics (University of Denver)
CoC - ceramic-on-ceramic
CoP - ceramic-on-polyethylene
CNS - central nervous system
CT - computed tomography
EMG - electromyography
EOS - low dose medical imaging system (EOS imaging®, Paris, France)
ex vivo - retrieved from patients body
FE - flexion-extension
FEA - finite element analysis
FEs - femoral epicondyles
GC - gait cycle
GCS - global coordinate system
HIP98 - online instrumented THR gait database (Bergmann, 2008)
IE - internal-external
in silico - simulated computationally
in vitro - while outside patients body in a controlled environment
in vivo - while in the patients body
ISO - International Organization for Standardization
ISB - International Society of Biomechanics
JCS - joint coordinate system
LBRC - Leeds Biomechanical Research Center (University of Leeds)
ML - medial-lateral
MoM - metal-on-metal

MoP - metal-on-polyethylene

OA - osteoarthritis

OPS™ - Optimized Positioning System™

PC - point cloud

PSIS - posterior superior iliac spine

RMSE - root mean square error

ROM - range of motion

SI - superior-inferior

SCS - segment coordinate system

THR - total hip replacement

UHMWPE - ultra high molecular weight polyethylene

+ve - positive

-ve - negative

Chapter 1

Introduction and Literature Review

1.1 Introduction

Total hip replacement (THR) surgery is a frequently undertaken arthroplasty procedure in the the UK, with around 90,000 surgeries performed in year 2017 (National Joint Registry UK, 2018). The THR surgery involves the full substitution of the natural diseased hip joint by the artificial components. Total hip replacement failures do occur and can cause severe risk to the patient's long-term health. The average age at implantation is reported to be 68 ± 11 years according to the National Joint Registry UK (2018), with life-expectancy of more than 15 years. Hence, the early detection of potential long-term failure is considered important.

Examination of failed total hip replacements removed during revision surgery showed that the devices, while *in vivo*, were loaded in a sub-optimal manner. Particularly, the damage indicated that the femoral head was in contact with the edge of the acetabular cup at some point during the activities. The loads during the head-on-rim contact at that point were significant enough to cause increased wear or rim damage (Nevelos et al., 1999; Komistek et al., 2002; Tower et al., 2007). The current total hip replacement standard, ISO 14242-1:2018, for wear testing addresses some of the head-rim induced damage. However, this standard does not include patient and activity specific data, which might also influence the success of the implant *in vivo*.

One of the head-rim contact types is edge contact, which belongs to a type of mechanism that cause long-term mechanical and biological total hip replacement failure. In some cases, in the literature, edge contact can also be referred to as the edge loading (Hua et al., 2016). The edge contact definition in this PhD

project is a scenario where the head remains concentric within the cup and the contact area falls onto the rim of the cup.

The implant failures associated with edge contact include high wear (Tian et al., 2017) and aseptic loosening due to wear (Abu-Amer et al., 2007), rim damage (Tower et al., 2007), and lysis due to altered loading and torques (Harris, 1995; Sariali et al., 2010). According to National Joint Registry UK (2018), aseptic loosening accounts for 50% , lysis 15%, implant wear 14% and implant fracture 4% of the revision surgeries.

Edge contact during daily activities can be avoided or minimised through well-planned surgical positioning. Current surgical positioning “safe zones” are based on the dislocation and severe impingement studies (Lewinnek et al., 1978; McLawhorn et al., 2015). It is easy to separate the failures caused by dislocation and severe impingement from other modes, in fact the National Joint Registry UK (2018) recognises these mechanisms as reasons for revision surgery. In a study by Lewinnek et al. (1978) the “safe zones” were identified through direct comparison between dislocation rates and cup positioning. Although, these “safe zones” are widely used, according to Seagrave et al. (2017) there is not enough evidence to support these orientation guides. McLawhorn et al. (2015) presents an updated approach for determining the “safe zones” by assessing the relationship between version angles and incidence of dislocation in a large-scale study of 553 THRs. However, same as the previous approach this was done in regards to dislocation only. There has been no study so far which combines all the mechanisms leading to THR failure with relation to cup positioning. In addition, edge contact has not yet been studied from an *in vivo* acetabular cup dynamic orientation perspective.

Possible method for *in vivo* edge contact detection is radiography. Marel et al. (2016) previously used radiography to determine the risk of edge contact in ceramic-on-ceramic failing THR replacements. Using computational modelling, the authors of the study have determined the change in functional cup orientation with change in pelvic position in sagittal plane. According to the results of the study, the cup orientations gained from typical anterior-posterior radiograph do not represent the dynamic bearing organisation throughout daily activities,

hence edge contact risk can be unnoticed. The possible non-static edge contact detection tool, could be video-fluoroscopy, which has been used for bearing separation measurement by Dennis et al. (2001). This method allows dynamic assessment of THR bearing alignment during patients motion. Video-fluoroscopy offers non-invasive method which can be combined with gait analysis, but there are multiple limitations due to equipment availability and associated costs.

Assessment of the effects of edge contact can be achieved through the *ex vivo* component analysis. In retrieval studies the challenge is to separate edge contact from other long-term failure mechanisms. In addition, explanted components are rarely available and are of older designs, and cup orientation data is often missing for those patients (Tower et al., 2007; Schroder et al., 2011).

Other methods of assessing component performance in relation to edge contact include *in vitro* wear and biomechanical studies (Korduba et al., 2014; Ali et al., 2017) and *in silico* contact mechanics studies (Hua et al., 2016). However, *in vitro* tests are lengthy and costly, hence are inefficient to assess a large patient cohort and determine the *in vivo* relevant edge contact risks. Meanwhile, up to date *in silico* studies, which provide more cost-effective solution, compared to *in vitro* studies, have not targeted edge contact from patient-specific *in vivo* perspective. A study by Hua et al. (2016) looked at the edge contact in one particular device for averaged patient with instrumented THR collected by Bergmann (2008). This study showed the importance of cup positioning and described riskiest activities in terms of edge contact occurrence and duration. However, it is yet unknown if the average patient activity biomechanics fully represents the THR population. Another limitation to the *in vitro* and *in silico* studies performed to date is the exclusion of pelvic motions, which is a movement present *in vivo* and for some patients shown to be of high range of motion (Miki et al., 2004).

1.1.1 Motivation for the project

The patient-specific edge contact occurrence knowledge would allow for enhancement of current ISO standard for assessment of total hip replacement design success. The analysis, either *in vitro* or *in silico*, with patient-specific data,

such as cup orientations, gait and weight, would broaden the assessment of device performance *in vivo* and would potentially eliminate revisions of total hip replacements from edge contact induced failure. In addition, combined with knowledge for “safe zones” in relation to dislocation and severe impingement this could form a combined cup orientation “safe zone” criteria. With more future work done on *in vivo* edge loading, mild impingement and other long term failure mechanisms the multi-mechanism “safe zone” reference system would be possible to generate. However, current *in vitro* and *in silico* tests with patient-specific parameters would be costly and time inefficient for large enough total hip replacement cohort to make some statistically significant judgment and analysis.

1.1.2 Aim of the project

The overall aim of the project was to establish the effect of patient-specific biomechanical activity features on the success of total hip replacement from an edge contact perspective.

Aim of studies within the project

1. The aim of the first study within this project was to develop a computational tool for fast patient-specific activity data processing with focus on edge contact risk assessment.
2. The aim of the second study was to use open-source activity database, for four patients and nine activities, to establish the potential patient-specific characteristics that influence the risk of edge contact.
3. Based on the conclusions of second study, the aim of the third study was to analyse a larger patient and more homogeneous cohort to establish the effect of patient-specific gait features, including pelvic motions, on the risk of edge contact.
4. The final study was aimed at exploring the potential use of video-fluoroscopy techniques in addressing the risk of edge contact specifically from dynamic pelvic orientation perspective.

1.2 Literature review introduction

The aim of the literature review of this thesis was to gain sufficient understanding into the topics relevant to this PhD project. The literature review for this thesis is extensive as the main aim of the project considers the combination of multiple disciplines within the orthopaedic area.

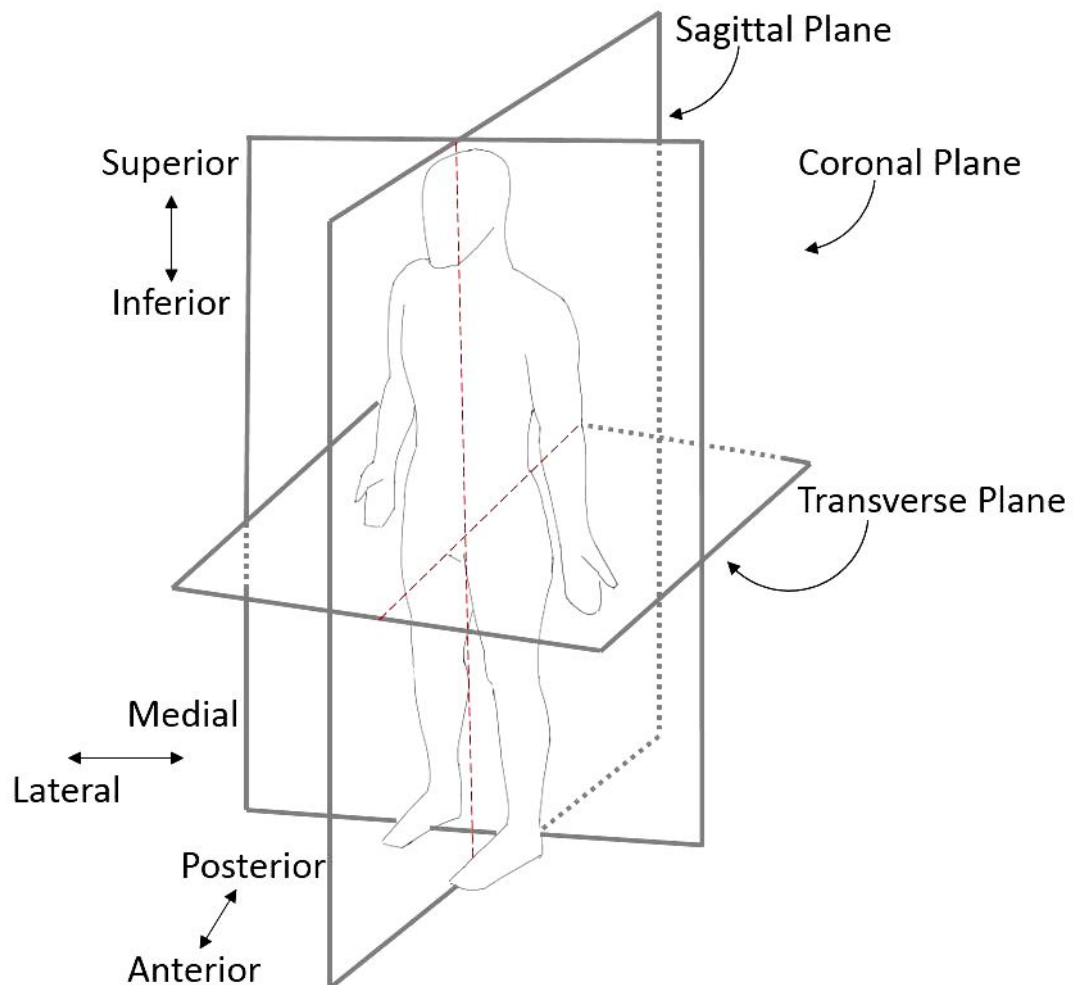


Figure 1.1: Schematics of the anatomical planes and anatomical terms of directions.

The names of the anatomical planes and terms of locations used in this thesis are presented in Figure 1.1. Here, the anatomical planes are orthogonal to each other and pass through the middle of the body. The terms of locations in Figure 1.1 are normalised to the right hip. The medial-lateral direction depends on the side of the body, where medial means the direction towards the mid line of the body.

1.3 Natural hip joint and surrounding structures

1.3.1 Anatomy and functionality

The human body has two symmetrical hip joints located laterally on the right and left side of the pelvis. The hip joint (Figure 1.2) is a connection between the pelvis and femur. The hip joint is considered a ball-and-socket articulation, where the ball is represented by a femoral head, and the socket is represented by an acetabular cup. In an asymptomatic joint, the femoral head is well-seated in the acetabular cup achieving large contact area during load-bearing activity (Hamill and Knutzen, 2006). Surrounded by a total of 27 muscles, the healthy hip joint provides a wide range of motions important in day-to-day activities and at the same time ensures overall stability. The hip joint provides a connection between the upper and lower body, supports and balances the inferior weight and transmits ground reaction forces in line with other lower extremity joints (Byrne et al., 2010).

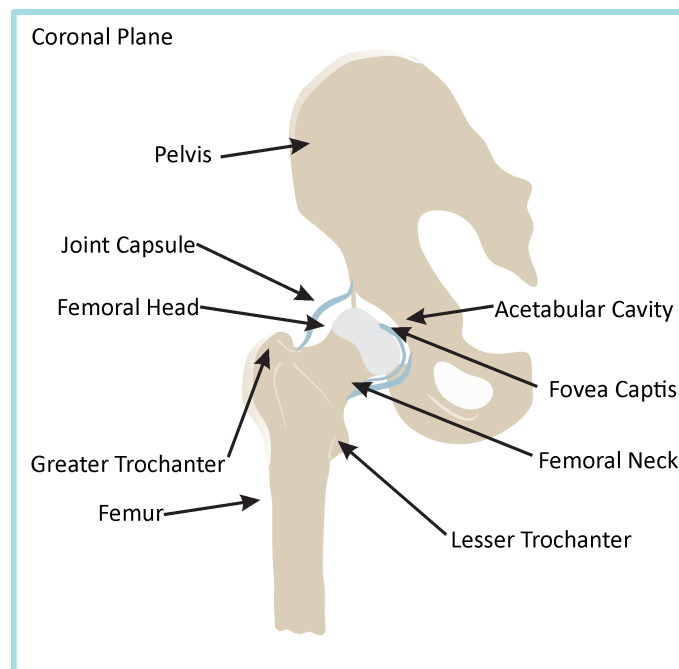


Figure 1.2: The anatomy of the right hip in the coronal plane, cross-section of the hip joint is shown exposing internal structures of the joint. Arrows direct to basic anatomical components of the hip joint.

Femur and femoral structures of the hip joint

The femur is the largest bone of the human skeleton, which is classified as long bone and provides structural support to the body. Femoral side of a hip joint is formed by head and neck, which extend to the femoral shaft as seen in Figure 1.2. A femoral head is spherical in its geometry, and according to Tönnis (2012) forms approximately two-thirds of a sphere. In healthy subjects, the femoral head is approximately 70% covered by articular cartilage. The central part of femoral head serves as weight-bearing area (Hamill and Knutzen, 2006). Medially (Figure 1.2), cartilage of the head is disturbed by fovea capitis which is an attachment point for ligamentum teres. Underneath the cartilage, femoral head structure is predominantly tubercular bone which allows a uniform strain distribution during loading (Van Rietbergen et al., 2003). The lateral and cartilage-less part of the femoral head extends to femoral neck (Hamill and Knutzen, 2006), forming a connection between hip joint and femur. The femoral neck is generally thin in the middle, formed by trabecular bone and lining of the cortical bone, which withstands compressive and tensile stresses preventing the neck from fracturing (Hamill and Knutzen, 2006). Just before the femoral shaft, two structures greater and lesser trochanters are present which are compromised of tubercular bone with a thin lining of the cortical bone on the outside. The femoral shaft extends down to the knee joint, slightly bowing anteriorly. The bowing of the femoral shaft largely depends on the exhibited compressive and tensile loads (Hoehn and Marieb, 2007).

Pelvic structures and acetabulum

Pelvis in contrast to the femur is classified as a flat bone. The pelvises preliminary role is the protection of the internal organs and provision of the soft-tissue attachment sites. Another role of the pelvis is to provide an adequate position of the hip joint during activity. The whole bone complex responsible for movement is called pelvic girdle. It is well known that pelvic griddle shape and structure is gender dependent, such that pelvic cavity in females is much broader than in males while bones are lighter and thinner (Hamill and Knutzen, 2006). The pelvic griddle is symmetrical along the sagittal plane and consists of three bony

structures ilium, ischium and pubis. The two sides of pelvis are connected anterior-inferiorly at the pubic symphysis and connected to trunk superiorly at the sacroiliac joint (Hamill and Knutzen, 2006). The acetabulum is located at the lateral fibrous connection of three pelvic bony structures which are lined with articular cartilage. The cartilage forms horseshoe-like geometry, or lunate surface, with an opening at the inferior rim. It is connected to the femoral head with ligamentum teres and is enveloped by the transverse ligament (Ranawat and Kelly, 2005; Tönnis, 2012). Around the edge, the acetabulum is protected by fibrocartilaginous rim called labrum. This structure forms a complete but asymmetrical circle that is thicker superiorly and posteriorly (Hoehn and Marieb, 2007). Jointly acetabulum and labrum conceal more than half of femoral head in the healthy hip joint. Hence, the labrum helps in preventing dislocation and excessive loading on the cartilage (Kim, 1987).

Articular capsule

The articular capsule is shown in Figure 1.2 in blue. The hip joint is classified as a synovial joint, as it is enclosed in the synovial membrane and its bearing surfaces are separated by the synovial fluid. The synovial membrane is formed by soft tissue which attaches itself to the distal part of the femoral neck from one side and just over the labrum on the acetabular side (Buckwalter et al., 2000; Hoehn and Marieb, 2007). In well-functioning joint membrane cells produce synovial fluid components, such as hyaluronic acid. The outer lining attaches externally to the intimal lining and includes mostly blood vessels, fat cells, and fibroblasts. In a healthy joint, synovial fluid plays a role in friction reduction for cartilage-to-cartilage and cartilage-to-synovium articulations (Buckwalter et al., 2000). Importantly, synovial fluid serves as a nutrition pathway for cartilage and ligaments distant from blood vessels of a joint (Murakami et al., 1996).

Exteriorly to the synovium, the hip joint is surrounded by the dense ligamentous tissue formation called fibrous layer which is attached to the acetabulum superiorly and wraps femoral neck inferiorly. The ligament complex encapsulates 95% of the femoral neck, leaving two-thirds of posterior part exposed for rotator muscle attachment (Ranawat and Kelly, 2005; Tönnis, 2012). Without the involvement

of muscles, purely due to high stiffness ligaments around the hip joint restrict the undesirable anterior translation when joint is extended or rotated externally and prevent joint from experiencing excessive motion at full extension (Ranawat and Kelly, 2005).

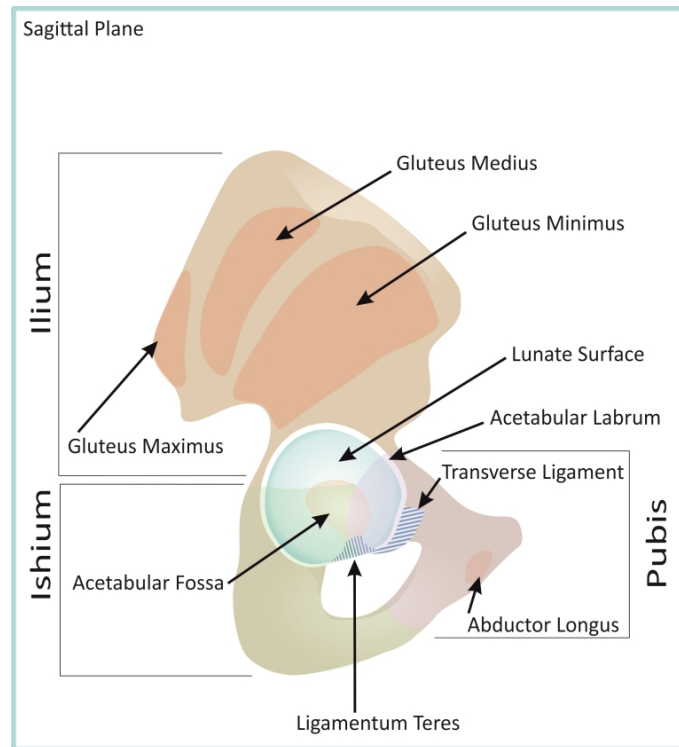


Figure 1.3: Right Hip. Anatomy of the natural hip joint's acetabular component in the sagittal plane. The unshaded area represents ilium bone, the green shaded area represents ischium bone and purple shaded area represents pubis.

Muscles and muscular actions

There are more than twenty muscles acting on the hip joint allowing for propelling and stabilising human body during the activity, which include muscles with attachment points at the femur, pelvis and trunk. There are several muscle groups acting on hip joint, performing flexion-extension, abduction-adduction, and external-internal rotation. It is not uncommon for some muscle to assist in various movements. Hip flexors are mainly responsible for bringing the leg forward during the activity. Hip flexors are considered two-joint muscles, which perform counter-actions at the other joint to allow for overall body stability. The strongest of those muscles is iliopsoas complex which has attachment sites at both thigh and lower spine. This muscle complex is activated greatly during hip

flexion exercises, while trunk is stabilised and vice versa. At the lower extremity level hip flexor, rectus femoris, also dictates the position of the knee and acting as the extensor to the knee joint. There are also secondary flexor muscles around the hip joint, which primary role is different but they do contribute flexion. In healthy individuals, the pelvis will be dragged anteriorly by hip flexors unless balanced by trunk motion (Hamill and Knutzen, 2006).

Position and clinical measurements

The most to assess the position and orientation of hip joint structures is conventional radiography, which allows two-dimensional imaging of the patient in a static position, either supine or standing. The standard radiographic plane used for measurements associated with the hip joint is taken parallel to coronal plane and is termed anterior-posterior (AP) radiograph (Callaghan et al., 2007a). For some studies and clinical assessment of patient's hip joint and pelvis the sagittal view is projected, which is termed lateral radiograph. Whereby in a supine position the patient has to turn on their side, which will ultimately change the orientation of the anatomical structure due to variable muscle recruitment between two positions (Jackson et al., 2016).

Alternative to radiography is tomography, such as computed tomography (CT) and magnetic resonance imaging (MRI), which allows for the capture of multiple slices across patient's body. The advantage of modern tomography over two-dimensional radiographs is a measurement of patient in same position from three radiographic planes coronal, sagittal and traverse. Clinically, the availability of a three-dimensional imaging technique might capture structural features which cannot be identified from two-dimensional projections. However, tomography is more expensive and less accessible than conventional radiography, hence the popularity of two-dimensional radiographic projections (Callaghan et al., 2007a; Tönnis, 2012).

One of the most novel methods of capturing hip joint orientations *in vivo* is video-fluoroscopy; and EOS (EOS imaging®, Paris, France), which tend to require lower dose of radiation than other imaging methods. Both imaging techniques,

allow for registration of dynamic motion. The planes can be adjusted to represent either sagittal or coronal radiographic planes or can be arbitrary dependent on the study aim (D'Isidoro et al., 2017; Westberry et al., 2018).

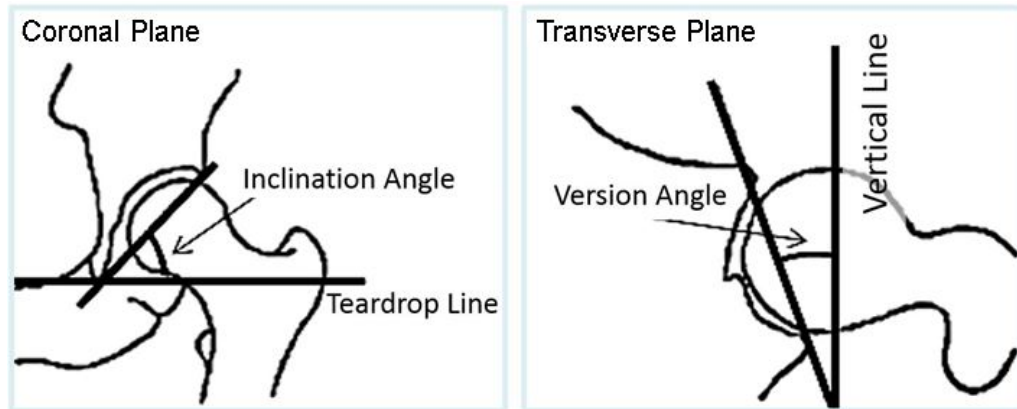


Figure 1.4: Left: left hip, coronal, acetabular inclination angle of the acetabulum measured between acetabular rims and teardrop line. Right: right hip, transverse, acetabular version measured between a vertical line and acetabular rims. (Saikia et al., 2008)

The complex position and orientation of the acetabulum can be identified through different planes. The transverse acetabular inclination in the coronal plane is commonly used. It is defined as the angle between a horizontal line drawn from the acetabular teardrop to the centre of the pelvis, and a line drawn from acetabular teardrop and superior rim of the acetabulum (Figure 1.5, left (Saikia et al., 2008)). In clinical practice version of acetabulum is quantified from the transverse plane if tomography is available. Version is measured as the angle between the line perpendicular to the line drawn between right and left iliums and the line drawn to the anterior margin from posterior margin of the acetabulum (Figure 1.4, right (Saikia et al., 2008)). The acetabulum can be evaluated as being anteverted or retroverted, where the acetabulum opening plane is facing anteriorly or posteriorly respectively. Apart from tomography, the version direction can be identified using standard AP radiographs. Anteversion is registered for acetabulum with no cross-over of the anterior and posterior rim projections of the acetabulum (Figure 1.5, left). Retroversion is registered for acetabular two-dimensional projection with intersection between anterior and posterior sides of the rim (Jamali et al., 2007).

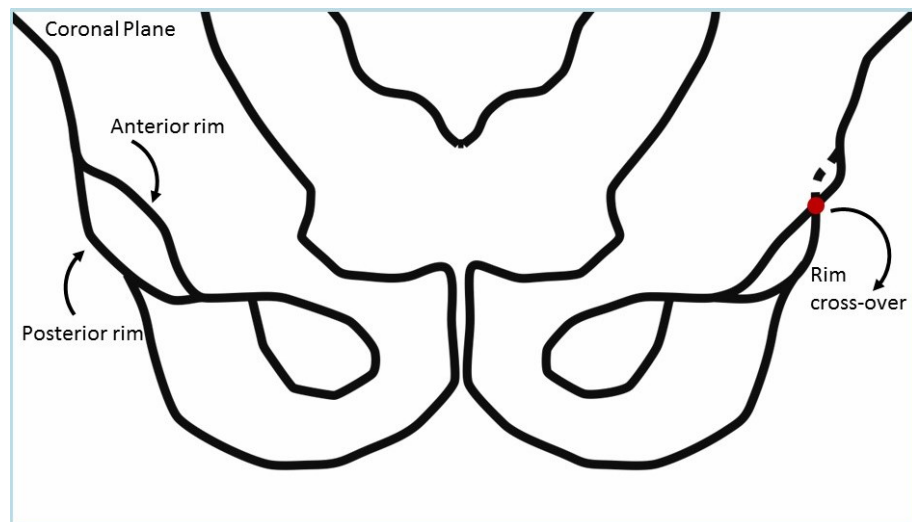


Figure 1.5: Two-dimensional projection of pelvis representing an AP radiograph. On the left, acetabulum with no rim cross-over, which is identified as anteversion. On the right, acetabulum with rim cross-over, marked by red dot, which is identified as retroversion.

In regard to pelvis the most commonly measured angle is pelvic sagittal tilt, which traditionally is measured from the sagittal radiograph as shown in Figure 1.6. The angle is measured either as the angle between vertical axis of the image and line connecting pubic tubercle and anterior iliac spines (ASIS). The left and right anterior iliac spines are defined by the most prominent anterior points of the ilium. The vertical axis of the image is either coincident with ASIS or pubic tubercle (Blondel et al., 2009; Maratt et al., 2015). According to Schache et al. (2000), pelvic tilt can also be measured as the angle between horizontal axis of lateral radiograph passing through posterior iliac spine (PSIS), and line connecting ASIS and PSIS. In this case, the horizontal image axis is constructed through PSIS, where PSIS is the most prominent posterior point of the ilium on sagittal plane (Figure 1.6).

The femoral head position is dictated by the orientation of femoral neck, which develops according to the direction and magnitude of the dominant compressive load and other functional stimuli (Tönnis, 2012). The two commonly measured positions of the femoral neck are neck to shaft angle and torsion, or neck version. The neck to shaft angle (Figure 2.6, left) is described as the inclination angle of the neck relative to the body of the shaft in the coronal plane (Saikia et al., 2008). The torsion angle (Figure 1.7, right) is a rotational offset in the transverse plane of the neck relative to an axis constructed between two femoral condyles (Figure

1.7, right) (Cibulka, 2004; Saikia et al., 2008).

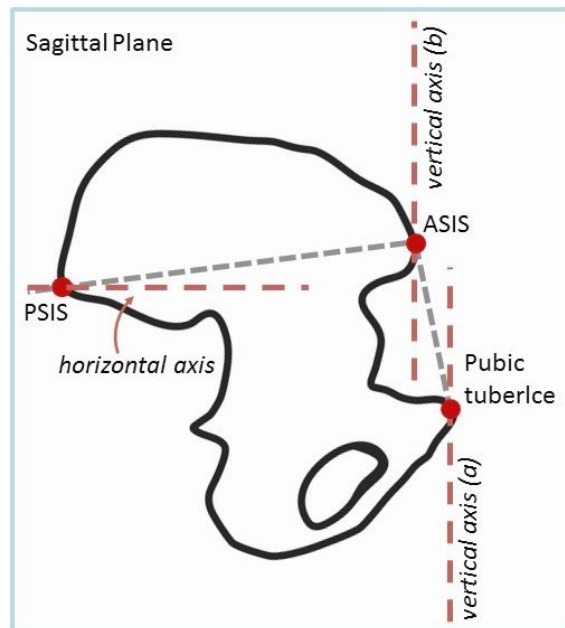


Figure 1.6: Two-dimensional projection of pelvis representing sagittal radiograph. Two methods of pelvic tilt measurement are shown. Red-dashed lines symbolise image axes built through bony landmarks of the pelvis, red reference points. ASIS for anterior for anterior superior iliac spine, PSIS for posterior superior iliac spine.

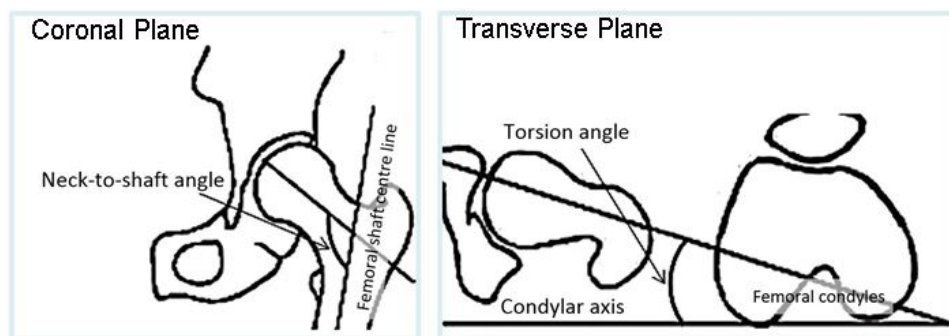


Figure 1.7: Left: left hip, coronal, femoral neck-to-shaft angle, measured between femoral shaft and femoral neck centre lines. Right: right hip, transverse, femoral neck torsion angle, measured between the condylar axis and femoral neck centre line.

Figure adapted from Saikia (2008).

Hip Joint Pathologies and Diseases

It has been mentioned in the previous sub-sections that the functionality of the anatomical structures is valid for non-pathological joint. However, due to the trauma or disease the functionality of the hip joint can be compromised, and lead to pain and loss of mobility. Within the scope of this project only several diseases affecting hip joint will be covered including osteoarthritis, osteonecrosis, dysplasia and osteoporosis as these are common reasons for THR (Crawford and Murray, 1997; Callaghan et al., 2007a).

Hip dysplasia is characterised by femoral head not being fully covered by the acetabulum, leading to joint subluxation, or in worst case dislocation. This disease can be classified both as congenital, present at birth, and developmental, developed during early stages of life. Dysplasia is characterised by under-developed or narrow acetabulum or inadequate femoral neck to shaft ratio. In the case of full dislocation a cavity, false acetabulum, to accommodate femoral head can be formed on the pelvic side. Apart from compromised functionality and pain, untreated hip joint affected by dysplasia commonly is diagnosed with secondary degenerative joint disease, or osteoarthritis (Callaghan et al., 2007a).

According to Callaghan et al. (2007a) approximately 2% of population suffers from painful osteoarthritis in one or multiple joints. Factors influencing the risk of osteoarthritis development include age, gender and genetics, as well as biomechanical factors such as abnormal mechanical stress and sub-optimal joint loading conditions. Osteoarthritis is commonly associated with joint pain and stiffness both during and after activity. Structurally, osteoarthritis involves change in cartilage thickness, loss of cartilage extracellular matrix components, formation of bony outgrowths and thickening of the articular capsule (Callaghan et al., 2007a).

Less common disease affecting performance of the hip joint is osteonecrosis of femoral head, or avascular necrosis, which according to Callaghan et al. (2007a) in some cases leads to osteoarthritis. Osteonecrosis is provoked by death of osteocytes, which is thought to be a result of loss or change in blood circulation

to the bone. In some cases femoral head osteonecrosis can be provoked by structural damage such as dislocation or fracture limiting vascular supply to the tissue. Osteonecrosis can also be induced by dysbarism, corticosteroids and alcohol intake (Callaghan et al., 2007a).

Avascular necrosis can be mistaken with some forms of osteoporosis (Balakrishnan et al., 2003). However, in contrast to avascular necrosis, osteoporotic joint is a metabolic disease induced by disturbance in normal bone remodelling processes. Osteoporosis involves loss in bone mass and can be developing undiagnosed until a fracture occurs. The disease can be diagnosed as type I, postmenopausal osteoporosis, or type II, senile osteoporosis, both types mostly occur in elderly individuals (Callaghan et al., 2007a).

1.4 Aspects of total hip arthroplasty

The hip joint diseases can be treated by non-invasive, minimally invasive or invasive treatments. Total hip arthroplasty, to total hip replacement (THR), is a frequently used treatment for painful and degenerated hip joint, when less invasive treatments fail. In the UK, 88.8% of THRs are proposed to patients suffering from osteoarthritis (OA) (National Joint Registry UK, 2018). According to Jain and Whitwell (2016) total hip replacement surgery is more uncommon for femoral neck fractures and in UK is a primary reason for 3.9% of THR. Across the western population, primary reason for THR is osteoarthritis, 69% and trauma 13% . However, conditions mentioned in section 1.3.1 of this chapter, also serve as primary causes for THR, and in other world regions might be more predominant causes for THR (Kumar et al., 2019).

Total hip replacement surgery requires full substitution of a hip joint, including acetabulum, femoral head and femoral neck. Typical THR design consists of an acetabular component and a femoral component as shown in Figure 1.8. The acetabular component either consists of the single liner which is cemented into an acetabulum, or is modular, and consists of outer shell press-fitted or cemented into the acetabulum, and inner liner (Figure 1.8). Femoral components in early designs are mono-block structures and are modular in modern designs, with the head being removable from the stem's neck, seen in Figure 1.8 (Buechel and Pappas, 2011).

Modular THR design type allows for variability in materials between bearing and non-bearing components of the total hip replacement acetabular and femoral parts. The modularity of modern THRs is advantageous during revision surgeries, allowing for bone preservation when only bearing components are to be replaced. For acetabular component modularity prevents of backside damage of the cup liner by providing backing in form of cup shell. For femoral component modularity allows for the use of materials such as ceramics and metal weight as bearing surfaces, which allow for reduction in friction coefficient and transmission of torques to fixation components. On the other hand, for the femoral stem tougher materials like titanium alloys and cobalt chrome are preferred, which provide

fracture resistance (Callaghan et al., 2007a; Berry, 2014).

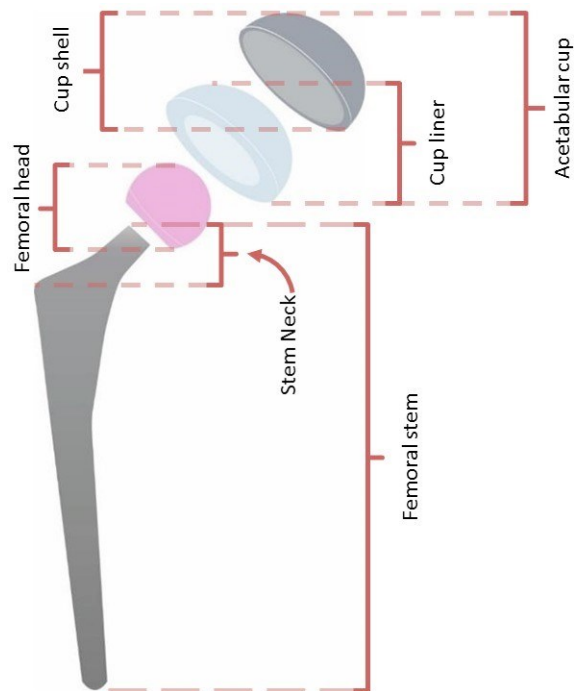


Figure 1.8: Modern modular total hip replacement. This design features acetabular shell and liner, femoral head and stem

According to the National Joint Registry UK (2018) in the United Kingdom, there are three types of fixation which are cemented, uncemented and hybrid. Cemented implants provide good stability straight after surgery, while uncemented have a porous surface to allow bone ingrowth. Bone ingrowth allows better long-term stability if fixation occurs and is preferable in younger patients. In some cases the uncemented implant, is press-fitted into the bony structure allowing for fixation through mechanically induced tissue bonding (Abdulkarim et al., 2013). The hybrid fixation is a combination between the later two. This design allows primary fixation and leaves a lot of space for future bone ingrowth (Baleani et al., 2000). In fact according to National Joint Registry UK (2018) in recent years hybrid fixation prosthesis became more prevalent and were used for 20.2% of UK THR patients.

There are four common articulation types used in THR, which are metal-on-polyethylene (MoP) and ceramic-on-polyethylene (CoP), metal-on-metal (MoM) and ceramic-on-ceramic (CoC) (National Joint Registry UK, 2018). According to

National Joint Registry UK (2018) the all cemented metal-on-polyethylene is most common bearing combination for primary THR, accounting for 26.9% of all primary THR procedures performed in the UK.

In early generations of MoP THR, ultra-high molecular weight polyethylene (UHMWPE) gamma-sterilised was used, which would articulate against cobalt chrome. However, the gamma radiation in air was found to increase the oxidation of UHMWPE with following reduction in mechanical properties. In retrieval and radiological studies, UHMWPE was proved to have poor wear properties. The wear debris produced from UHMWPE was noticed to be biologically active and provoke osteolysis, or bone resorption around the THR (Kurtz, 2009). In subsequent implant generations, mechanical and tribological properties of UHMWPE were enhanced by improving the manufacturing and sterilisation techniques. Gamma sterilisation environment was switched to inert gases or near vacuum and storage became vacuum-sealed. The cross-linking of UHMWPE molecules was also introduced to improve the wear resistance of the material (Buechel and Pappas, 2011). Cross-linking is also performed under gamma radiation, hence *in vivo*, surrounded by body fluids, oxidation takes place. Currently it is common to stabilise free radicals by anti-oxidant additives, such as Vitamin E, before irradiation (Kurtz, 2009; Buechel and Pappas, 2011).

The ceramic materials used in CoP or CoC bearing combinations have also gone through the several transformations over the past years. First generation ceramics consisted of mainly industrial grade aluminium oxide, which had unfavourable wear resistance and was prone to fracture, both due to large grain size. Over the years, the homogeneity and purity was improved leading to better performance clinically (Callaghan et al., 2007a). The fourth generation ceramic-on-ceramic components are alumina matrix composites (BIOLOX® Delta), which combine the strength, toughness and wear resistance of both alumina and zirconia oxides. According to recent study by Lim et al. (2018), after 6.5-year implantation period Delta THRs had high survivorship rate, 98.6% across 677 patients.

Now infrequently used, metal-on-metal THRs were proved to be biologically harmful due to the release of metal ions into the blood and surrounding tissues.

The design and materials for MoM were changed and improved through the years and were introduced again. Metal-on-metal bearings *in vitro* demonstrated to have superior tribological properties when compared to metal-on-polyethylene bearings in standard wear testing. However, metal-on-metal devices were shown to be very sensitive to component positioning. The occurrence of head-on-rim contact *in vivo* has caused increased wear rates of such material combination and led to high revision rates and currently are not recommended for implantation (0.1% UK) (Buechel and Pappas, 2011; National Joint Registry UK, 2018).

THR bearings are designed to be well-positioned, conforming and concentric with each other. The nominal radius of head and cup are the same, but some space, clearance, is allowed for the synovial fluid and motion. Conformity and concentricity ensure the central location and wide spread of contact area across the two bearing surfaces. Prior to the *in vivo* implantation preclinical, *in vitro*, test are performed (ISO 14242-1:2014) to make sure tribological characteristics of the prosthesis are acceptable (Buechel and Pappas, 2011). In recent years, a new testing standard ISO 14242-4:2018 has been introduced to address the wear and mechanical damage issue of mal-positioned implants.

There is a vast number of commercially available bearing combinations in terms of material and geometry design which are selected to suit the needs of patient. The generic THR has a hemispherical acetabular component and almost spherical femoral head. The geometry features such as fillets and chamfers are added to acetabular liners to reduce tensile stresses at the cup rim (Mak et al., 2011). The more complex designs of the acetabular cup are used for patient-specific approach. These include anatomical fit cups, which have both flares for minimisation of instability and material reduction for prevention of undesirable effects.

In addition, other joint arthroplasty procedures exist. These include hip-resurfacing (Callaghan et al., 2007b) targeted for younger patients, ensuring preservation of the bone. Another procedure is hemiarthroplasty or unipolar joint substitution which is a common treatment for fractures of femoral neck, where only one side of the joint is replaced by artificial implant (Callaghan et al., 2007b).

The surgical techniques used in THR can substantially affect the rehabilitation period and biomechanics of the hip joint. The surgical techniques for the THR are classified by location of the incision. There are six common surgical approaches used in THR, which are anterior, anterior-lateral, direct lateral, lateral transtrochanteric, posterior and minimally invasive approaches (Kelmanovich et al., 2003). Each approach has its own unique advantage, but naturally involve the disruption of soft-tissues surrounding the joint. For example the restoration of function after the THR was found to be faster for patients who undergone anterior THR compared to posterior approach as shown by Barrett et al. (2013). However, the posterior approach is simpler technically than other approaches, as reported by Kelmanovich et al. (2003). At the same time minimally invasive procedures, both posterior and anterior, ensure low blood loss, decreased procedure time, as well as faster patient recovery, compared to other approaches (Kelmanovich et al., 2003).

1.4.1 Contact mechanics principles affecting total hip replacement bearing performance

Contact mechanics is a crucial aspect to consider in total hip replacement bearing design and pre-clinical testing. The contact between two bearings can be subdivided into modes where contact is non-frictional and frictional. The non-frictional contact is associated with normal stresses between two surfaces such as tension and compression and no sliding between two surfaces. In contrast, frictional contact is associated with both normal and tangential stresses, as well as relative motion between two surfaces (Fischer-Cripps et al., 2000).

The pressure can be defined by normal force acting to the surface of a body per unit area. In contact theory, the contact area is described by contact extent between two surfaces, and contact pressure is pattern of pressure within contact patch. However, definition of contact is complex combination of many factors. A widely used theoretical approximation of contact was proposed by Hertz (1896), Hertzian contact theory, which describes contact of two non-conformal surfaces. The solution was derived from theory of elasticity specifically for two contacting surfaces of infinite half-spaces having homogeneous material, elastic behaviour

and exhibiting small strains. According to these assumptions, the theory can be applied for derivation of contact pressures for parabolic shapes in contact with each other or flat surface. The Hertzian contact theory defines the contact radius as a function of applied normal load, dimensions of contacting objects and contact modulus as seen from the Equation 1.1. Here P is applied normal load, R is the effective radius of two surfaces, E^* is contact modulus which is a function of Poissons ratio and Young's modulus for each bearing material (Fischer-Cripps et al., 2000). The Hertzian contact theory is applicable for sphere-on-plane and sphere-on-sphere contact.

$$a = \left[\frac{3PR}{4E^*} \right]^{\frac{1}{3}} \quad (1.1)$$

The maximum pressure for that contact type can be found as a function of contact radius and applied force described in Equation 1.2, where P is the applied load and a is contact radius calculated in 1.1.

$$p_{max} = \frac{3P}{2\pi a^2} \quad (1.2)$$

The theory suggested by Hertz (1896) is not always valid, for example when objects in contact are conforming or when objects are of finite thickness. Based on the theory of elasticity, Bartel et al. (1985) derived a solution which improves the later theory by removing the restriction of contact area being small in relation to radii of the contacting objects. The solution takes into account the angle between axis of symmetry and radial displacement of the surface, adding complexity to the solution which has to be solved iteratively. In brief, the relationship between load, indentation and radial pressure can be described through Equation 1.3, where σ_r is the pressure for radial displacement, Δ is displacement of an indenting sphere with respect to concave surface and θ is the angle between axis of symmetry and

edge of contact radius.

$$P = \pi \int_0^{\theta_{max}} \sigma_r \Delta^2 \sin(2\theta) d\theta \quad (1.3)$$

Nevertheless, both of these theories do not include a chance of plastic deformation, provoked by high loads (Bhushan, 2000). Stress from surface contact is the highest below the surface of the object, hence it is below the surface where the plastic deformation originates. Moreover, within the object, the contact induces shear stresses which are normally higher towards the edge of the contact. The materials used for total hip replacement bearing can be both brittle such as ceramics and ductile such as polyethylene, hence behave differently under the load. The brittle materials do not exhibit substantial plastic behaviour and fail while deformation is elastic. In contrast, ductile materials experience plastic flow and exhibit a yield point after which the deformation becomes permanent, reaching plastic region. For both material types, fracture or mechanical failure, occurs as a results of crack propagation originating at stress concentration points, such as notches, micro-cracks, pores and impurities.

The plastic deformation is not the only concern in implant design. Creep and cyclic fatigue are shown to occur before the yield point within the elastic region, which can not be predicted by ultimate tensile, or compressive, strength testing (Ashby and Jones, 2012).

The second contact mode, including friction and sliding, can be described by tribology which is the study of wear, friction and lubrication of the interacting surfaces which are in relative motion to each other. The performance of an artificial hip joint depends on the tribological properties and behaviour between bearing surfaces. As relative motion still exists between the bone and the implant, and between the modular component parts, these are also the focus of tribological studies. The aspects described in this section are friction and wear, as they are the common focus of THR research studies.

There are several types of friction, but in this section mostly sliding friction will be

discussed as it is a type found between artificial hip bearings. It can be described as the force which opposes the relative motion between contacting unchangeable surfaces, and is dependent on the force applied to cause the motion and friction coefficient (Budinski, 2013). The basic mathematical formulation of friction is described by Equation 1.4, where μ_{fric} is friction coefficient and P is normal load.

$$F_{fric} = \mu_{fric}P \quad (1.4)$$

The coefficient of friction depends on multiple factors including surface geometry, as well as material characteristics. On the macroscopic level, the contact between the two bodies is achieved through the bonding of their asperities. In order to move two surfaces relative to each other, these bonds must be broken, or sheared, hence the friction is equal to the shear strength of the bonds. At the same time, the real contact area is also controlled by the indentation hardness of each surface material (Budinski, 2013). There are two components to sliding friction, static and kinetic, where the first type of friction, F_s , is the force required to start the macroscopic motion and second type, F_k , is the force required to maintain this motion. Thus, theoretically, the μ_s should be higher than μ_k . However, for real materials this is not always true, for example, plastic-to-plastic contact can result in lower μ_s than μ_k , as well as in some cases the μ_k never stabilises indicating the continuous surface change on a macroscopic level. This constant change might occur due to third bodies formed by wear process (Budinski, 2013). In this case, the friction is not actually measured between two surfaces but between two surfaces and formed bodies. The other phenomenon in friction behaviour is called “stick-slip”, when there is a constant average μ_k which oscillates harmonically, the squeaking (Affatato et al., 2009) between two unlubricated surfaces is one of those occasions (Budinski, 2013).

Two types of wear between the THR bearing surfaces have been identified, abrasion, and adhesion, as well as the fretting wear between head-neck junction, and implant and cement or bone interface. Adhesive wear includes bonding of the asperities of two opposing surfaces, on the atomic level of like-to-like materials, such as in hard-on-hard bearings. In metal-on-metal THR bearings, adhesion manifests itself by forming third bodies which either localise between

surfaces or distribute within the joint. Depending on the loading conditions, these particles might serve as a lubricant or in contrast increase wear. In metal-on-polyethylene bearings the manifestation of adhesion is different, causing polyethylene to deposit on the metal surface and form pits on the polyethylene surface due to material fracture (Budinski, 2013). Another wear process, abrasion, contributes to the softer surface damage by a hard surface, due to the combination of sharpness and hardness of rough surface geometry. Abrasion is characterised by the removal of softer material with formation of wear debris. In addition, as a counter action to wear, molecular chains of cross-linked UHMWPE, in MoP and CoP articulations, have a tendency to align along motion path and increase the wear resistance in this direction (Kurtz et al., 2009). This process is called strain hardening. However, in the orthogonal direction the wear resistance properties are reduced and if motion suddenly changes its course the material removal dramatically increases (Budinski, 2013; Di Puccio and Mattei, 2015)

In general terms, fretting wear is referred to material removal due to cyclic micro-motion between two surfaces, for example in the presence of vibration. In THR, fretting, for example at the head-neck taper junction, in most cases causes corrosion of metallic components, hence is called tribocorrosion (Gilbert et al., 1993; Swaminathan and Gilbert, 2012).

To lower the wear or in some cases totally eliminate it, the separation of interacting surfaces by the fluid is used. This is called lubrication and synovial fluid is the lubricant in the natural hip joint. The effectiveness of lubrication is directly dependent on the level of separation, thickness of lubricant film, between two mating surfaces. The higher the load applied to the lubricated bearing couple the higher is the friction between them (Equation 1.4). The higher the velocity and dynamic viscosity of lubricant during the sliding the lower is the friction coefficient. The lubrication regimes can be classified as boundary, mixed and hydrodynamic lubrication regimes. Boundary regime is commonly registered during high load and low speed periods. The regime is characterised by collision of asperities between two contacting surfaces. For hydrodynamic regime two surfaces must be fully separated by the fluid film, where the asperities of contacting surfaces do not interact with each other. Mixed regime depends on the

roughness of the surfaces, and is characterised by both presence of fluid film and interaction between asperities. For THR the lower the wear the better, hence the hydrodynamic regime is preferable (Budinski, 2013).

1.4.2 Standard pre-clinical testing

The long-established pre-clinical testing performed on total hip replacement bearings is standard *in vitro* wear simulation, which is based on either ISO 14242-1:2014 or adapted Paul's cycle gait kinetic and kinematic profiles (Barbour et al., 1999). The data which these profiles were based on is gait for healthy volunteers collected by Paul (1966). It is important to note that both profiles were generated with the aim of reproducing wear rates comparable to ones seen *in vivo* or *ex vivo*, and other parameters such as deformation, fracture or contact area location of bearing surfaces were not taken into account. The loads during normal walking, which were measured in three axial directions on the hip joint, were simplified to one vertical load as in Figure 1.9, that resembled the resultant of three forces in terms of magnitude. In terms of kinematics the profiles include flexion-extension, abduction-adduction and internal-external rotation of the femur, also collected by Paul (1966). For standard conditions the head and cup are assumed to be concentric. Even though the loads and motions for these profiles are approximated and simplified, they allow for the assessment of wear under standard conditions of various THR designs (ISO 14242:2014, (Dowson and Jobbins, 1988) (Figure 1.9)).

Wear is not the only factor, associated with bearing couples, which can contribute to the mechanical failure of artificial hips. Such occurrences as rim damage seen on the retrievals (Tower et al., 2007), or migration of the component *in vivo* post-operatively (Nevelos et al., 1999; Leslie et al., 2009) raised a question of improved THR testing. Currently, the tests involving separation of component centres (Williams et al., 2003), extreme component positioning (Al-Hajjar et al., 2013), and friction simulation (Brockett et al., 2007) are performed. Separation tests, involve the translation of one bearing component relative to another. In general, separation tests are designed to move the contact area closer to the rim to simulate edge contact mechanics. One of the methods to achieve the relative

motion between bearing centres is by applying small medial displacement to the cup during swing phase (Al-Hajjar et al., 2013). As was mentioned above the new testing protocol to mimic the component mismatch was recently introduced in ISO 14242-4:2018. These tests produced results similar to *in vivo* bearing damage patterns. However, the tests are still performed using standardised gait profiles, which do not represent in full the motions experienced *in vivo*. Dowson and Jobbins (1988) stated that the designed hip joint simulators are used to perform basic studies on THR performance. For these the healthy volunteer physiological data was used, as precise data for artificial hip did not exist. Currently, there is more available data on *in vivo* kinetic and kinematics of THR patients, including walking and daily activities, which potentially can be adopted for pre-clinical testing.

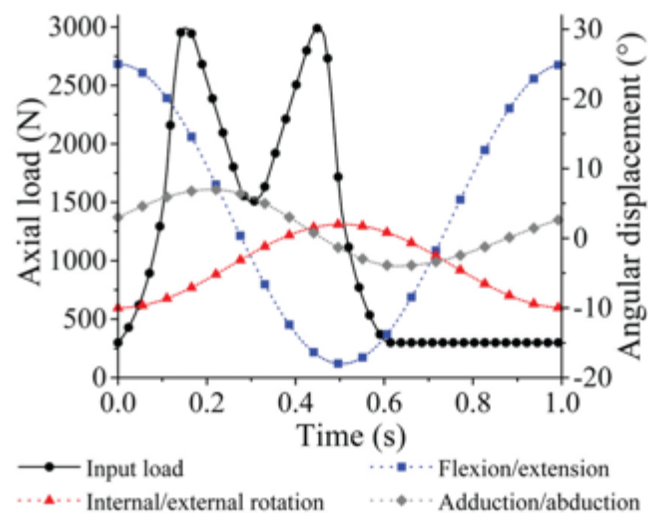


Figure 1.9: Example *in vitro* testing loading and motion profiles by (Ali et al., 2016) for THR *in vitro* wear testing. The curve represents resultant force derived from medial-lateral, anterior-posterior, vertical loads.

1.5 Dynamic *in vivo* alignment of total hip replacement

1.5.1 *In vivo* organisation of total hip replacement

Despite thoughtful design and pre-clinical tests THR failure still occurs. Mechanically driven failures are associated with deviations from the optimal organisation of artificial joint. Similarly to the natural hip joint, artificial joint components *in vivo* vary in terms of position depending on patients anatomy, but also on the surgical technique. The component selection and orientation, joint tissue laxity and patient specific biomechanics can provoke separation, impingement, subluxation or full dislocation. The occurrence of these deviations from ideal THR performance depends on multiple factors described further in this section and summarised in Figure 1.10. The gait and activity biomechanics will be described in further sections.

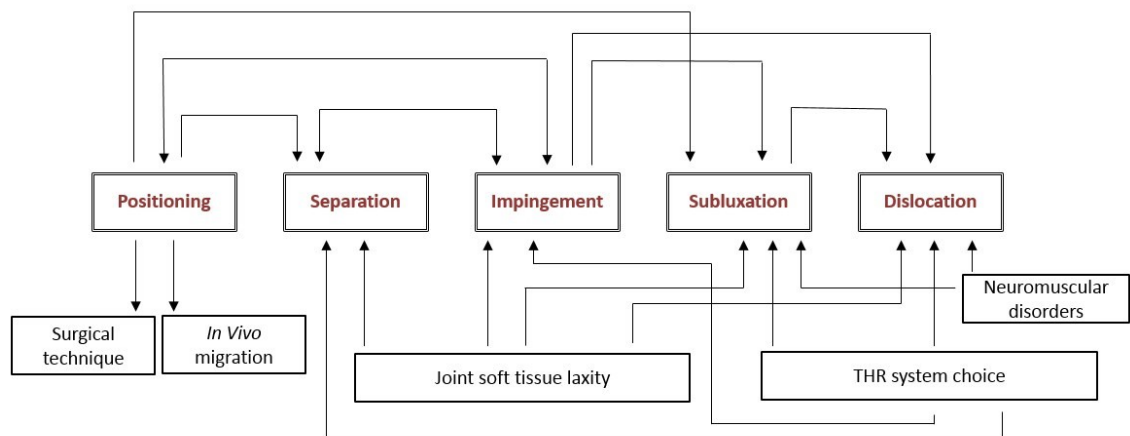


Figure 1.10: Factors influencing the risk of sub-optimal dynamic joint organisation occurrence, excluding gait biomechanics.

The position of the THR *in vivo*, within bone structures, is dictated by the surgical technique or post-surgical migration. The common angles considered during component positioning are acetabular inclination in coronal plane (Figure 1.11a) and version in transverse plane (Figure 1.11b). Similar to natural hip joint measurements, the inclination is the angle between the line drawn between superior and inferior edges of the cup and horizontal axis. Version angle is the angle between the line drawn between anterior and superior edges of the cup and

the vertical axis. Femoral version in transverse plane (Figure 1.11) is defined as the angle between femoral neck centre line and axis drawn at the base of two knee condyles. There are no strict guidelines for THR positioning in terms of cup inclination and version, as these parameters depend on patient's anatomy and are determined during preoperative planing. In study by Lewinnek et al. (1978) the cup orientation "safe zones" were identified through direct comparison between dislocation rates and cup positioning. Although, these "safe zones" are widely used, according to Seagrave et al. (2017) there is not enough evidence to support those orientation guides. In fact, in the recent study by McLawhorn et al. (2015) the large patient cohort of 553 THR patients was assessed in terms of dislocation and cup orientations. This study evaluated both Lewinnek "safe-zones" and target zones driven by patients anatomy. There was no relationship found between the dislocation incidence and both of the orientation zones, which suggests that there are other factors that influence the incidence of dislocation. The post-surgical migration might also affect cup orientation angles. Nevelos et al. (1999) observed an increase in inclination angle by up to 15° from the operative one, in post-surgical radiographs of THR patients with CoC bearing systems, suggesting the migration of the cup.

Other positioning considerations in total hip arthroplasty include femoral offset and stem subsidence. Femoral offset is identified in the coronal plane and is defined as the horizontal distance between the central axis of femoral shaft and centre of rotation of the femoral head in natural joint. If the stem is positioned correctly, the artificial head centre would match the native femoral head centre. Any deviation from this value is called offset deficiency and strongly depends on the component dimensions and geometry chosen for the surgery (O'Brien, 2014). The offset deficiency can cause soft tissue laxity, increasing the risk of separation, impingement, subluxation and dislocation as seen in Figure 1.10. Similar to the offset deficiency stem subsidence can result in joint soft tissue laxity. Stem subsidence rate is measured as a distance between the tip of the stem and fixed point in the femoral bone, superiorly. The measurement depends on the design of the prosthesis. In 1980 in *in vivo* study, Loudon and Charnley (1980) and Tangsataporn et al. (2015) compared conventional femoral stem design and one including a dorsal flange, both cemented. Using radiographic measurements

it was established that the excessive stem subsidence is higher in conventional designs, with average of 1.92mm, than in prosthesis with dorsal flange, with average subsidence of 0.53mm (Loudon and Charnley, 1980). In uncemented femoral components low osteointegration increases the risk of stem subsidence. The variation among patients with same prosthesis design can be significantly different. Pentlow and Heal (2012) found that for collarless stems the subsidence in trauma patients, ranges between 4 and 5 cm, which is much higher than in non-trauma patients, which ranges between 1 and 2 cm.

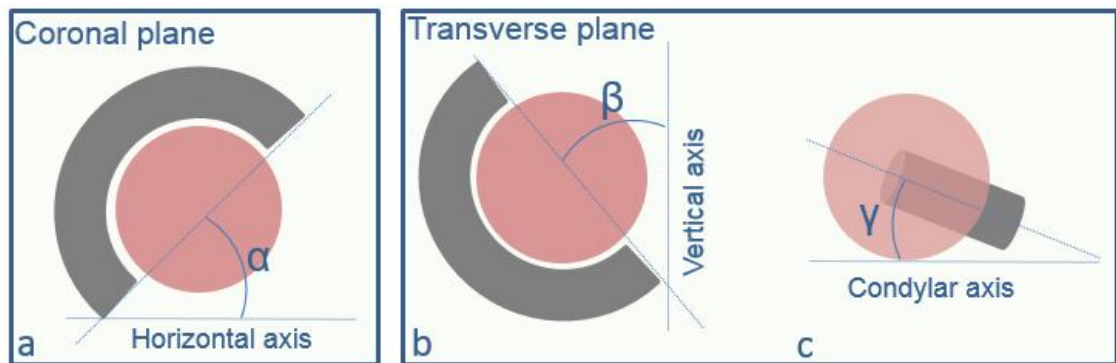


Figure 1.11: Left hip schematics of radiographic measurements a) cup inclination angle α measurement in coronal plane b) cup version angle β measurement in the transverse plane. In this particular case the angle is positive and is called anteversion, the deviation from the vertical axis to the right will produce negative angle – retroversion c) femoral neck version (torsion) angle γ measurement in the transverse plane.

Evidence of *in vivo* separation was first reported by Northcut et al. (1998) using mobile video-fluoroscopy. The medical images were taken for well-functioning THR patients during normal walking. According to the results, the medial-lateral separation of 0.5mm occurred between the head and cup of the implant. In following studies, the separation was observed during other daily activities (Komistek et al., 2002; Blumenfeld et al., 2011), which included treadmill walking pivoting side-to-side while standing, tying shoes, sitting down and standing up from the chair. As mentioned previously, the separation of THR bearings could be caused by stem subsidence and femoral offset deficiency, as the distance between bearing centres increases. In addition, Komistek et al. (2002) relates separation to surgical damage of the soft-tissue surrounding the joint, termed soft-tissue laxity.

Separation could also be a result of the femoral component leveraging against the acetabular cup caused by impingement. In the natural hip joint, impingement might occur between iliopsoas tendon and joint surfaces, between trochanters and acetabular structures, as well as femoral neck and acetabulum. These impingement types were also studied for THR patients. The risk of impingement for the patients is believed to be increased by the combination of factors which may include an excessive range of motion of the hip, positioning, geometry and design of THR (Marchetti et al., 2011). The iliopsoas tendon impingement most commonly occurs at the anterior site of acetabular rim. The recognised reason for this type of impingement is sub-optimal positioning or component design and sizing for a particular patient. Strangulation of the tendon, especially at high hip flexion, causes severe pain and often is treated by revision surgery (Dora et al., 2007). In the case of trochanteric impingement, there is no direct evidence in THR patients. Isaacson et al. (2015) presented several case reports for THR patients with severe pain and small horizontal distance, 10-18mm, between ilium and greater trochanter. After increasing the distance 21-30mm, by changing the bearing couple to one that was more geometrically suitable, the pain was eliminated. For patients with no evident reasons for pain trochanteric impingement was stated to be a possible cause (Isaacson et al., 2015). The most commonly discussed, in regards to THRs impingement type, is femoral-acetabular, which is defined by an impingement of the femoral neck and the acetabular cup. In some cases, it can be a reason for revision surgery, but according to Marchetti et al. (2011) *ex vivo* study, out of 416 retrieved components, with signs of neck-cup contact, only five were explanted due to symptomatic impingement. Thus impingement can take place unregistered but contribute to future THR failure.

In most severe cases, the excessive leverage due to impingement might either lead to subluxation or dislocation (Marchetti et al., 2011). Both subluxation and dislocation are the consequences of THR instability caused by one or a combination of various risk factors, such as neuromuscular disorders, muscle weakness either related to surgical intervention or to patients health in general, positioning of the implant and impingement (Werner and Brown, 2012). Clinically recognised subluxation is defined as the partial displacement of femoral head outside the acetabular cup, with further hip joint reduction. In general, this

type of joint instability is more likely to occur for primary THR than revision. In some cases, subluxation can be followed by dislocation, but more frequently, if registered, is corrected by adjustment to patient's daily activity range or revision surgery (McGrory et al., 2010).

Compared to subluxation, dislocation is more symptomatic and is the third most common reason for THR failure after aseptic loosening and pain (National Joint Registry UK, 2018). It is defined by complete displacement of the femoral head outside the acetabular cup. Dislocation of THR bearings commonly occurs between 3 to 12 month postoperatively, straight after the post-surgical rehabilitation period (Meek et al., 2008).

1.5.2 Head-to-rim contact and implant damage

Under idealised conditions THR bearings are well-positioned and concentric, so that the contact area location is central during the gait cycle and is away from the rim of the cup (Figure 1.12a). However, the joint is dynamic organisation variation *in vivo*, described in the previously, causes the cup and the head alignment to change during the gait cycle. This could potentially shift the contact area away from the centre of the cup closer to the rim. In this section the two consequences of dynamic malalignment, are discussed in terms of *in vivo* evidence, causes and consequences. The first consequence of the dynamic malalignment is called edge contact and is defined by the contact area falling onto the rim of the cup due to THR component orientation and contact force magnitude and direction, when bearing centres remain concentric (Figure 1.12b). In this scenario, the separation between the bearing centres is negligible, and remains less than the radial clearance. In contrast to edge contact, edge loading (Figure 1.12c) is present when the rim of the cup comes in contact with femoral head due to translation of the cup centre relatively to femoral head centre. In this case, the contact area is narrow line-like and separation exceeds clearance value in one or multiple directions.

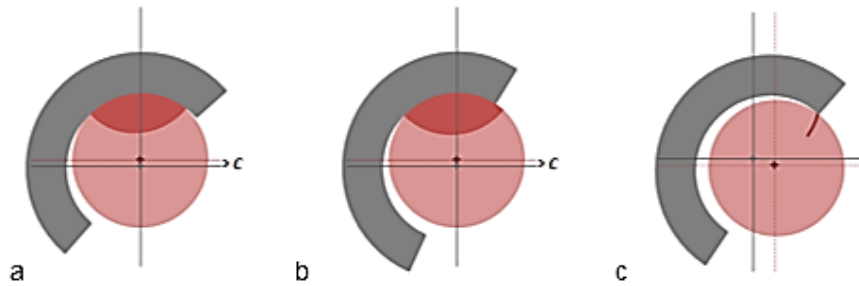


Figure 1.12: Left hip coronal plane, possible modes of dynamic alignment of THR *in vivo*. *c* denotes radial clearance. a) Ideal conditions, when the cup and head are well-positioned and concentric; the contact area (in red) falls between head and cup, the separation between centres is negligible - clearance. b) Edge contact, when the cup's and the head's position deviates from ideal and theoretical contact area shifts partially outside of the cup; head and cup remain concentric and separation between centres is negligible - clearance. c) Edge loading, when the cup's centre translates away from head's centre, and the stripe-like contact area falls between the head and cup rim only. The separation between head and cup centres is significant – higher than clearance.

Metal-on-polyethylene and ceramic-on-polyethylene

In relation to MoP and CoP bearings, information on a head-on-rim contact *in vivo* is limited. In a retrieval study by Tower et al. (2007) focusing on large diameter cross-linked UHMWPE liners, substantial fatigue damage in the form of liner rim cracking was observed in the four available explants.

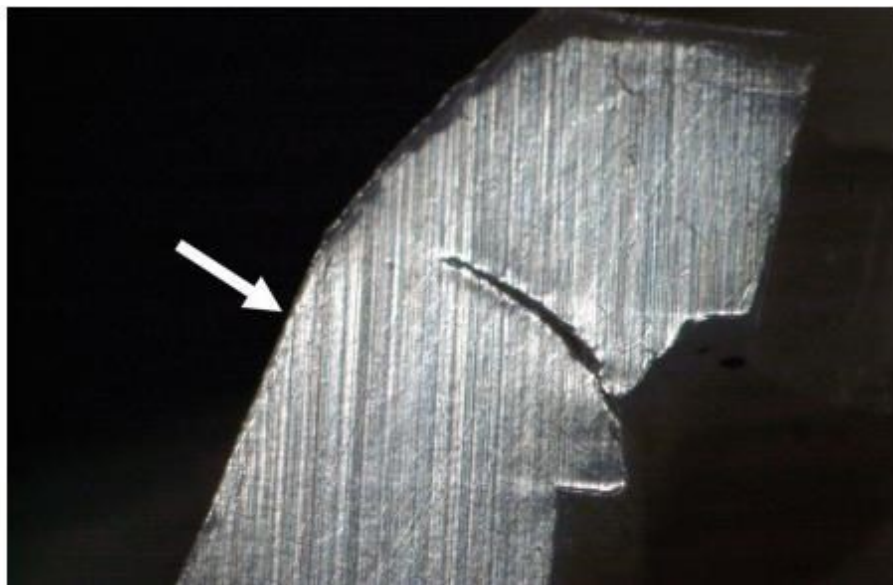


Figure 1.13: The figure shows the cracked rim cross-section of cross-linked polyethylene THR liner. White arrow shows the direction of loading on the rim (Tower et al., 2007).

Figure 1.13 demonstrates typical fracture type identified in the study. The crack was formed superiorly, in relation to cup position *in vivo*, and originated at the outer side of the rim above shell locking ridge. The white arrow, in Figure 1.13, symbolises the approximate direction of the contact force, which most likely defined the location of contact area near the rim, hence resulted in edge contact. Here the major contributing factor supposedly was the increased cup inclination angle of more than 60° , observed radiographically in all four THR specimens. The dramatic rim damage could also be attributed to a fairly low thickness of the liner, which in combination with edge contact could have resulted in crack initiation and propagation. In contrast to non-cross-linked UHMWPE, these liners did not experience any considerable degradation or oxidation, and the wear rates were reported as moderate. For some patients, the dissociation of the MoP liners has been reported due to the locking mechanism failure, which results in the femoral head articulating against the metal shell. Yun et al. (2016) reported that particular designs of the acetabular cup locking mechanism between liner and shell are not resilient enough to *in vivo* conditions. The reasons for locking mechanism damage are not clear, but liner dissociations have been associated with sub-optimal cup orientation, which as mentioned previously contribute to rim loading either in form of impingement, edge loading or edge contact (Gray et al., 2012). Another possible cause of the rim cracking could have been edge loading rather than edge contact, as patients in the study by Tower et al. (2007) suffered from recurring dislocations and subluxations.

In a video-fluoroscopy study, Blumenfeld et al. (2011) found evidence of edge loading in well-functioning unilateral metal-on- cross-linked UHMWPE THRs'. The results of the study suggest that during daily activities the contact area shifts towards superior-lateral edge of the liner which is consistent with Tower et al. (2007) findings. The identifiable difference between two studies was that Tower et al. (2007) studied highly cross-linked UHMWPE and Blumenfeld et al. (2011) studied moderately cross-linked UHMWPE. The cup inclination angles in Blumenfeld et al. (2011) study were not reported. It might be speculated that the occurrence of both edge contact and edge loading in modern MoP and CoP may cause dramatic mechanical implant failure rather than increased wear volumes. An *in vitro* study by (Williams et al., 2003) showed lower wear under edge loading

compared to standard testing condition. This phenomenon was suggested to be caused by the improved lubrication under separation due to damping effect of lubricant film squeezing. However, the polyethylene wear *in vivo* was shown to increase with the increased inclination angles, over 45° , which can be provoked by both edge contact and edge loading, or other conditions (Tian et al., 2018).

In an 11-year THR follow-up study by Bobman et al. (2016), it was shown that the orientation of acetabular does not influence the overall patient-reported functional outcomes of metal-on-polyethylene or ceramic-on-polyethylene primary THRs. It was shown that the difference in patient-reported pain, function and joint stiffness between components inside and outside Lewinnek "safe zones" (Lewinnek et al., 1978) is not significant. However, authors stressed that this is true only if the combined cup and stem anteversion were within normal range, 0.5° - 47.5° , and hip joint was balanced (Bobman et al., 2016). In terms of rim loading, the results of this study could indicate that either the Lewinnek "safe zones" (Lewinnek et al., 1978) do not represent dynamic *in vivo* component orientation, or that the effects of edge contact in metal-on-polyethylene or ceramic-on-polyethylene can be undiagnosed for many years.

Metal-on-metal

The latest design iteration, of metal-on-metal hip resurfacing and total hip replacement implants were brought to the market as a solution for younger hip replacement patients. These implants were suggested to allow for wider range of motion, due to larger head diameter 38-45mm, and lower femoral head coverage, 156° - 165° . The MoM were proposed as a good alternative for MoP, as the wear rates under ISO 14242-1:2002 conditions were proved to be much lower (Mabilleau et al., 2008). Despite the outlined advantages of MoM hip replacements, the failure rates of some designs were high, inducing the adverse tissue reaction (National Joint Registry UK, 2018). The rim-loading is thought to play a major role in dramatic failure rates of MoM implants. In the MoM retrieval study, Morlock et al. (2008) identified signs of rim-loading in 54% implant pairs from total of 267 explants. The inclination angle was found to significantly affect the occurrence of rim wear. The *in vitro* study by Williams et al. (2008) showed that the increase of

inclination angle from 45° to 55° for MoM under concentric conditions increases wear substantially. In the same study, the shift of contact-wear patch towards the superior edge of the cup was observed, indicating edge contact. However, the rate of wear increase seen by Williams et al. (2008) is much lower than seen by Morlock et al. (2008). In the same study by Williams et al. (2008) the lateralisation of the cup from the concentric condition in combination with higher inclination angle proved to produce significantly higher wear than just changing the inclination angle. Hence, a possible reason for high rim wear *in vivo* could be edge loading. This is consistent with another *in vitro* study by Leslie et al. (2009), in which the 17-fold increase in wear rates was observed with increase in cup inclination angle (to 60°) and introduction of medial-lateral separation between bearing centres.

It was shown that in MoM, 21% to 46% of wear is down to corrosive wear, which manifests itself in terms of pitting and blistering of metal surface (Yan et al., 2006). The edge contact or edge loading mechanisms could potentially disrupt the oxidative film on the metal surface and provoke release of metal ions into the surrounding tissues, as well as induce corrosive wear of the implant. The ions provoke tissue inflammation, which leads to local necrosis, pain, lymphocytic infiltration and the occurrence of pseudotumors (Leslie et al., 2009). Another consequence of edge contact or edge loading is high-torque generated by the shift in lubrication regime and roughening of the surface. These torques can lead to both loosening of components and repeated fracture of oxide film within taper and shaft interface, resulting in additional metal ion release (Gilbert et al., 1993; Fisher, 2011).

Ceramic-on-ceramic

For CoC bearings there are two types of head-rim damage recognised which are stripe wear and severe wear near the edge of the cup (Nevelos et al., 1999). The stripe-wear on the head is commonly reported wear pattern and was seen in old and new generation of CoC bearings. This type of wear is associated with edge loading, as the wear patch is narrow and line-like (Nevelos et al., 1999). Stripe-wear was identified for both steep and well-positioned cups, which suggests

potential separation. Nevelos et al. (1999) found stripe-wear in most of retrieved BIOLOX® components, with the wear rates relatively low except for one cup. Esposito et al. (2012b) identified stripe wear on the BIOLOX® forte retrieved liners occurring as frequently as severe edge wear, and more often than no edge wear. Stripe-wear was previously identified to occur posteriorly and anterior-superiorly, with wear rates being higher anterior-superiorly. In addition, this study found that a combination of inclination and anteversion is influencing the severity of edge loading, rather than a single orientation angle. For the BIOLOX® Forte combination, Esposito et al. (2012b) identified that the increased wear occurred at 35° inclination and 15° anteversion, as well as for the 55° inclination and 25° anteversion. The insignificance of cup inclination, in terms of wear for BIOLOX® Delta, as a single factor was also proved by Al-Hajjar et al. (2013) *in vitro* study, where with the increase in cup inclination angle from 45° to 65°, no significant change in wear rate was observed. In terms of BIOLOX® Delta, there is only little information available on the retrievals, as usage of this material is relatively recent. In retrieval study by Esposito et al. (2012a) the BIOLOX® Delta was shown to be significantly more wear resistant than BIOLOX® Forte, 0.06mm³year⁻¹ and 0.96mm³year⁻¹ respectively. This relation was confirmed in *in vitro* studies, where the wear of BIOLOX® delta was found to be lower than BIOLOX® Forte under the same medial-lateral separation condition of 0.4mm to 0.5mm (Stewart et al., 2003; Al-Hajjar et al., 2013).

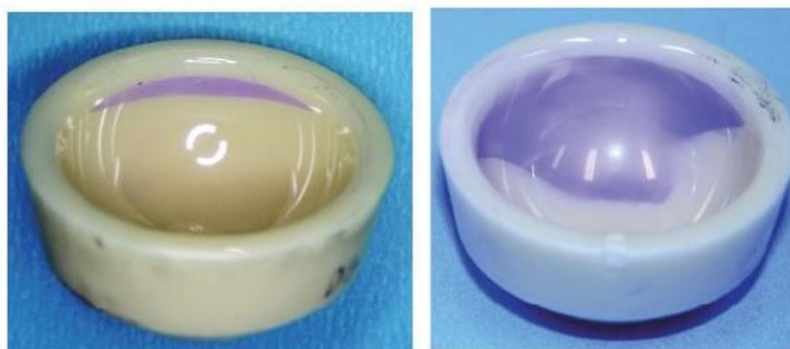


Figure 1.14: Left: BIOLOX® Forte with stripe wear indicated in purple, revised after 2.6 years *in vivo* due to pain. Right: BIOLOX® Forte liner with severe edge wear indicated in purple, revised after 1.7 years *in vivo* due to constant squeaking Esposito et al. (2012b).

The severe edge wear which is represented by wide-spread wear patch of irregular shape was reported for the early generation of CoC, BIOLOX®, by Nevelos et al. (1999). The similar contact patch was also reported by Esposito et al. (2012b) for BIOLOX®Forte components retrieved due to squeaking (Figure 1.14, right). Probably due to the enhancement of the material properties, the reported volumetric wear per year by Esposito et al. (2012b) of $0.299\text{mm}^3\text{year}^{-1}$ is much lower than reported by Nevelos et al. (1999) 9 to $110\text{mm}^3\text{year}^{-1}$. In addition, the increased wear might be associated with a larger bearing diameter in Nevelos et al. (1999) compared to Esposito et al. (2012b) study, 32 - 38mm and 28 - 32mm respectively. Al-Hajjar et al. (2013) also stated that *in vitro* 28mm diameter bearings wear less than 36mm diameter for edge loading conditions. In case of severe edge wear, it is arguable which dynamic alignment type is prevalent, as from patient to patient, the conditions of the joint varied in both studies Nevelos et al. (1999) and Esposito et al. (2012b). For example, in two patients in Nevelos et al. (1999) study, the only obvious deviation from the normal organisation was found to be increased cup inclination angle of 70° and 75° . This could be a case of edge contact where the contact area falls onto the rim of the cup. The analysis of the bearing couples also revealed an increase in roughness from $0.005\ \mu/\text{m}$ up to $0.4\ \mu/\text{m}$, most likely caused by lubrication regime shift from fluid to mixed or even boundary. In addition, it was suggested by Nevelos et al. (1999) that the worsening of lubrication regime could have been partially influenced by the poor condition of peri-prosthetic soft tissues of the patients. This suggests that joint laxity and further separation and edge loading could have taken place *in vivo*. For latest generation CoC bearings, for example BIOLOX®Delta, severe edge wear was not yet reported by retrieval studies.

It is important to note that increased wear of CoC bearings followed by distinct wear patches is more complex and depends on multiple factors such as the occurrence of impingement, dislocation, and subluxation. In Nevelos et al. (1999) study two severe cases were reported, accompanied by recurring dislocation and wear rate $262\ \text{mm}^3\text{year}^{-1}$, as well as loosening of the prosthesis and wear rate $120\text{mm}^3\text{year}^{-1}$. In study by Lusty et al. (2007) authors report on a wide edge loading stripe-wear (Figure 1.15), which visually resembles the severe edge wear reported by Esposito et al. (2012b), but has also signs of impingement in

terms of metal deposition on the surface. In ceramics-on-ceramics bearings, the wear debris, and hence potential for aseptic loosening has been showed to be minimum. However, the roughness, of bearings due to wear, either through edge contact or loading tends to increase, for example from $0.010\mu\text{m}$ to $0.016\mu\text{m}$ for BIOLOX®Delta (Al-Hajjar et al., 2013). This change in roughness values, in combination with mixed or boundary lubrication regime, might increase frictional torques and cause unwanted squeaking and possibly mechanical instability. Theoretically, edge loading can cause subluxation or dislocation as seen in Figure 1.15 (Lusty et al., 2007). It is hard to assess whether the edge loading or whether contact occurred first, or it is a consequence of recurring subluxation followed by dislocation. Furthermore, high torques may increase the fretting between the head taper and neck, and thus cause corrosion similar to one seen in MoM bearings (Gilbert et al., 1993; Al-Hajjar et al., 2013) but to a lesser extent (Kurtz et al., 2013).



Figure 1.15: BIOLOX®Forte liner with severe wear indicated in purple, and deposited titanium metal material, as a result of dislocation (Lusty et al., 2007)

1.6 Biomechanical motion analysis background and considerations

Gait is defined as the sequence of lower limb activities during bipedal locomotion, for example walking, running and stair climbing. In addition to gait, non-locomotor activities are also a subject of biomechanical motion studies, which can include sitting down, raising from the chair or even rowing. In line with widely used orthopaedic and patient satisfaction scoring, biomechanical motion analysis is used to evaluate the performance of lower limb joints. For example, in patients with hip joint pathologies, gait adaptation is a common sign of pain and discomfort. Activity is usually screened over one full cycle of motions also called stride. For the hip joint, walking is the most commonly investigated activity. In general, there are two major events which are stance, when a foot is in contact with the floor, and swing, when a foot is off the floor. Each event then can be described as a set of other minor events, discussed in detail in following sections (Nordin and Frankel, 2001). There are at least four common parameters assessed by biomechanical motion analysis, including temporal and spatial analysis, which is a study of characteristic aspects of gait such as stride length and walking speed. A second analysis type is kinematic which is a study of body movement and a third type is kinetic analysis which is a study of motion causes, such as forces and moments. Lastly, muscle activity analysis which is a study of muscle involvement in physical activity. Depending on the aim of the study, these analyses can provide data such as gait symmetry between two hips or patients motion similarity to healthy motion patterns (Jim, 2008; Ewen et al., 2012).

1.6.1 Reference systems used for gait analysis

For biomechanical measurements of musculoskeletal motion variable reference frames are used according to the purpose of the study. The spatial reference system is essential for biomechanical motion data processing, allowing for measurement of body position. Most common coordinate system type used for biomechanical activity assessment is Cartesian one, either two-dimensional or three-dimensional. The orientation and naming of the axes is arbitrary and does vary from study to study. One of the most widely used reference frames is

laboratory coordinate system, which is constant throughout the activity cycle. The a laboratory coordinate system is often referred to the global coordinate system (GCS) and its axes are usually parallel to the walls of the laboratory space. Apart from GCS, the local joint or segment coordinate systems are also used (Hamill and Knutzen, 2006).

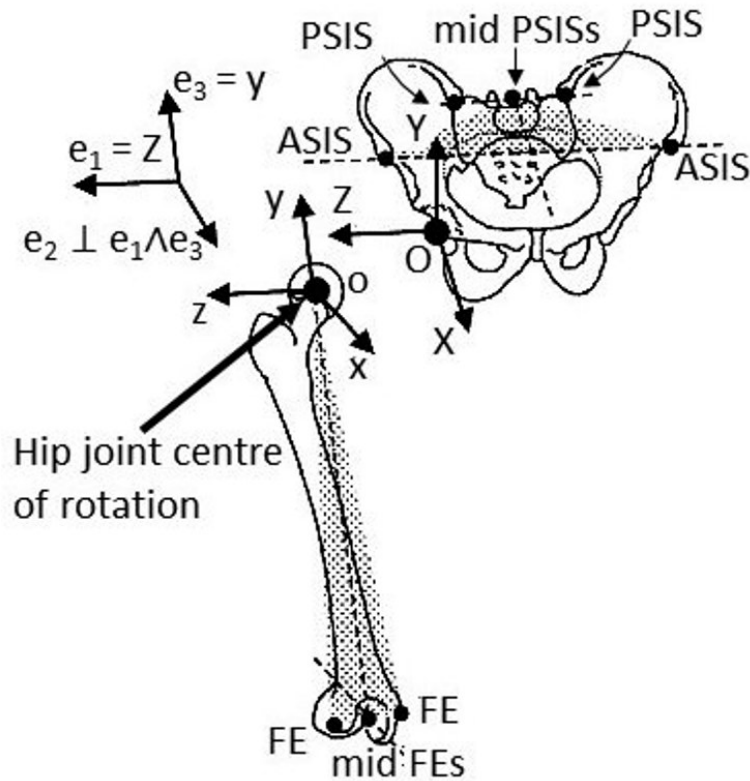


Figure 1.16: Joint coordinate system and segment coordinate systems at the hip joint defined by ISB (Wu et al., 2002), with respect to right leg. Figure adopted from Wu et al. (2002). PSIS - posterior superior iliac spine, ASIS - anterior superior iliac spine, FEs - femoral epicondyles.

The definition of joint coordinate system (JCS) and segment coordinate systems (SCS) heavily depends on the availability of information about bony landmarks. Even though the definition of the reference systems vary across the studies, International Society of Biomechanics (ISB) proposed a general JCS definition for reporting the results to wider research community. The reference frame definition is based on a proposal by Grood and Suntay (1983), which also included recommendations on SCS definition. Adapted by Wu et al. (2002), the JCS and SCS for the hip joint and surrounding structures is defined according to Figure

1.16, where hip JCS system is defined by axes $[\mathbf{e}_1 \mathbf{e}_2 \mathbf{e}_3]$.

According to Wu et al. (2002), the hip joint coordinate system is defined by the axes of both femoral and pelvic SCSs'. Here the femoral SCS has the origin at the centre of femoral head and is constructed such that the superior-inferior axis is joining midpoint between two femoral epicondyles (FEs) and origin. The medial-lateral axis is constructed such that it is perpendicular to the plane formed by the origin and FEs, pointing laterally. The anterior-posterior axis for the femoral SCS is perpendicular to both superior-inferior and medial-lateral axes of the femoral SCS, denoted in Figure 1.16 as $[\mathbf{x} \mathbf{y} \mathbf{z}]$ with origin \mathbf{o} . The pelvic SCS centre is coincident with right acetabulum centre, and the system is defined by ASIS and PSIS locations. The medial-lateral axis of the pelvic SCS is the connection between the pelvic centre and line passing through the origin, also parallel to the connecting line between two ASISs. The anterior-posterior axis is the line lying on the pelvic plane and perpendicular to medial-lateral axis. In this case pelvic plane is defined by the two ASISs and midpoint between two PSISs. The superior-inferior axis of the pelvic SCS constructed such that it is perpendicular to two other axes of the SCS, denoted in Figure 1.16 as $[\mathbf{X} \mathbf{Y} \mathbf{Z}]$ with origin \mathbf{O} . The hip JCS superior-inferior axis is parallel to superior-inferior axis of the pelvic SCS, JCS medial-lateral axis is parallel to medial-lateral axis of femoral SCS, and anterior-posterior axis is orthogonal to later two pointing anteriorly (Wu et al., 2002). The axes of hip JCS might not be orthogonal, which can be used in calculation of torques and power generated at the hip joint (Sado et al., 2017).

1.6.2 Kinematic analysis

In kinematic analysis the variations in hip joint angles are studied. These include flexion-extension, internal-external rotation, and abduction-adduction, which are typically observed in coronal, sagittal and transverse planes respectively (Figure 1.17). These angles can be recorded in GCS, JCS and SCS systems depending on the aim of the research.

In addition to movements performed around the femur, total hip joint motion includes movement of the pelvis. Pelvic motion can be measured as the angles

in three anatomical planes. Pelvic tilt is measured in the sagittal plane, pelvic obliquity measured in the coronal plane and pelvic rotations measured in the transverse plane as shown in Figure 1.18 (Jim, 2008).

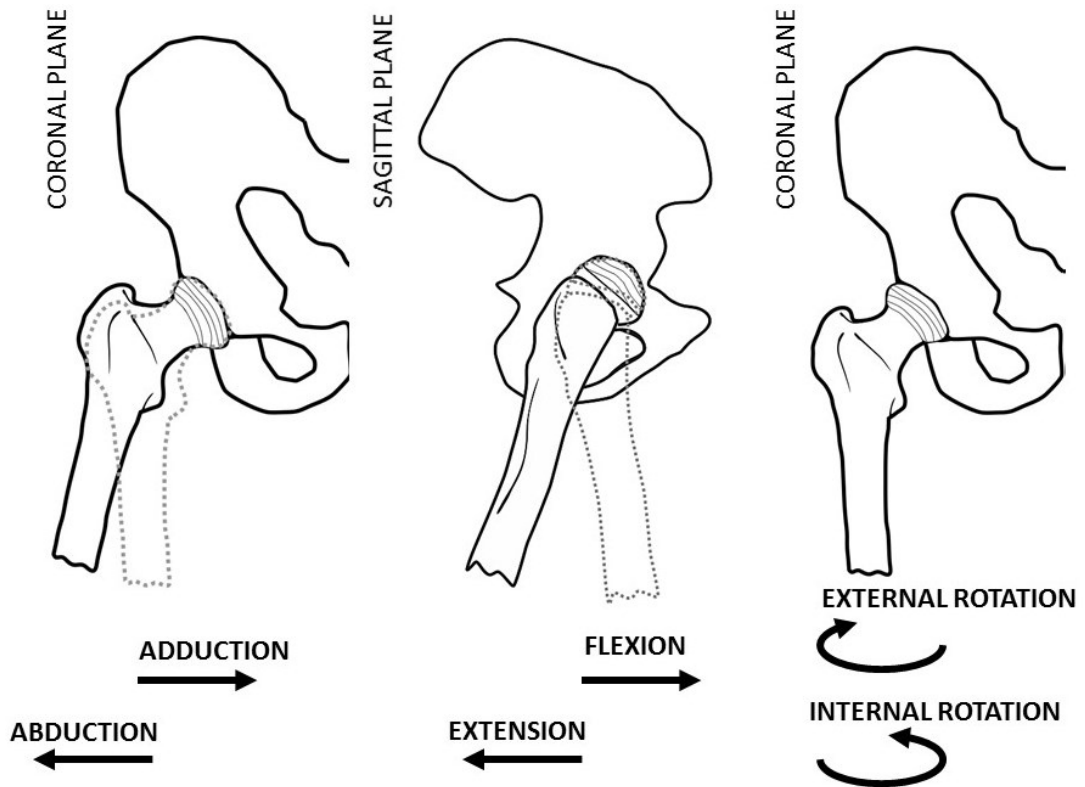


Figure 1.17: Possible movements of the femur at the hip in regard to the right side. Angles for specified movements are measured in following planes, starting from left, coronal, sagittal, transverse.

The simplest method for acquiring kinematic data is by the use of goniometers and potentiometers. Both devices can be attached to the patient's skin or specialised clothing. The devices record the change in voltage output, in response to linear or angular displacement. These devices are relatively inexpensive and allow for real-time data acquisition. They are more practical for the assessment of single hip joint motions in terms of flexion-extension and/or abduction-adduction due to their attachment technique (Jim, 2008). These devices are prone to skin movement errors, and can adjust motion patterns due to their weight (Smith, 2000).

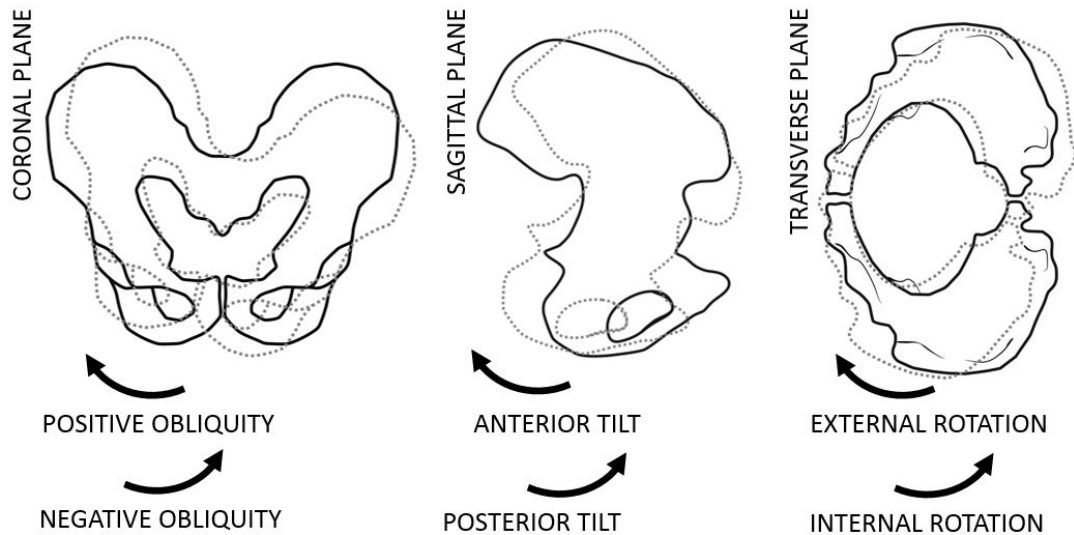


Figure 1.18: Possible rotations of the pelvis in coronal, sagittal and transverse planes. The motion in the coronal plane - obliquity, the motion in the sagittal plane - tilt, the motion in transverse plane - rotation around superior-inferior axis.

The most common and sophisticated method of measuring joint angles during activity requires movement analysis systems. These usually consist of marker sets, attached to patient's anatomical landmarks, which are tracked by the cameras (Cole et al., 1993). The anatomical landmarks provide the references for constructing limb segments. Cameras are usually positioned around the walkway 90° relative to each other. For two-dimensional analysis of hip flexion-extension, only one camera can be sufficient. For three-dimensional analysis, at least two are essential. However, when using small number of cameras, some markers might not be in a view at particular points during the activity. A higher number of cameras provide a more complete dataset and fewer approximations are required. Marker sets are either reflective, which are illuminated by infrared lights attached to the camera, or LED markers, which are light emitting themselves (Smith, 2000; Jim, 2008). Most commonly markers are attached laterally and medially around the joint at both ends of the femoral segment. The rotation angles can be measured between axes of hip JCS and GCS axes, or between SCS axes of pelvis and femur. The centre of the hip joint is identified either radiographically or as the percentage offset from the particular marker set according to predefined anatomical characteristics. Using joint and segment information the anatomical body models are constructed in specialised software, such as Visual3D (C-Motion 2016, Inc.) or AnyBody (AnyBody Technology A/S, 2017©). The translational and

rotational displacements of markers are recorded and applied to each joint, creating linear and angular motion data for coronal, sagittal and transverse planes (Robertson, 2009).

Another kinematic measurement approach is based on video-fluoroscopy, and has been used more extensively for the total knee replacements (Dennis et al., 2003; Tsai et al., 2015). This measurement method involves three-dimensional joint reconstruction in computer-aided design (CAD) software, using successive fluoroscopic images captured during the motion (Banks et al., 1997). The fluoroscopic data for THR's provides not only angles for motions but also relative positions of bearing components (Tsai et al., 2015). This allows identification of the gait abnormalities during joint articulation, such as head separation in THR (Komistek et al., 2002).

1.6.3 Kinetic analysis

In motion analysis, kinetic components such as forces and torques, or moments around the joint, are commonly identified with help of instrumented force platforms. The platforms record ground reaction forces and their point of application. There are two types of platforms, piezoelectric and strain gauge. Both platforms produce raw voltage data by measuring electric dipole moment or resistance, induced by deformation of piezoelectric crystals or strain gauge. Piezoelectric platforms generate data for three-dimensional forces, while strain gauge platforms generate data for both forces and moments around axes of force application. The moment in all three planes can be calculated using the force direction vectors origin generated by piezoelectric platform. The raw output data from the force platforms is transformed using inverse rigid body dynamics to acquire joint contact forces and moment around the joints. The technique allows for mathematical modelling of the mechanical behaviour of body segment under a set of assumptions, which can include segment mass and proportions (Jim, 2008).

For THR patients, there is a possibility, to record contact forces *in vivo* using instrumented hip implants. It usually consists of data recording and transmitting

module located in femoral component, articulating against traditional acetabular components (Bergmann et al., 2001). The device consists of the main femoral shaft, which accommodates strain gauges, a telemetry unit and a power coil. The strain gauge signals were transmitted by an antenna to the radio frequency receiver. Signal is then processed in measurement software and further converted to joint contact forces in three directions. Moments around other were easily calculated by using data for the neck-shaft interface and head centres (Bergmann et al., 2001; Westerhoff et al., 2009; Damm et al., 2013).

1.6.4 Temporal and spatial parameters

Useful information on gait patterns and possible pathologies can be provided by temporal and spatial parameters. These parameters can be assessed using marker systems. There is also another method to assess and record temporal and spatial parameters by using pressure mat systems, such as MatScan™ (Tekscan, Inc., US). They consist of printed pressure sensors that record pressure maps created by foot. This allows for estimation of foot positions during gait cycle, stride length, step frequency, speed, and cadence. In contrast to marker systems, pressure mat systems allow faster set up and can be easily transported (Jim, 2008).

1.6.5 Muscle activity

Muscle activity can be measured by electromyography (EMG) which involves placing electrodes on the skin surface, or directly into the muscle, and measuring electrical signal of muscle during activity. In simple terms increasing EMG signal represents increasing muscle activity and decreasing represents relaxation of the muscle. The most commonly used clinically, is the surface EMG (Leighton, 2006), but the thick layer of skin between electrode and muscle introduces more noise compared to intramuscular EMG. The invasive EMG measurement technique might be used during rehabilitation to assess the influence of procedures on the restoration of damaged muscles (Jim, 2008).

1.7 Natural hip joint gait biomechanics

In natural and healthy lower extremity joints, gait is considered to be symmetrical in terms of kinematics, kinetics, and muscle activation. The gait cycle for normal walking is described for one limb at a time. The stance phase lasts for about 60% of the cycle. The remaining 40% is occupied by swing phase. Figure 1.19 shows the sequence of gait events during the cycle (Nordin and Frankel, 2001). The initial foot contact, as seen in Figure 1.19, overlaps with terminal foot contact for opposite limb, hence the 0% of the cycle ([GC]) is called double limb support, or heel strike, and continues until toe-off of opposite foot (10% GC). Mid-stance coincides with the end of pre-swing for opposite limb and lasts from foot being fully flat on the ground until the point when contact with the ground transfers to the front part of the foot. Then limb enters the terminal stance phase, where the load is fully transferred to the toe area and enters the pre-swing phase. In the meantime opposite limb goes through the mid-swing and terminal swing. At the end of the cycle, both feet are in contact with the ground and are found in terminal double limb support stage. The kinematic and kinetic, muscle activity and temporal-spatial parameters are described in detail in following sections (Nordin and Frankel, 2001).

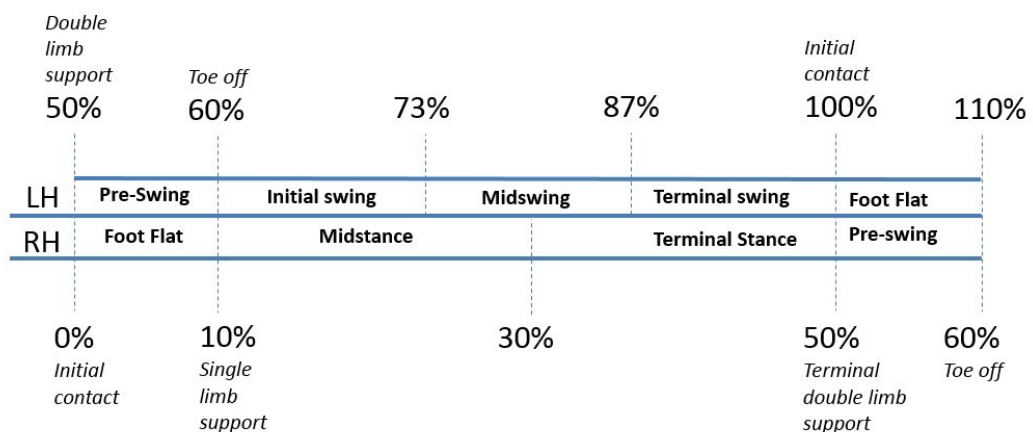


Figure 1.19: The schematic of the gait cycle, during normal walking. LH - left hip, RH - right hip.

1.7.1 Kinematic analysis

The data collected from kinematic analysis is sensitive to the measurement coordinate system chosen for the study (section 1.6). The raw data should be examined with care prior to comparison. The *trends* in kinematic gait profiles are easier to compare. For example, the symmetry of biomechanics between opposing hips. Aside from movement angles, multiple studies state the range of motion (ROM) for the movement of interest, which makes it more comparable with other studies. In this section, the gait trends and patterns in natural healthy and abnormal hip joints are discussed.

In terms of movements of a natural healthy hip joint, studies show that both left and right joint behave almost identically in terms of spatial-temporal parameters and low asymmetry in terms of motions in sagittal plane (Sutherland and Hagy, 1972; Kadaba et al., 1990; Forczek and Staszkiwicz, 2012). In an early biomechanics study by Kadaba et al. (1990) and external marker system was used, alongside mathematical algorithms, to effectively track joint and pelvic motions. The method is used currently (Miki et al., 2004; Bennett et al., 2008), and the study provides a baseline for recognising pathological kinematic gait patterns. Table 1.1 shows results for studies by Kadaba et al. (1990) and Bennett et al. (2008), which used the same measurement techniques for measuring hip and pelvic angles with almost 20 year between the studies and different age groups. Even though, the age groups are different and method improved with time the ROMs are similar between two studies.

Table 1.1: Full ROMs' for gait kinematic angles identified by two studies Kadaba et al. (1990) and Bennett et al. (2008). The ROM is from +ve and -ve

Study [sample size]	Kadaba et al. (1990) [40]	Bennett et al. (2008) [10]
Age [years]	18-40	> 54
Pelvic Tilt [°]	2.8	2.9
Pelvic Obliquity [°]	8.4	9.6
Pelvic Rotation [°]	9.2	11.4
Femoral Hip Flexion [°]	43.2	45.9
Femoral Hip Adduction [°]	11.6	12.7
Femoral Hip Rotation [°]	13	15.5

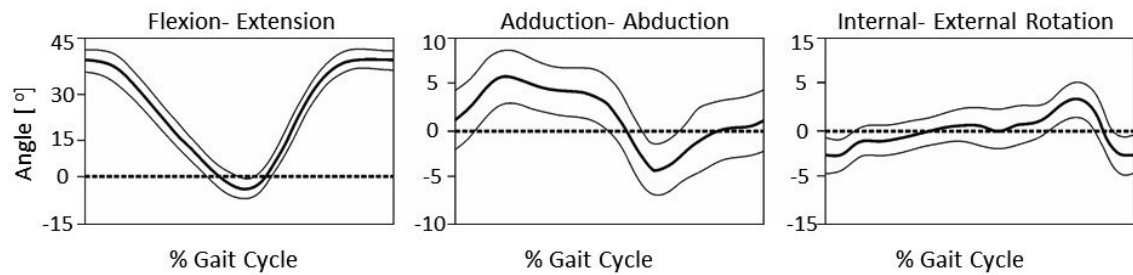


Figure 1.20: The motions of the natural hip joint, left: sagittal plane; centre: coronal plane; right: transverse plane. Vertical axis represents degrees, where +ve are flexion, adduction and internal rotation angles (Kadaba et al., 1990).

According to results published by Kadaba et al. (1990), the maximum values for flexion (Figure 1.20, left) for the healthy hip joint during level walking were reached from the end of mid-swing, 80% GC, up until single limb support point at 10% GC. The maximum extension is achieved at the terminal double limb support, 50% GC, just before the pre-swing. The ROM for flexion-extension is the highest ROM across all the hip joint movements, 43°. During gait the maximum adduction angle occurred at single limb support point, 10% GC, when the weight of the body shifts to one side. The adduction angle (Figure 1.20, centre) remains relatively high until terminal double limb support at 50% GC, where it starts to decrease towards neutral position angle. Near toe-off the weight shifts towards the opposite hip creating a negative adduction angle, or abduction. The abduction is at its highest during the initial swing at 60-73% GC and then gradually decreases towards the neutral position and switches to adduction. The adduction starts from the middle of mid-swing, 80% GC, and gradually rises towards single limb support point. In terms of hip internal-external rotation, the angles deviate away from the base line only slightly for most of the gait cycle (Figure 1.20, right). The maximum internal rotation occurs during mid-swing at 73-87% GC. The maximum external rotation lasts throughout terminal swing, up until initial contact of the foot with the floor at 100% GC.

Pelvic motions (Figure 1.21) contribute to an effective walking pattern for subjects with healthy hip joints. Pelvic tilt (Figure 1.21, left) ROM is reported to be 2° during normal walking and is not pronounced for a healthy individual. Pelvic obliquity (Figure 1.21, centre) follows the adduction pattern of healthy proximal femurs. On the side of standing limb, the pelvis lifts up in coronal plane to the maximum of single limb support point, 10% GC, while the opposite side

is in swing phase and drops, creating a increased obliquity angle (Figure 1.21, centre). The obliquity reverses just after toe-off and lasts through initial swing phase, 60-73% GC. Pelvic rotation (Figure 1.21, right) is opposite to the direction of femur internal-external rotation, with the internal pelvic rotation at maximum from initial ground contact, 0% GC, up until middle of the mid-stance at 30% GC (Kadaba et al., 1990). However, these values are averaged between all the participants. In reality, due to the anatomical differences in males and females, the pelvic obliquity in particular varies. Smith et al. (2002) showed that ROM of pelvic obliquity during the normal walking in females and males is significantly different ($p = 0.0024$), $9.4 \pm 3.5^\circ$ and $7.4 \pm 3.4^\circ$ respectively.

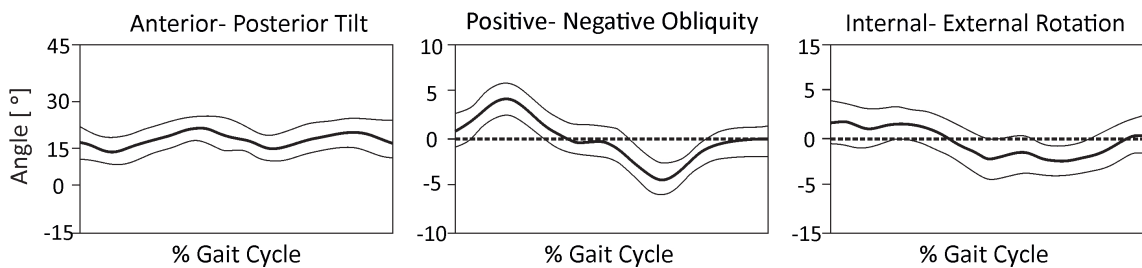


Figure 1.21: The motions of the pelvis, left: sagittal plane; centre: coronal plane; right: transverse plane. Vertical axis represents degrees (Kadaba et al., 1990).

In the diseased hip joint, the motion patterns are altered by the person usually in order to eliminate pain and these alterations can lead to secondary discomfort and diseases in other joints, as well as back pain (Leigh et al., 2016). In the study by Leigh et al. (2016), researchers examined gait patterns of patients with mild and moderate OA in comparison to healthy control volunteers. The kinematics of hip joint was different between the control group and OA patients, such that during mid-stance, 10-30% GC, the maximum adduction angle was significantly lower for OA group ($p = 0.003$), than for others. During terminal double limb support, 50% GC, maximum extension angles for control group were significantly higher than for OA group ($p = 0.005$). The low angle for hip extension were also determined by other studies in severe OA (Hurwitz et al., 1997), and hence it could be suggested that this gait pattern is typical for this disease. In contrast, at toe-off the maximum external rotation was significantly higher for OA group compared to healthy subjects ($p = 0.006$). In terms of pelvic motions,

during phases of single limb support, 10-50% GC, there was identified significant increases in all three pelvic movements ($p \leq 0.01$). The study by Leigh et al. (2016) showed no correlation between gait adaptation and pain. The change in pelvic biomechanics could be explained by changes in soft tissues surrounding the joint. The compensatory mechanism for motion adaptation is thought to be an increase in pelvic range of motions, which aid retaining stability during walking (Leigh et al., 2016).

1.7.2 Kinetic analysis

For healthy individual the resultant contact force magnitude during gait is dominated by the magnitude and direction of the vertical contact force component. The resultant force, in healthy hip joints forms a double peak profile (Figure 1.22) through the walking cycle. The peaks occur near the periods of single limb support (Paul, 1966).

According to Paul (1966), at the hip joint the weight bearing phase during walking starts from the initial floor contact, 0% GC, for healthy individual. The first peak is achieved at just before single limb support point, 10% GC, with the contact force approximately three-times higher than the person's body weight, which for a 65kg subject equates to 1.9kN. The resultant contact force decreases during mid-stance to one and a half-times higher than person's body weight, then increases again until the second force peak. The second peak occurs just before toe-off during pre-swing phase, 50-60% GC, and increases up to 3.8-times person's body weight, which equates to 2.5N for a 65kg individual. The horizontal forces contribute less to resultant force magnitude but define the direction of the resultant force vector. The anterior-posterior force at the first peak of vertical force is positive, or anterior, where maximum either occurs just before the first peak or at the initial contact point, 0% GC. At the stage of the resultant force's second peak, 50-60% GC, the anterior-posterior force reaches the same force magnitude as at the first peak but in the posterior direction. During mid-stance anterior-posterior force intersects the zero value. The medial-lateral force is mirroring the vertical, resultant, force, hence at first and second peaks the hip joint experiences contact force laterally. During the mid-stance, lateral contact

force decreases slightly. All the contact forces are close to zero during swing phase, with maximum resultant contact force just below one-times person's body weight (Paul, 1966). It is important to note that these values can vary according to the factors such as velocity and age, and data collection method (Nordin and Frankel, 2001).

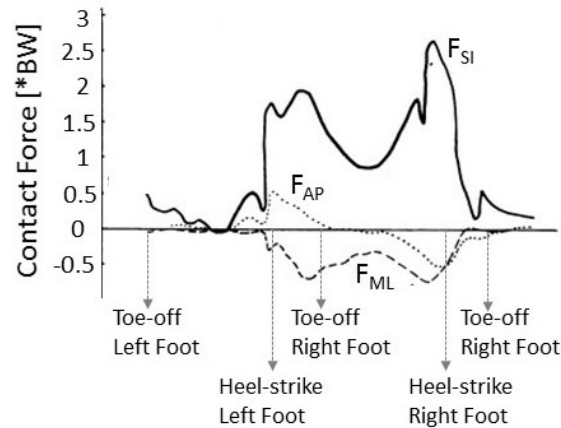


Figure 1.22: Figure adapted from Paul (1966), representing joint contact force at the right hip. F_{Si} for superior-inferior force, F_{ML} for medial-lateral force, F_{AP} for anterior-posterior force. The contact forces are averaged for healthy patients.

The hip joint forces can vary substantially due to disease and due to the BMI of an individual. For example, when comparing the function of healthy and high BMI children it was found that in terms of resultant force, the first peak force magnitude for children with high BMI is similar to healthy, but the second peak is significantly lower for children with high BMI compared to healthy ($p = 0.004$) (Lerner and Browning, 2016). For the OA patients, the resultant hip joint contact force was found to be significantly lower in OA hip compared to healthy hip ($p = 0.03$) for two peaks, but kept following the same pattern. In this case, the data suggests asymmetry between hips, hence the healthy hip becomes more weight bearing compared to healthy subject. In many cases the asymmetry leads to the development of OA in the opposite healthy hip (Aqil et al., 2016).

1.7.3 Temporal and spatial parameters

According to Kadaba et al. (1990) and Paoloni et al. (2012) the typical cadence, number of full cycles within a minute, for a healthy individual is approximately $113 \frac{\text{steps}}{\text{min}}$. However, for OA patients the cadence decreases to $95.5 \frac{\text{steps}}{\text{min}}$. Similar trends are observed with velocity and stride length between healthy and OA patients, $1.3 \frac{\text{m}}{\text{sec}}$ and $0.76 \frac{\text{m}}{\text{sec}}$, 1.3 m and 0.99 m respectively. The decrease in those values were attributed either to pain or gait adaptations (Kadaba et al., 1990; Paoloni et al., 2012).

1.8 Artificial hip joint gait biomechanics

There are two types of gait studies usually performed for THR, which vary by the choice of the control group. In studies by Bennett et al. (2008) and Nantel et al. (2009) the gait of THR patients was compared to the gait of healthy volunteers, as the aim of both studies was to identify the level of gait restoration after total hip replacement surgery. Foucher and Freels (2015), on the other hand, examined the level of gait improvement after THR, where the preoperative data was chosen as a control. Some studies consider successful gait restoration to have been achieved if biomechanical symmetry between two hips is achieved. In these studies, there is no control as such, but the gait data for operated hip is compared to the non-operated one (Hodge et al., 1991; Tsai et al., 2015). The number of subjects recruited, therefore the sample size, for a study, is another source of variation between studies. Obviously, the higher the sample size the more viable statistical analysis is likely to be. The number of recruits can vary from minimum of four (Loizeau et al., 1995), up to more than a hundred (Bennett et al., 2008). The reason for low numbers of recruits hugely depends on the selection criteria. For example, Bergmann et al. (2001) recruited patients with instrumented hip implant, which is an uncommon and customised type of THR. Therefore, the number of recruits in this study was very low compared to conventional hip gait analysis studies. Since THR surgery aims to restore normal function of the hip, many studies compare their results with the results for healthy individuals. In many studies it is observed that the gait of the patient after THR does not resemble that of a healthy individual (Perron et al., 2000; Beaulieu et al., 2010; Bennett et al., 2008).

1.8.1 Comparison of THR patient biomechanics to a healthy control group

Flexion-extension deviations

In the sagittal plane a significant reduction in ROM, moment around the joint and mechanical power was established by Perron et al. (2000) for women with a unilateral hip replacement implanted within 18 month prior to the gait study, aged 50-75. The peak extensor moment, at 50% GC, established for THR patients was

20% less in magnitude than for healthy subjects. The deviation corresponded to a significant reduction in flexion-extension angle ($p = 0.002$) (Perron et al., 2000). This finding is consistent with one identified by Bennett et al. (2008) for a large study group, including males and females aged 50 and higher. Kinematic data, at 10 years follow up, showed that flexion-extension motion was significantly reduced ($p < 0.05$) for the whole age range of THR patients, 33.82° , compared to healthy subjects of the same age, 45.9° (Bennett et al., 2008). A reduction in hip flexion-extension results in compromised step and stride length, as well as gait speed. This dramatic decrease is commonly attributed to the change in muscle activity levels (Perron et al., 2000; Nantel et al., 2009).

Increased average activation of the extensor muscles over the gait cycle in THR patients compared to healthy individuals was previously identified ($p < 0.001$) (Perron et al., 2000; Horstmann et al., 2013). There are two likely causes for muscle activation increase, preoperative gait adaptation and postoperative muscle weakness. Perron et al. (2000) hypothesises that the increased muscle activations are the consequence of passive resistance of hip flexors, which are opposing the extension. In this case, the resistance is developed by patient during OA due to pain or instability (Hurwitz et al., 1997), and persists after THR surgery. Horstmann et al. (2013) suggests that this increase is the compensation for post-operative muscle weakness, as non-restored muscles require higher activity to produce the same moment around the joint, in other words desirable extension. Both groups do not give any data supporting these theories, hence this information should be treated with care. A study by Madsen et al. (2004) could support Horstmann et al. (2013)'s hypothesis, they found that patients who underwent an anterior-lateral surgical approach, which affects the extensor muscles, have gait which has less resemblance to the healthy gait kinematics than those who underwent a posterior approach, which affects the rotator muscles. Nevertheless, the flexion-extension ROM in both groups, 34.0° for anterior-lateral and 39.4° for posterior approaches, were significantly lower than in the healthy subjects, 46.4° .

Abduction-adduction and internal-external rotation deviations

In contrast to flexion-extension, motions in the coronal and transverse planes during walking are mainly responsible for hip joint stability rather than forward progression. Horstmann et al. (2013) observed a significant increase in adductor muscle activation in THR patients ($p < 0.001$) compared to their control group. The preoperative and postoperative data for adductor muscle in this study does not differ, hence the activation could be both attributed to post-operative muscle weakness or gait adaptations due to pain. With regard to coronal plane motions, adduction-abduction, the only significant difference found by Perron et al. (2000) was in moment around the joint ($p = 0.0002$). The double-peak moment profile, at 10% GC and 50%-60% GC, in healthy subjects is distinct and pronounced, with the first peak being higher in magnitude compared to the second peak (Perron et al., 2000). For THR patients, the first peak was found to be significantly lower ($p = 0.0002$) and closer to the value of the second peak. In line with Perron et al. (2000)'s finding, the results of the large sample size study by Bennett et al. (2008) showed significant reduction in adduction-abduction ROM in THR patients, compared to healthy individuals ($p < 0.05$). For these patients the difference in internal-external rotation was found to be not significant, which is consistent with a more recent study by Lunn et al. (2019). For patients in the study by Perron et al. (2000) only a 66% decrease in moment in transverse plane in THR patients was found, compared to healthy subjects.

Pelvis and trunk deviations

The compensation for altered hip joint movement, may result in deviation of pelvic and trunk positions. Perron et al. (2000) reports, that during toe-off, 60% GC, pelvis tilts anteriorly around the medial-lateral axis, possibly to help with propagation of whole body and compensate for low extension moment around the hip joint. This pelvic angle is significantly higher ($p = 0.02$) for THR patients than for healthy individuals. However pelvic sagittal tilt ROMs were found to be 4° for THR patients and 7° for healthy subjects. In contrast, Bennett et al. (2008) found no significant differences in pelvic tilt or other pelvic motions between THR patients and healthy control group. The differences were observed

in medial-lateral trunk inclination towards the stance side ($p = 0.0003$) at initial foot contact stage, 10% GC, in THR female patients compared to healthy subjects. The authors speculate, that this excessive inclination observed for THR patients, is justified by body adaptation, aimed at reduction of activation demand for weak muscles and improvement of the stability in coronal plane (Perron et al., 2000). In male patients, no such differences were observed (Vogt et al., 2003), which might suggest that there is a possible difference in gait adaptations between females and males after THR.

Contact force deviations

Using ground reaction platform method Li et al. (2014) showed that ISO 14242-1:2014 profile used in wear simulation and healthy individual gait profiles are comparable. The double-peak profiles for ISO 14242-1:2014 and normal individuals involve a higher second peak compared to first peak, $3.1 \frac{N}{BW}$ versus $3.89 \frac{N}{BW}$. However, in THR patients, while first peak corresponds to the healthy group, the second peak is significantly lower, $2.1 \frac{N}{BW}$. The kinematic data presented by Li et al. (2014), corresponds to Bennett et al. (2008), decrease in ROM in flexion-extension, 41.2° , and adduction-abduction, 10.5° , compared to normal subjects, 48.6° and 15.7° respectively. Therefore, it could be speculated that the whole biomechanics of the gait is compromised by OA and THR surgery compared in relation to healthy subjects and in fact is not represented by the ISO 14242-1:2014 standard. In the recent study by De Pieri et al. (2019) it was also shown that contact forces during gait are also much lower compared to ISO 14242-1:2014. However, for patients with normal walking speeds higher than average the contact force profiles resembles ISO 14242-1:2014, which is not seen for patients with average or low walking speed. As in study by Li et al. (2014), the resultant contact force profiles for average and low walking speed displayed decreased second load peak in comparison with the first one. Possible explanation for the decreased contact force at the second peak, is the age difference between healthy subjects, 44.97 mean age, and THR group, 64.27 mean age. Interestingly, Anderson and Madigan (2013) observed the decrease in contact force at second peak for elderly non-THR subjects, 79.4 years, compared to younger non-THR subjects, 25 years, $5.29 \frac{N}{BW}$ and $4.28 \frac{N}{BW}$ respectively.

In addition to conventional gait platform studies, Bergmann et al. (2001) studied the contact forces of four patients, aged between 51 and 76 years, with unilateral instrumented THR. This study showed single peak contact force profiles in two patients during normal walking, with no distinct mid-stance region. However, the follow up time was 11-31 months after implantation, hence the performance might have not yet been stabilised due to muscle and soft tissue weakness after surgery. Interestingly, the data presented by Bergmann et al. (2001) and Li et al. (2014) shows a similar trend of first peak, or single peak in some cases, being higher than second peak. This suggests, that most probably the kinetics, same as kinematics of THR patients does not restore to a healthy gait biomechanics.

1.8.2 Comparison of operated hip biomechanics to opposite non-operated hip

Even though, the THR patient's gait does not restore to a healthy, the THR is still considered to be a successful surgery with positive outcomes. The main purpose of the surgery is to eliminate pain and discomfort caused by OA, or other diseases. As mentioned previously, the asymmetry in gait might be a sign of the pain and discomfort, hence comparing biomechanics parameters between two hips, usually operated and non-operated or in case of bilateral THR between two hip replacements, can serve as indicator of gait improvement (Bennett et al., 2008).

Flexion-extension deviations

For hip joint motions in the sagittal plane, most of the studies show that the biomechanics between two hips becomes symmetrical, or gets close to symmetry, gradually. Miki et al. (2004) studied the gait of 17 unilateral THR patients over a 12 month period after surgery and found significant improvements after THR. For example, prior to the surgery the difference between flexion-extension ROM for the affected and non-affected hip was significant ($p < 0.0001$), with average angles of 21.3° and 46.7° respectively. The highest difference between two hips was recorded at the end of the swing phase 90%-100% GC. During the one year period the flexion-extension ROM had become more symmetrical, but the difference was still significant ($p = 0.0002$). However, the flexion-extension moment around

the joint which was asymmetrical ($p = 0.004$) for both hips preoperatively during early stance phase, 0%- 10% GC, reached symmetry one month post-surgery respectively. This suggests that motions would possibly reach symmetry in a longer time period with an appropriate rehabilitation programme (Miki et al., 2004). The sudden improvement in gait symmetry after surgery, is a possible sign of pain reduction. However, the asymmetrical flexion-extension ROM suggests that gait compensatory mechanisms acquired preoperatively are still present.

In fact, Bennett et al. (2008), who studied gait of THR patients 10 years after surgery found no significant differences between operated and non-operated hips for flexion-extension ROM. Tsai et al. (2015) found that there was no significant differences between the two hips, even after a mean period of 8.3 months postoperatively. However, the study revealed significantly increased anterior-posterior translation between joint bearing surfaces in non-operated hips compared to operated hips ($p = 0.008$). Since all three studies focused on posterior surgical approach, the variation between Miki et al. (2004) and other two studies can be attributed to the primary reason for THR. Bennett et al. (2008) states clearly that the main reason for surgery was degenerative arthritis and Tsai et al. (2015) mentions only this disease in the article, which suggests that OA was primary cause, but it is not clearly stated. Furthermore, in both studies the contralateral hip was healthy. In contrast, Miki et al. (2004) who did not observe symmetry in flexion-extension ROM, used data from patients treated with THR as a result of femoral necrosis and hip dysplasia. In addition, the contralateral hip in all patients was symptomatic, two with femoral head necrosis and one affected by dysplasia. Such differences, between the studies, suggest that THR is not affecting all the patients in similar way and other factors such as, contralateral hip joint condition, and the reason for surgery should be considered.

In terms of temporal and spatial parameters, the statistical analysis of walking speed correlation to the flexion-extension ROM, showed that these parameters are directly correlated at one month for both hips (Miki et al., 2004). Difference in walking speed, cadence, step length and stride length between two hips were not significant in studies by Miki et al. (2004) and Bennett et al. (2008).

Abduction-adduction and Internal-external rotation deviations

The adduction-abduction moment around the joint was found to be asymmetrical, for the first peak period of the gait cycle (10%-20% GC), prior to the surgery and six months afterwards (Miki et al., 2004). Asymmetry, in terms of angular motions for both adduction-abduction and internal-external rotation, were not reported by Miki et al. (2004) and Bennett et al. (2008). However, Tsai et al. (2015) found significant differences in adduction angle during swing phase, 80%-100% GC, between two hips, with the operated hip showing increases in the motion angle. In addition, increased hip internal rotation was observed on the THR side. Authors speculate that the increase could be attributed to compensation due to abductor muscle weakness, as higher internal rotation would provoke abduction, hence lead to greater stability. Other possible explanation is that the measurements were performed while walking on the treadmill which could potentially alter gait patterns (Tsai et al., 2015).

Tsai et al. (2015) also reported significant asymmetry in medial-lateral and superior-inferior translation of the head centre relative to the cup. For both translation types the distance was significantly decreased on the THR side compared to the non-operated one, $p = 0.008$ and $p = 0.039$ respectively. Authors suppose that the improved conformity of THRs, compared to the natural hip, is the cause for lower femoral head translation. However, the conformity is not only achieved by the component design. The vertical translation could be correlated with the leg discrepancy (Kaufman et al., 1996) which was found to be significant between both hips ($p = 0.008$) and reach up to 8mm (Tsai et al., 2015). In fact, Li et al. (2015) found that the asymmetry between two hips is significantly higher in subjects with leg length discrepancy than in asymptomatic THR control group. The differences were found in terms of internal-external rotations during heel strike ($p = 0.0011$), in adduction-abduction and internal-external rotation during mid-stance, $p = 0.026$ and $p = 0.0001$ respectively, as well as at toe-off, $p = 0.029$ and 0.0019 respectively Li et al. (2015). Therefore, the tension of the muscles and soft tissues could also play a crucial role in maintaining low translations.

Pelvic movement deviations

Interestingly, the pelvic tilt and obliquity showed symmetry between the two hips in the study by Bennett et al. (2008) but not in the other two (Miki et al., 2004; Tsai et al., 2015). Miki et al. (2004) found that the pelvic obliquity was symmetrical one month after surgery and continued to be so. However, pelvic internal-external rotations became symmetrical between first and third month post-surgery, after which symmetry disappeared ($p = 0.004$). The most likely reason for asymmetry could be further degeneration of contralateral hip, as the external rotation on this side reached 7.6° towards twelve months post-operative period compared to 3° preoperatively. For the THR side the external rotation angle did not differ from three to twelve months, remaining 4° . In the study by Tsai et al. (2015) there was found a significant increase in anterior pelvic tilt during terminal stance, 32%-54% GC, of the operated side compared to non-operated side. In contrast, during swing phase and early stance, 65%-15% GC, the anterior pelvic tilt was significantly decreased compared to collateral hip. Change could be attributed to patients walking on the treadmill which might require greater stability.

Contact force deviations

In terms of contact forces, studies including instrument implants (Bergmann et al., 2001), could not provide data for symmetry. In force platform study, Li et al. (2014) showed that the resultant contact force between two hips was identical. Li et al. (2014) identified that the asymmetry in contact forces was present between two hips in patients with substantial leg lengthening of more than 10 mm after THR. In this case, the main difference is at the first peak, 20% GC, where contact force was more pronounced on a non-operated side. However, the differences between two hips were found not to be significant, $p > 0.05$. Symmetry in loading for the THR patients, also depends on the time since surgery and rehabilitation. In a study by Caplan et al. (2014), the authors found that for THR patients the non-operated leg was overloaded during a sit-stand task, which might be the habit developed preoperatively as a result of pain. Twelve months post-surgery, loading between operated and non-operated hips had reached symmetry.

1.9 Previous computational studies on total hip replacement biomechanics

A limiting factor in studying the performance of the total hip replacement *in vitro*, *in vivo* and *ex vivo* is inability to monitor many factors contributing to mechanical performance. Computational, or *in silico*, modelling can be used to estimate some of these factors. Examples of computational modelling include mechanical, electrical, biological systems and many more, which are set up in order to replicate existing or theoretical events. In general, the term computational modelling can be applicable to a mathematical representation of some physical phenomenon.

For investigation into THR performance, computational models to simulate contact mechanics between bearing surfaces were previously used (Jin et al., 1999; Hua et al., 2014; Hua et al., 2016). The advantages of these models over the *in vitro*, *in vivo* and *ex vivo* studies include possibility of estimation of the contact area, stress distributions and concentrations. Multiple experimental studies tried to identify the contact area between hip replacement bearing surfaces *in vitro* using staining ink or similar alternatives (Korhonen et al., 2005). However, there are two issues in using this method. Firstly, of all the ink alters the clearance between bearings and hence alters the result. Secondly, there are number of experimental limitations such as repeatability of the result, material expenses and time inefficiency. In addition, even if the contact areas are retrieved experimentally the contact pressures, highlighting the severity of the contact, are even more complicated to examine. Similar to the staining ink, sensor films (Anderson and Madigan, 2013), used in pressure recording, would most likely alter the clearance, slip away and get damaged at high loads, reducing accuracy of the measurement. In contrast computational analysis allows for estimation of contact area and contact pressures, without altering initial input parameters. Nevertheless, the computational model serves more as an addition to experimental tests, rather than as a separate tool. Computational model outputs, could contribute to investigation into failure of the implant. In addition, models can aid in examining the differences between device design and device features (Korhonen et al., 2005). Currently computational tests are commonly validated by *in vitro* studies, rather than *in vivo*, as the loading and constraints are less

complex in first than the second scenario. In a case where *in vitro* results match computational, the model is assumed to be reliable for this particular system. The long term goal of computational modelling, similar to *in vitro* studies, is to simulate and replicate complex *in vivo* events and have predictable models.

Table 1.2: The list of the computational studies on THR performance, including contact mechanics and tribology.

Author (year)	Clearance	Thickness	Backing	Design	Position	Edge contact	Edge loading	Biomechanics
Carter et al. (1982)			✓					
Bartel et al. (1985)	✓	✓	✓					
Jin et al. (1999)	✓	✓	✓					
Korhonen et al. (2005)	✓	✓		✓	✓			✓
Zeng et al. (2008)							✓	
Mak et al. (2011)				✓			✓	
Underwood et al. (2012)	✓			✓	✓	✓		
Hua et al. (2012)					✓	✓		
Hua et al. (2014)					✓		✓	
Hua et al. (2016)					✓	✓	✓	
Pierrepont et al. (2016b)					✓			✓
Peng et al. (2019)					✓			✓

1.9.1 Variation in computational methodologies

Computational models, performed for the analysis of THR bearing components' contact mechanics, can be divided into analytical models and finite element models. Analytical methods are based on the idea of obtaining a solution through logical reasoning and generating a continuous solution. For mechanical problems, physical quantities are identified through the mathematical solutions derived from laws of physics, exclusively for a specific situation (Bartel et al., 1985). For example, there are number of Equations describing behaviour of beams with different cross-sectional areas, which are used to predict the exact performance of a structure. However, the analytical solution involves a lot of simplifications in order to formulate and solve the problem. Thus, if the cross-sectional area of the beam becomes irregular throughout the length, it may not be feasible or even impossible to derive an analytical solution for the problem (Fagan, 1992). For more complex structures finite element analysis (FEA) is used, which is a type of numerical solution. It allows for the discretion of a complex solid into simple and

regular elements such as rectangles, triangles or pyramids. The simpler Equations for regular elements are assembled into larger numerical systems. Finite element analysis is an approximation which is aimed to approach the true analytical solution. In steady state problems, static, physical entity behaviour is assessed when system reaches equilibrium. In static structural analysis problems, the displacements for each element of the system are estimated in order to derive strains and stresses exhibited by the body. Dynamic finite element method, allows for the analysis of inertia force effects in addition to stress and strain. In general, static models are time independent and dynamic models are time dependant (Fagan, 1992). The main benefits of FEA over analytical solutions is the possibility to track the local effects simultaneously with gross behaviour (Zienkiewicz et al., 2005). However, analytical models can be faster at computing and can be adjusted through algorithms.

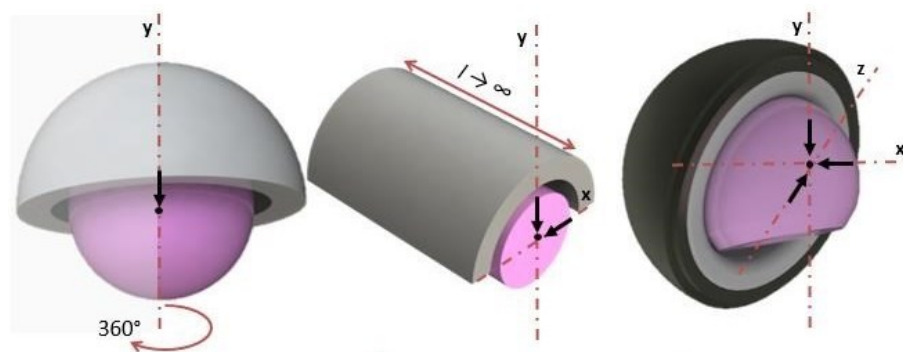


Figure 1.23: Illustration of different types finite element models: a) axisymmetric model, b) 2D model and c) 3D model in three-dimensional space. The x,y,z arrows represent contact loads which are reasonable or possible to apply in these models. In figure a) and b) the depth if component is assumed to be infinitely long.

Commonly model set-ups for THR contact mechanics studies are axisymmetric , two-dimensional and three-dimensional models shown in Figure 1.23 left, middle and right respectively. The best approximation of reality would be achieved through the three-dimensional models. However, the higher dimensionality the more degrees of freedom are included into the overall system of Equations to achieve the end solution (Fagan, 1992). To reduce the computational time required to analyse the behaviour of the three-dimensional system, real life problems can be simplified to axis-symmetric or two-dimensional problems.

Axisymmetric models, are commonly used to look at loading or displacement effects from one direction, along the chosen axis. The addition, of horizontal displacement would only be valid if modelling squeezing or stretching of a body from both sides. These types of models can provide information about contact radius, contact pressures and stress. Information on contact area and distributed stresses over the area could be available, but would be treated as symmetrical in the third dimension (Jin et al., 1999). The main assumption of two-dimensional models is that its shape only represents the true geometry of a THR in cross-section in chosen plane. If the two-dimensional model would be transferred into three-dimensional space the shape of the THR would be cylindrical and of infinitely long. The example of two-dimensional analytical solutions are Hertzian contact and elasticity solutions described in section 1.4.1 of this chapter. Three-dimensional models, in contrast to axis-symmetric and two-dimensional ones, allow for irregular distributions in contact area and contact pressure irregular distribution. In addition, *in vitro* tests can be replicated, hence potentially eliminating the costs of additional *in vitro* tests. Replicating *in vivo* conditions using computational tools proves to be a challenge due to complexity of human body performance and structure (Korhonen et al., 2005; Hua et al., 2014).

1.9.2 Previous studies on total hip replacement contact mechanics

Table 1.2 shows the focus of each study discussed below. In this sub-section three study themes are identified and discussed. The first theme is focused on the investigation into fundamental THR bearing performance under concentric conditions. The second addresses effects of edge contact and edge loading under standard ISO conditions. The last section focuses on the incorporation of patient-specific gait features including pelvic movement.

Concentric conditions and basic design variables

The first studies on contact mechanics in THR involved investigation of such factors as conformity, elastic modulus, thickness and addition of liner backing. These studies were conducted for metal-on-UHMWPE implants, almost exclusively, per-

haps due to wide use of these bearings. Bartel et al. (1985) studied the effect of clearance and cup thickness on the contact stresses exhibited by polyethylene cup during uniaxial loading. The model was set up as two-dimensional, and cup orientation was not assumed. This study showed that small increases in clearance resulted in large increases in contact stresses, for example a change in radial clearance, from 0 to 0.1mm resulted in a three-fold increase in contact stress. Another factor contributing to increased contact stress between bearings, was found to be cup thickness. For components surrounded by a metal shell, nearly conforming a thickness of liner less than 4mm resulted in significantly higher contact stresses of approximately 45MPa, compared to 20MPa for cup thickness above 4mm. Finally, the study found that introducing a metal shell into the component set up lowered the tensile stresses near the edge of the cup. Ten years later Jin et al. (1999) also found the same trend in terms of clearance and cup thickness for almost identical finite element model set up. In contrast to Bartel et al. (1985), who validated results using an analytical solution, these results were proven to be accurate by validation through analytical and experimental studies. In addition, Carter et al. (1982) prior to the previous findings, studied the effect of cement thickness and addition of a metal shell on the distribution of contact stresses by using a two-dimensional model. The cup was modelled intact with pelvic bone in coronal plane with cement layer between the two structures. Both analyses were conducted with or without metal shell. Similar to previously described studies, Carter et al. (1982) identified that increasing the polyethylene cup's stiffness, by adding the shell or increasing thickness, provided more effective stress distribution. Such additional support minimised the risk of cup loosening and migration. These studies provided a basic overview on contact mechanics in THR, with insufficient representation of the *in vivo* and *in vitro* conditions. However, the data provides more of a starting point for future studies rather than guidance for successful THR design. To investigate further and provide more sophisticated data for the THR manufacturers, as well as clinicians the previously described studies were taken further by the implementation of three-dimensional analytical and finite element models, in line with efficient model validation and verification.

In terms of conformity and clearance, a three-dimensional FEA study by Korhonen

et al. (2005) confirmed the trend for an increase in contact pressure with an increase in radial clearance and decrease in cup thickness. Compared to Bartel et al. (1985) and Jin et al. (1999) simulations, this study featured the real geometry of femoral head, acetabular liner and shell. The study was validated using experimental results for the same components under the same loading and positioning conditions.

Edge contact and edge loading

As the positioning of the components may provoke in an adverse conditions such as edge loading or edge contact, multiple FEA studies have been conducted to address this issue. Korhonen et al. (2005) found head-on-rim contact under high inclination angles, which were 60° and 80° clinically. Hua et al. (2012) observed a transfer of contact area centre closer to the cup rim, with an increase in cup inclination angle, but no significant contact pressure increase was noticed in this study with rim contact. This suggests, similar to previous findings that contact pressures depend hugely on the design of the cup. Korhonen et al. (2005) focused on other geometry variation in chamfered and non-chamfered cups. The results of the study suggested that the specific design features adjust the performance of THR bearings in relation to contact mechanics. For example, chamfered cups examined in this study exhibited high contact pressures near the edge under specific positioning conditions, when unchamfered cups did not show the increase (Korhonen et al., 2005). The addition of a chamfer did not necessarily result high contact stresses, in fact, most of the current THR designs have this feature. In a three-dimensional ceramic-on-ceramic study, Mak et al. (2011) established that the addition of a small chamfer is very effective in reducing tensile stresses at the rim, from 174MPa to 98MPa during edge contact conditions. Hua et al. (2012) analysed the Charnley hip system with smaller chamfer, hence not as compromising on bearing diameter. It is important to note, however, that for the aforementioned studies the huge limitations were uniaxial loading and concentric conditions.

The acetabular cup orientation and head coverage angle was also addressed by Underwood et al. (2012) after a world-wide increase in MoM THR revision

surgeries, which was linked to head-rim damage as mentioned in section 1.5. In contrast, to studies mentioned previously in this sub-section, Underwood et al. (2012) used an analytical method which allowed for measurement of contact area proximity to the rim of the cup in sagittal plane. One position of the contact force vector with magnitude of 3kN was used for this study. The contact area magnitude was approximated using Hertzian contact theory. The simplifications for the model allowed for fast processing of data for 122 patients in terms of cup inclination angle and head-coverage angle. The results of the study showed that for patients with edge worn retrieved cups the contact was closer to the rim, however this was not significant, than for patients with non-edge worn retrieved metal cups (Underwood et al., 2012).

As it was described in sections 1.5 and 1.8 of this chapter, the performance of the THR *in vivo* is far more complex than proposed in ISO 14242-1:2014, which was recently modified by ISO 14242-1:2018 to address some of the *in vivo* aspects. Many studies have been conducted in computational research, identical to adverse *in vitro* tests, specifically on medial-lateral separation. Both Hua et al. (2014) and Mak et al. (2011) looked at simulating *in vitro* tests, under separation conditions and uniaxial loading only for MoP and CoC respectively. The common finding of these studies was the increase in contact area shift towards the edge of the cup, which was consistent with *in vitro* studies, where the wear patch moved closer to the edge with increased medial-lateral separation of the cup. In study by Hua et al. (2014) the dramatic increase in contact pressures were found to occur as a combination of increased cup inclination and separation, under low separation conditions of 800µm in medial-lateral direction. Under high separation 1000-2000 µm, the effect of cup inclination was negligible. The results showed that the plastic strain in the liner near the edge increase significantly during high separation conditions compared to standard conditions. That could be linked to the rim cracking in retrieved THRs. Mak et al. (2011) observed increasing tensile stresses at the outer edge of the liner with increase in separation. As ceramics are much weaker in tension than in compression, this parameter is determinant for the material performance. Some of the designs in the study exhibited 469MPa tensile stress, which is close to the ceramic flexural strength. This increase can explain the occurrence of stripe wear, as a result of intergranular surface fracture,

which is consistent with an explant study by Zeng et al. (2008). The results of the study depend on the granular size of ceramics used as well as whole microstructure of the material. Thus, simulation of CoC is proved to be more complex and requires more material inputs than elastic and plastic properties.

Incidence of edge contact with activity variation

A step further towards simulating computationally *in vivo* conditions, rather than *in vitro* can be achieved through the application of loads and motions experienced by THR during gait or activity. One of the first studies to link patient functional activity biomechanics and edge contact was by Hua et al. (2016), in which the hip joint motion cycles of THR patients were analysed for MoP combination. The study was performed based on the *in vivo* motion data published by Bergmann et al. (2001). In contrast to previous studies, the direction of the force vector governed by axial, medial-lateral and posterior-anterior forces were included in FEA model. Here the effect of anteversion angles on the contact area was studied, in addition to inclination angles. The group found that for 36mm MoP THRs from six daily activities, only the ones where single limb support occurred resulting in edge contact. The increased cup inclination angle also increased a chance of edge contact. For example, during normal walking, both the contact pressures and plastic strain increased by 18% -26% and 234%-306% respectively, when the cup inclination angle changed from 55° to 75°. In addition, the duration of edge contact during the gait cycle was shown to be increasing with increasing inclination angle. On the other hand, anteversion angle for this bearing couple and activities were shown not to increase the risk of edge contact occurrence. The elevated plastic strain near the rim suggests that the edge contact can be regarded as a risk factor for cup fatigue damage, deformation and associated failures. Even though, the study shows the performance of THR in more clinically relevant conditions the limitations to this study pose the area for future studies. For example, the effect of gait profiles were assessed only for one design where the component size, thickness and feature geometry were very specific. The model, similarly to those in previous studies, does not include soft tissues surrounding the joints. In addition, the gait profiles studied here were the averages for set of patients, rather than patient specific (Hua et al., 2016). Therefore, this

study presents the baseline knowledge on the occurrence of edge contact *in vivo* and further in depth studies are required to establish “risk zones” for positioning, thickness and other THR relevant parameters.

In *in vitro* and *in silico* studies mentioned throughout this chapter the effect of pelvic motions on head rim damage was neglected. However, as mentioned in section 1.6 pelvic motions are substantial during gait, and even more so for THR patients. A step towards understanding the role of pelvic motions on the functional position of the acetabular cup and hence risk of head rim damage was done by Pierrepont et al. (2016b). The group developed an analytical computational tool, Optimized Positioning System™ (OPS™), which determines change in cup functional orientation during static standing, flexed seated and stepping up. Three patients were assessed in this study. The inputs to the tool were sagittal CT scans and joint reaction force directions for each static activity calculated externally. The outputs of the tool were contact patch paths and sagittal pelvic tilt angles. The results for three patients showed that those outputs are specific for each patient and previously defined "safe zones" by Lewinnek et al. (1978) do not reflect functional acetabular cup orientation.

Even though Pierrepont et al. (2016b) assessed pelvic orientation contribution to functional acetabular position, the study was limited to only assessing one pelvic angle and non-dynamic activities. The latest FEA study on the wear of MoP THR by Peng et al. (2019) incorporated kinematics for the hip joint of 48 THR patients, including pelvis and femur, into the model. The kinematics was extracted from video-fluoroscopy imaging. The group used contact forces from OrthoLoad database Bergmann (2008). No edge wear was reported in this study. The results, similarly to previous studies showed that for 36mm MoP patient-specific kinematics and joint forces significantly influenced the wear results (Peng et al., 2019).

1.10 Literature review summary

- Natural hip joint is a ball-and-socket synovial joint experiencing motions in all three anatomical planes. The healthy function of the hip joint depends

on the nutritional supply, muscle strength, exhibited loads and orientation of the bony structures forming the joint;

- In the event where the aforementioned anatomical and functional features are sub-optimal, pathologies and diseases of the hip joint can develop. The joint abnormalities might influence persons lifestyle by causing pain and limiting range of hip motion;
- Hip joint diseases include osteoarthritis, avascular necrosis and displasia. Common treatment for severe hip disease is total hip replacement surgery, where the native diseased joint is substituted by artificial components;
- The total hip replacement is considered a successful arthroplasty surgery, eliminating pain and restoring joint function, as reported by National Joint Registry UK (2018). However, failures still occur which in some cases cause dramatic consequences;
- Failure causes in total hip replacements range from increased material wear, sub-optimal component positioning, impingement, joint laxity and more. One of the known failure contributors is edge contact, which is characterised by contact between bearing surfaces of the implant to relocate fully or partially to the edge of the cup;
- Edge contact can provoke rim deformation, component cracking and line-shell dissociation. Edge contact can occur asymptotically. In addition, detection of edge contact on the retrievals is not always possible and can be confused with other damage mechanisms;
- Edge contact is believed to be caused by sub-optimal implant positioning, which can be influenced by surgical technique, anatomical consideration and patients activity biomechanics. Patient-specific joint biomechanics was proved to be changed post-surgery. The motions experienced around hip joint depend on pelvic and femoral dynamic orientation;
- The total hip replacement activity analysis can help to identify the gait characteristics developed due to age, life-style and BMI, which can be further used in pre-clinical device assessment. However, care should be

taken interpreting the data as it depends on the measurement reference system used;

- ISO 14242-4 hip joint contact force profile was originally simplification of the average gait profile. This allows for the tribological comparison between THR devices rather than to assess the patient-specific characteristics. Despite some modifications, the current ISO 14242-4:2018 contact force profile does not reflect patient specific gait characteristics;
- Computational modelling is time and resource efficient method of assessing total hip joint performance is computational modelling, which allows for variable inputs and parametric testing. To date, only few computational studies have addressed patient-specific hip joint motion biomechanics in relation to edge contact, mostly using the standardised gait cycle for pre-clinical testing.

Chapter 2

Development of the computational tool to determine the location of contact between total hip replacement bearings

This chapter describes the development of a bespoke analytical tool for assessment of the risk of edge contact from patient-specific and activity specific perspective. Broadly, this tool measures the proximity of the contact to the rim of the acetabular cup, hence is referred to as a proximity tool throughout this thesis.

As discussed in Section 1.9, computational modelling is a time and resource efficient method that can be used to evaluate the success of THR *in vivo*, compared to *in vitro* simulations. Hence, prior to pre-clinical experimental testing, computational tools can be used to investigate the feasibility of the research or to determine *in vitro* scenarios of most interest. The motivation behind the proximity tool development was the estimation of the patient-specific biomechanical activity features which put the THR bearings at most risk of edge contact.

This chapter provides a detailed description of development processes of computational proximity tool. The related considerations in terms of biomechanics data processing are also addressed in the scope of this chapter. In section 2.1 the general purpose, function and example of the outputs are presented. Section 2.2 covers the specifics of the identified input to the tool in relation to the THR device, patient and biomechanics activity data. The following sections, 2.3 and 2.4, are focused on the description of the datasets used during the tool development process and their coordinate system definitions. Section 2.5 of this chapter describes the approach and general tool structure prior to the detailed description of separate methods in Section 2.6. Method section, is followed by

two case studies, where the two types of patient data were analysed using the developed tool. Section 2.8 summarises the tool itself and the development process including challenges, limitations and future work discussion.

2.1 Overview of the analytical proximity tool purpose, function and output

Two possible approaches were considered to achieve the aim of this work, one of which was finite element modelling using ABAQUS/CAE 6.14 (©Dassault Systèmes, US). Other approach was to develop a custom set of algorithms using MATLAB R2017a (©The MathWorks, Inc., US). The choice of these particular software packages was based on the availability within the institute. The finite element analysis (FEA) is an established way of assessing edge contact (Hua et al., 2016), which predicts contact area and related stresses directly. However, there were disadvantages to the FEA in regards to the processing of the biomechanical data. Firstly, FEA can be costly in terms of computational solution time, which could be an issue when processing large amounts of data. Secondly, the finite element models require specialist knowledge in software, hence the user variability would be limited. Thirdly, ABAQUS/CAE (©Dassault Systèmes, US) is only widely available within the engineering institutes, again limiting the number and type of users. The upgrade of testing profiles could be of interest for future studies, beyond the deadline of the work described in this thesis. Hence, consideration of the tool future use was defined to be important.

In contrast to finite element model development, the analytical approach would require bespoke development, using an algorithm development environment such as MATLAB (©The MathWorks, Inc., US). The analytical tool development approach allows for customisation in terms of output, simulation time and user variability. In addition, MATLAB (©The MathWorks, Inc., US) package as a scripting environment, is more popular within research groups than finite element software. Set of algorithms can be compiled in a stand-alone executable, which does not require any software installation.

Considering the aim of the project, which requires patient-specific processing, custom algorithm development was chosen as the main method in this project,

although finite element modelling was used to generate one sub-set of the input data.

Prior to analytical proximity tool development general requirements were identified for successful fulfilment of the aim. Firstly, the tool had to incorporate metrics for the edge contact risk assessment for THR bearings. Secondly, the tool had to be developed so that it allows for processing of each individual patient gait data. Since the required amount of data to establish any trends must be large, it was identified that the tool's run time should be minimised as much as possible to allow for fast data processing. Other requirement was the ability of the tool to include patient-specific pelvic motions and cup orientation.

According to the requirements described previously and definition of edge contact, custom computational tool was developed which measures the proximity of the contact centre and contact area to the rim of the cup. To allow for relevant *in vivo* condition simulations, inputs from gait data were selected to be both, joint contact forces and pelvic motions. Two types of data were used in the development process to allow for versatility of the tool. These included instrumented implant and motion marker combination taken from HIP98 dataset (Bergmann, 2008), and more conventional force platform and motion marker combination provided by Leeds Biomechanical Research Centre (LBRC, ©Leeds Teaching Hospitals NHS Trust).

Main output metrics were chosen according to the definition of edge contact, which is described by the contact falling partially on the rim of the cup. Hence, the determination of the contact centre and contact area location in relation to the rim of the cup was considered to be sufficient in determining the deviations in risk of edge contact. Proximity tool's functionality is presented in Figure 2.1 and is discussed in detailed in Section 2.5. To measure the proximity of the contact centre and contact area to the rim of the cup two measurements were identified as detailed in Section 2.6. Firstly, the centre proximity angle was defined as an angle between the contact force vector, blue arrow in Figure 2.1, and cup pole. Secondly, edge proximity angle was defined as the angle between the cup pole and the most distal edge of the theoretical contact area, in red, to the cup pole.

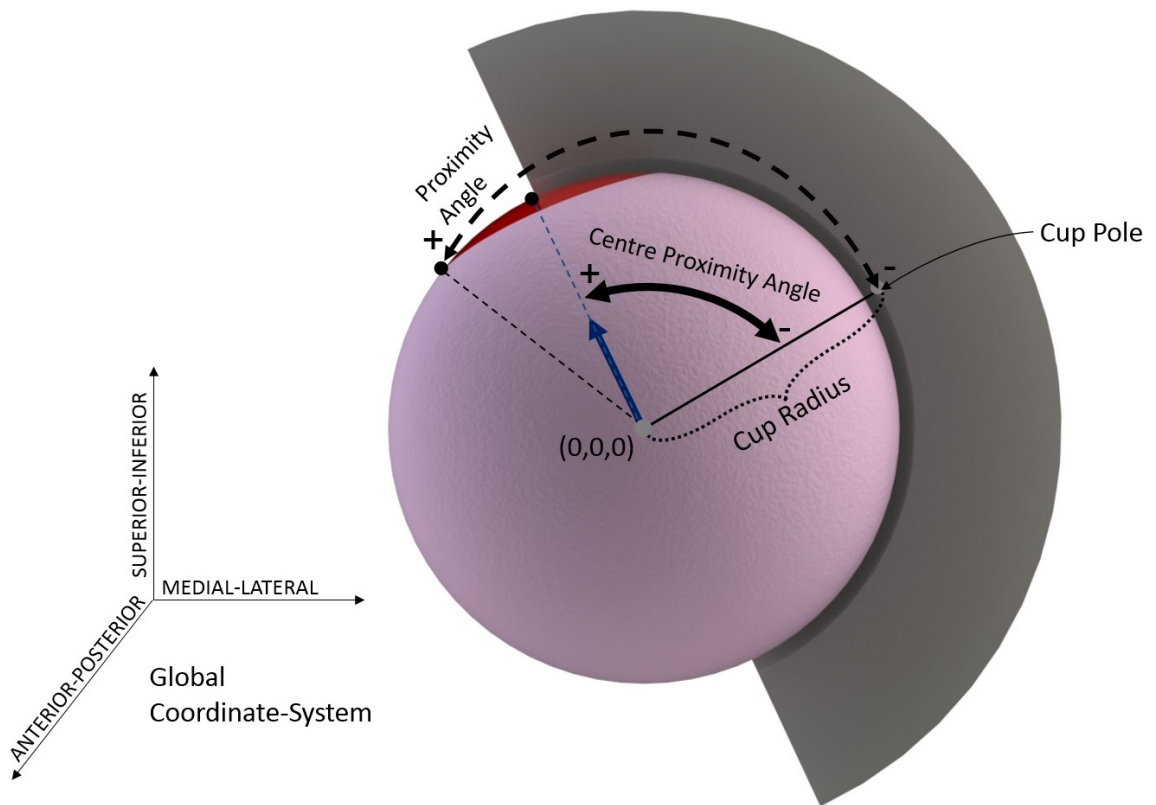


Figure 2.1: Illustration of the proximity tool's output, where THR is presented in cross-section and with global coordinate system marked. The theoretical contact area is in red and force vector, in blue, determines the centre of contact determined by resultant contact force vector.

As the tool was developed to establish trends in patient-specific data using a rapid approach, rather than assess the particular THR device performance, simplifications in cup design and contact area definitions were made (Section 2.2). Firstly, acetabular cup was modelled as featureless and set to maintain spherical geometry throughout the simulation. Secondly, the contact area was chosen to maintain circular base, which eliminates the additional computational costs of re-calculating contact area shape. The larger the magnitudes of both proximity angles the higher the risk of edge contact. Throughout this thesis this area is called theoretical contact area.

An example of the proximity tool's graphical output is presented in Figure 2.2. Here the orange curve represents centre proximity angles and blue curve represents the edge proximity angles through the activity cycle. The dotted line at 90° provides a reference measure. This represents the edge of the cup with head-coverage angle of 180° , this cup would have a rim at 90° from cup pole. Setting this reference line allows to establish identify the cases with or without edge

contact, if required. The red arrow symbolises the maximum risk of edge contact. The distance between centre proximity angle and edge proximity angle represent half of the contact area closest to the rim of the cup, which can also be seen from Figure 2.1.

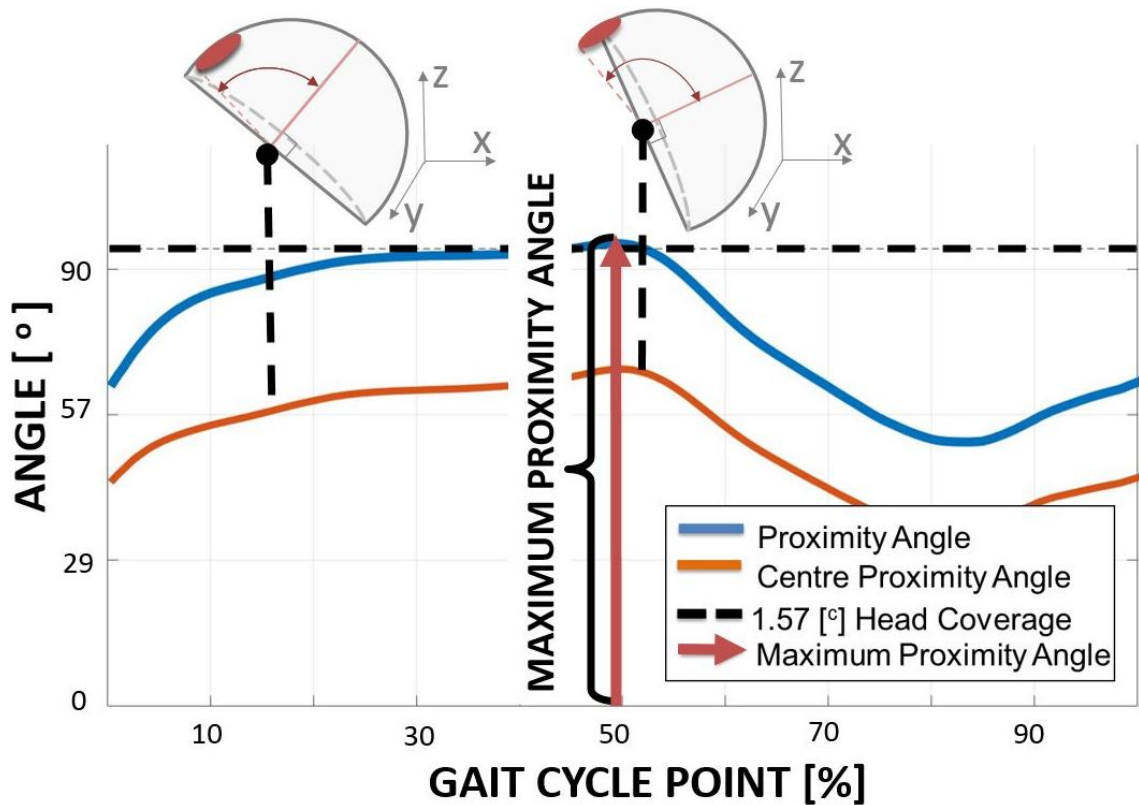


Figure 2.2: Sample output of the proximity tool where orange curve is for centre proximity angle and blue for edge proximity angle. The dotted line marks the 90° head coverage.

2.2 Description of the required input type and format for the proximity tool

There were three types of input identified for the tool, device specific, patient specific and gait cycle point specific. The input to the tool from device specific perspective was the diameter of the acetabular cup and the head-coverage angle. As mentioned previously the cup was chosen to be featureless to avoid the output being product specific, which meant the exclusion of the design features such as chamfers, fillets and variable head-coverage angle. To find the relationship between contact force and contact area, the material properties, THR bearings' radial clearance, diameter of the cup and the range of contact forces were also identified as the necessary inputs. This included the THR bearing material specification.

The side, left or right, of the THR or the side to which the inputs are normalised was set as another input requirement, which establishes the position of the cup in tool's coordinate system. For following chapters and future uses, for the cases when the patient-specific cup alignment is known, the definition of version and inclination angle must be clearly stated in the image system, and the relationship between this coordinate system and global coordinate system must be stated or discussed. Otherwise the arbitrary position depending on the aim of the simulation was defined as an input. The patient-specific inputs were identified to be dependent on the nature of the data. Therefore, in future use, the assumptions for each data type must be clearly stated and explored prior to the use of the tool.

The three components of the contact force at the hip joint and pelvic motions for each point of the cycle were selected as the dynamic inputs. The combination of those inputs was established to be essential in order to find the change in proximity angles throughout the activity cycle and detection of the cycle point of highest edge contact risk. The definitions of pelvic motions were different for HIP98 data and LBRC data, which are described in Section 2.3.

2.3 The detailed description of the datasets used in the *proximity tool* development and input selection

2.3.1 HIP98 dataset format and input assumptions description

HIP98 is an online dataset which was available through the OrthoLoad website (Bergmann, 2008). The dataset contained information for four patients and nine activities (Chapter 3). In the context of the analytical tool development, data for one patient was taken from this dataset, patient HSR, walking at self-selected speed. The patient had a 32mm diameter ceramic-on-polyethylene instrumented THR implanted.

The dataset itself was composed of the THR patient gait data recorded through motion marker system, six-camera Vicon, and instrumented implant, HIP II with one 9-channel transmitter. The motion marker data included dynamic joint angles in individual joint coordinate systems as well as in the global, laboratory, coordinate system. The hip contact forces, normalised for body weight (BW), were also provided which were recorded by the instrumented hip implant. The trial video-recording was also available for each activity performed by each patient. Only two pelvic motions, coronal obliquity and sagittal tilt, were available within the dataset. In addition the joint centres were provided for knee, ankle and hip, as well as pelvis centre, which was defined by junction between L5-S1 vertebrae (Bergmann, 2008).

For this specific dataset, the group of inputs was extracted according to the requirements discussed in Section 2.2. The device material combination from HIP98 specification together with all three hip joint contact forces were set as an input. As only two pelvic angles were explicitly provided in the dataset, it was decided to use hip joints centre locations during each activity cycle point to establish pelvic motions through the activity cycle.

The version and inclination angles of the acetabular cup were set to be within Lewinnek "safe-zone" and have 45° inclination and 7° version in the imaging coordinate system (Lewinnek et al., 1978) for the test case within the scope of

this chapter. Two assumptions were made regarding the HIP98 dataset, due to the missing link between cup orientation in a radiographics definition and the corresponding pelvic orientation. First, the orientation coordinate system was set to be identical to the pelvic coordinate system during standing up-right position. Second, the pelvic coordinate system orientation prior to application of pelvic motions was set to be equal to the orientation of the global coordinate system.

2.3.2 LBRC format and input assumptions description

The dataset from Leeds Biomechanical Research Centre, (LBRC, ©Leeds Teaching Hospitals NHS Trust) was acquired for twenty patients discussed in detail in Chapter 4. Ethical approval was obtained via the UK national NHS ethics (IRAS project ID 151079) system and all participants provided informed, written consent. From the whole patient cohort of 137 (Lunn et al., 2019) twenty high-functioning patients walking at self-selected speeds were chosen. In the scope of this chapter, one patient, 001, was chosen for analytical solution development and testing. In contrast to HIP98 data this set was measured using a conventional method described in Section 1.8 of Chapter 1 using force platform, AMTI (©Advanced Mechanical Technology, Inc.) and motion marker, ten camera Vicon system & cast market set, combination. The data was further processed through Visual 3D (©C-Motion, Inc. 2016) for pelvic motions, and AnyBody (AnyBody Technology A/S 2017©), inverse kinematics method, to acquire hip contact forces. In contrast to the HIP98 dataset the pelvic motion input data was defined by actual pelvic angles measured from motion marker system, all three rotations were present namely coronal obliquity, sagittal tilt and internal-external rotation.

For this specific dataset the group of inputs were extracted according to the selection criteria discussed in Section 2.2. The THR device was set to be identical to HIP98 specification, as it was not provided for the LBRC dataset. The three pelvic angles were used to identify the three-dimensional pelvic motion during each gait time point. As no cup positioning data was provided the assumption was made that the cup was positioned according to surgical guidelines. The inclination and version cup angles were used for this data type test case as for

HIP98 within the scope of this chapter. Similar to the LBRC dataset the assumption was made that pelvic coordinate system prior to application of pelvic motions was equal to global coordinate system.

2.4 Description of the coordinate systems defined in datasets used for tool development

2.4.1 HIP98 dataset laboratory, image and pelvic coordinate system definition

The definition of coordinate systems was defined within the dataset supplementary information (Bergmann, 2008). There were three coordinate systems in which the selected input data was expressed, these were laboratory, image and pelvic coordinate systems. The laboratory coordinate system was defined in terms of $[X_L, Y_L, Z_L]$ components, where X_L was the axis in anterior-posterior direction from posterior illiac spine to level of the anterior illiac spines, Y_L is the axis in the medial-lateral direction from right hip centre to left hip centre, Z_L is the axis in the superior-inferior direction (Figure 2.3).

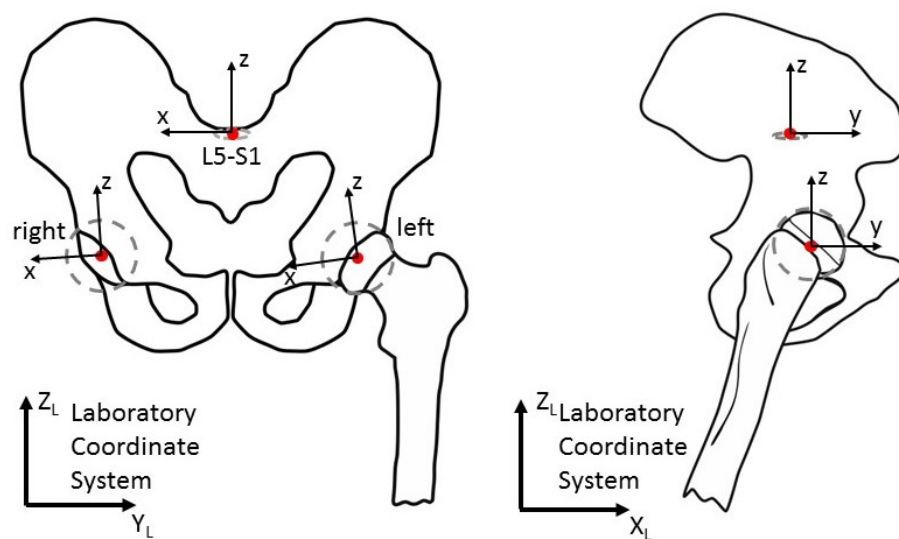


Figure 2.3: Definition of the laboratory coordinate system for HIP98 dataset in relation to the patient lower body in coronal and sagittal planes marked as Z_L and Y_L and X_L . The local coordinate system of the pelvis has its origin at left hip joint centre (Adapted from (Bergmann, 2008)).

Each joint centre is also presented in terms of $[x, y, z]$ components as seen in Figure 2.3, where x is for the medial-lateral direction, y is for the anterior-posterior direction and z is for the superior-inferior direction. The pelvic coordinate system was defined by the left, right hip joints and L5-S1 centres. The origin of the pelvic coordinate system was reported to be at the left hip, as all the data was normalised to it. The x axis was defined as the connection of the centres of two femoral heads in the direction from left to right hip. The z axis was defined as being perpendicular to x axis and went through the centre of the L5-S1 vertebral body junction in the sagittal plane in the superior-inferior direction. The y axis was defined to be constructed from posterior iliac spine to anterior iliac spine and perpendicular to both x and z axis.

2.4.2 LBRC coordinate systems

The pelvic motions in the LBRC dataset were given in terms of rotations around the axes. The definitions of the contact forces were given in the laboratory coordinate system. In relation to the cup and pelvis, the coordinate system was reported in $[X_L, Y_L, Z_L]$ components where X_L axis is in the medial-lateral direction from left hip to right hip, Y_L axis is in the anterior-posterior direction from posterior iliac spine to anterior iliac spine, Z_L axis is in the inferior-superior direction (Figure 2.4).

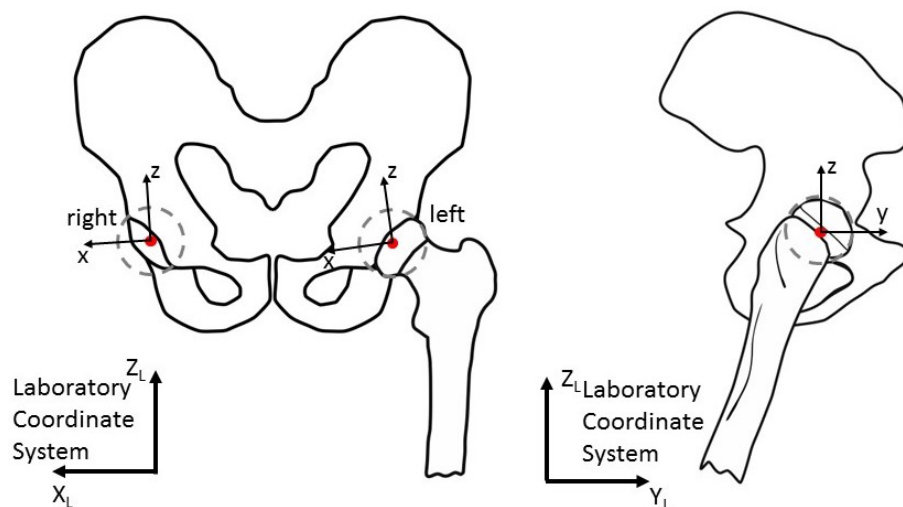


Figure 2.4: Definition of the laboratory coordinate system for LBRC dataset in relation to pelvis in the frontal plane.

The coordinate system is defined as global, laboratory, coordinate system and the joint contact forces are defined in this system, hence depending on which hip was studied, the direction of the medial-lateral force will change. The rotations, however, are defined independent of the operated hip side as seen in Table 2.1. Rotations for right hip and left hip are described in Figure 2.5, these rotations are compared to *right-hand rule* rotations which is a standard convention in engineering mathematics. The positive rotation around medial-lateral axis, sagittal tilt was set to be always in the anterior direction. The positive rotation around the anterior-posterior axis, coronal obliquity, was set to be always in the upwards direction. The positive rotation around superior-inferior axis, internal-external rotation, was set to be always in the internal direction.

Table 2.1: Rotation direction definitions in relation to the acetabular cup. The definitions apply independently of the hip side

Pelvic Rotation	+ ve	Axis of rotation
Sagittal Tilt	Anterior	x, medial-lateral
Coronal Obliquity	Upwards	y, anterior-posterior
Internal-External Rotation	Internal	z, inferior-superior

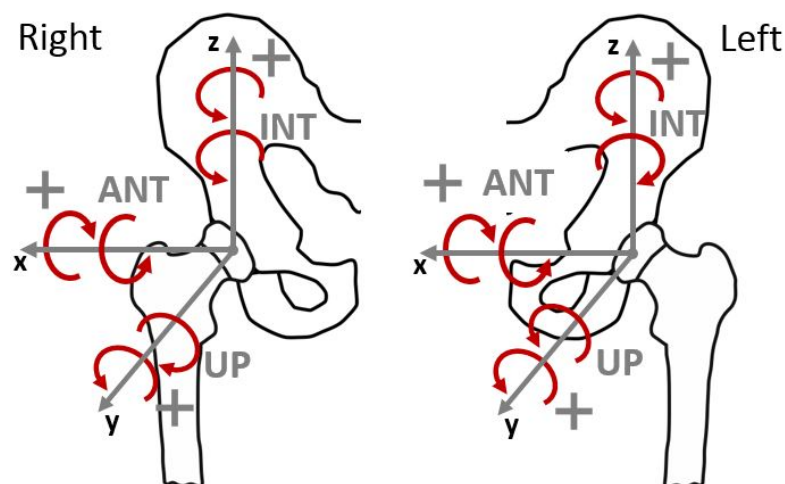


Figure 2.5: Rotation direction definitions for LBRC dataset in relation to the right and left side acetabular cups. The \oplus denotes rotation direction around the axis according to the *right-hand rule*. ANT - anterior tilt, INT - internal rotation, UP -upwards obliquity.

2.5 Overview of the approach taken in the analytical tool development

The initial proximity tool algorithms were developed on the basis of HIP98 data (Bergmann, 2008), with further additions and adaptations from biomechanical data provided by LBRC. As previously mentioned the risk of edge contact was measured in terms of contact location relative to the rim of the acetabular cup and the main outputs from the tool were centre proximity angles and edge proximity angles.

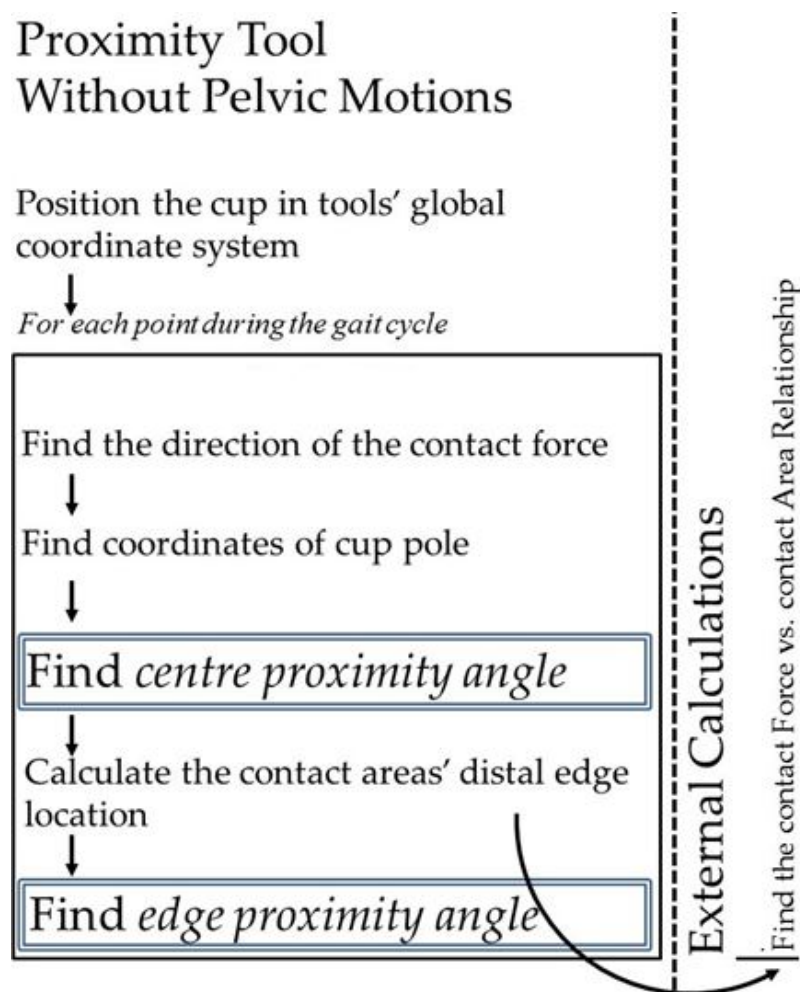


Figure 2.6: Flow chart describes the actions executed in the proximity tool during the simulation both with and without pelvic motion addition.

A flow chart of simplified proximity execution without pelvic motion addition algorithm is shown in Figure 2.6. First, the cup was set to be positioned in the global coordinate system, which corresponds to the MATLAB (©The MathWorks,

Inc., US) one (Figure 2.1). In following algorithms of the tool, the cup was set to remain stationary. Second, the direction of the force vector originating from the centre of the cup was scripted to be established for each gait cycle point of the activity. The direction of force was represented by the unit vector derived from the contact force component data. Third, knowing the cup position the vector's coordinates defined by cup origin and cup pole were set to be recorded for future use. The angle between the two vectors described in step two and three was defined as the centre proximity angle. The angle between the centre of contact and edge of contact area was then calculated. Here the calculation of the contact force and contact area relationship was performed externally to the tool using finite element solver, ABAQUS/CAE 6.14 (©Dassault Systèmes, US) for the range of clinically relevant contact forces. From this relationship the magnitude of the contact area for each gait cycle point can be determined and further used to find the required angle between centre of contact and edge of contact area. Finally, the centre proximity angle and contact edge to centre angle were set to be summed up in order to compute the edge proximity angle.

In order to add the pelvic motion effect, the extra algorithms were added to the tool, shown on Figure 2.7 in red, prior to the proximity angles calculations. The approach taken to add the effect of pelvic motion was based on translating the force vector into the dynamic pelvic coordinate system for each gait cycle point. This eliminated the need to rotate the cup itself which would be a much more complicated process as the rotations would have to be performed around three axes. In addition, this method would allow for the use of joint contact centres rather than pelvic motion angles which is the case in HIP98 data. Therefore, the first step in pelvic motion addition was set to be the construction of the dynamic pelvic coordinate system that varied throughout the activity cycle. The next step was the translation of the force vector into the dynamic pelvic coordinate system for each activity point. Hence, this would simulate the relative motions between force vector and acetabular cup, without moving the cup itself.

During the development process the additional algorithm was added to the main tool. The algorithm was aimed at finding the potential clockwise location of the maximum proximity angle along the rim. This algorithm was thought to be

beneficial in future during examination of the *ex vivo* THR components which show rim damage.

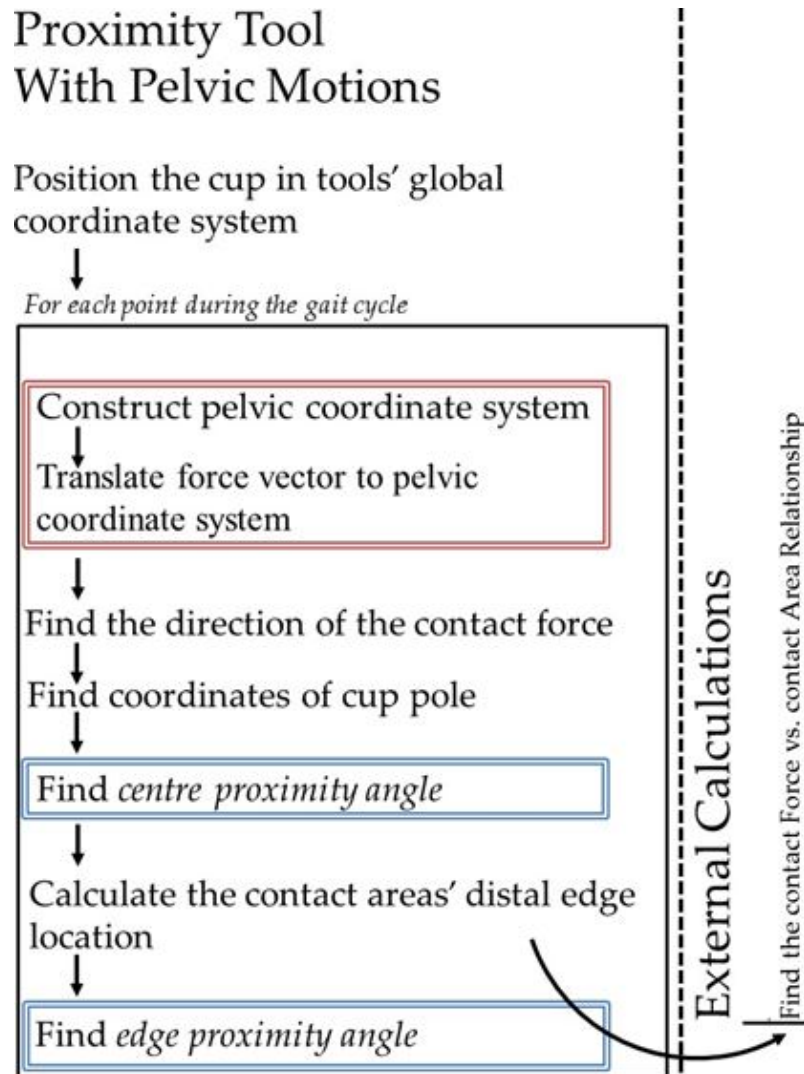


Figure 2.7: Flow chart describes the actions executed in the proximity tool during the simulation both with and without pelvic motion addition.

2.6 Detailed description of actions taken prior and during proximity tool execution

2.6.1 Global coordinate system set-up

The relationship between the proximity tool's coordinate system used within the proximity tool and coordinate systems associated with the imported data was crucial to consider during the tool operation. Therefore, the default tool's coordinate system was specified prior to the development. The tool's coordinate system was defined according to standard definition for a Cartesian coordinate system, expressed in terms of three orthogonal axes going through common origin. The origin in this case was set to be centre of the cup. The positive rotation direction was counter-clockwise according to the *right-hand rule*, as discussed in Section 2.4 of this chapter. The default tool's axes in relation to the acetabular cup were set to be X for medial-lateral, Y for anterior-posterior and Z for superior-inferior.

2.6.2 Detailed description of the centre proximity angle and edge proximity angle algorithm

The angle between the force vector and cup pole was defined as centre proximity angle, and the angle between the cup pole and most distal edge of the contact area was identified as the edge proximity angle (Figure 2.1). To calculate both of these proximity angles, the equations for spherical cap, circular segment and angle between two vectors were used (Weisstein, 2018a; Weisstein, 2018c; Weisstein, 2018e). A schematic of these calculations is presented in Figure 2.8. Two vectors were used for centre proximity angle algorithm development. First, the contact centre vector, which initial point was set to be at the origin, 0, of the cup and was defined by three contact force components, medial-lateral, anterior-posterior, superior-inferior or [X, Y, Z] spatial coordinates, according to global coordinate system definition of the tool. Secondly, the cup pole vector was set to have the initial point at the origin of cup and terminal point at the pole of the cup. The angle between these two vectors was set to be derived from

Equation 2.1 (Weisstein, 2018c).

$$v_1 \cdot v_2 = |v_1||v_2| \cos \theta \quad (2.1)$$

In the Equation 2.1, v_1 is contact centre vector shown in blue in Figure 2.8, and v_2 is cup pole vector shown in red in Figure 2.8. Angle θ in the Equation 2.1 is the angle between two vectors, which is centre proximity angle.

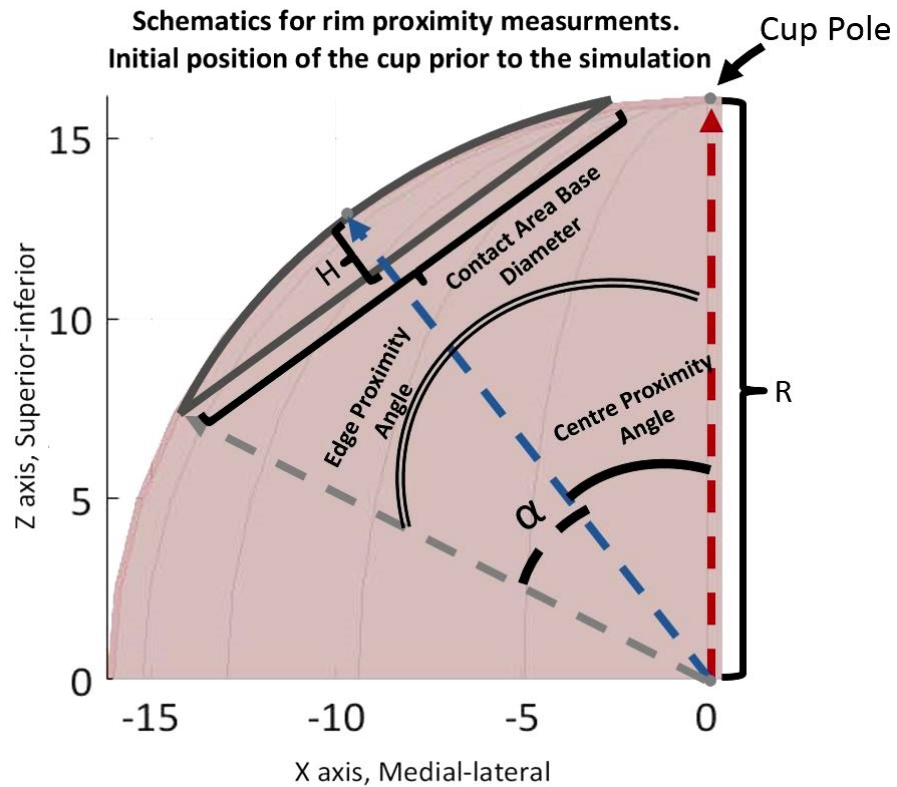


Figure 2.8: Simplified 2D schematics of the acetabular cup, where H is the height of the theoretical contact area, α is the angle between edge of the theoretical contact and joint contact force vector. Radius of the cup is marked by R which extends from cup origin to cup pole. Anterior-posterior axis, Y, is not presented but is orthogonal to both X and Z axes.

To identify edge proximity angle the relation between contact area and contact force was used in the algorithm, which is further discussed later in this section. The magnitude of the contact area was selected to represent the surface area of the spherical cap of the surface of the cup, or arc formed by contact area base as shown in Figure 2.8. Calculation of the angle between the contact force vector and edge of the contact area, α (Figure 2.8) was performed using the equations

for surface area of the sphere and its features. The height of the spherical cap was calculated using Equation 2.2a. By knowing the height of the cap, the chord of the circle (cup cross-section) was found. The chord of a circle was equal to the diameter of contact area base and could be found from the definition of surface area of the spherical cap (Equation 2.2b). From Figure 2.8 it can be seen that the half of the contact area base diameter and cap height formed a 90° angle. At the same time radius of the acetabular cup, in grey in Figure 2.8 formed a right triangle with radius of the spherical base. Hence, the angle α was found from Equation 2.2c, which is the angle between contact force and edge of the contact area. Finally, the edge proximity angle was set to be equal to the sum of α and centre proximity angle.

$$H = S_{\text{cap}} \div (2\pi R) \quad (2.2a)$$

$$S_{\text{cap}} = \pi(A^2 + H^2) \quad (2.2b)$$

$$\alpha = \sin^{-1}(A \div R) \quad (2.2c)$$

In the Equations 2.2a, 2.2b, 2.2c H is height of the spherical cap, R is radius of the acetabular cup, S_{cap} is surface area of the spherical cap which is equal to generated contact area. Angle α is the angle between contact centre vector and contact edge vector. The chord A is perpendicular to contact centre vector. The edge proximity angle is equal to $\alpha + \text{centre proximity angle}$.

Verification of the algorithm for identification of force vector location relative to the rim of the cup

To verify the algorithm the location of the force vector was tested for (1) 45°, $\begin{bmatrix} 0.7071 \\ 0 \\ 0.7071 \end{bmatrix}$ and (2) 90° $\begin{bmatrix} 1 \\ 0 \\ 0 \end{bmatrix}$ for cup in initial position (Figure 2.13). The contact area was selected to be equal to the surface area of the cup, hence angle α should be equal to 90°. For the first set up (1) the centre contact proximity was found to be 45° and α was set to 90°. For the second set up (2) the centre contact proximity

was found to be 90° and α was found to be 90° . Both tests showed the expected results, hence the algorithm was verified.

2.6.3 Detailed description of finite element model for estimation of contact force and contact area relationship

The contact area to contact force relationship was established, in order to allow measurement of proximity of the contact area edge to the rim of the cup. A finite element model was constructed in ABAQUS/CAE 6.14 (©Dassault Systèmes, US). Contact forces were applied from 0.2kN up to 5kN which take into account contact forces range seen in HIP98 (Bergmann, 2008) and LBRC data. The dimensions for the cup and head were chosen to be 32mm ceramic-on-polyethylene which was in accordance to the HIP98 data (Bergmann, 2008). The cup was chosen to deform only elastically and have an Elastic modulus of 1GPa and Poisson's ratio of 0.4 identical to Hua et al. (2016). The head was assigned properties of an alumina matrix composite with an Elastic modulus of 380GPa and Poisson's ratio of 0.26 (Liu and Fisher, 2017). The radial clearance was set to 0.5mm. As mentioned previously geometrical features such as chamfers, backing of the cup (shell) were neglected. The thickness of the acetabular cup was not device specific. The acetabular cup was designed as a hollow sphere with the head being in the core of it (Figure 2.9). By eliminating the rim in general, it was guaranteed that the contact area remain circular and not device specific. The resultant contact force was applied vertically along the Y axis of the ABAQUS default coordinate system from the head centre as seen from Figure 2.9. Although any direction would have generated the same results. Thirty force iterations cases were simulated for the range defined previously, which corresponded to the number of cases used in literature (Hua et al., 2016). The outputs of the finite element solution were minimised to only contact area between THR bearings, which reduced the simulation time. Using gained theoretical contact area data, Equation representing the relationship between contact force and contact area was created by interpolating a mathematical function through the data points.

$$f(x) = a * x^b \quad (2.3)$$

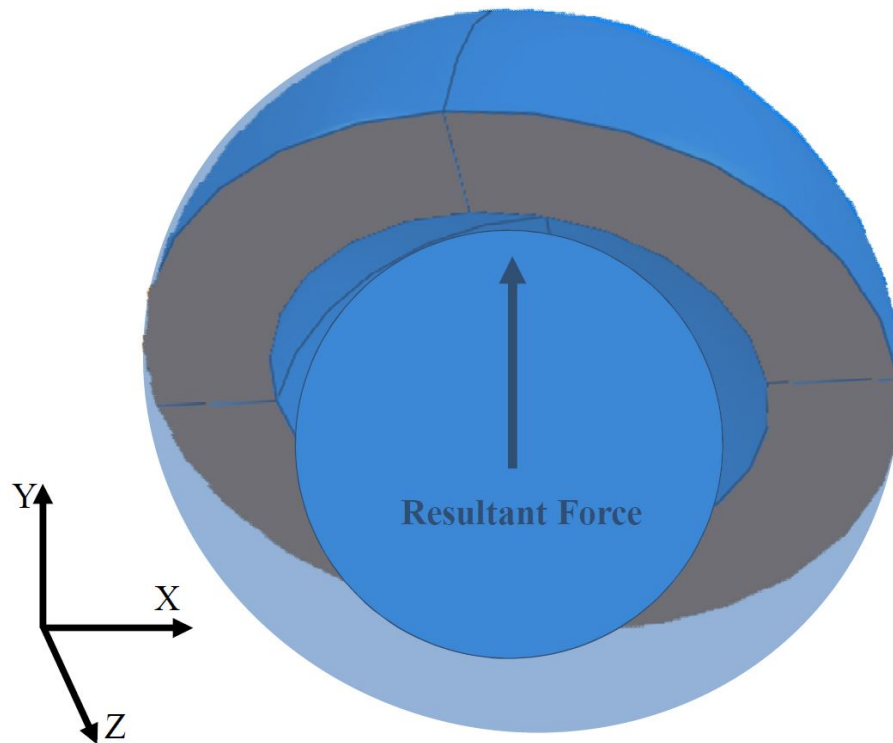


Figure 2.9: Acetabular cup cross-section, X-Z plane, of the generalised total hip replacement model used to find the contact force and contact area relationship. Resultant force acting in vertical direction. Half of the cup rendered for visualisation purposes.

The curve fitting tool, which is a built-in application in MATLAB (©The MathWorks, Inc., US), was used to find the relationship. The mathematical functions to construct the curve that would describe the relationship were exponential, Fourier series, Gaussian, linear, polynomial and power-law fitting models. The most accurate fit for the contact force versus contact area relationship was expressed by the power law function defined by Equation 2.3, where x is variable and a and b are scaling factors. The power law curve to the data is shown in Figure 2.4 and expressed by Equation 2.4

$$ContactArea = 102.5 * (ContactForce)^{0.58} \quad (2.4)$$

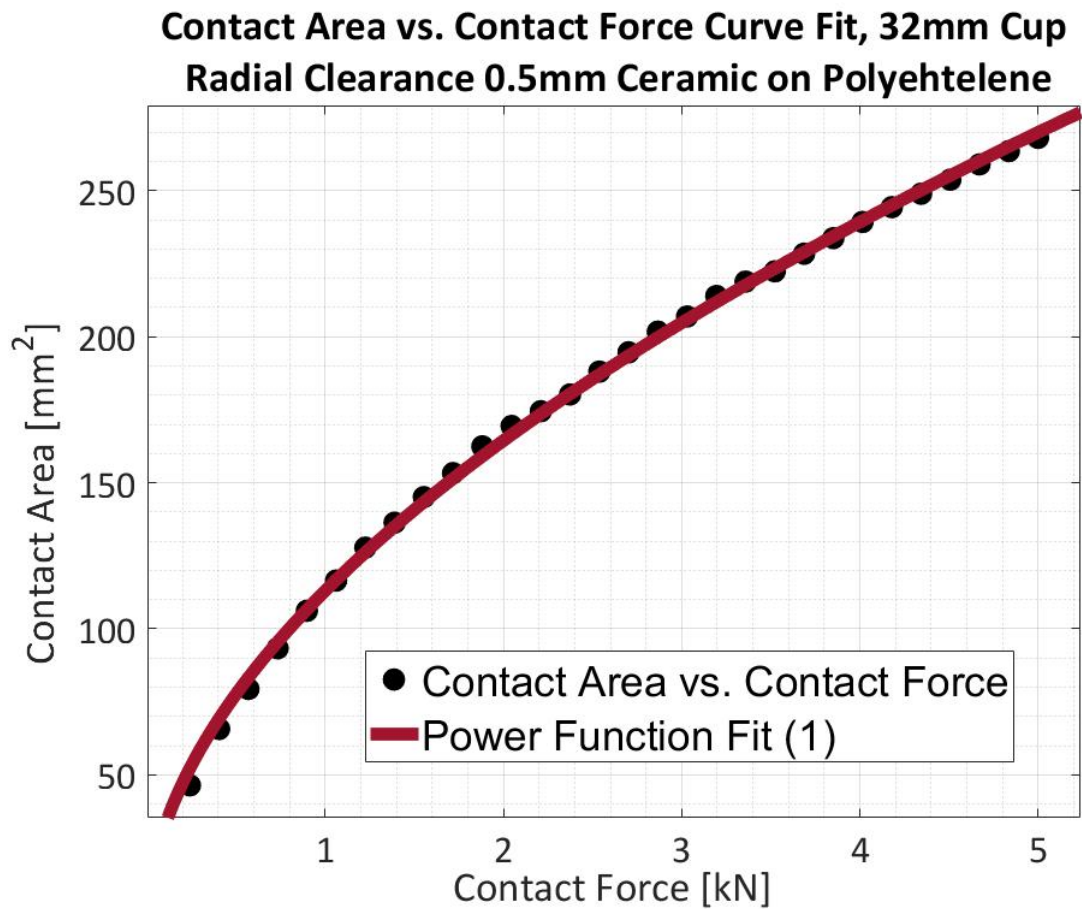


Figure 2.10: Output of the finite element simulation, contact force versus contact area marked in black. The power-law function fit, characterising the relationship between contact force and contact area, shown in red.

Two sensitivity studies were performed. These were mesh convergence and cup radial clearance tests, which are described further. The cup thickness sensitivity was not performed as a part of this study. According to Kurtz et al. (1997) and Bartel et al. (1985) the change in average contact stresses, which is proportional to contact area, lowers after polyethylene cup thickness reaches 8mm. After the point where thickness reached 8mm the contact stresses remained the same with cup thickness increase. Hence it was decided to use 8mm cup thickness in the model, which is also close to the combined thickness of acetabular liner and shell (Hua et al., 2016).

Mesh convergence test and acetabular cup geometry sensitivity tests.

The mesh element size between two contacting bodies was chosen to be one-to-one, based on the contact study by Jahani (2017). The mesh elements were chosen to consist of linear hexahedral elements (continuum three dimensional 8-node reduced integration) for both hollow sphere and head.

The convergence study was performed to determine optimal element global size. One of the requirements was time efficiency. The finite element simulations were performed on a desktop PC with Intel® Xeon® at 3.5GHz with 12 logical processors and 32GB of RAM. Each simulation was performed using 10 logical processors. It was identified that for mesh sizes of 0.4mm and lower the simulation time increases from just below 1 hour to above 12 hours compared to coarser meshes, which run-time is just under one hour. Therefore, mesh of 0.5mm was chosen as the minimum that can be used in this work.

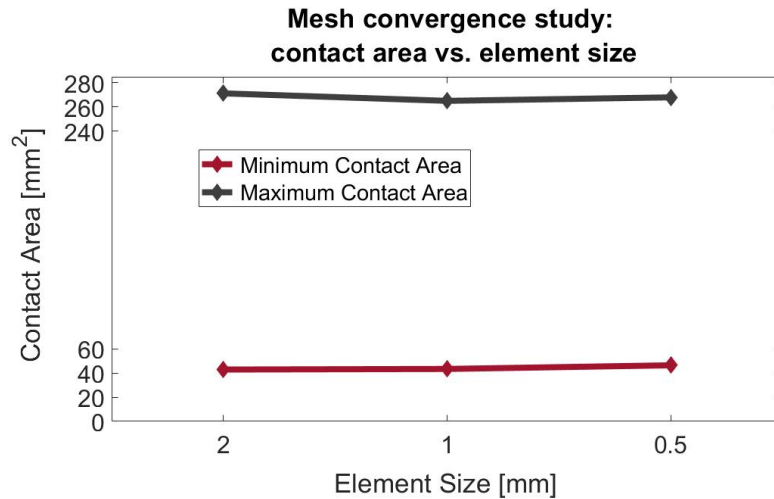


Figure 2.11: Mesh convergence results for the element size between 2mm and 0.4mm for maximum and minimum contact area values.

Mesh convergence tests were performed for three element sizes, 0.5mm, 1mm and 2mm. The measurements taken for the convergence test were maximum and minimum contact area values.

The results of the mesh convergence study are shown in Figure 2.11 and Tables 2.2 and 2.3. For maximum contact area values, the difference between 2mm & 1mm was higher than for 1mm & 0.5mm (Table 2.2). Hence it can be assumed that the mesh will continue to converge with halving of the element size, 0.25mm. The error between 1 mm and 0.5 element sizes in terms of α (Figure 2.8) was shown to be 0.2° as shown in Table 2.3.

Table 2.2: Mesh convergence test results for element sizes 2mm, 1mm and 0.5mm. Contact area difference (B) between element size 2mm and 1mm, (C) between element size 1mm and 0.5mm. CA - contact area, Diff. - difference.

Case	Element Size [mm]	Minimum Contact Area CA [mm²]	Diff.[mm²]	Maximum Contact Area CA [mm²]	Diff. [mm²]	Time [hrs]
A	2	42.9		271.3		0.3
B	1	43.4	-0.5	265.1	6.2	0.6
C	0.5	46.64	3	268.1	-2.9	0.9

For minimum contact area values, the difference between 2mm&1mm was lower than for 1mm&0.5 mm (Table 2.2). This suggested that the mesh element size required for the convergence will have to be less than 0.25mm. Due to the lack of convergence the error in a 0.5mm mesh remains uncertain. Hence, the

overall error in the 0.5mm mesh could be better estimated by the difference between 2mm and 0.5mm mesh global size. The measured error in α for 0.5mm was measured to be 0.5°, as seen from Table 2.3. The errors in α for minimum and maximum contact areas and element size for 0.5mm mesh describe the uncertainty in the results in the work throughout the thesis. This is only true for edge proximity CA angles, which values depend on contact area.

Table 2.3: The finite element mesh error for minimum and maximum contact areas. Compariosn to 0.5mm element size. CA - contact area, Diff. - difference.

	CA 0.5mm [mm ²]	Diff. 0.5mm to [mesh size]	Alpha angle ° (0.5mm) ± mesh error
Min CA	46.4	3.5 [2mm]	13.8 ± 0.5
Max CA	268.1	3 [1mm]	33.6 ± 0.2

The radial clearance test was performed to check the effect of the differences between head and cup size on the output of the model. Throughout this test the clearance difference affecting the model response in α angle was identified for future reference between radial clearances, which are relevant to hard-on-soft bearing combination. The radial clearance 0.5mm is typical for a ceramic-on-polyethylene THR, which was measured experimentally using coordinate measurement machine (©2019 RedLux Ltd) as a part of Groves et al. (2017) study. The data for other radial clearances was based on the literature (Hua et al., 2016; Bartel et al., 1985; O'Dwyer Lancaster-Jones, 2017). The clearances from literature and internal to the institute experimental data were also tested. The interval between the clearances was chosen to be 0.1mm based on the existent clearance values.

The results show that clearance affects the contact area output and the effect is the highest for largest contact force of 5kN. The smaller clearances are more typical for hard-on-hard bearings. For larger clearances, which are more typical for hard-on-soft bearings and shown in Figure 2.12 by dotted curves, the difference in maximum areas and related to them α angle are shown in Table 2.4. The largest error was recorded for radial clearance of 0.5mm in comparison to 0.3mm radial clearance, which resulted in deviation of 4°. The difference of 0.1mm was shown

to affect the contact area size and α more for decreasing clearance (1.8°) rather than increasing clearance (1.4°) as seen from Table 2.4.

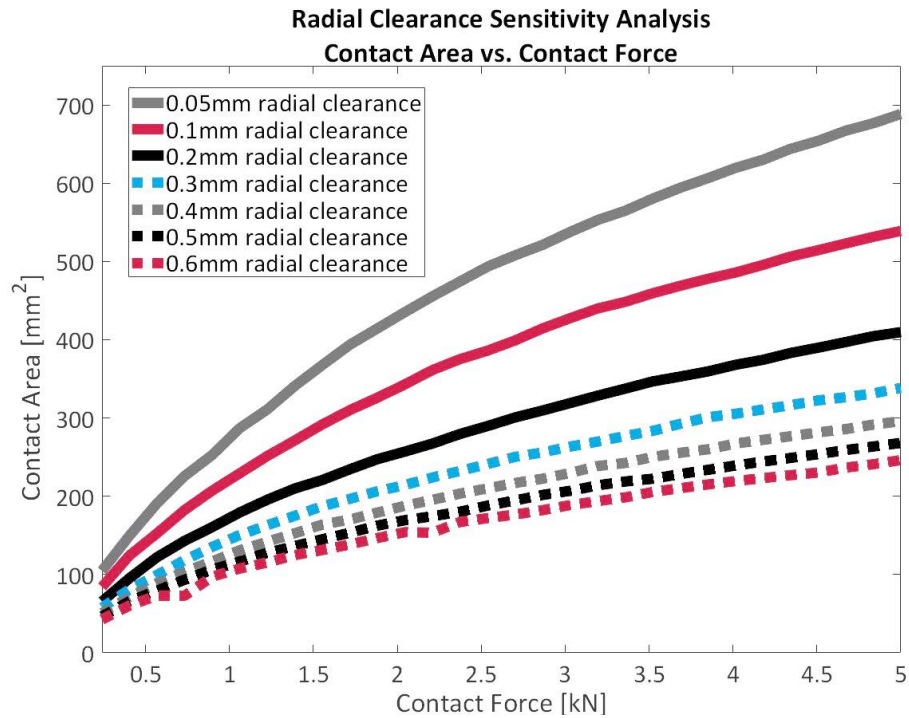


Figure 2.12: Sensitivity study for radial clearance between THR bearings, for 32mm ceramic-on-polyethylene combination. The tested radial clearances were 0.05mm, and 0.1mm to 0.6mm. The dotted curves are representative of radial clearances for hard-on-soft bearings and solid curves for radial clearance representative of hard-on-hard bearings.

Table 2.4: Contact area and contact force variation and uncertainty depending on radial clearance value. Comparison to 0.5mm radial clearance. Diff. - difference, CA - contact area.

Radial Clearance [mm]	CA Diff. to 0.5mm	Alpha angle ° (0.5mm) ± clearance effect
0.3	70.3	33.6 ± 4
0.4	26.9	33.6 ± 1.8
0.6	-21.9	33.6 ± 1.4

2.6.4 Detailed description of the algorithm used for the positioning of the acetabular cup within the proximity tool environment

At the initial point, before processing activity data, the cup was positioned according to selected inclination and version angles, which during tool development

were 45° inclination and 7° version. The origin of the cup at the initial time-point, was set to coincide with $[0, 0, 0]$ coordinates of the global coordinate system as shown in Figure 2.13. The plane of the acetabular cup was set to coincide with X-Y plane of the global coordinate system, where normal to the cup plane would be coincident with the Z axis.

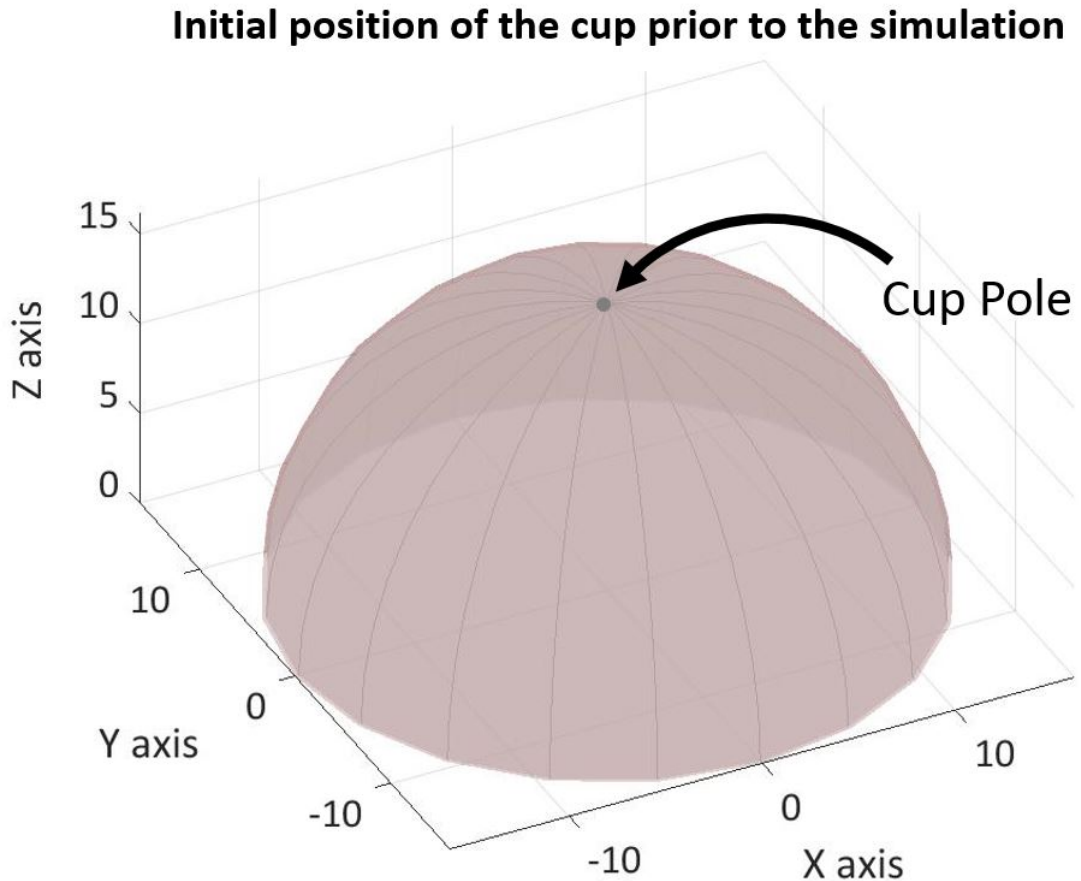


Figure 2.13: The initial position of the acetabular cup within the proximity tool environment.

The order of the rotations was set so that inclination was applied before version. An example of the final position of the cup shown in Figure 2.14. This particular sequence was important, as the version was rotation around Z axis hence, if the cup was lying on the X-Y plane and rotation around Z is applied the normal to the cup plane would not change. The sequence would have to be changed by a future user if the initial position of the cup was changed. Importantly the version here was defined as the three-dimensional rotation around the version

axis rather than the two-dimensional angle, that is usually measured clinically. Hence, the relevant three-dimensional rotations need to be calculated if only two-dimensional angles are available. A radiographic 7° version angle used for the case study, would in fact result in 10° rotation around the three-dimensional version axis. The detailed explanation of the method used to determine two dimensional angle is described in Section 3.2.2 of Chapter 3.

Two rotation methods were considered in this study, the rotation matrix approach and a quaternion approach. The rotation matrix is considered a type of transformation matrix in the Euclidean space. To rotate an object around some arbitrary axis, the object has to be rotated in terms of [X, Y, Z] components of the global coordinate system. The rotation by the means of quaternion is defined by a single rotation around an arbitrary axis fixed at some arbitrary point in the Euclidean space. For applications requiring multiple rotations around arbitrary axes, such as aerospace and robotics, quaternions are most popular choice (Yan et al., 2017). The reason being that quaternion rotations are more compact than rotation matrices, reducing storage space, and also avoid "Gimbal lock". This phenomenon is characterised by loss of degree of freedom, which can occur during the use of rotation matrices (Conway and Smith, 2003). The quaternion approach was chosen, as cup positioning at the initial point the rotation would have to be performed around arbitrary axes.

The inclination was applied first, followed by version. The cup position was defined by normal unit vector to cup plane, which is equal to the unit vector originating at cup origin pointing in the direction of cup pole. Hence, at the initial positioning point cup defining vector was equal to [0, 0, 1]. To generate a new cup position, \vec{v}_{new} , an angle, γ , was applied by conjugation of cup defining vector, \vec{v} and quaternion, q , representing the rotation through the angle around desired axis, $[u_x, u_y, u_z]$ (eq. 2.5).

$$\vec{v}_{new} = q * \vec{v} * q^{-1} \quad (2.5)$$

To apply the desired rotation the three-dimensional vector $[u_x, u_y, u_z]$, was converted to quaternion q using Equation 2.6. Here quaternion is presented in terms of its real part and imaginary parts $[0, i, j, k]$ which represent components of

three-dimensional space.

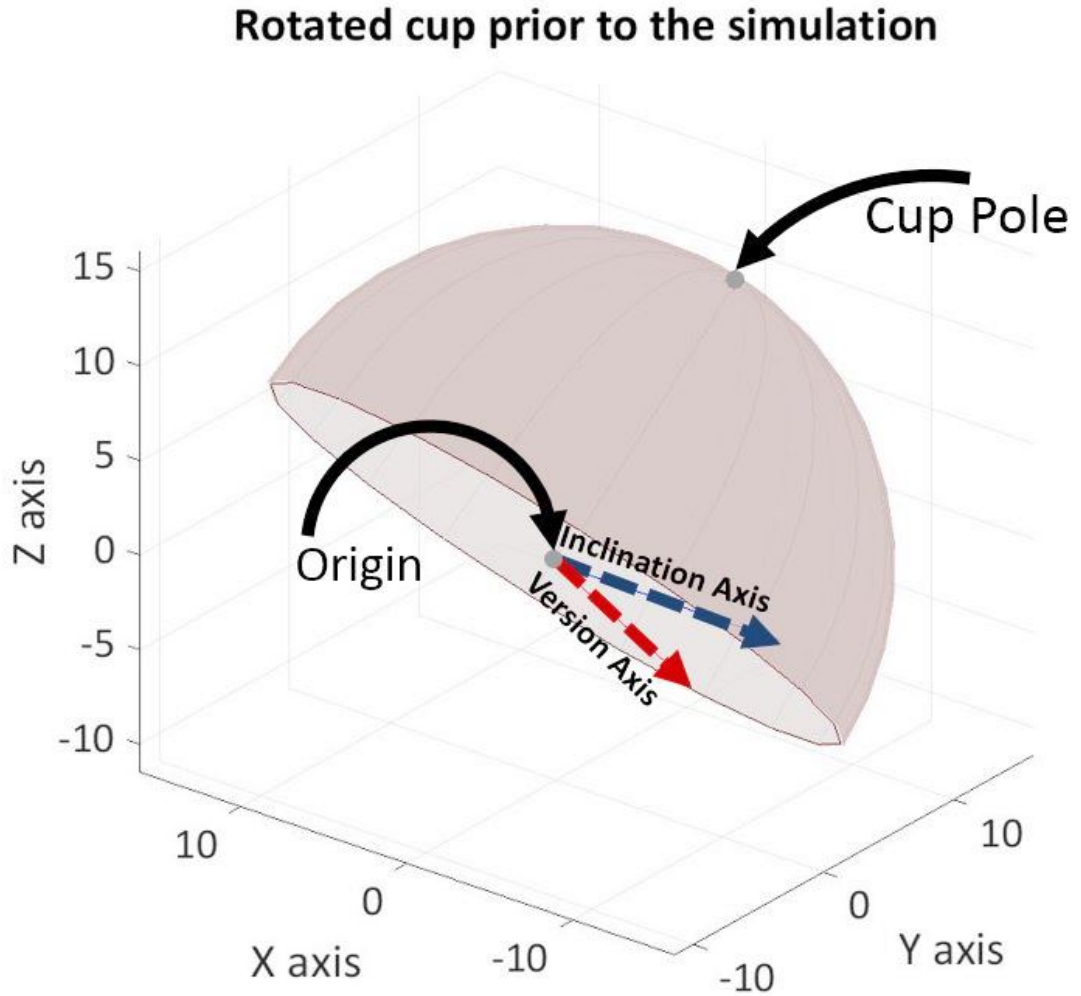


Figure 2.14: Cup positioned within the proximity tool environment using inclination and version angles. Where, X axis is medial-lateral axis and Y is anterior-posterior axis and Z axis is superior-inferior axis.

$$q = \cos \frac{\gamma}{2} + (u_x \mathbf{i} + u_y \mathbf{j} + u_z \mathbf{k}) \sin \frac{\gamma}{2} \quad (2.6)$$

Equation 2.5 was further expanded as explained in study by Yan et al. (2017) using definition of quaternion as shown in Equation 2.7. Here, real part of the quaternion $\cos \frac{\gamma}{2}$ is presented by w .

$$\vec{v}_{new} = [0, (-2w * u_z + 2u_x * u_y) \mathbf{i}, (w^2 - u_x^2 + u_y^2 - u_z^2) \mathbf{j}, (2 * w * u_x + 2u_y * u_z) \mathbf{k}] \quad (2.7)$$

The axes definitions for inclination and version rotations are presented in Figure 1.11, which were defined at initial position as unit vectors. The inclination axis was defined by unit vector $[0, 1, 0]$ and version axis was defined by vector $[1, 0, 0]$ at the initial set-up point. The version axis will change its orientation after the inclination is applied as seen in Figure 1.11, so it is always on the cup face. These axes will depend on the global coordinate system definition of the biochemical gait data study.

2.6.5 Detailed description of the data-specific algorithms used in the proximity tool for the addition of the pelvic motions into the simulation

As illustrated in Figure 2.7, the pelvic motion addition was separated into two parts. First, the dynamic pelvic coordinate system was generated for each gait cycle point and second, the force vector was expressed in terms of that coordinate system. As the datasets, HIP98 and LBRC, are different in nature the dynamic coordinate system generation had to be adapted for each data type. The starting position for simulation of the pelvic coordinate system was identified to be identical to the global coordinate system, due to the lack of information in the dataset on the cup position in relation to the pelvis position. Hence, cup position shown in Figure 1.11 was used as the start of simulation for the cases studies in the scope of this chapter.

Algorithm for dynamic pelvic coordinate system construction using joint centres location

This algorithm was developed for processing of the joint centres location for each gait cycle point. The provided in HIP98 hip joints centres and pelvis centre coordinates in the laboratory space during the activity were used within this algorithm. Each of these centre serves as the reference point for dynamic pelvic coordinate system generation. For the HIP98 (Bergmann, 2008) dataset the image origin was set by authors to coincide with acetabular cup centre. Medial-lateral axis, x_p , was defined as the one connecting the left and right hip joint centres. The vertical axis, z_p , was set to be perpendicular to x_p axis and coincide with L5-S1 junction projection on the anterior-posterior plane of the image. And the anterior-posterior axis, y_p , was set to be perpendicular to those defined previously. Equation 2.1 was used to ensure the orthogonality between the axes. As the pelvic system is dynamic throughout the gait cycle this step was set to be repeated for each gait cycle point. The algorithm was designed so it can be tailored for other definitions of coordinate system that describes the motions of pelvis as long as it's origin is at the origin of the acetabular cup.

Algorithm for dynamic pelvic coordinate system construction using measured pelvic angles

A separate algorithm was developed for the data where the two-dimensional angles were available. In this algorithm, the pelvic coordinate system at time point zero was set to be identical to global coordinate system. The algorithm was designed such that each two-dimensional angle was applied to pelvic coordinate system at every gait cycle point. The aforementioned quaternion approach, Section 2.7, was used to apply the angles. However, the rotations *in vivo* are happening simultaneously, as one rotation around some dynamic arbitrary axis. As the motions in conventional biomechanical studies are expressed as two-dimensional angles this arbitrary axis is unknown. To achieve the simultaneity, for each time point the angles representing three pelvic motion rotations were set to be executed in small steps, iteratively.

For example, let the angle of pelvic tilt at particular time point was equal to θ pelvic obliquity to γ and pelvic internal-external rotation to ω and number of iteration was chosen to be n . Then the sequence would look like $[\frac{\theta}{n}, \frac{\gamma}{n}, \frac{\omega}{n}, \frac{\theta}{n}, \dots, \frac{\omega}{n}]$ until the sum of iterations would reach the whole rotation for the given time-point.

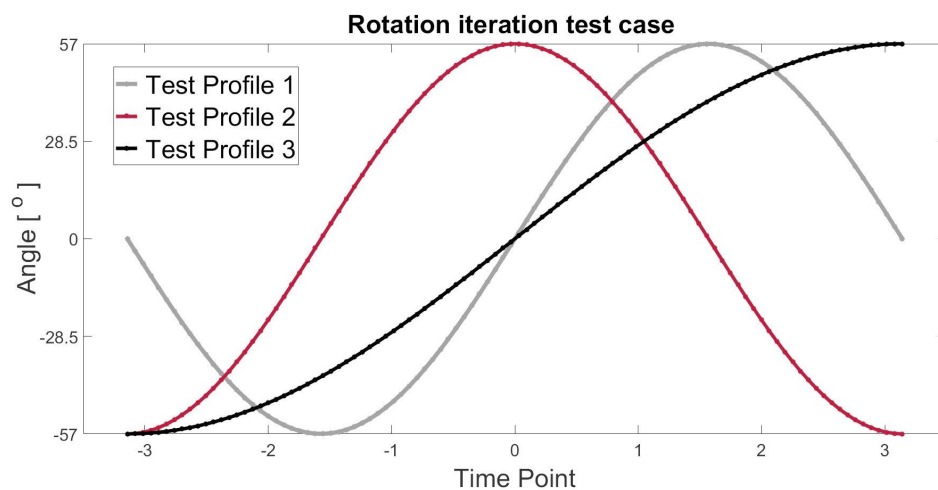
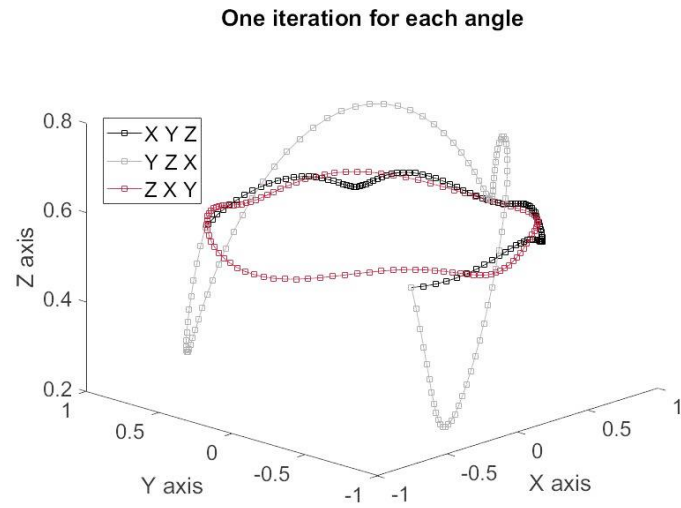
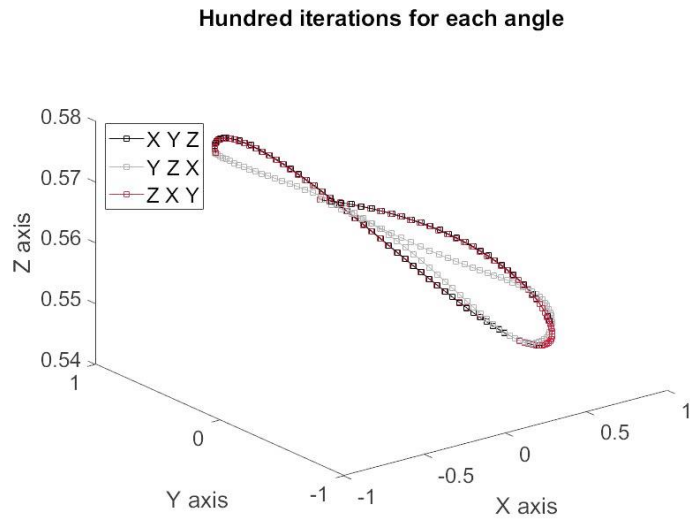


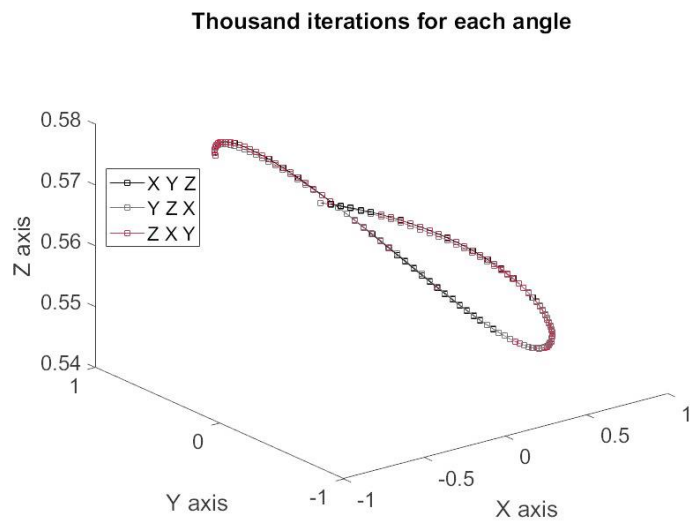
Figure 2.15: Custom profiles, sine waves, to test the dynamic pelvic coordinate system rotation order and iteration count



(a)



(b)



(c)

Figure 2.16: Rotation test with variable step iterations per each angle. The outputs are generated using angle profiles in Figure 2.15.

Before the integration of this algorithm into the proximity tool the test case was created. The rotations were performed around three axes $[x, y, z]$ of the global coordinate space (Figure 2.16). The method algorithm was tested using three profiles shown in Figure 2.15, where profile 1 was rotation around x-axis, profile 2 around y-axis and profile 3 rotation around z-axis. The arbitrary point, $[1, 0, 0]$, was rotated in space around each global coordinate system axis using three test profiles. Each angle per time-point of each curve was subdivided into 1, 100 and 1000 iterations. The example of 1 iteration, 100 iterations and 1000 iterations is shown in 2.16a, 2.16b and 2.16c. For this example required number of iterations to achieve simultaneity should be above hundred iterations. However, the number of iterations is specific to the angle profile range and their combination.

The test case revealed that variation in the order of the rotation results in different final position of the reference point, or different coordinate system final position, when implemented into the proximity tool. For all patients in LBRC data the number of suitable iterations, 10, was derived by testing the final position of arbitrary point, $[1, 0, 0]$, with variable order of rotation for pelvic motion data. To identify number of iterations for all the patients in dataset, data for 5 randomly selected patients' was used. The number of iterations was defined using pelvic motion data for patient 001 from LBRC dataset, as seen in Figure 2.17. Figure 2.18 shows that even at one iteration the angular profiles of the reference point are more alike compared to the test case, which explains the reduced number of iterations. The reason for this difference between required iterations is the range of the motion for profiles, between the test case, 114° , and LBRC patient case, 8° .

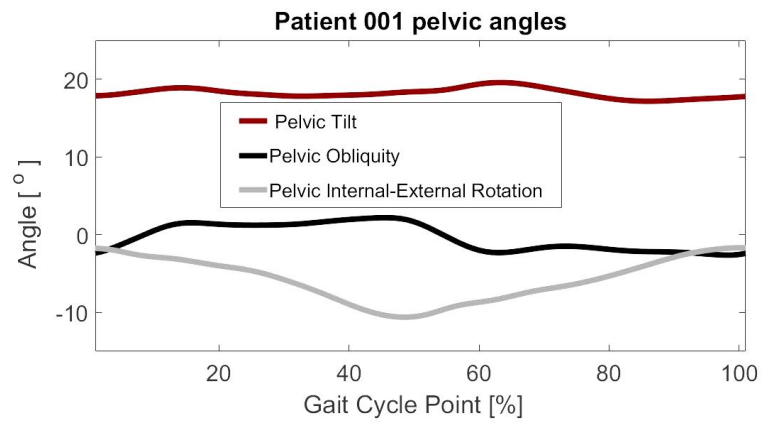


Figure 2.17: Patient 001 (LBRC) two-dimensional angle profiles for pelvic motion through the gait cycle.

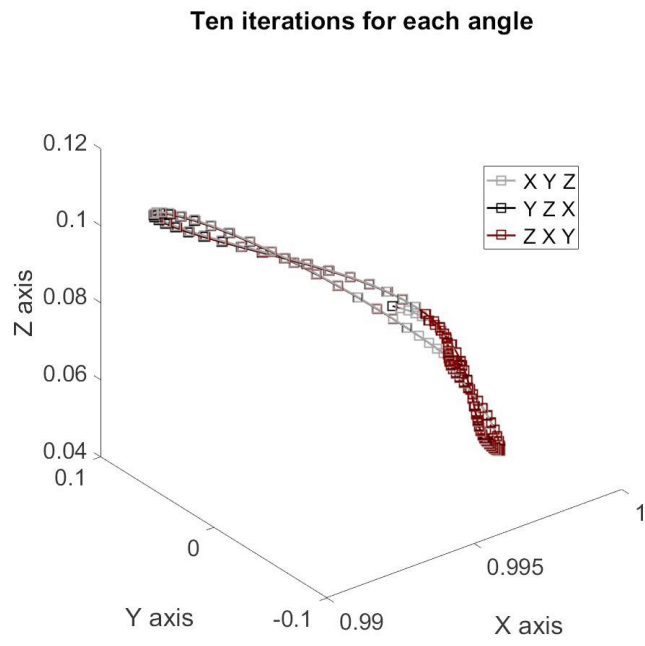
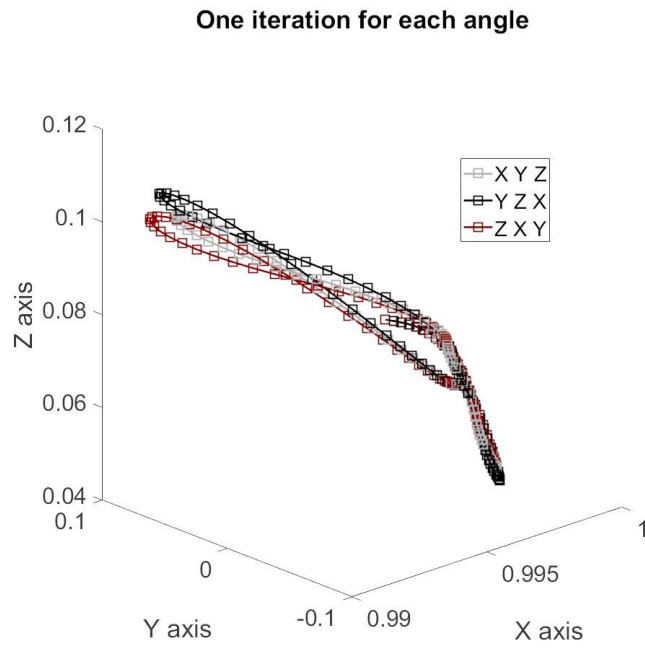


Figure 2.18: Rotation test with variable step iterations per each angle for patient 001 from LBRC dataset. The rotations were applied around three axes x, y, z for vector [1, 0, 0]. (a) one rotation iteration, (b) 10 rotation iterations.

Expression of force vector in the dynamic pelvic different coordinate system

To suit both methods instead of rotating the cup defining vector through the activity cycle, the force vector was rotated in relation to the motion of pelvis. To achieve that the force vector was translated into the dynamic pelvic coordinate system for each activity cycle point. Each component of the force vector $[x_f, y_f, z_f]$ was projected onto the related axis of the new dynamic pelvic coordinate system according to Equation 2.8. Here a is vector to be projected and u is axis to be projected on. The combination of three projections would give coordinate of three-dimensional projection of the force vector in dynamic pelvic coordinate system.

$$v_{proj}^{\rightarrow} = \frac{a * u}{|u|^2} * u \quad (2.8)$$

The new force unit vector, v_{proj}^{\rightarrow} , was composed from $[\cos \theta_x, \cos \theta_y, \cos \theta_z]$ according to direction cosines rule (Weisstein, 2018b) where θ is angle between force unit vector and coordinate system axis.

Verification of the algorithm for force vector expression in the variable coordinate systems

To verify the projection algorithm a test vector defined as $[1, 1]$, was originally set up in the coordinate system where x-axis was set to $[1, 0]$, y-axis to $[0, 1]$. Using the method described above, the test vector was expressed in terms of new coordinate system where x-axis was set to $[1, 0]$ and y-axis to $[0, -1]$. Unit vector of the test vector was found to be equal to $[0.7071, 0.7071]$. The projection of this unit vector on the x-axis was found to be 0.7071 and on the y-axis -0.707 , hence the coordinates of the new unit vector were found to be $[0.7071, -0.7071]$. Resizing the new unit vector by the magnitude of the test vector, 1.4142 gave the coordinates of the new vector in relation to the new coordinate system $[1, -1]$. Figure 2.19 shows the vector viewed in the original coordinate system, left, and in the new coordinate system, right.

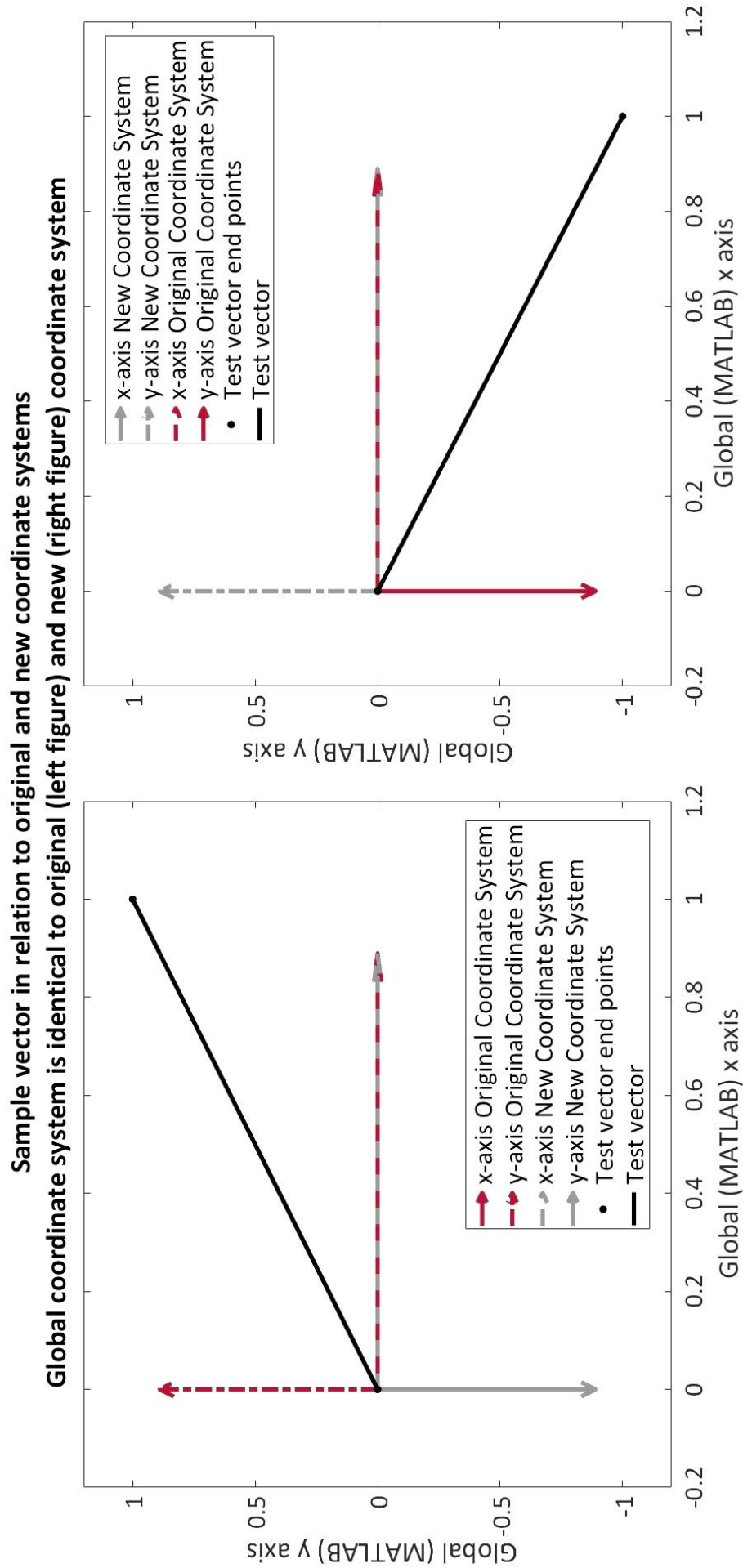


Figure 2.19: 2D sample vector expression in relation to two different 2D coordinate systems.

2.6.6 Orientation of the contact along the acetabular cup rim

An additional algorithm was developed to identify the location of the force vector along the rim. This algorithm can be further used to establish the potential damage location caused by edge contact, as when studying damage on cup retrievals it is not always clear on the causes of damage.

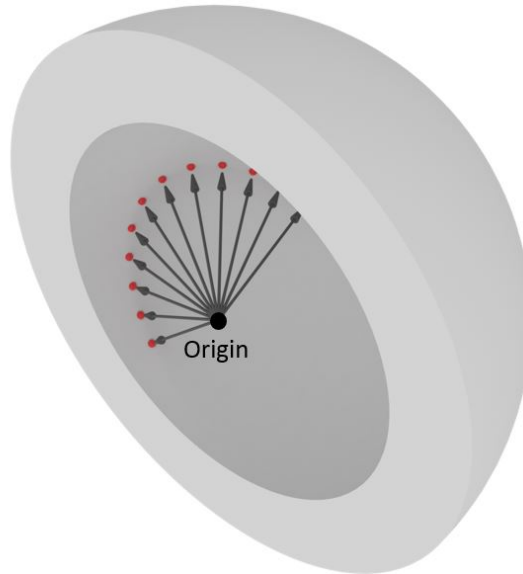


Figure 2.20: The schematic of acetabular cup with the contact force path through the arbitrary activity cycle. The red dots are the locations of the centre contact within the cup, the grey arrows are contact force vectors which cover the centre contact location.

The location of the force vector at every time-point within the acetabular cup was also recorded as the contact centre track as seen in Figure 2.20. To ensure that the force vector was projected onto the acetabular cup plane according to Equation 2.9, where \vec{v}_{force} is the force vector to be projected and n_c is the cup defining vector, or cup plane normal. An additional vector, \vec{v}_{sup} , was defined which represented the most superior point of the cup point at original cup positioning 1.11 (This vector was constructed by rotating version axis 180° in the cup plane). The angle between reference vector, \vec{v}_{sup} , and projected force vector, \vec{v}_{proj} , was used for evaluation of contact region along the rim using Equation 2.1, where v_1

and v_2 are \vec{v}_{sup} and \vec{v}_{proj} respectively.

$$\vec{v}_{proj} = \vec{v}_{force} - \frac{\vec{v}_{force} \cdot n_c}{|n_c|^2} n_c \quad (2.9)$$

For reference purposes, the cup was separated into four quadrants encompassing 90° angular distance (Figure 2.21). The angle between two vectors, θ , from -180° to -90° represents fourth (IV) quadrant, from -90° to 0° represents first (I) quadrant, from 0° to 90° represents second (II) quadrant and from 90° to 180° represents third (III) quadrant.

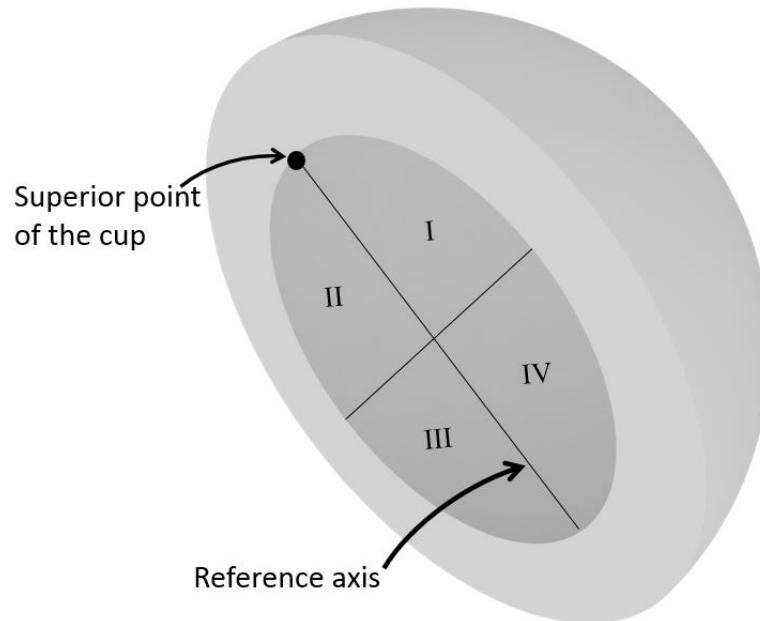


Figure 2.21: The schematics of acetabular cup implanted on the right side. I, II, III, IV regions marked for assessment of rim damage location. (I) quadrant is superior-anterior region, (II) quadrant superior-posterior, (III) quadrant is inferior-posterior and (IV) quadrant is for inferior-anterior.

2.7 Proximity tool testing for one patient from each dataset

The proximity tool was tested upon the development completion using one patient from each of the datasets used in the development process. The proximity angles were measured in degrees and round off to whole number to account for maximum mesh convergence error of 0.5° (Section 2.6). Walking at self-selected speed was the chosen activity for the tool testing. Both patients were chosen so that they had similar demographics to each other. The HIP98 patient, HSR, was assigned to be *Case 1* and LBRC, patient 001, was set to be *Case 2*. The demographics data for those patients is presented in Chapters 3 and 4. Two scenarios were simulated first, when three pelvic motions were included and second, when three pelvic motions were excluded. Both centre and edge proximity angles were measured. During both cases the tool was set to apply cup angles of 45° inclination and 7° version which are within common *safe zone* positioning angle guidelines (Callanan et al., 2011).

An additional *Case 1a* was performed using two available pelvic motions in the HIP98, using the pelvic motion algorithm described in Section 2.6.5. This was the algorithm using two-dimensional pelvic angles, which was developed based on LBRC data. This was done to check that both algorithms for the pelvic motion application worked in a similar way, and did not produce unreasonable results. For this case also, both centre and edge proximity angles were measured and initial cup position was 45° inclination and 7° version.

Finally for both *Case 1* and *Case 2* the observations on the risk of edge contact and effect of pelvic motion on the risk of edge contact were discussed.

2.7.1 Case 1: HIP98 patient

The results for *Case 1* are presented in Figure 2.22, red curves are the output for the first scenario where three pelvic motions are included. The black curves are for the output for the second scenario, where three pelvic motions are excluded from the simulation. The solid curves are for centre proximity angles, and dashed curves are for edge proximity. The distance between the centre proximity angle

and edge proximity angle for one instance represents the magnitude of the contact area half, and hence gives an idea on the highest force regions. The increase in contact force magnitude results in increase in contact area (Section 2.6.3).

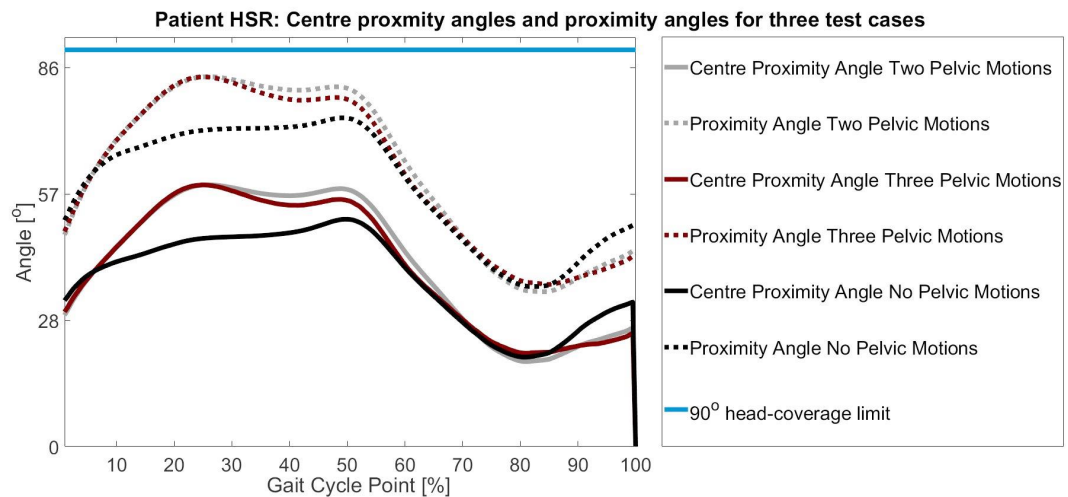


Figure 2.22: Case 1 and Case 1a, patient HSR output of the proximity tool for three simulation scenarios. Three pelvic motions (red), no pelvic motions (black) and two pelvic motions (grey). The blue line marks the rim of the cup with head-coverage angle of 180° . The dotted curves are for edge proximity angles and solid centre proximity angles.

It can be seen from Figure 2.22, case 1, that for patient HSR the pelvic motions included, in red, showed higher risk of edge contact than pelvic motions excluded, in black. The risk of edge contact was higher during the stance phase for both simulation scenarios, pelvic motions included and excluded. As it can be seen from Figure 2.22 the maximum proximity angles are consistent with the regions of highest contact force. The maximum centre proximity angle for the first scenario was 60° , and edge proximity was 84° . For second scenario, the maximum centre proximity angle was equal to 51° , and 74° . The location of maximum proximity angles throughout the stance phase changed between pelvic motions included and pelvic motions excluded scenarios.

Finally, it can be seen from Figure 2.22 that proximity angles curves, both for centre and edge of contact, resemble the two-peak contact force curve. This pattern is more prevalent for first simulation scenario, where pelvic motions are

included into the simulation.

2.7.2 Case 2: LBRC patient

The same analysis as for *Case 1*, was performed for *Case 2*. Figure 2.23 shows the output for both centre and edge proximity angles. For this figure the same color-coding as for *Case 1* was used.

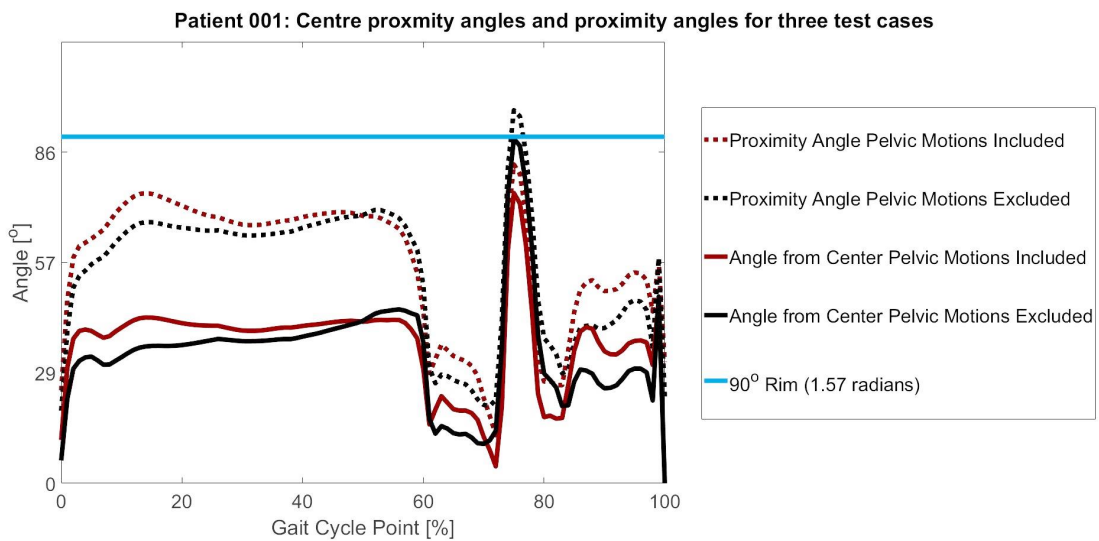


Figure 2.23: Case 2, patient 001 (LBRC) output of the proximity tool for two simulation scenarios. Three pelvic motions (red), no pelvic motions (black). The blue line marks the rim of the cup with head-coverage angle of 180° . The dotted curves are for edge proximity angles and solid for centre proximity angles.

It can be seen from figure 2.23 that for patient 001 the exclusion of pelvic motions decreases both centre and edge proximity angles for the most of stance phase. However, for the stance phase region 51% onwards the exclusion of pelvic motions slightly increased the risk of edge contact, both centre proximity and edge proximity. The risk of edge contact was higher during the stance phase for both simulation scenarios, pelvic motions included and excluded, except for sharp peak during the swing phase at 78% gait cycle. Apart from that, the maximum proximity angles are consistent with the regions of highest contact force. The maximum centre proximity angle for the first scenario was 42° , and edge proximity was 74° during stance phase. For the second scenario, these angles were equivalent to 45° and 73° for centre and edge proximity respectively. The location of maximum proximity angles throughout the stance phase changed

between pelvic motions included and pelvic motions excluded scenarios.

Similar to *Case 1*, the proximity curves during swing phase represented the two-peak contact force curve. For *Case 2*, this pattern is more prevalent for edge proximity angles. This can be explained by the contact area and contact force relationship.

In terms of swing phase, it is uncertain if these results are actually representative of *in vivo* contact locations. This is because during swing phase there is no force platform data, as the leg is off the ground, and the forces generated by the muscle activations are assumed (Jim, 2008). These forces are very close to zero and hence any small deviation would result in sudden direction change. Hence, in the further analysis of LBRC data the swing phase was not considered.

2.7.3 Case 1a: HIP98 patient, two motions

The algorithm verification test is shown in Figure 2.22 in grey for both centre and edge proximity angles. The results did not show huge difference between three pelvic motions included and two pelvic motions included. This, suggests that both algorithms developed for pelvic motion application in the tool are working. This can only be properly verified if the all three pelvic motion angles are known, which is not the case for HIP98 data. The certainty in both algorithms function was previously tested by the tests cases in Section 2.6.5.

In terms of data analysis, the difference between three and two pelvic motions included scenarios suggests that the third motion, which in this case is internal-external rotation, decreases the risk of edge contact in the second half of the stance phase. This type of analysis was used within this thesis (Chapter 4), to test which pelvic motion or combination of two motions contributes to the overall, three, pelvic motion effect on the risk of edge contact.

2.7.4 Initial patient-specific analysis

In summary, two gait profiles from two patients were analysed within this preliminary study. It was found that for both patients pelvic motions substantially

affect the contact location between total hip replacement bearings. The pelvic motion exclusion from the simulation resulted in a change in the risk of edge contact, and also the location of maximum edge contact risk throughout the gait cycle.

Comparing two patients within this study, shows that for pelvic motions included scenario the risk of edge contact was higher for patient from HIP98 dataset, than for patient from LBRC dataset. This was despite the equivalent cup orientation at the the initial set-up between two cases.

In addition, for all the cases within this preliminary study the run-time of the simulation was just below 1 minute per scenario, where the simulations were performed on a desktop PC with Intel® Xeon® at 3.5GHz with 12 logical processors and 32GB of RAM.

2.8 Summary of proximity tool development and usage

Edge contact was previously shown to affect component performance *in vivo* by analysing the THR retrievals and through the *in vitro* studies (Williams et al., 2003; Tower et al., 2007). However, current "safe zone" positioning studies mostly take into account clinical cases for dislocation and painful impingement (McLawnhorn et al., 2015; Lewinnek et al., 1978), neglecting edge contact and other mechanisms (Chapter 1, Section 2.3.1). The current study was aimed to develop a feasible method to address some of these gaps using patient-specific biomechanical activity data in relation to the risk of edge contact.

2.8.1 Tool capabilities and study achievements

1. Developed tool establishes the contact location within the acetabular cup in relation to the rim of the THR cup. The closer contact is to the rim the higher the risk of edge contact;
2. Compared to finite element simulations, the current tool is more time-efficient. The run-time of the finite element model used to establish the contact area and contact force relationship was just under 54 minutes, compared to 1 minute for proximity tool simulation on the same computer. This gives the current tool an advantage in rapid data processing involving large patient cohorts;
3. Tool also allows for processing of biomechanical activity data measured with variable techniques, and with different format of the motion data;
4. Tool allows to separate assessment the effect of joint contact forces, pelvic motions and acetabular cup orientation on the risk of edge contact;
5. Tool can be used to identify patients at most risk of edge contact, or to identify a set of activity features that greatly contribute to the risk of edge contact.

2.8.2 Limitations and considerations of the tool

1. Developed tool allows for estimation of edge contact, but does not provide

a measure of edge contact severity. A finite element model would need to be used to identify those parameters, after the activity profiles of most interest are identified;

2. There is a level of uncertainty from the finite element mesh resolution which was used to establish contact area and contact force relationship. This error only affects the edge proximity results. The uncertainty error was shown to be no more than 0.5° . Hence, the difference in edge proximity results of more than $\pm 0.5^\circ$ would not be substantial;
3. Proximity tool at its current settings is for a ceramic-on-polyethylene combination, and specific radial clearance. The error in contact area and contact force relationship found for current radial clearance compared to other relevant clearances 1.4° and 4° . This is more substantial than finite element mesh error. Hence, for the other material combinations and clearances to the ones used within this work, the new contact force and contact area relationship would have to be derived;
4. Both results for centre and edge proximity are affected by uncertainty and variability in the motion and force capture methods. Hence, in the studies presented in this thesis the three-trials will be used where possible to account for the errors associated with data capture.

2.8.3 Upcoming studies and future uses of the tool

In the upcoming studies described in this thesis the tool was used to analyse both datasets, HIP98 and LBRC. The tool was used to evaluate multiple aspects of gait that influence the risk of edge contact on the patient specific basis. The sub-studies that were performed using the proximity tool are listed below:

1. Comparison between the centre proximity angles generated with and without the addition of pelvic motions, both from the patient-specific and activity-specific perspective.
2. Comparison of centre proximity results generated on a patient-specific basis to the ones generated for *in vitro* testing profiles.

3. Location of possible damage along the rim between various activities, and in comparison to *in vitro* test profiles.
4. Effect of each pelvic motion and combination of two pelvic motions on the overall effect of three pelvic motions on the risk of edge contact.
5. Role of static pelvic orientation on the the overall effect of pelvic movement on the risk of edge contact.
6. Dependence of patient-specific characteristics and demographics on the risk of edge contact in THRs.

In and beyond the scope of the work described in this thesis, the analysis performed with the tool can contribute to the development of new *in vitro* testing protocols, based on the patient-specific data. Secondly, the data gathered using the tool can contribute to evaluation of suitable component orientation, again on patient-specific basis. Lastly, the output of the tool can aid in distinguishing edge contact associated damage during the analysis of the *ex vivo* THR acetabular components.

Chapter 3

The investigation into risk of edge contact with patient and activity variability

3.1 Introduction

This chapter describes the analysis of patient-specific activity data processed through the developed proximity tool. The tool's development process is detailed in Chapter 2 of this thesis. The HIP98 OrthoLoad[©] (Bergmann, 2008) database was used to acquire the relevant data for this study. The study was composed of data processing and qualitative analysis of the generated data for edge contact risk. This chapter also includes suggestions for further studies, and limitations for the current one.

The main aim of this study was to investigate of the patient specific gait characteristics influence on the risk of edge contact during different daily activities. Possible applications of the proximity tool's output data for the enhancement of THR pre-clinical testing were also addressed. The current study was split into three sub-studies. The first sub-study was covering the risk of edge contact across the activities and patients. The second sub-study was focused on the assessment of the effects caused by exclusion of pelvic motions from the activity data on the estimation of risk of edge contact. The final sub-study was based on comparison of patient proximity tool data to the output of the tool under force and alignment conditions typically used in *in vitro* testing. The aforementioned sub-studies contribute to the overall aim of the PhD project of establishing the effect of patient or population gait variation, in terms of rotations and forces in THR on the risk of edge loading.

3.2 Patients and general methods

3.2.1 Patient selection and description

The data used in this study was acquired from OrthoLoad[®] (Bergmann, 2008) website, from HIP98 database. The total number of patients was four. The data for this study included pelvic motions, hip joint contact forces, hip joint centre coordinates and pelvic centre coordinates. All data was extracted in respect to the laboratory coordinate system. Detailed information about nature of data in HIP98 set is provided in Chapter 2, Section 2.3.1.

The patient data which was used as an input for current study is presented in table 3.1. The names by which patients are referred to were HSR, PFL, KWR and IBL, with the same abbreviations used in the current study. According to Bergmann et al. (2001) three out of four patients had osteoarthritis as their primary cause for THR and for one patient it was femoral head necrosis. Patient IBL had a THR in both hip joints. In addition, this patient had asymmetrical gait due to pain in opposite side to instrumented THR joint. In total, nine activities were performed across the patients which are listed in table 3.1. The activities included walking with self-selected speed, walking fast and slow, ascending and descending stairs, rising up from the chair and sitting down on the chair, as well as standing on *two-one-two* legs and bending knees. Not all patients performed every activity. Table 3.1 displays the activities performed by each patient and number of trials available for each activity.

Figure 3.1 shows the magnitude of patient's resultant contact forces for every patient and across the daily activities analysed in this study. The gait cycle curves for all walking modes, displayed both double load peak profiles as well as single peak load profiles (Figures 3.1a - 3.1c). Similar to gait, the regions during stair ascent and descent were split into toe-off, mid-stance and heel-strike. The region split was done with assistance of video-recordings provided with HIP98 data. The beginning of rising from the chair and end of sitting down on the chair cycles corresponds to patient being fully seated on the chair.

Table 3.1: Detailed patient demographics and cup orientation information for HIP98 dataset. Number of trials for each activity is displayed next to activity name.

Patient	HSR	PFL	KWR	IBL
Gender	Male	Male	Male	Female
Age at Implantation [years]	55	51	61	76
Operated Joint	Right	Left	Right	Left
Total Body Weight [N]	860	980	702	800
Cup Inclination [°]	42	59	46	43
Cup Version [°]	28	18	11	22
Cup Rotation for Version [°]	19.5	15.5	8	15.5
Activity	Trials per patient			
Walking	3	3	3	3
Walking Fast	3	3	3	×
Walking Slow	1	3	3	×
Stairs up	3	2	3	3
Stairs down	3	1	3	×
Chair up	3	3	3	3
Chair down	3	3	3	3
Standing	3	3	3	×
Knee bend	3	3	3	×

Each patient from Bergmann et al. (2001) had a 32mm diameter ceramic-on-polyethylene instrumented THR implant. For each patient, both acetabular cup version and inclination angles were provided from three-dimensional CT supine scans. The inclination angle was measured by that group as a projection of acetabular cup rim centre-line onto the coronal plane. Similarly, the acetabular version angle was measured as projected acetabular rim centre-line onto the transverse plane of the CT scan.

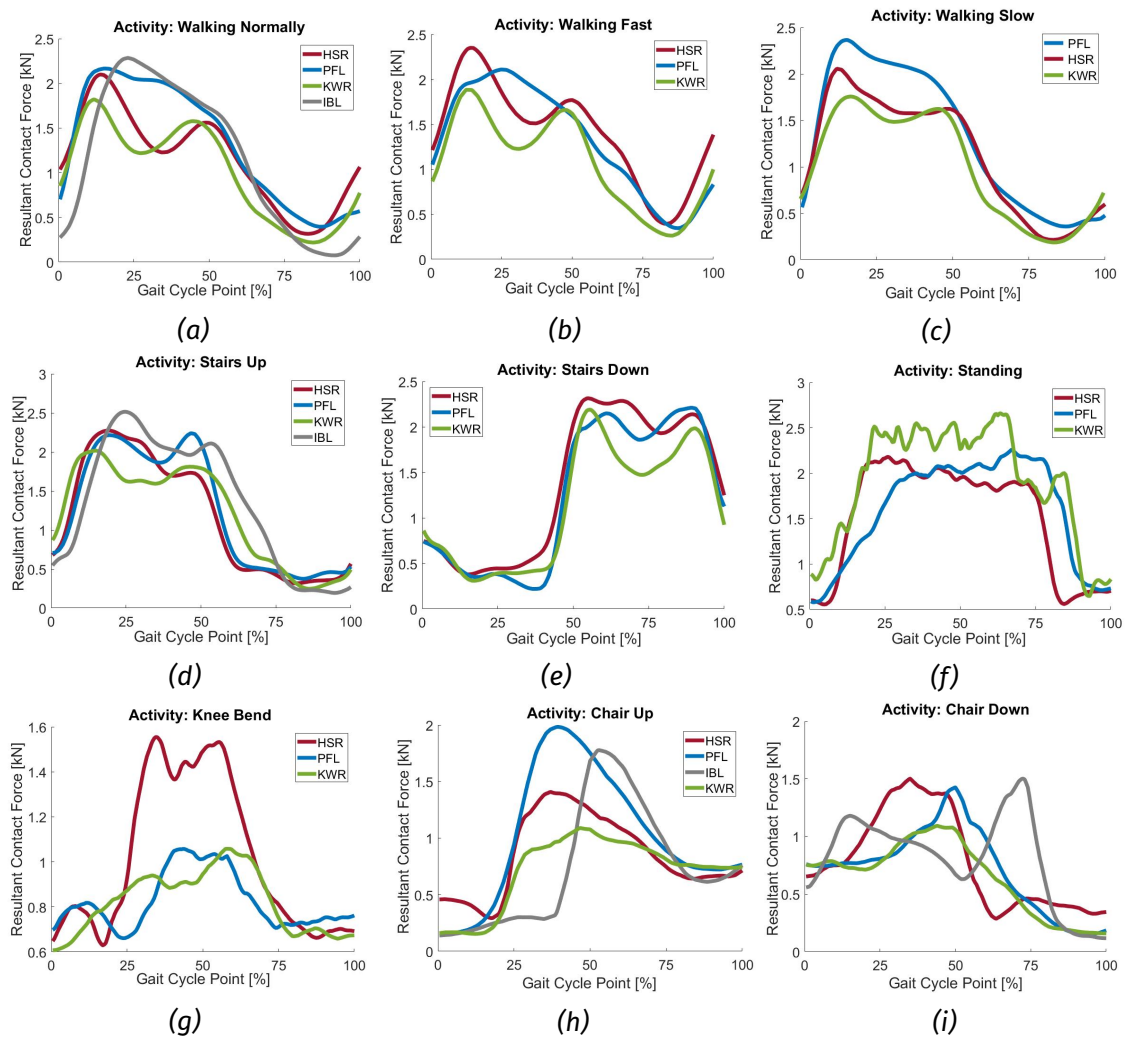


Figure 3.1: Magnitudes of resultant contact force for all nine activities for each HIP98 patient. The contact force profiles are averaged out from trials per activity per patient, where available multiple trials are available.

3.2.2 Cup positioning reference table development

According to Section 2.6.4 of Chapter 2 the inclination was applied first hence will actually represent the measured projected inclination angle. To ensure that appropriate rotation was applied for projected version angle, a specialised look-up table was compiled. Figure 3.2 shows the inclination and version angles which correspond to the ones measured in HIP98 database (Bergmann, 2008) from CT scans.

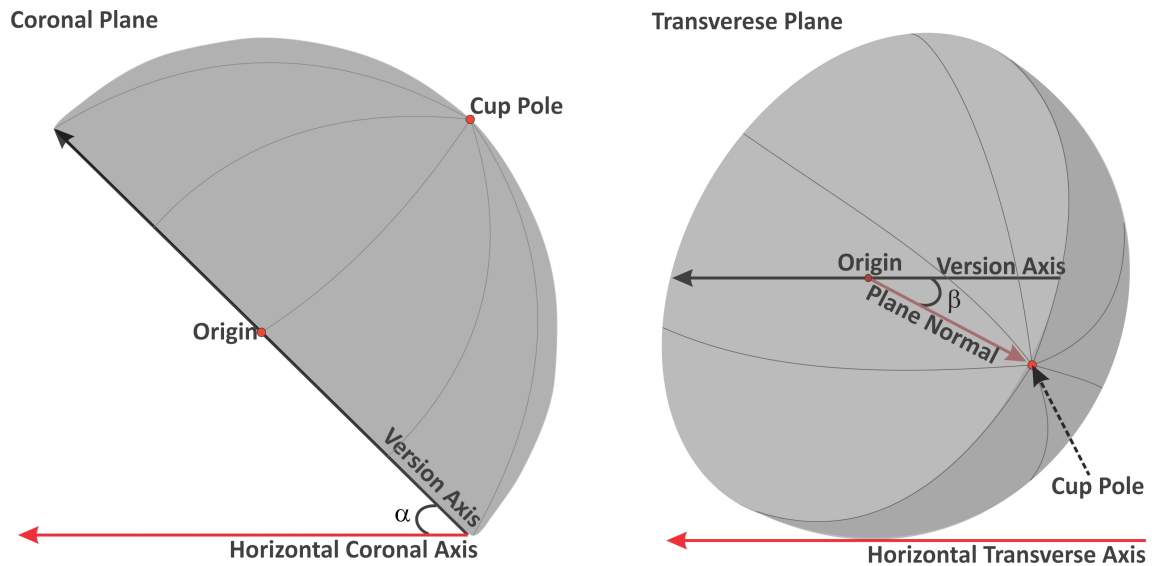


Figure 3.2: Cup orientation schematics for creation of reference table, which combined two-dimensional inclination and version angles, and rotation which has to be applied to get the desired version angle. Cup in the transverse plane, on the right, is pictured from above and is semi-transparent for visualisation purposes. Angle α is for inclination angle, β is for version angle. Version axis is used to apply rotation which produces the two-dimensional version. Version axis in transverse plane is parallel to horizontal axis of the transverse plane.

The table displayed in Appendix A was developed by applying set of inclination and version rotations to encompass range of cup orientations in the HIP98 data. The schematics of cup orientation measurements are presented in Figure 3.2. Applied rotations were from 40° to 70° for inclination angle α , and from 20° to 35° rotations around version axis shown in Figure 3.2. Each inclination rotation was paired with each rotation around version axis. The two-dimensional version angle, β , was found as the angle between normal of the cup's rim plane and version axis projected onto transverse plane of the global coordinate space. The projected version axis was parallel to horizontal axis of the transverse plane. The projection was performed using Equation 3.1, where v is the vector to be projected, v_p is the projection of this vector and n_p is normal to the transverse plane which in this study is defined as $\begin{bmatrix} 0 & 0 & 1 \end{bmatrix}$. The angle between two projected vectors was found from Equation 3.2, where va_p is projected version axis and n_{cr} is the normal to cup rim. The results are summarised in Table 3.1 under *Cup*

Rotation for Version heading.

$$v_p = v - \frac{v \cdot n_p}{|n_p|^2} n_p \quad (3.1)$$

$$version_{2D}^{\vec{}} = \cos^{-1} \left(\frac{v\vec{a}_p \cdot n_{cr}^{\vec{}}}{|va_p| |n_{cr}|} \right) \quad (3.2)$$

There was an assumption that during the cup positioning that the global coordinate system was identical to the imaging coordinate system and laboratory coordinate system, this was due to no specified relationship between the later two.

3.2.3 Study set-up and considerations

For this study proximity tool developed in Chapter 2 was used. To establish the effects of variable daily activity features the proximity tools' version (Section 2.6.5, Chapter 2) for implementing joint and pelvic centres location was used. Three types of output were generated for each activity and patient. First output was the angle between cup pole and centre of the theoretical contact area, or centre proximity angle. Second output was the angle between cup pole and furthest edge of contact area, or edge proximity angle. Finally, the third output was the angle between most superior point of the cup, during initial positioning, and location of the maximum edge proximity angle along the rim of the cup. Angular distance between the centre and edge proximity angle illustrates the size of contact area half (Chapter 2, Section 2.1). A large contact area would signify higher contact forces. The acetabular cup was assumed to have head-coverage angle of 90° , hence the proximity angles equal or above the head-coverage value would indicate edge contact event. Contact forces were used to derive the contact force versus contact area relationship for the proximity tool (Section 2.6.3, Chapter 2).

3.3 Risk of edge contact for patients across all activities

The first sub-study was aimed to identify the risk of edge contact for all patients and across all the activities. Patients were not compared to each other in terms of proximity angle magnitudes due to variation in cup orientation. Instead, the most at risk of edge contact activities were identified. The findings of this sub-study were used to define the selection criteria for second sub-study described in Section 3.4.

3.3.1 Method

Results for each of the four patients were analysed separately. Activities were separated into locomotor and non-locomotor ones. Walking, going up and going down the stairs were counted as locomotor activities. Sitting down on the chair, rising from the chair, bending knees and standing up were defined as non-locomotor. The analysis included a description of edge proximity angles and evaluation of maximum edge proximity angles for a scenario where pelvic motions were included. The analysis was performed only for outputs when pelvic motions were included in simulation as this case represents the *in vivo* conditions of a THR more closely than when pelvic motions were excluded from the simulation. For each activity, three trials, when available, were taken into account to define the average of the edge proximity angles for each activity cycle point as seen in Figure 3.3 dashed black curve. For the purpose of this sub-study the average edge proximity angle was referred to as edge proximity angle.

In addition, for every patient the region of high proximity angles and the associated contact forces were analysed, including the force and gait cycle point for each maximum proximity angle. Figure 3.3 shows an example output for the current sub-study, where edge proximity results are presented along side resultant contact force. The maximum edge proximity angle and maximum contact force are also marked in the Figure 3.3.

Additional bar charts were presented for each patient that allows comparison of risk of edge contact between activities. All the activities across the patients

were analysed in terms of the edge contact risk, using maximum and mean of average edge proximity angles. Mean edge proximity angles were used to assess the duration of high edge proximity angles, the higher mean angle is in relation to maximum proximity angle the longer was the duration of the high proximity angles.

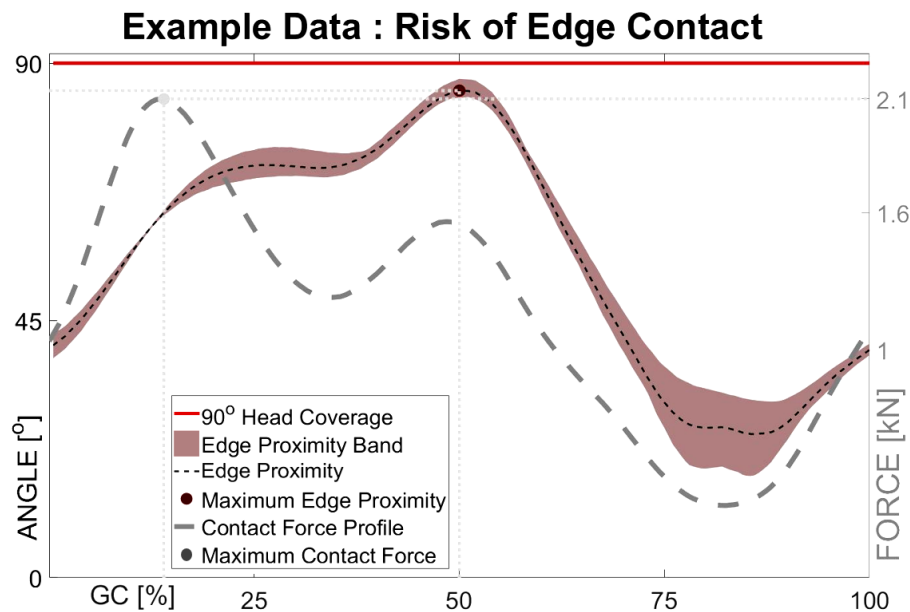


Figure 3.3: Example of output for sub-study 1 of HIP98 data analysis. The Figure presents the edge proximity angles and resultant contact force magnitude during one activity cycle for one patient. Plot also shows maximum edge proximity angle and maximum contact force during the cycle. Pale-dashed grey lines are for navigation purposes.

3.3.2 Results

Results for edge proximity angles are presented in Table 3.2, where the maximum edge proximity angles are summarised for each patient and activity. These values will be further discussed in detail.

*Table 3.2: The proximity result comparison between different patients and activities. PA - angle measured in degrees [°], for maximum edge proximity angle. In square brackets, A.C. is for gait cycle instance of the maximum proximity. F_p - contact force of maximum proximity angles, F_{max} - maximum contact force during activity cycle. * symbolises edge contact occurrence.*

Row	Activity	Measure	Patient: HSR	Patient: PFL	Patient: KWR	Patient: IBL
1	Walking Normally	PA ° [A.C. %]	85 [51]	100 [23.5]*	68 [17.5]	72 [53]
		F_p kN [F_{max} kN]	1.6 [2.1]	2.06 [2.17]	1.58 [1.82]	1.66 [2.29]
2	Walking Fast	PA ° [A.C. %]	75 [50]	99 [26.5] *	67 [12.5]	
		F_p kN [F_{max} kN]	1.8 [2.35]	2.11 [2.11]	1.68 [1.88]	
3	Walking Slow	PA ° [A.C. %]	72 [52.5]	99 [22.5]*	68 [19]	
		F_p kN [F_{max} kN]	1.55 [2.06]	2.2 [2.4]	1.74 [1.76]	
4	Stairs Up	PA ° [A.C. %]	57 [49.5]	97 [24.5]*	67 [18.5]	71 [54.5]
		F_p kN [F_{max} kN]	1.68 [2.27]	2.14 [2.24]	1.92 [2.01]	0.20, 2.09 [2.51]
5	Stairs Down	PA ° [A.C. %]	72 [85]	101 [84]*	71 [58]	
		F_p kN [F_{max} kN]	2 [2.3]	2.17 [2.21]	2.1 [2.19]	
6	Chair Up	PA ° [A.C. %]	66 [17.5]	69 [99.5]	61 [28.5]	73 [47.5]
		F_p kN [F_{max} kN]	1.2 [1.48]	0.76 [1.98]	0.85 [1.09]	1.37 [1.78]
7	Chair Down	PA ° [A.C. %]	66 [95.5]	72 [1]	60 [50]	82 [99.5]
		F_p kN [F_{max} kN]	1.36 [1.5]	0.76 [1.43]	1.06 [1.09]	0.12 [1.05]
8	Knee Bend	PA ° [A.C. %]	59 [43]	69 [5]	56 [52]	
		F_p kN [F_{max} kN]	1.43 [1.56]	0.78 [1.05]	0.98 [1.06]	
9	Standing	PA ° [A.C. %]	69 [44.5]	89 [46]	65 [36.5]	
		F_p kN [F_{max} kN]	2.03 [2.17]	2.19 [2.19]	1.03 [2.43]	

Patient HSR edge proximity data analysis

For patient HSR graphical results are shown in Figures 3.4 and 3.5, where all the locomotor activities are presented in Figures 3.4a - 3.4e and non-locomotor activities are shown in Figures 3.5a- 3.5d.

For all locomotor activities the high proximity angles were registered during second half of the stance phase. The range of maximum edge proximity angles for those activities was between 57° and 85° as seen from Table 3.2 Patient; HSR rows one to five. For most locomotor activities, but stair descend, gait cycle point at which maximum proximity angles were recorded was between 50% and 53% of the gait cycle. For stair descend, due to the nature of the activity (Figure 3.4e), gait cycle point for maximum proximity angle was at 85% of the gait cycle. Contact

forces of maximum proximity angles for locomotor activities were between 1.55 kN and 2 kN. The maximum contact forces for these activities were recorded during first peak of stance phase and ranged from 2.1 kN to 2.4 kN. In contrast to most locomotor activities, during walking slowly proximity angles were almost identical between just-after first load peak and just-after second load peak, 12% to 53% of the gait cycle (Figure 3.4c). For other locomotor activities, maximum proximity angles were more prominent as seen in Figures 3.4a, 3.4b, 3.4d and 3.4e around second load peak. The variation between trials for all activities was below 10°, except for stair descend. The maximum variation for going down the stairs activity was around 13°.

Non-locomotor activities for patient HSR included rising from the chair, sitting down on the chair, bending knees and standing. For all non-locomotor activities the maximum proximity angles were established to occurred around maximum contact force. For rising from the chair and knee-bend activities the maximum proximity angles were found just before maximum contact force at 1.2 kN and 1.43 kN respectively. For chair down the maximum proximity angles were recorded just after maximum contact force at 1.36 kN. The maximum proximity angles for standing activity were established during high contact force region, similar to locomotor activities, after maximum force of 2.2 kN. The maximum edge proximity angles for non-locomotor activities ranged from 59° to 69°. For all the activities but standing the maximum proximity angles were in the first region of the activity cycle between 29% to 47%. For standing activity the maximum proximity angles were found at 71.5% of the gait cycle. The variation between trials for all activities but standing was high, where the highest variation between trials was for knee-bend activity, approximately 30°.

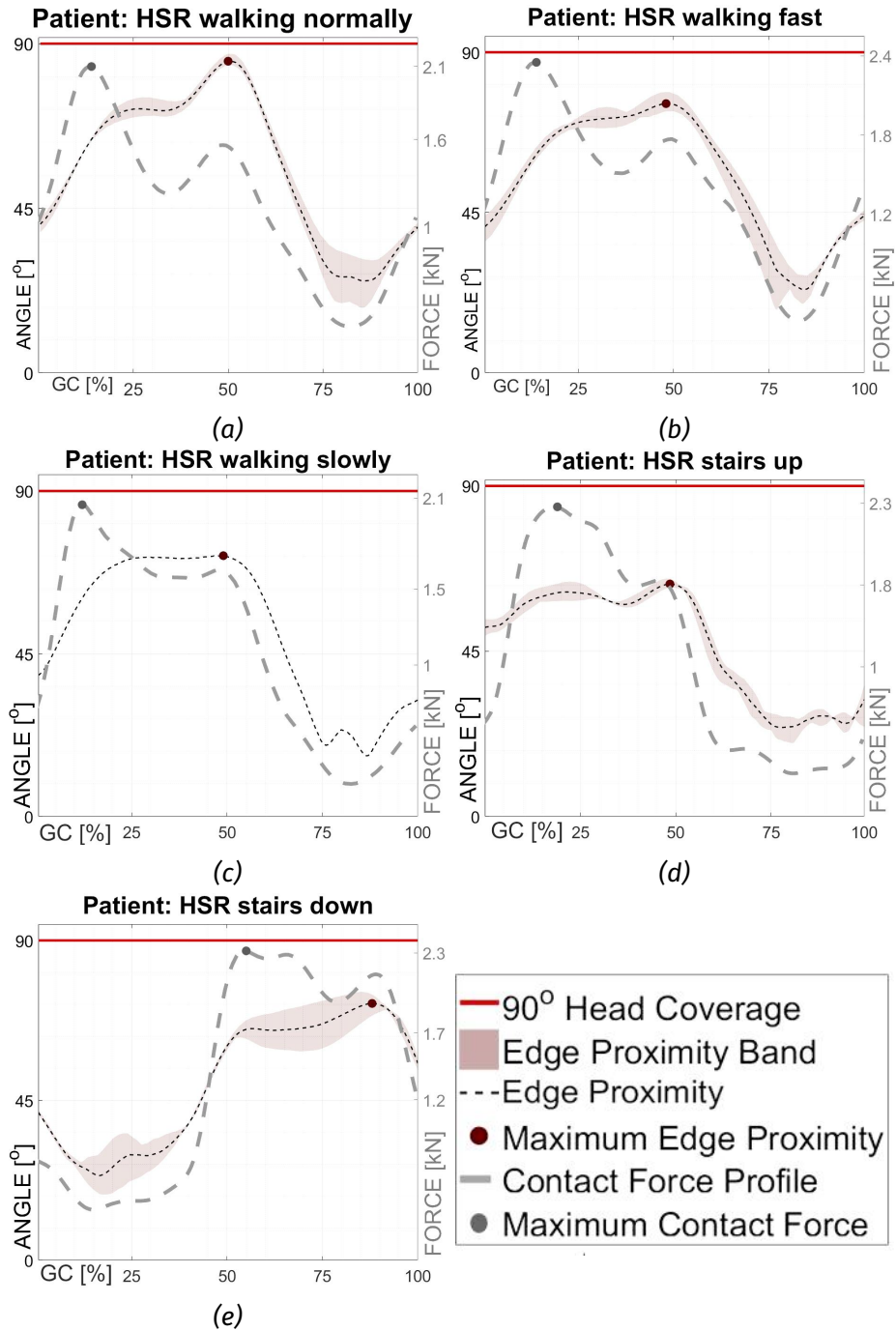


Figure 3.4: Edge proximity angles and resultant contact force magnitude for locomotor activities for patient HSR. The legend presented is valid for all the graphs. The instances of maximum edge proximity angle and contact force are also presented

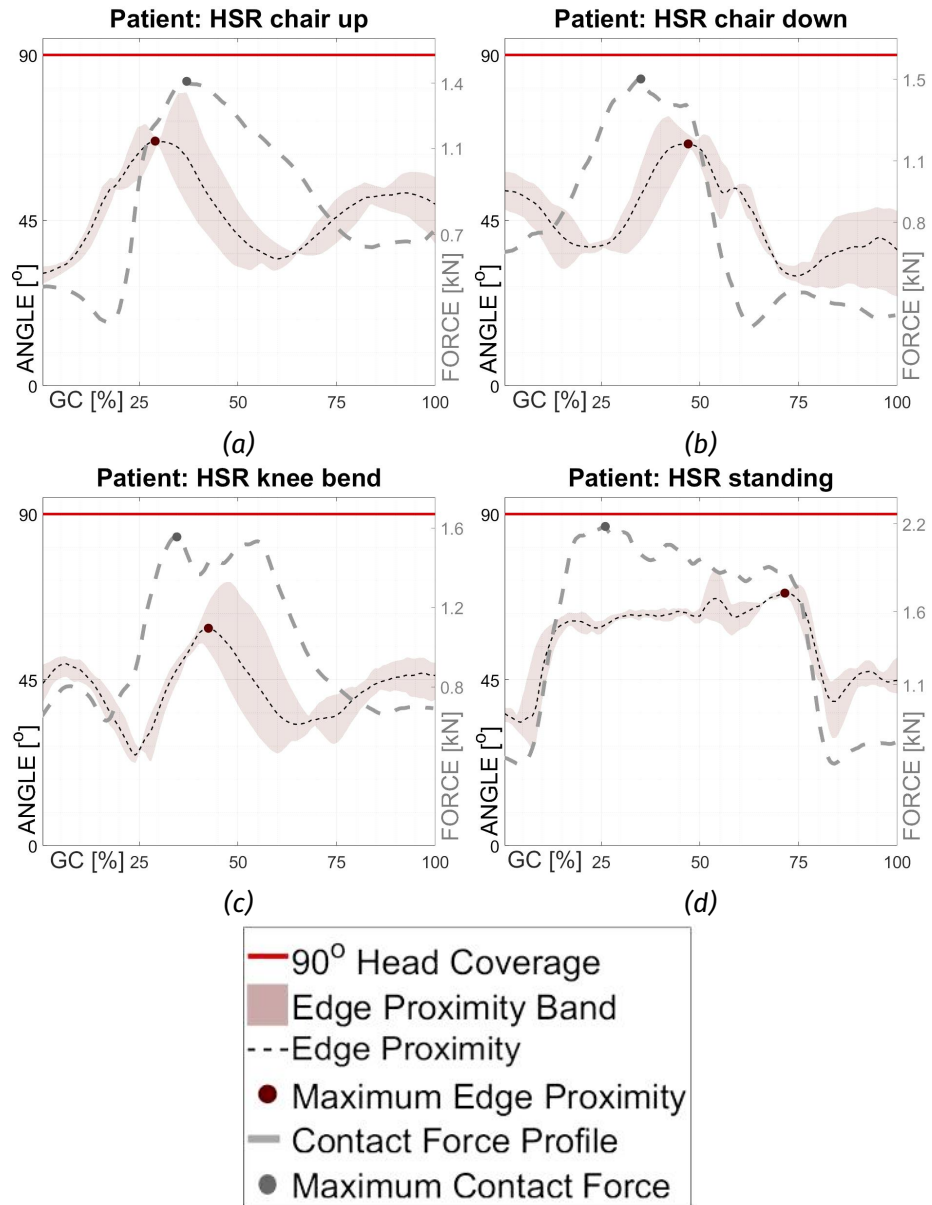


Figure 3.5: Edge proximity angles and resultant contact force magnitude for non-locomotor activities for patient HSR. The legend presented is valid for all the graphs. The instances of maximum edge proximity angle and contact force are also presented.

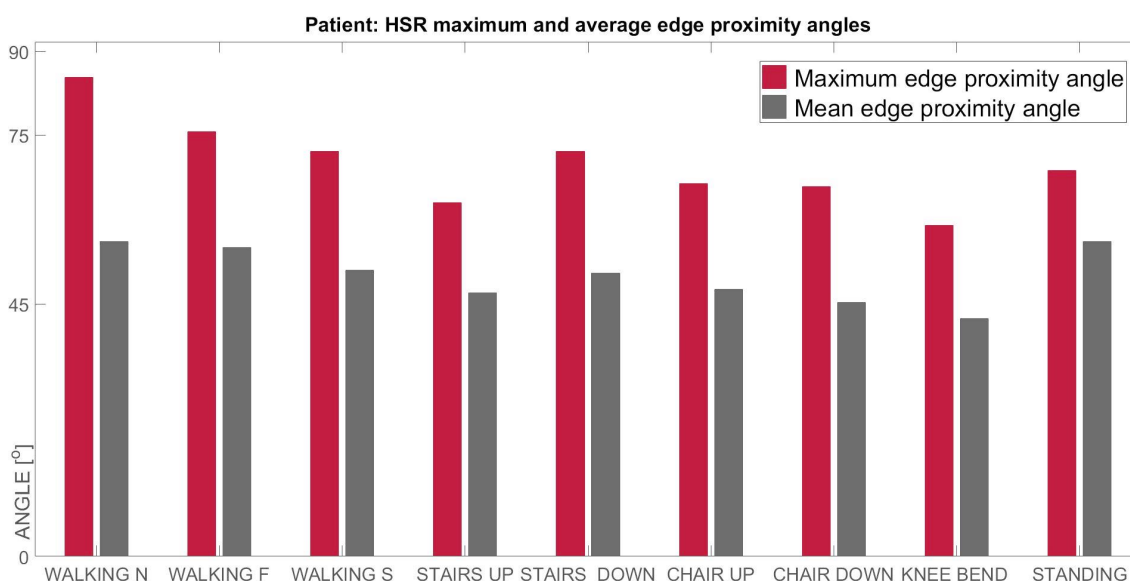


Figure 3.6: Risk of edge contact for patient HSR. Maximum edge proximity angles in red, average edge proximity angles in grey.

The comparison of the risk of edge contact between activities is shown in Figure 3.6, where both maximum and mean edge proximity angles are presented. According to the result, highest risk of edge contact for patient HSR occurred during walking with self-selected speed. The edge proximity angle was equivalent to 85.4° , Figure 3.6). Mean proximity angles for patient HSR were the highest during walking with self-selected speed and standing 56° as seen from Figure 3.6.

Patient PFL edge proximity data analysis

The results for patient PFL are shown in Figures 3.7 and 3.8, where all the locomotor activities are presented in Figures 3.7a - 3.7e and non-locomotor activities are shown in Figures 3.8a- 3.8d.

For all the locomotor activities, but stair descend, the maximum proximity angles were registered in the region from heel-strike to mid-stance. For stair descend activity the high proximity angles were found to be within gait cycle region of second force peak. The range of maximum edge proximity angles was between 97° and 101° as seen from Table 3.2 *Patient: PFL* rows one to five. The proximity angle results, also suggest that during all locomotor activities the edge of the contact area exceeded head-coverage angle. For most locomotor activities, but

going down the stairs, the gait cycle point at which maximum proximity angles occurred was between 22.5% and 26.5%. For stair descend (Figure 3.7e) the gait cycle point for maximum proximity angle was 84%. The contact force at the maximum proximity angles for all locomotor activities was between 2.06 kN and 2.2 kN. As seen from Figures 3.1a - 3.1c, blue curve, patient PFL has only one force peak for all the walking activities, which occurred before maximum proximity angle incidence. The maximum contact forces going up the stairs and going down the stairs were at the second force peak, which occurred after maximum edge proximity angle instance. The maximum contact force magnitude across all the locomotor activities was between 2.11 kN and 2.4 kN. For these activities the variation between trials did not exceed 12°, which was recorded for walking slow activity during swing phase.

Non-locomotor activities for patient PFL included rising from the chair, sitting down on the chair, bending knees and standing up. In contrast to patient HSR, maximum proximity angles for the current patient were recorded during low contact forces of the activity. The exception was standing, where the maximum edge proximity angle instance corresponded to maximum contact force. For rising from the chair, sitting down on the chair and bending knees the maximum edge proximity angle ranged between 69° to 72°. The contact forces at maximum proximity angle ranged between 0.76 kN to 0.78 kN (Table 3.2 *Patient: PFL* rows from six onwards). Maximum contact forces for rising from the chair, sitting down on the chair and bending knees were between 1.06 kN to 1.98 kN. Interestingly, for rising from the chair and sitting down on the chair, the maximum proximity angle was recorded at the beginning and the end of the cycle respectively. This instance for both activities corresponded to patient being sat on the chair. For standing, the maximum contact force corresponded to contact force at maximum proximity angle, which was equal to 2.19 kN. The maximum edge proximity angle during standing was registered in the middle of a cycle, 46%, and was equal to 89°. The variation for non-locomotor activities was higher than for locomotor activities, with the highest variation for standing activity reaching approximately 30°.

For patient PFL, no distinct maximum edge proximity was recorded across the

activities. However, the highest maximum edge proximity angles were all for locomotor activities, which also were above the head-coverage angle (Figure 3.9). The highest mean edge proximity angle was recorded for walking activities, descending stairs and standing, with average mean angle across activities of 77° , Figure 3.9.

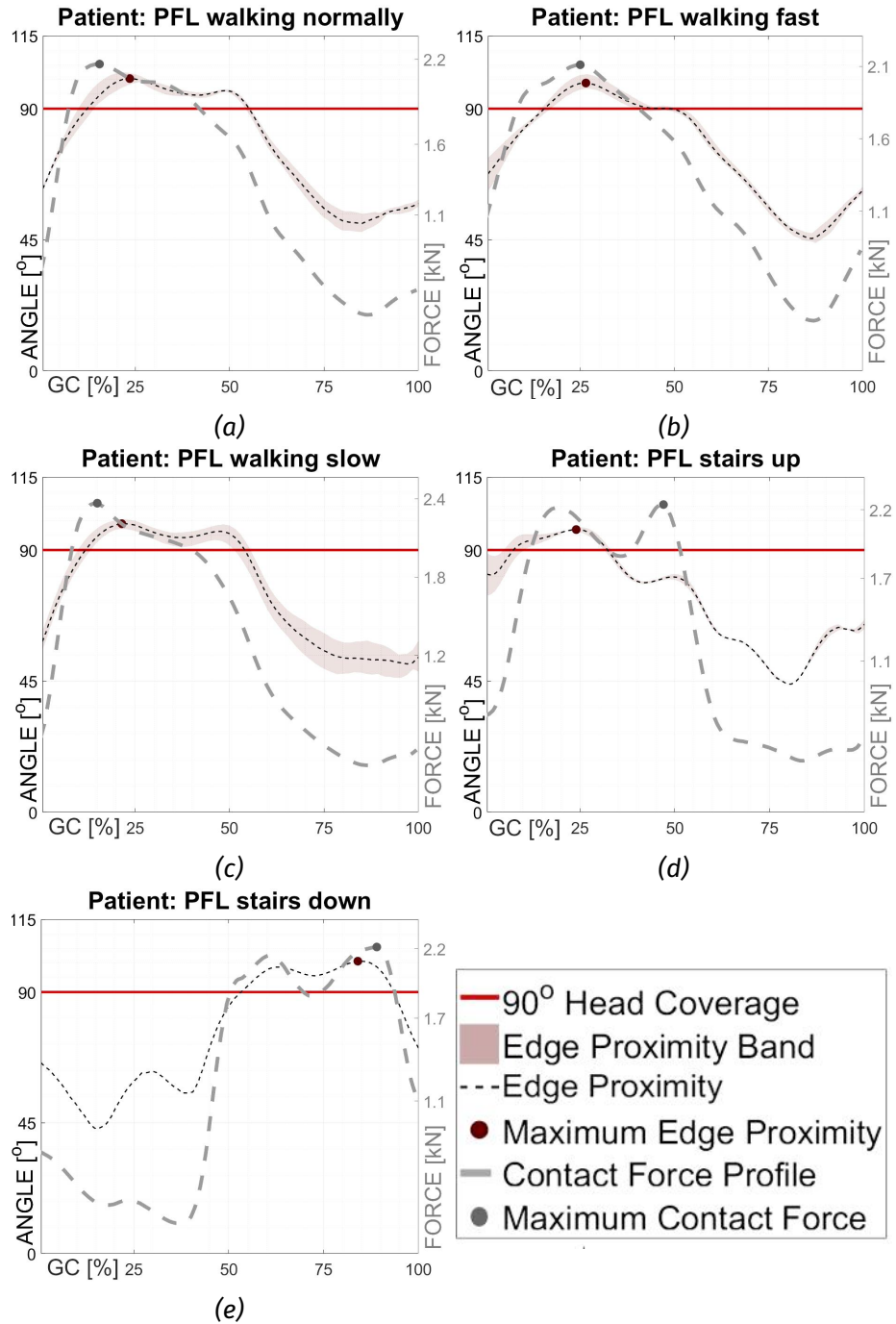


Figure 3.7: Edge proximity angles and resultant contact force magnitude for locomotor activities for patient PFL. The legend presented is valid for all the graphs. The instances of maximum edge proximity angle and contact force are also presented.

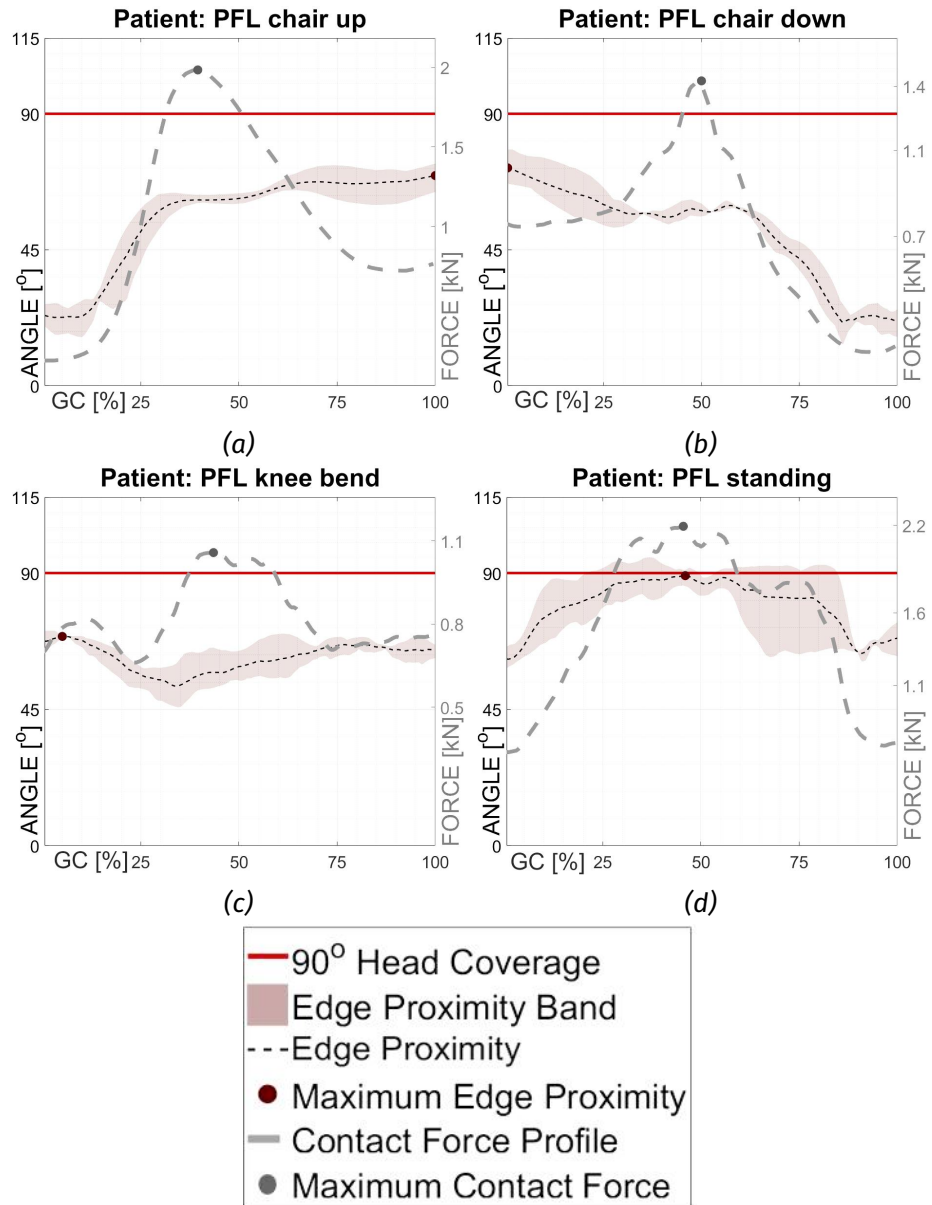


Figure 3.8: Edge proximity angles and resultant contact force magnitude for non-locomotor activities for patient PFL. The legend presented is valid for all the graphs. The instances of maximum edge proximity angle and contact force are also presented.

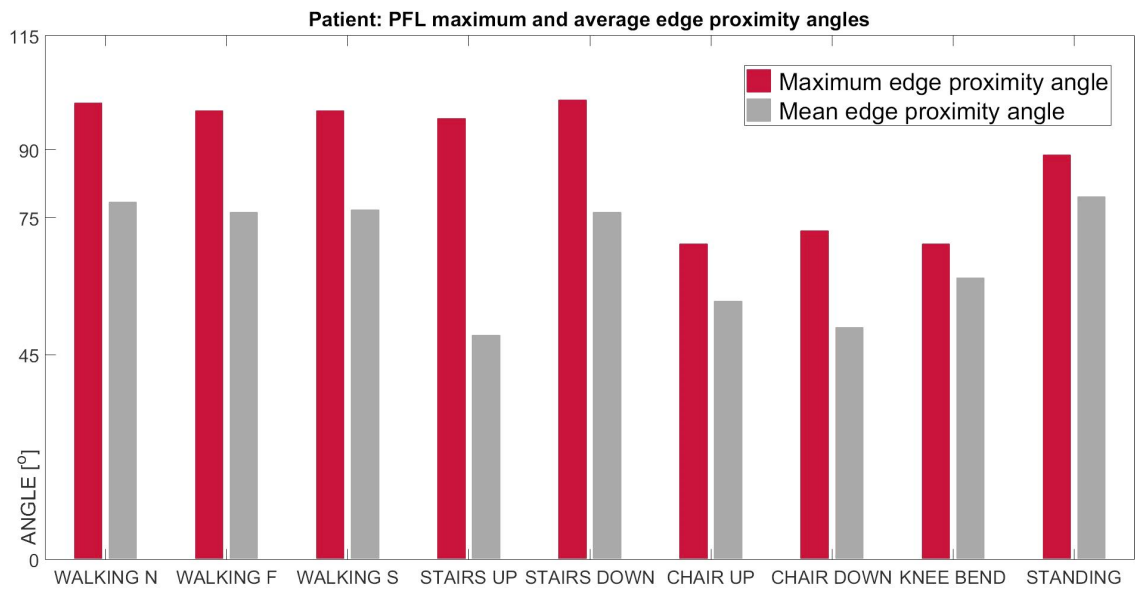


Figure 3.9: Risk of edge contact for patient PFL. Maximum edge proximity angles in red, mean edge proximity angles in grey.

Patient KWR edge proximity data analysis

The graphical representation of the results is shown in Figures 3.10 and 3.11, where all the locomotor activities are presented in Figures 3.10a - 3.10e and non-locomotor activities are shown in Figures 3.11a- 3.11d.

For patient KWR the available locomotor activities were walking with self-selected speed, fast and slow, going up and going down the stairs. The high proximity angle region for all the locomotor activities corresponded to the region from heel-strike to mid-stance. The range of maximum edge proximity angle across the activities was between 66° and 71° (Table 3.2 *Patient: KWR* from rows one up to row five). For most locomotor activities, except stair descent, the gait cycle point at which maximum proximity angles were established was between 12.5% and 18.5%. For stair descent (Figure 3.10e) the gait cycle point for maximum proximity angle was at 58%. The contact forces at maximum proximity angles for all locomotor activities were between 1.6 kN and 2.1 kN. The maximum contact force magnitudes across all locomotor activities were between 1.82 kN and 2.2 kN. For the walking fast activity the maximum proximity angles corresponded to the maximum contact force instance, or first force peak, 12.5% of the gait cycle. For the rest of the locomotor activities, the maximum edge proximity angle was recorded for the period just after the first force peak, within 4% of the activity cycle. The variation between trials for all activities but ascending stairs was below 15° . However, for ascending stairs the trial variation reached approximately 30° (Figure 3.10d).

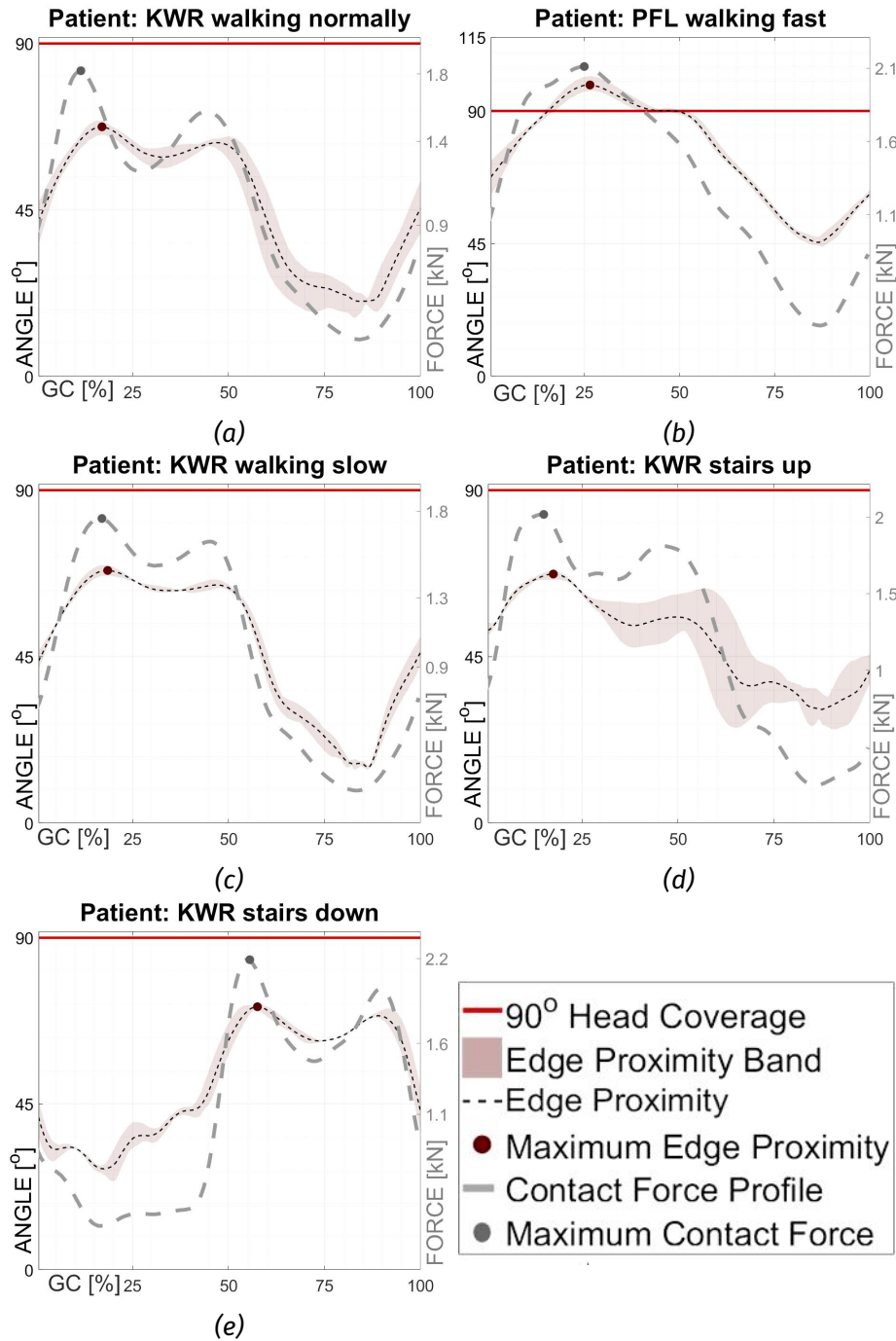


Figure 3.10: Edge proximity angles and resultant contact force magnitude for locomotor activities for patient KWR. The legend presented is valid for all the graphs. The instances of maximum edge proximity angle and contact force are also presented.

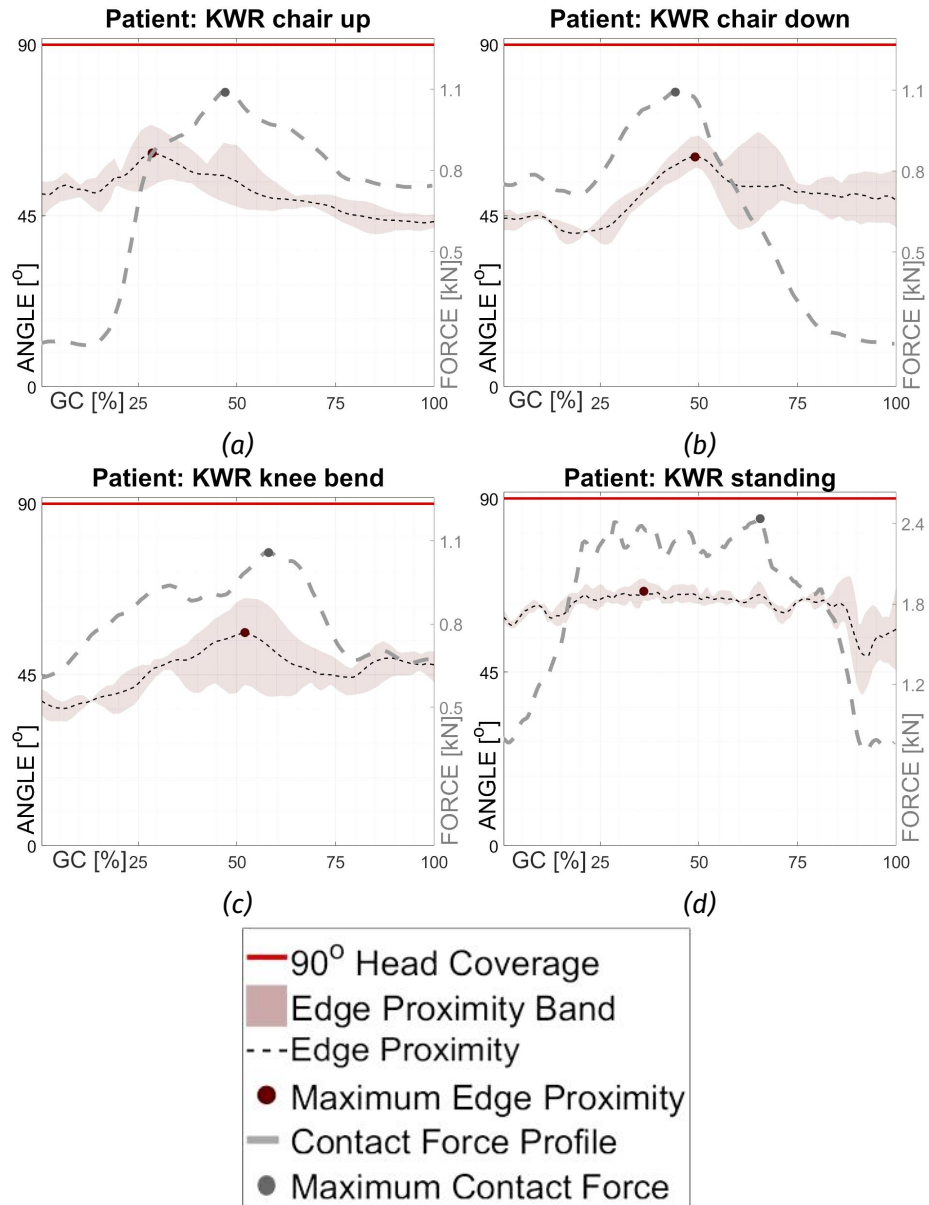


Figure 3.11: Edge proximity angles and resultant contact force magnitude for non-locomotor activities for patient KWR. The legend presented is valid for all the graphs. The instances of maximum edge proximity angle and contact force are also presented.

Non-locomotor activities for patient KWR included rising from chair, sitting down on the chair, bending knees and standing up. Similar to patient HSR, high proximity angles for the current patient occurred during high contact force region of the activity. For non-locomotor activities the edge proximity angle ranged from 56° to 65°. The contact forces during maximum proximity angle ranged between 0.9 kN to 2.5 kN, where maximum contact forces for these activities were between 1.1 kN to 2.4 kN. The variation between trials for rising from chair, sitting down on the chair, bending knees was similar to ascending stairs activity, reaching up to 23° for knee bend activity. For standing activity the variation was

less than 20° .

For patient KWR the highest edge proximity angles were recorded for locomotor activities and standing activity (Figure 3.12). The maximum mean edge proximity angle was found for standing activity and was equivalent to 62° as seen in Figure 3.12.

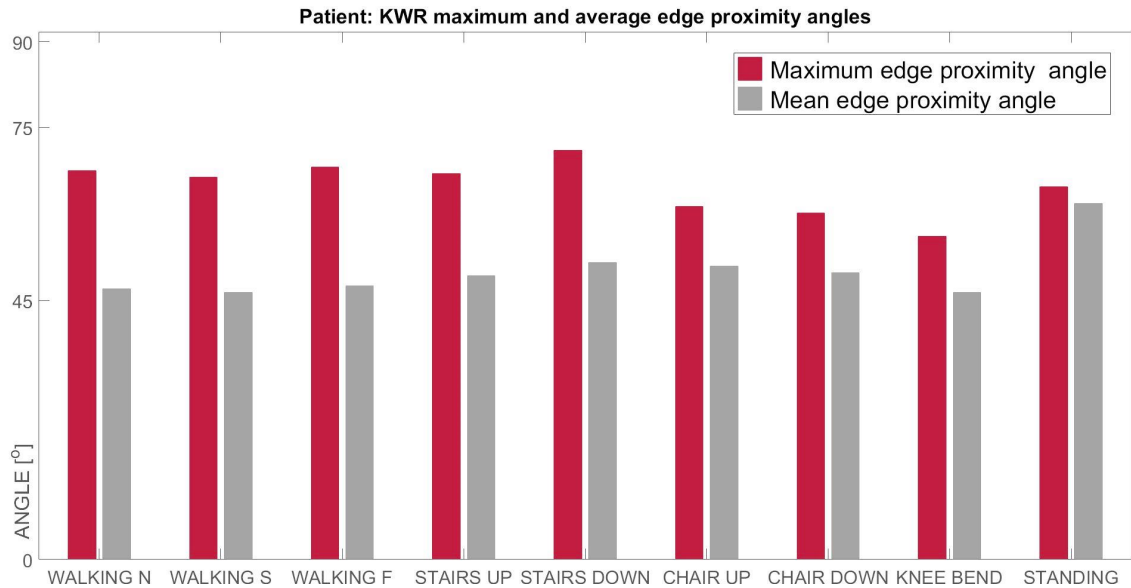


Figure 3.12: Risk of edge contact for patient KWR. Maximum edge proximity angles in red, mean edge proximity angles in grey.

Patient IBL edge proximity data analysis

The graphical representation of the results for patient IBL is shown in Figure 3.13, where all the locomotor activities are presented in Figures 3.13a - 3.13b and non-locomotor activities are shown in Figures 3.14a- 3.14b.

For patient IBL there were only two locomotor activities available, walking with self-selected speed and stair ascent. For the first activity the maximum edge proximity angle occurred for gait cycle point 53%, which corresponded to the second half of the stance phase. The edge angle for this point was equal to 72° . The contact force at maximum proximity angle was 1.65kN, when the maximum force was 2.29 kN. For going up the stairs activity, the maximum edge proximity angle was equal to 71° and registered during stance phase, at gait cycle point 55%.

Contact force for this instance was equivalent to 2.1kN. The variation between activity trials was not higher than 15° , with the exception of swing phase during stair ascent, when reached 42° (Figure 3.13b).

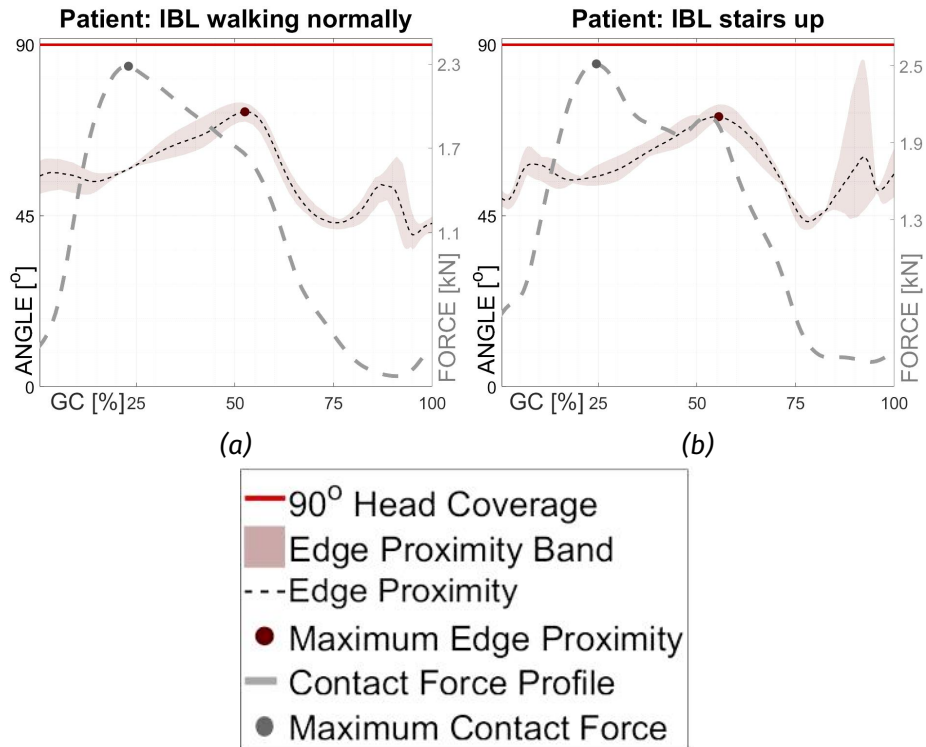


Figure 3.13: Edge proximity angles and resultant contact force magnitude for locomotor activities for patient IBL. The legend presented is valid for all the graphs. The instances of maximum edge proximity angle and contact force are also presented.

Non-locomotor activities for patient IBL included rising from chair and sitting down on the chair. For rising from the chair, maximum edge proximity angle was recorded for gait cycle point 53% and was equal to 73° . Contact force for this angle was found to be 1.37 kN, which occurred just before maximum contact force of 1.78 kN. For sitting down on the chair, maximum edge proximity angle was registered at the end of the cycle, 100%, and was equal to 47° . Contact force for this gait cycle point was 0.12 kN, when the maximum contact force was 1.05 kN. The variation between trials for rising from the chair was below 20° . This was true for sitting down on the chair activity until last quarter of the gait cycle, where the variation between trials reached 64° .

In contrast to other patients, for patient IBL the maximum risk of edge contact was identified for non-locomotor activity, sitting down on the chair (Figure 3.15).

For patient IBL and all the activities almost identical mean edge proximity angle was found, with average mean angle across the activities equal to 57°.

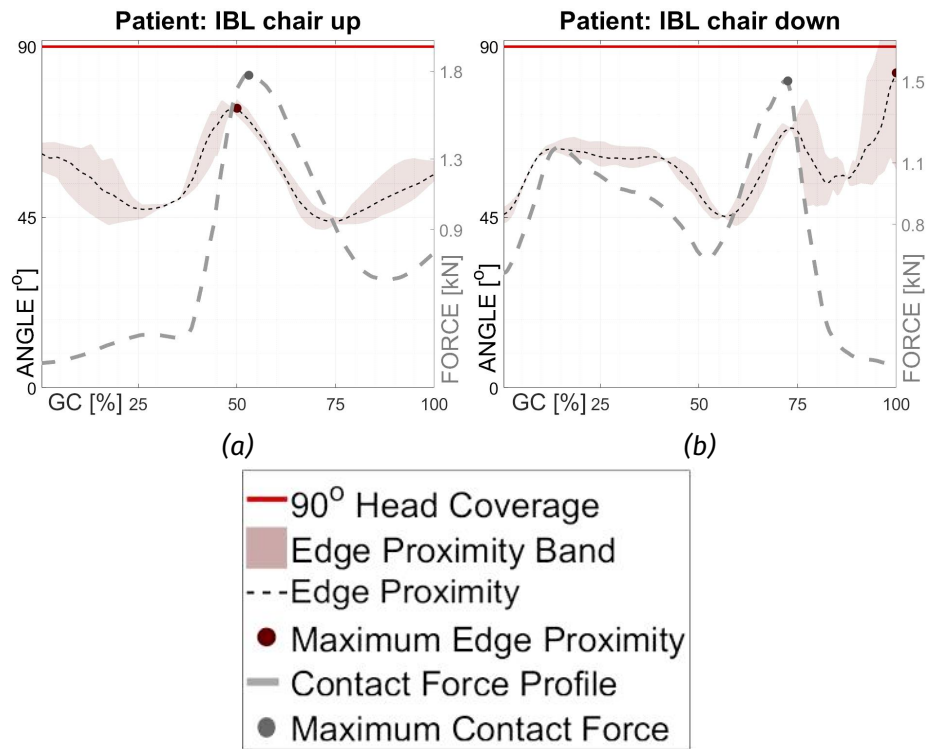


Figure 3.14: Edge proximity angles and resultant contact force magnitude for non-locomotor activities for patient IBL. The legend presented is valid for all the graphs. The instances of maximum edge proximity angle and contact force are also presented.

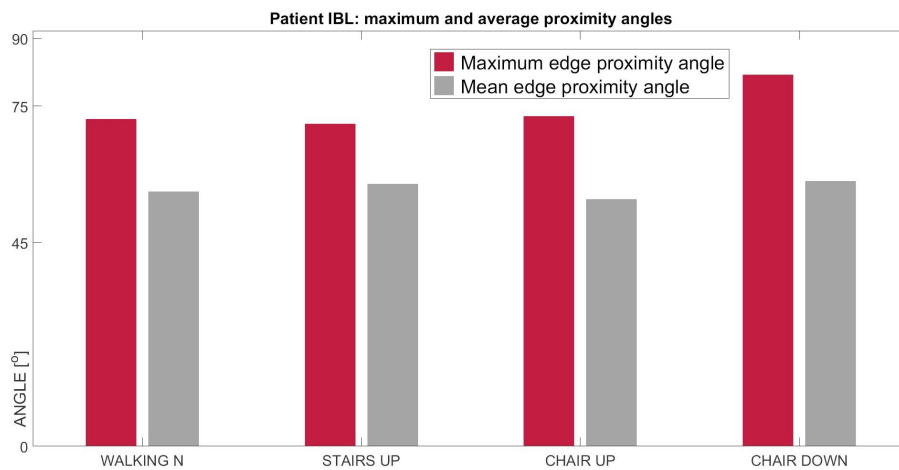


Figure 3.15: Risk of edge contact for patient IBL. Maximum edge proximity angles in red, mean edge proximity angles in grey.

3.3.3 Conclusions and observations

- The maximum risk of edge contact, during locomotor activities, corresponded to high load region of the cycle for all patients. For patients IBL and HSR the maximum risk of edge contact was established for gait cycle region from mid-stance to the end of high contact force region. For patient KWR the maximum edge proximity angles occurred in region from heel-strike to mid-stance. The same was found for patient PFL, except for descending stairs activity, where the maximum risk of edge contact was recorded in the region from mid-stance to toe-off;
- For all patients but IBL, the locomotor activity curves resembled resultant contact force magnitude profiles, with edge proximity angles being substantially higher during stance phase than during swing phase;
- For non-locomotor activities the maximum proximity angle occurred during high or low load regions. The variation between profile patterns across the patients for same activity was high. This was true for all non-locomotor activities but standing;
- The risk of edge contact was the highest for locomotor activities and standing for all patients but IBL;
- For patient IBL the highest risk of edge contact occurred during sitting down on the chair activity;
- The longest duration of the high edge contact risk was found to be during standing activity, based on mean edge proximity results;
- The variation between trials was generally higher for non-locomotor activities with some exceptions;
- The only patient for whom the edge proximity angles were higher than head-coverage angle of 90° was patient PFL. Patient PFL also has the highest cup inclination angle across all the patients (Table 3.1).

3.4 Effect of pelvic motions onto the risk of edge contact

The aim of this sub-study was to investigate the effect of excluding pelvic motions from the simulation on the risk of edge contact for set of activities which showed the highest edge proximity angles in previous sub-study (Section 3.3).

3.4.1 Method

Analysis description

The effect of pelvic motion exclusion on the risk of edge contact was assessed. The centre proximity angle was used in order to avoid the effect of contact force magnitude. Figure 3.16 represents, as example of the output data for this sub-study, where centre proximity angles with both pelvic motions included and excluded cases are shown. The maximum centre proximity is also marked in the Figure for two cases. In contrast to first sub-study, this analysis is reported per activity rather than per patient to analyse the effect of pelvic motion addition for each activity. For this analysis all three trials (Table 3.1) were used to establish the confidence band for each activity during both pelvic motions included and excluded cases. The confidence band for each case was represented by an uncertainty region between the maximum and minimum registered centre proximity angles, for each gait cycle point across all the trials. This was done to determine if the difference between with and without pelvic motions in the simulation is substantial. In Figure 3.16, the confidence band for pelvic motions included case is in dark red, and for case where pelvic motions are excluded in dark grey. The overlap of two confidence bands would signify no substantial change. Average of the three trials was used to establish the change in centre maximum proximity angles between pelvic motions included and excluded simulation.

Three different angles, were measured in this study. First was the difference between two maximum centre proximity angles, measured as absolute value. In Figure 3.16 this difference is marked in blue under title " Diff. maximum centre proximity ". The second value measured in this sub-study was the difference between centre proximity angles of two cases, at the gait cycle point where

centre proximity angle is maximum for pelvic motion included case. The gait cycle point for this measurement is marked with pink vertical dashed line in Figure 3.16. The difference for second measurement is in bright red and titled "Diff. max pelvic motions included". For the third measurement the instance of maximum centre proximity for pelvic motions excluded case was used. The difference was measured for this particular gait cycle point between maximum centre proximity for pelvic motions excluded case and corresponding proximity angle of pelvic motions included case. The difference for third measurement is in bright red and titled "Diff. max pelvic motions excluded". The gait cycle point for this value is marked by grey vertical dashed line.

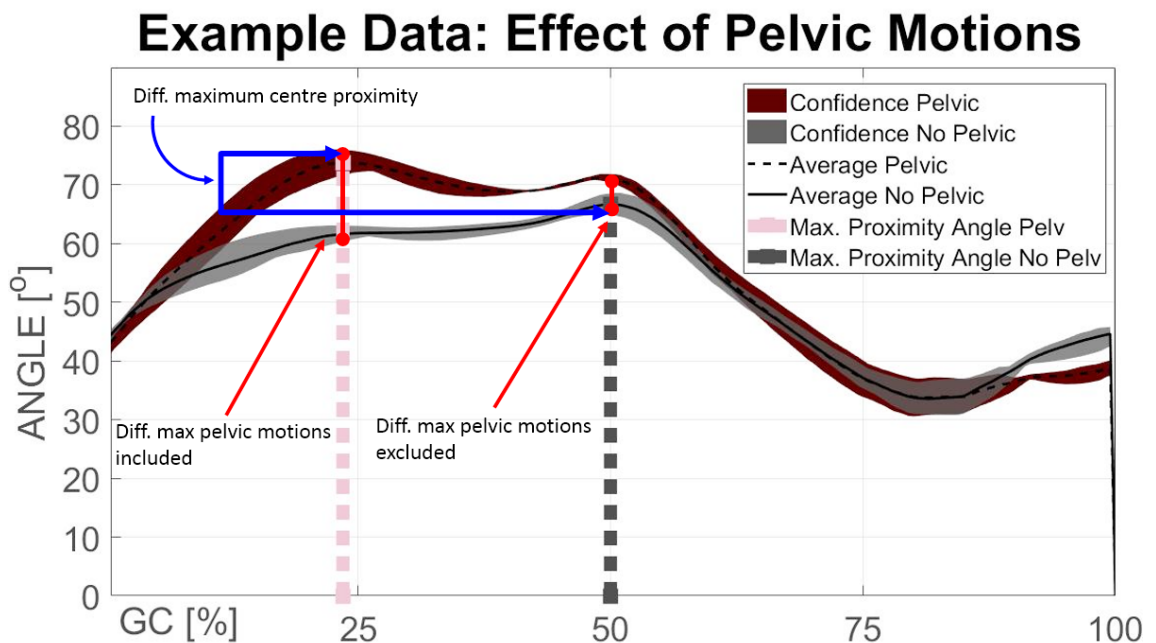


Figure 3.16: Example of output for sub-study 2 of HIP98 data analysis. A plot of centre proximity angles where pelvic motions included and excluded during one activity cycle for one patient. Plot also shows maximum centre proximity angles during the cycle during pelvic motions included and excluded cases, in pink and grey respectively. GC is for gait cycle point. Diff. is for measured difference.

Patient and activity selection

The activities which showed the higher degree of edge contact risk in Section 3.3 were selected for this sub-study. This included locomotor activities and the standing activity. Activities which had all three trials provided were investigated (Table 3.1.) The exclusion of sitting down on the chair, rising up from the chair and knee bend, was due to the high variability between trials for those activities. Data for patient IBL was not included in this particular study for several reasons. First, the patient performed only a limited number of activities and some of the activities were done differently to other patients. Secondly, the IBL patient edge proximity angle patterns did not resemble those of other patients. In total patients HSR, KWR and PFL were selected for this study. The activities included walking with normal speed, walking fast and standing.

3.4.2 Results

Table 3.3 shows the summary of results for the second sub-study of this chapter. The results include maximum centre proximity angle for each activity, patient for two pelvic motion cases, included or excluded. The results also include gait cycle point at which maximum centre proximity angle was recorded, GC. *Delta*, Δ , is the difference between centre proximity angles for pelvic motions included and excluded cases. The odd rows in Table 3.3 show results for pelvic motions included case, and even rows show results for pelvic motions excluded case. For odd rows Δ is for "Diff. max pelvic motions included" as described in Section 3.4.1 of this section and show in Figure 3.16. For even rows in Table 3.3 Δ stands for "Diff. max pelvic motions excluded" as seen in Figure 3.16. The negative value of *Delta* signifies a decrease in edge of risk contact by amount of degrees $^{\circ}$.

Table 3.3: Centre proximity results comparison between different patients and activities with pelvic motion included/excluded. PI - pelvic motion included, PE - pelvic motion excluded. PA - angle measured in degrees [$^{\circ}$], for maximum edge proximity angle. GC - gait cycle point of the maximum centre proximity incidence. Δ - the difference in centre proximity angles between pelvic motions included and excluded at GC. Δ measures the difference in relation to scenario of interest for that row, PI or PE. " - " signifies that scenario of interest decreases the centre proximity angle and " + " that signifies an increase.

Row	Activity	Patient: HSR			Patient: PFL			Patient: KWR		
		PA $^{\circ}$	GC %	Δ°	PA $^{\circ}$	GC %	Δ°	PA $^{\circ}$	GC %	Δ°
1	Walking Normally PI	61	51	+8	74	23.5	+12.4	50	48	+6.4
2	Walking Normally PE	53	51	-8	67	50	-4.6	44	50	-6
3	Walking Fast PI	50	48	+6.4	72	26.5	+11	42	20	+2.4
4	Walking Fast PE	44	50	-6.3	64	50	-1	39	50	+4.8
5	Standing PI	43	71.5	0	62	46	-2.6	40	8	+2.5
6	Standing PE	45	44.5	+8	65	42.5	+3.3	46	65	+9

Walking with self-selected speed

The results for walking with self-selected speed show that pelvic motion exclusion affects patients differently. One common attribute in all three patients was a decrease in edge contact risk at some point during the first quarter of the gait cycle (Figure 3.17). The decrease corresponds to a region around the first load peak (Figure 3.1a).

As seen in Figure 3.17a, the exclusion of pelvic motions, for patient HSR, resulted in substantial decrease of edge contact risk for gait cycle points between 13.5% to 68.5%, encompassing most of the high contact force region. The substantial increase in edge contact risk with exclusion of pelvic motions for patient HSR was found for low load regions in first 13% of gait cycle and in the last 12% of the gait cycle.

Similar to patient HSR, for patient PFL the decrease in edge contact risk with exclusion of pelvic motions was established for region of high contact force, from 12% to 52.5% of the gait cycle (Figure 3.17b). In contrast to patient HSR, the decrease was more substantial in the first half of that region, around maximum contact force. The substantial increase with pelvic motion exclusion was only noted for last 10% of the gait cycle.

In contrast to both patient HSR and PFL, the results for patient KWR did not show much variability between pelvic motions included and excluded cases. Some substantial increase in edge contact risk with exclusion of pelvic motions was found in the first 5% of the gait cycle, as well as decrease in proximity angle from 16.5% to 24.5% of the gait cycle.

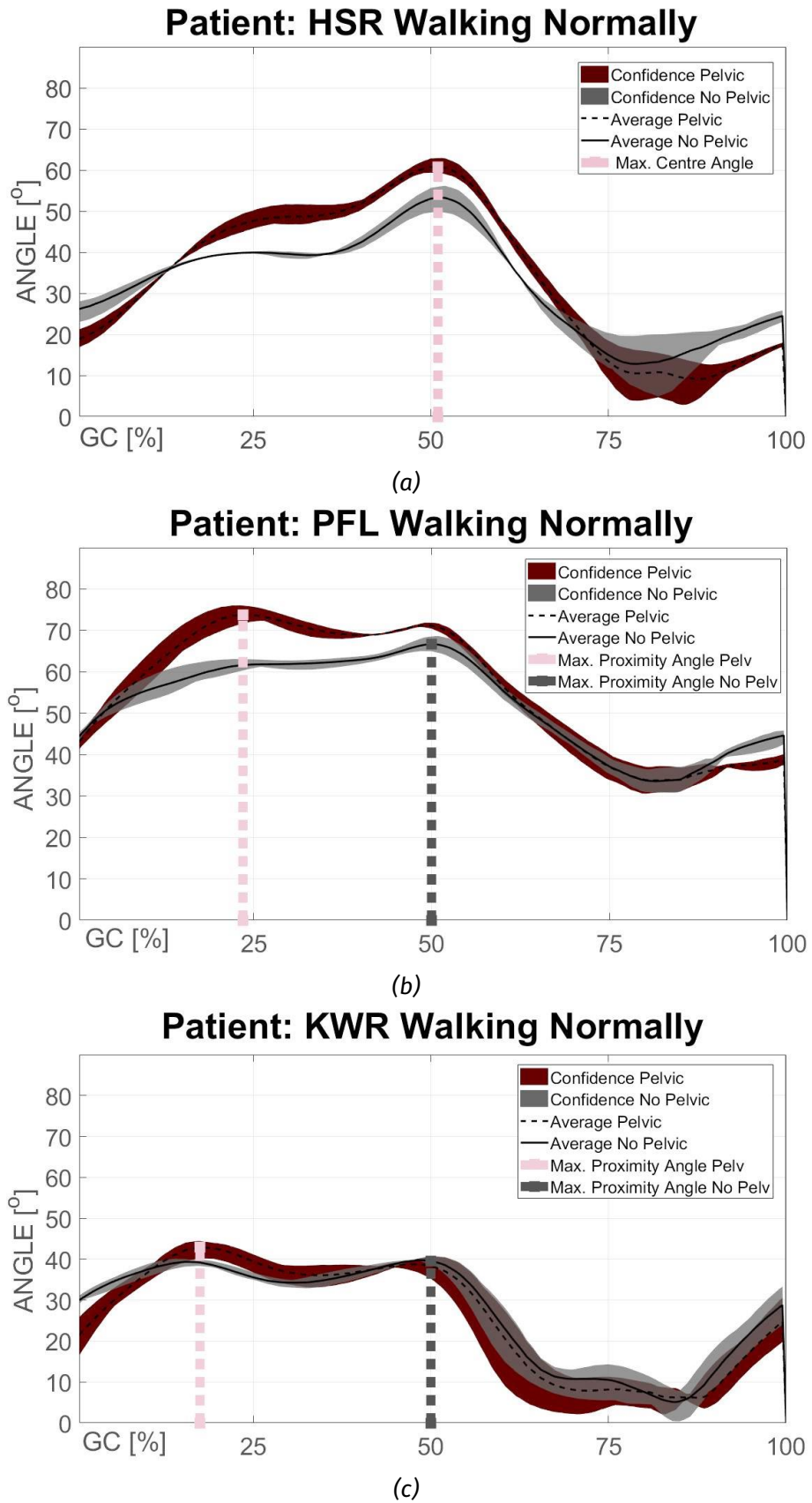


Figure 3.17: Walking with self-selected speed centre proximity angles for pelvic motions included and excluded cases for patients HSR, PFL, KWR.

The difference in maximum centre proximity angles was found to be 8°, 7° and 6° for patients HSR, PFL and KWR respectively. As seen in Table 3.3 row one, the difference, Δ , between maximum centre proximity angle for pelvic motion included and corresponding centre angle for pelvic motion excluded cases was the highest for patient PFL and reached 12.4°. This instance is highlighted in Figure 3.17b by pink dashed line. The difference for maximum proximity angle instance during pelvic motions excluded case, was the highest for patient HSR and reached 8° (Table 3.3). This instance is highlighted in Figure 3.17a by grey dashed line.

For pelvic motions excluded, the maximum centre proximity angles were found in the middle of the gait cycle between mid-stance to toe-off. Same was identified for patient HSR for pelvic motions included case. For two other patients, inclusion of pelvic motions switched maximum centre proximity angles to the first quarter of the gait cycle 3.17.

Walking with faster speed

Slight changes in centre proximity profiles were found for increased walking speed, when compared to walking with self-selected speed. The results showed even greater variability in the effects of exclusion of pelvic motions on risk of edge contact between patients as seen in Figure 3.18.

As seen in Figure 3.18a, the exclusion of pelvic motions, for patient HSR, resulted in substantial decrease of edge contact risk for gait cycle points between 20% to 60.5%, which corresponded to some part of stance phase. As in previous activity, the substantial increase in edge contact risk with exclusion of pelvic motions for patient HSR was found for low load regions in first 5.5% of gait cycle and in the last 15% of the gait cycle.

For patient PFL the substantial decrease in edge contact risk with exclusion of pelvic motions was established for earlier region of the stance phase compared to patient HSR, from 7% to 42.5% of the gait cycle (Figure 3.17b). This region corresponded to highest contact force for this activity for patient PFL (Figure

3.1b). The substantial increase with pelvic motion exclusion was found for last 7.5% of the gait cycle.

Similar to walking with self-selected speed, the exclusion of pelvic motions from simulation for patient KWR did not change much. Some decrease in centre proximity angles were established between 35% to 40% of gait cycle. The substantial increase in edge contact risk with exclusion of pelvic motions was found in the first 5% of the gait cycle, and during some instances between 66% and 100% of the gait cycle.

The difference in maximum centre proximity angles was found to be 6° , 8° and 3° for patients HSR, PFL and KWR respectively. As seen in Table 3.3 row three, the difference, Δ , between maximum centre proximity angle for pelvic motion included and corresponding centre angle for pelvic motion excluded cases, as for previous activity, was the highest for patient PFL and reached 11° . The gait cycle point is highlighted in Figure 3.18b by pink dashed line. The difference for maximum proximity angle instance during pelvic motions excluded case, was the highest for patient KWR and reached 4.8° (Table 3.3). The maximum centre proximity angle's instance for this patient is highlighted in Figure 3.18c by grey dashed line. However, for patient HSR this angle was greatest in magnitude across all patients, while representing decrease. This instance is highlighted in Figure 3.18a by grey dashed line. The location of maximum centre proximity angles during gait was identical to walking with self-selected speed, where all the pelvic motions excluded cases showed maximum risk of edge contact half way through the cycle. This was also true for patient HSR when pelvic motions were included into simulation. For other two patients the maximum risk of edge contact was in the first half of the stance phase.

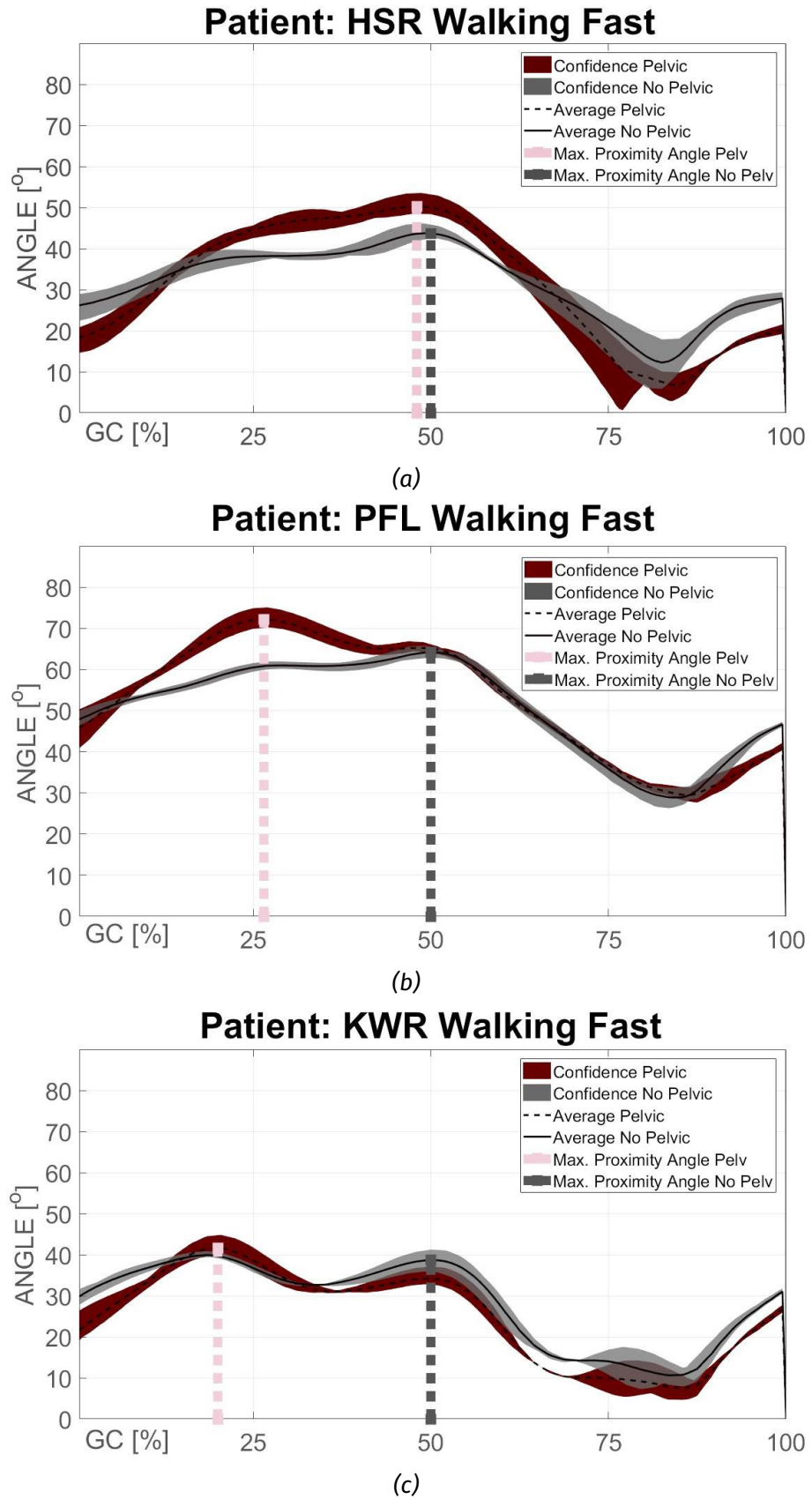


Figure 3.18: Walking fast centre proximity angles for pelvic motions included and excluded cases for patients HSR, PFL, KWR.

Standing on two-one-two legs

For standing on two-one-two legs the maximum results were also varied between patients as for walking activities. For patient HSR the exclusion of pelvic motions increased the risk of edge contact substantially for most of the cycle, from 12% to 67.5% of the gait cycle. Some increase was also registered at the beginning and the end of the gait cycle. For patient PFL no substantial difference was found between the cases. Similar to patient HSR, the exclusion of pelvic motions for patient KWR did result in a substantial increase in centre proximity angles, from 16.5% to 79.5% of the gait cycle.

The difference in maximum centre proximity angles was found to be 2°, 3° and 6° for patients HSR, PFL and KWR respectively. As seen in Table 3.3 row five, the difference, Δ , between maximum centre proximity angle for pelvic motion included and corresponding centre angle for pelvic motion excluded cases, was the highest for patient KWR and reached 2.5°. The gait cycle point is highlighted in Figure 3.19c by pink dashed line. The difference for the maximum proximity angle instance during pelvic motions excluded case, was highest for patient KWR and was found to be 4.8° (Table 3.3, row six). The gait cycle for this occurrence is highlighted in Figure 3.19c by grey dashed line. For pelvic motions included, the maximum centre proximity angles were found across the cycle as seen in Figure 3.19. For pelvic motions excluded case, the maximum centre proximity angles occurred near the middle of the cycle for patients HSR and PFL, and at 65% of the gait cycle for patient KWR.

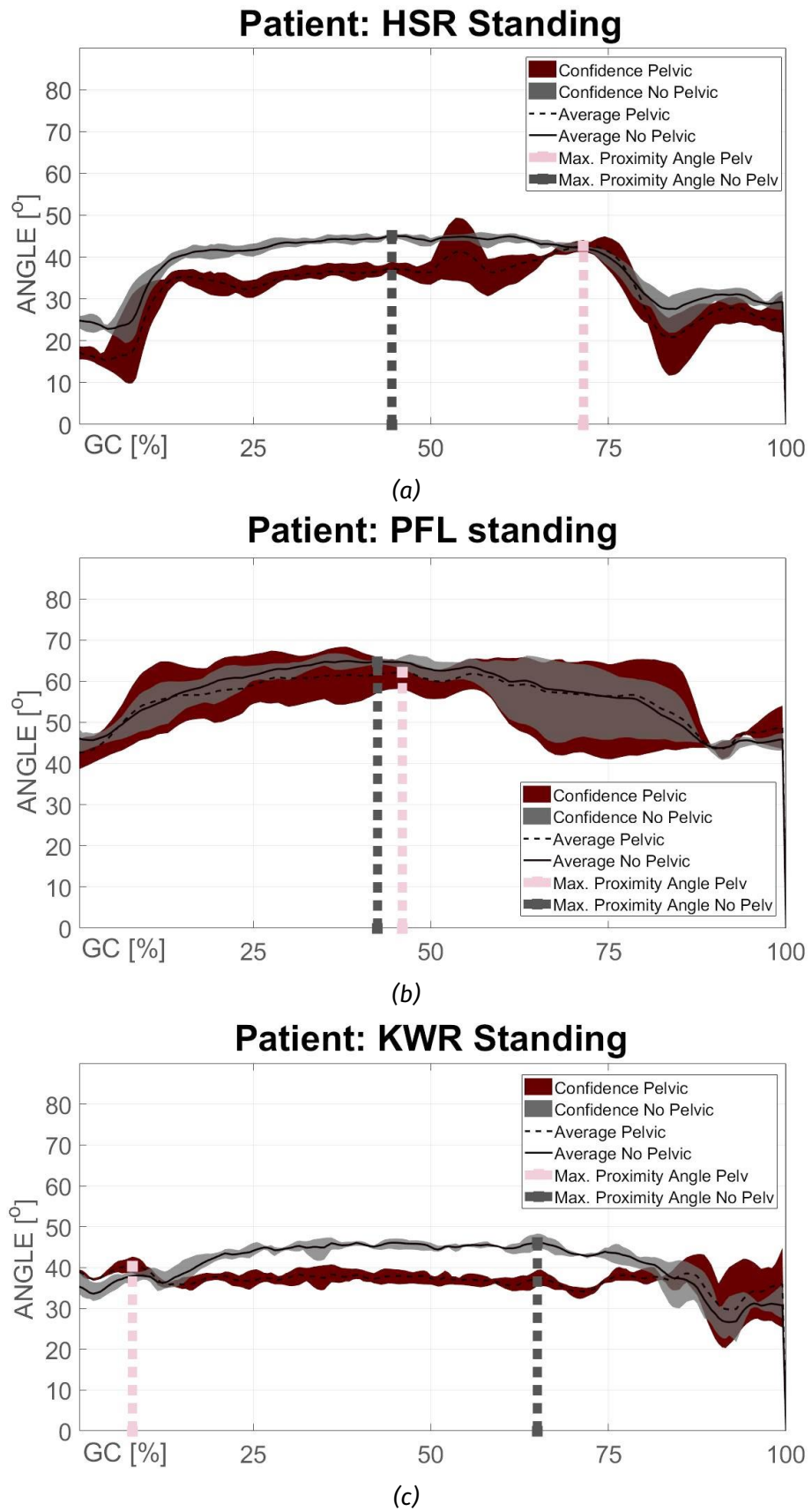


Figure 3.19: Standing activity centre proximity angles for pelvic motions included and excluded cases for patients HSR, PFL, KWR.

3.4.3 Conclusions

- For walking activities the exclusion of pelvic motions resulted in a decrease in risk of edge contact during the high contact force region. In some patient the exclusion of pelvic motions substantially increased the risk of edge contact during low contact force regions;
- In contrast to the results observed for walking activities, when pelvic motion was excluded in standing a substantial increase in risk of edge contact was observed;
- The greatest difference in maximum proximity angles when pelvic pelvic motions were included and excluded was 8° ;
- The maximum change in centre proximity angles between two cases, at the gait cycle point of maximum proximity angle for pelvic motions included case, was 12.4° ;
- The maximum change in centre proximity angles between two cases, at the gait cycle point of maximum proximity angle for pelvic motions excluded case, was 9° ;
- The results of this sub-study suggest that there is variability between patients in terms of the effect of pelvic motion exclusion from the simulation.

3.5 Comparison to Paul cycle of edge contact risk and location of potential rim damage location

As described in Chapter 1, Section 1.5.5, the *Paul Cycle* is a profile commonly used in pre-clinical tests either as it is or in a modified form. The aim of this sub-study was to compare THR patient gait data with pre-clinical testing profile.

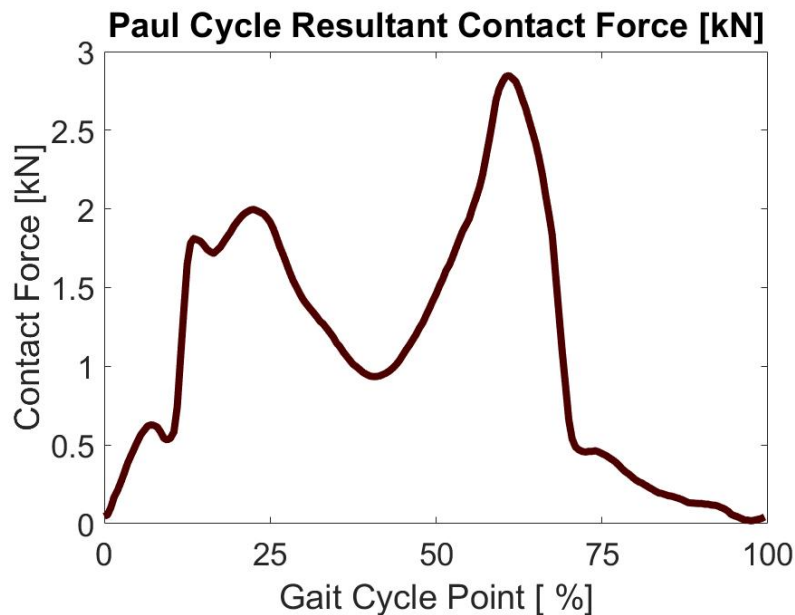


Figure 3.20: Paul Cycle resultant contact force gait profile (Paul, 1966).

3.5.1 Method

The contact forces for the profiles were sourced from Paul (1966), which did not include motions of the pelvis. Hence, only the case where pelvic motions are excluded was simulated for this sub-study. The contact forces were formatted identically to HIP98 data and the cup was positioned at 45° inclination and 7° version in the global coordinate space, which fits with the “safe zone” description by Lewinnek et al. (1978). This cup orientation is most similar to the cup orientation for patient KWR, where inclination was 46° and version was 11° . The *Paul Cycle* adapted resultant force profile is shown in Figure 3.20. In comparison to all the patients in HIP98 data, for *Paul Cycle* gait the maximum contact force was established for the second half of the stance phase. The contact force profile also had two distinct contact force peaks which are not seen for patients PFL

and IBL.

The edge proximity angle results for *Paul Cycle* were compared to walking with self-selected speed results for HIP98. The results for HIP98 discussed in Section 3.3 in order to identify the potential differences in *in vitro* and *in vivo* joint performance. In addition to edge proximity angles, the centre proximity angles were added to the output graphs.

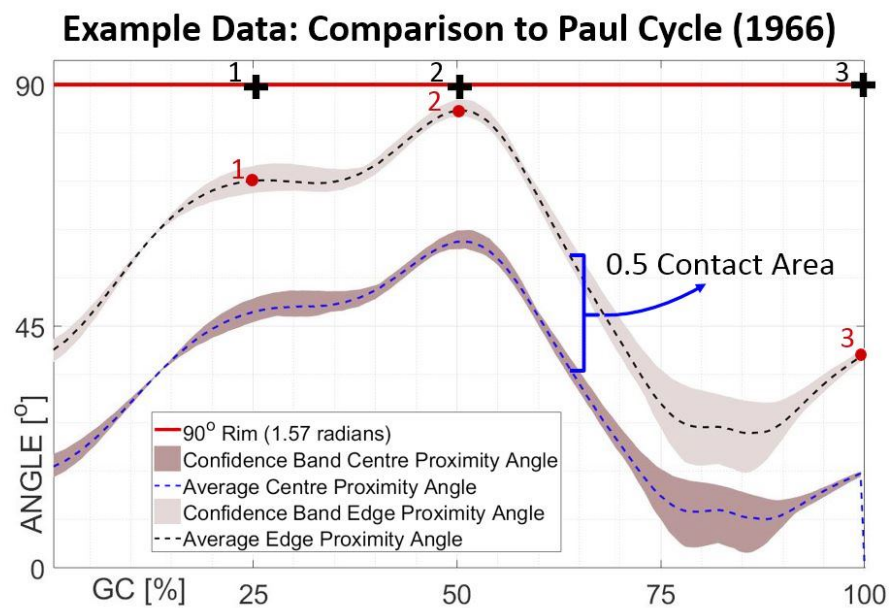


Figure 3.21: Example of output for sub-study 3 of HIP98 data analysis. The figure presents a plot for centre and edge proximity angles, and location of maximum contact along the rim for pelvic motions included case. The red dots are for locations of resultant contact force vector for maximum proximity angles, the black crosses are for locations of corresponding maximum proximity angle along the rim of the cup. These markers correspond to markers in 3.22. The distance between centre and edge proximity angles for one instance shows the magnitude of contact area half, for that gait cycle point. GC is for gait cycle point.

To address the difference in potential cup damage between THR under *Paul Cycle* gait conditions and under gait HIP98 conditions, the locations of maximum angles along the acetabular rim were established using algorithm described in Chapter 2, Section 2.6.7. The measurements were taken for maximum edge proximity angles during heel-strike to mid-stance, mid-stance to toe-off and swing phase regions for walking with self-selected speed.

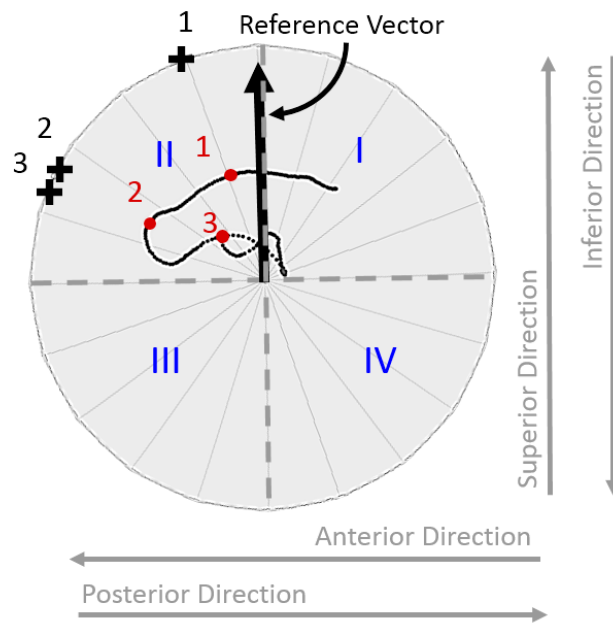


Figure 3.22: The red dots and black crosses are markers that correspond to 3.21. The red dots are for location of centre of contact area for maximum centre proximity angles, the black crosses are for locations of corresponding maximum proximity angle along the rim of the cup. The black curve represents the path of contact area centre through the cycle. Cup is split in four quadrants as marked in blue. Reference vector is the vector from cup origin to the superior part of the cup for initial orientation.

For pelvic motions included, the maximum centre proximity angles were found across the cycle as seen in Figure 3.19. For pelvic motions excluded case, the maximum centre proximity angles occurred near the middle of the cycle for patients HSR and PFL, and at 65% of the gait cycle for patient KWR.

Finally, the potential damage locations for other available activities were also assessed. For locomotor activities the same three measurement were taken as for walking with self-selected speed. For non-locomotor activities only one measurement for maximum proximity angles were taken. All the data for HIP98 used in this sub-study was for simulations where pelvic motions were included into simulation.

3.5.2 Results

Analysis of proximity angles

The results for this sub-study are presented in Figure 3.23 for the proximity angle profiles. The maximum edge proximity angle for *Paul Cycle* profile was found in the first quarter of the stance phase, similarly to patients HSR and KWR. The maximum edge proximity angle was established to be 70° , which is lower than for all the patients but patient KWR. The proximity angles profile curves for *Paul Cycle* were most similar to patient's IBL, with no dramatic drop in proximity angles after just-before toe-off point. This suggests that for *Paul Cycle* contact is close to the rim during both low and high load periods, compared to patients HSR, PFL and KWR. There was also established drop in proximity angles in the middle of the gait cycle, which was also true for patients HSR, PFL and KWR. However, for *Paul Cycle*, the duration of that drop was visually longer.

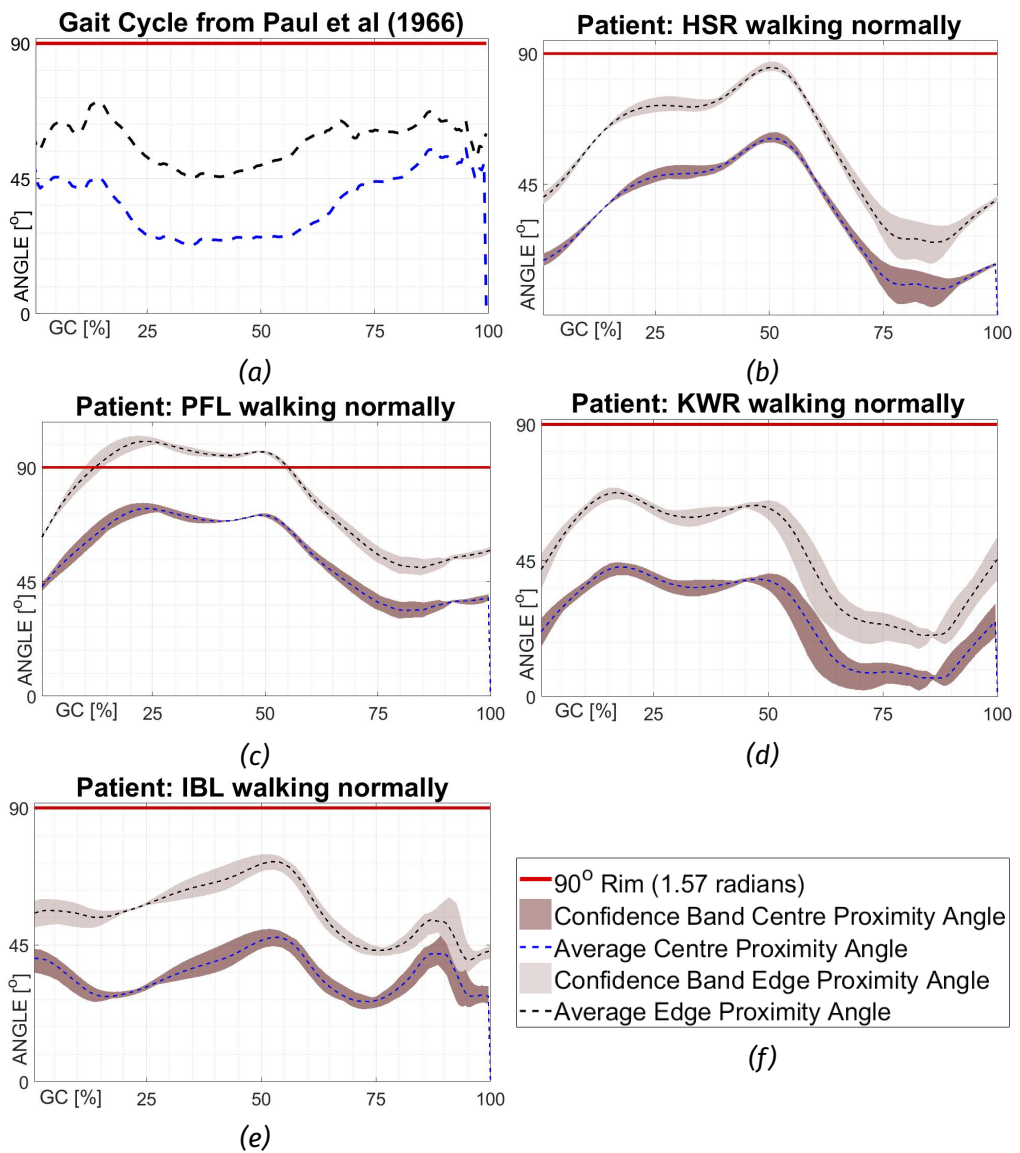


Figure 3.23: Centre and edge proximity angles for (a) Paul Cycle, (b) - (e) for HIP98 patients during walking with self-selected speed. Figure (f) - legend.

Analysis of risk of edge contact location along the rim for walking

Figure 3.24 shows the output for location of maximum edge proximity angles for *Paul Cycle* simulation, for three regions during the gait cycle.

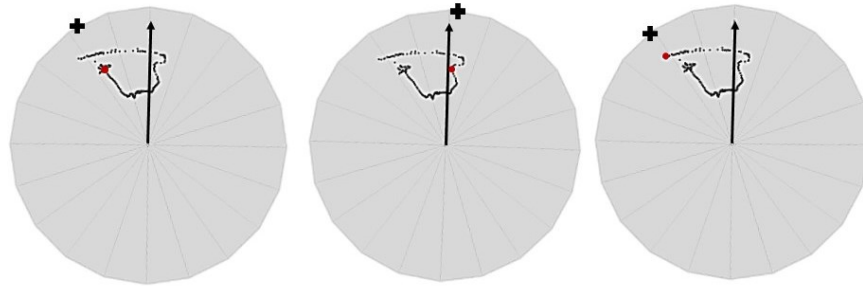


Figure 3.24: Location of the maximum proximity angles for heel-strike to mid-stance (left), mid-stance to toe-off (middle) and swing phase (right) for **Paul Cycle**. Left direction - posterior, right direction - anterior. Black arrow - reference vector. Grey curve - contact path along the cycle, in red - contact path point for maximum risk of edge contact. Location along the rim - black cross. One division on the cup is 18°.

The locations along the rim were registered in superior part of the cup either in first or second quadrant (Chapter 2, section 2.6.7). The angle deviation from reference vector, co-linear with version axis, was 31° for heel-strike to mid-stance region, 3° for mid-stance to toe-off region, and 39° for swing phase region. The results for walking with self-selected speed are presented in Figure 3.25. The contact locations along the rim for HIP98 patients for walking with self-selected speed were similar to *Paul Cycle*, covering superior part of the acetabular liner. The maximum deviation from the reference vector was found for patient HSR 3.25a and was equal to 51°. In contrast to *Paul Cycle* the location of maximum contact during swing phase was found closer to the reference vector, with maximum deviation of 28°.

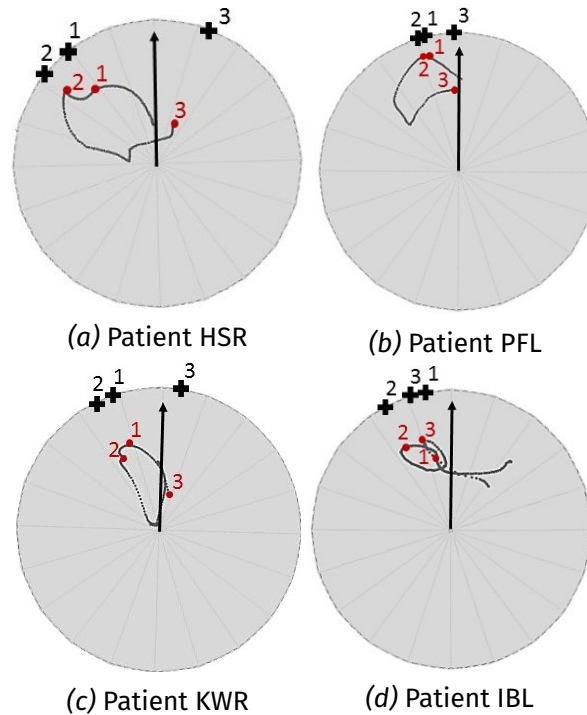


Figure 3.25: Location of the maximum proximity angles for heel-strike to mid-stance (1), mid-stance to toe-off (2) and swing phase (3) across all patients for **walking with self-selected speed (normally)**. Black arrow- reference vector. Grey curve - contact path along the cycle, in red - contact path point for maximum risk of edge contact. Location along the rim - black cross. One division on the cup is 18° . Left direction- posterior, right direction - anterior.

Analysis of risk of edge contact location along the rim different activities

The results for walking fast are presented in Figure 3.26. The contact locations along the rim for HIP98 patients for current activity were similar to *Paul Cycle*, covering superior part of the acetabular liner. The maximum deviation from the reference vector was found for patient KWR 3.26c and was equal to 38° . Similar to walking with self-selected speed the for patient HSR and KWR location of maximum proximity angle along the rim for swing phase was registered in first quadrant, with maximum deviation of 29° for patient HSR. Similar to other walking modes, for walking slow the maximum edge proximity angle along the rim was located in the superior region of the acetabular cup. The maximum deviation from reference vector was established to be 41° , which was close to values found for *Paul Cycle*. Swing phase location was closer to the reference vector than for the other two walking activities, with maximum reaching 9° .

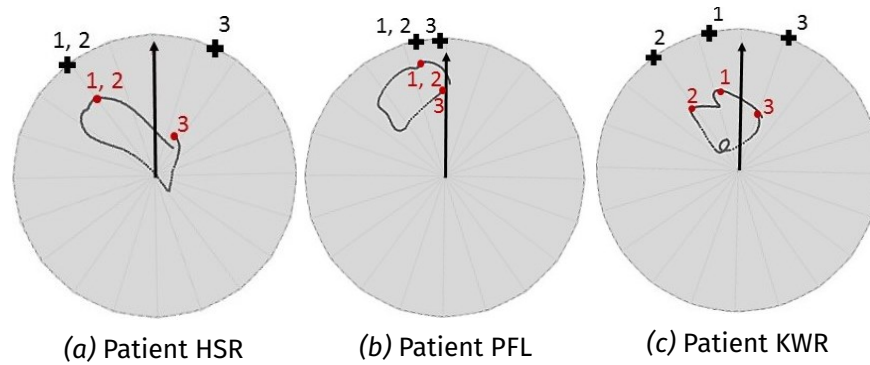


Figure 3.26: Location of the maximum proximity angles for heel-strike to mid-stance (1), mid-stance to toe-off (2) and swing phase (3) across all patients for **walking with faster speed**. Black arrow- reference vector. Grey curve - contact path along the cycle, in red - contact path point for maximum risk of edge contact. Location along the rim - black cross. One division on the cup is 18° . Left direction- posterior, right direction - anterior.

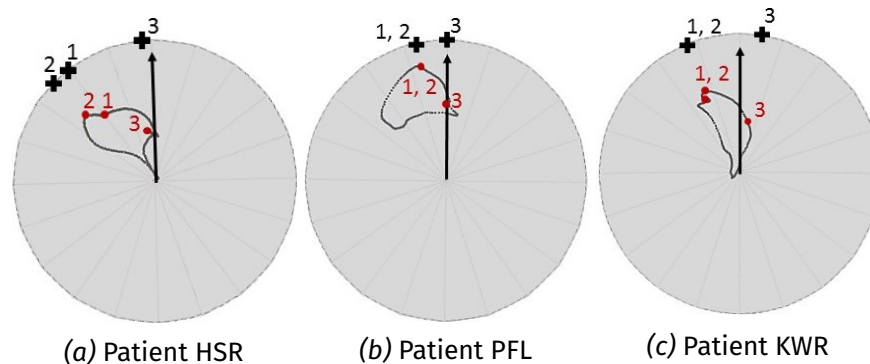


Figure 3.27: Location of the maximum proximity angles for heel-strike to mid-stance (1), mid-stance to toe-off (2) and swing phase (3) across all patients for **walking with slower speed**. Black arrow- reference vector. Grey curve - contact path along the cycle, in red - contact path point for maximum risk of edge contact. Location along the rim - black cross. One division on the cup is 18° . Left direction- posterior, right direction - anterior.

The location of maximum edge proximity along the rim for stair ascent was variable between patients. For patients HSR, PFL and KWR the angles were all located in the superior part of the second quadrant, with maximum deviation from reference vector equivalent to 63° (patient HSR). This deviation was almost 20° more than for *Paul Cycle*. For patient IBL during the second half of the activity cycle the locations of the maximum proximity angles were also established for superior region of the cup. However, for the first half of the stance phase the location of the maximum proximity angle reached inferior part of the first quadrant. The deviation for that instance was found to be 61° .

For stairs down activity results also showed the occurrence of maximum proximity angles along the rim in the superior part of cup, more specifically in the second

quadrant. The maximum deviation from reference vector registered for between three patients was 57° for patient PFL at swing phase. For stance phase the maximum deviation from the reference vector was equal to 35° .

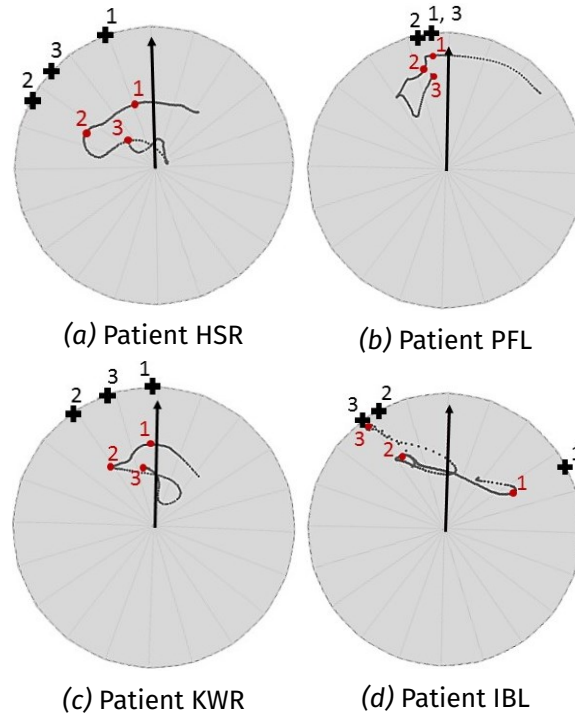


Figure 3.28: Location of the maximum proximity angles for heel-strike to mid-stance (1), mid-stance to toe-off (2) and swing phase (3) across all patients for **stair ascent**. Black arrow- reference vector. Grey curve - contact path along the cycle, in red - contact path point for maximum risk of edge contact. Location along the rim - black cross. One division on the cup is 18° . Left direction- posterior, right direction - anterior.

For raising from the chair, only for one patient (PFL) the maximum edge proximity angle location along the rim was registered in the superior part of the cup. For other patients the location of maximum contact along the rim was found in the fourth quadrant, with maximum deviation from the reference vector of 119° in clock-wise direction.

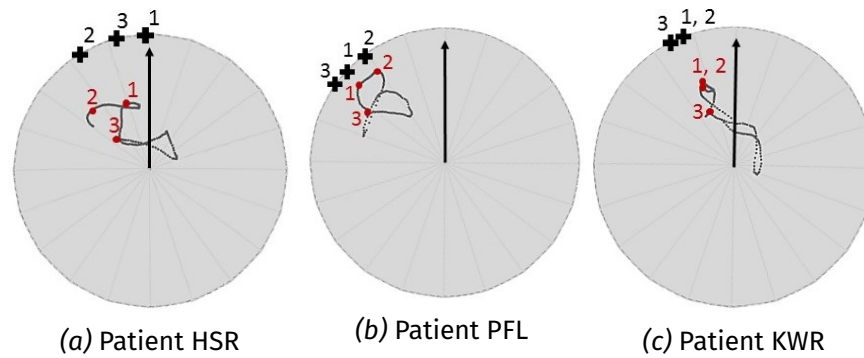


Figure 3.29: Location of the maximum proximity angles for heel-strike to mid-stance (1), mid-stance to toe-off (2) and swing phase (3) across all patients for **stair descend**. Black arrow- reference vector. Grey curve - contact path along the cycle, in red - contact path point for maximum risk of edge contact. Location along the rim - black cross. One division on the cup is 18°. Left direction- posterior, right direction - anterior.

For sitting down on the chair maximum edge contact risk in terms of location along the rim was inferior as seen in Figure 3.31d. The maximum deviation from the reference vector was seen for patient IBL and was equivalent to 116° in clockwise direction. Only exception, as for previous activity, was patient PFL with location of maximum proximity angle in superior region of the cup.

Data for bending knees activity was available only for three patients, HSR, PFL and KWR, and showed similar location of the maximum proximity angle as for previous two non-locomotor activities. For patient PFL, the location was found to occur in the anterior-superior region of the cup. For patients HSR and KWR the location along the rim was recorded in the posterior-inferior part of the cup, with maximum deviation from reference vector of 115° in clockwise direction.

Finally, for standing the location of maximum edge contact risk along the rim was also in superior region of the cup as for locomotor activities and *Paul Cycle* (Figure 3.33). The maximum deviation away from the reference vector was smaller than for other activities and was equal to 31°.

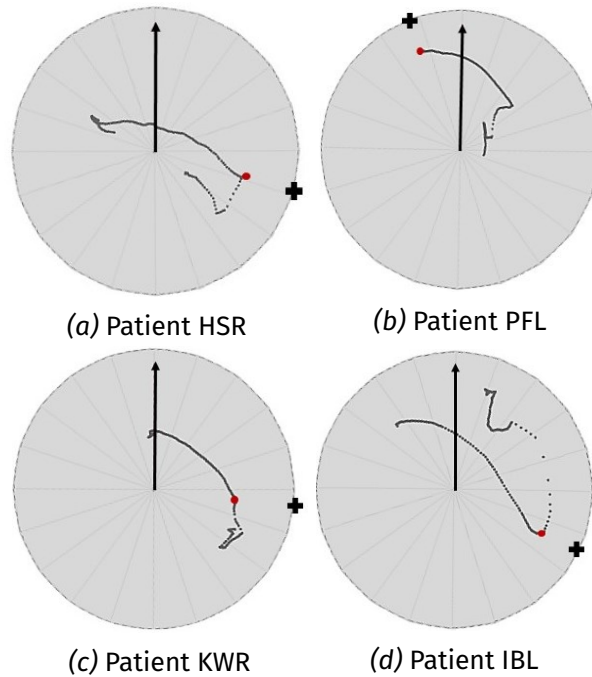


Figure 3.30: Location of the maximum proximity angles for maximum proximity angle occurrence across all patients for **raising from the chair**. Black arrow- reference vector. Grey curve - contact path along the cycle, in red - contact path point for maximum risk of edge contact. Location along the rim - black cross. One division on the cup is 18° . Left direction- posterior, right direction - anterior.

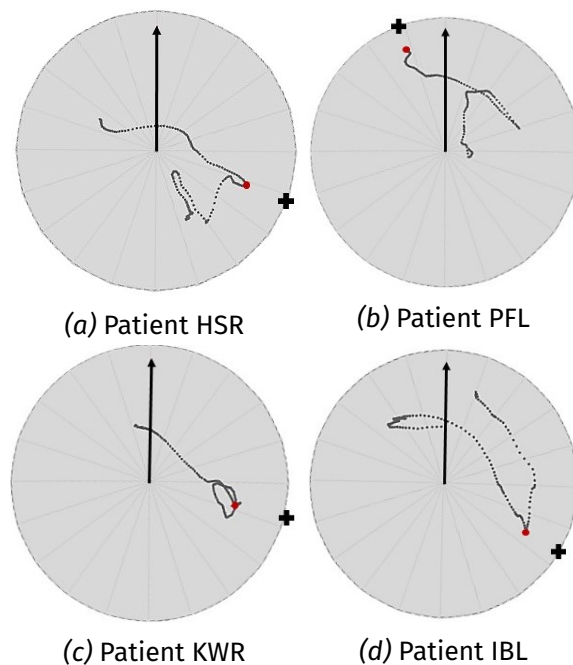


Figure 3.31: Location of the maximum proximity angles for maximum proximity angle occurrence across all patients for **sitting down on the chair**. Black arrow- reference vector. Grey curve - contact path along the cycle, in red - contact path point for maximum risk of edge contact. Location along the rim - black cross. One division on the cup is 18° . Left direction- posterior, right direction - anterior.

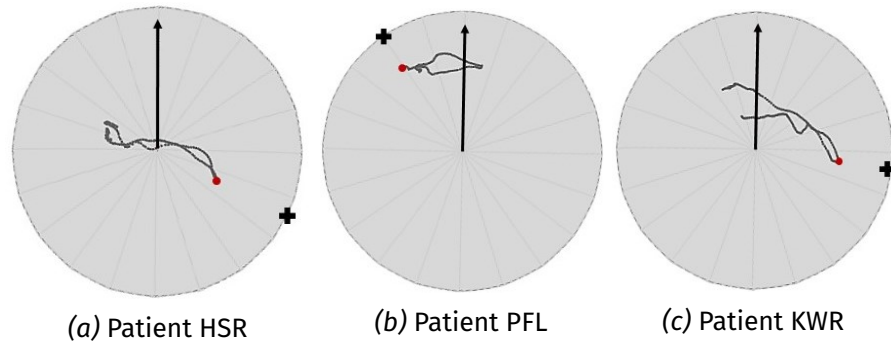


Figure 3.32: Location of the maximum proximity angles for maximum proximity angle occurrence across all patients for **bending knees**. Black arrow- reference vector. Grey curve - contact path along the cycle, in red - contact path point for maximum risk of edge contact. Location along the rim - black cross. One division on the cup is 18° . Left direction- posterior, right direction - anterior.

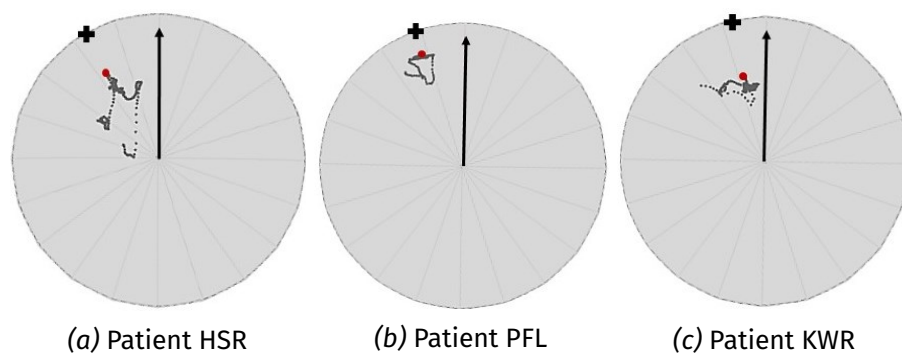


Figure 3.33: Location of the maximum proximity angles for maximum proximity angle occurrence across all patients for **standing on two-one-two legs**. Black arrow- reference vector. Grey curve - contact path along the cycle, in red - contact path point for maximum risk of edge contact. Location along the rim - black cross. One division on the cup is 18° . Left direction- posterior, right direction - anterior.

3.5.3 Conclusions

- Analysis of the risk of edge contact for THR performance under the *Paul Cycle* with the cup positioned at 45° inclination and 7° anteversion was performed. The analysis revealed that the edge proximity angle profile does not represent the profiles for THR patients within HIP98 dataset (Bergmann, 2008);
- Maximum proximity angle for THR under *Paul Cycle* conditions was lower than for most of the patients except for KWR. The acetabular cup orientation for patient KWR was the closest to *Paul Cycle*, with 46° inclination and 8° anteversion. This suggests that *Paul Cycle* testing conditions might over estimate the risk of edge contact for some patients;
- In contrast to patients HSR, PFL and KWR, under *Paul Cycle* conditions swing proximity angles during swing phase are as high as during stance phase;
- Location of the maximum proximity angles for *Paul Cycle* conditions were found in the superior region of the cup. In general, for tests under *Paul Cycle* conditions the location of highest risk of edge contact is comparable to locomotor activities for all patients. The exclusion to this pattern was patient IBL;
- Proximity angle locations along the rim for *Paul Cycle* and non-locomotor activities from HIP98 database varied substantially, except for standing. For most patients, but PFL, the locations along the rim were found in posterior-inferior region of the cup. For patient PFL, the location was established in the anterior-superior region of the cup. Hence, it can be speculated that *Paul Cycle* does not include damage of the acetabular component which may occurred while performing non-locomotor activity;
- For standing on two-one-two legs the location of maximum proximity angle was similar to *Paul Cycle* and locomotor activities. This is most likely result of dominant vertical direction of the resultant contact force during aforementioned activities.

3.6 Overall conclusions and summary

3.6.1 Main findings

The main findings and observations of the sub-studies of Chapter 3 are listed below:

1. Across all the patients, the region of high risk of edge contact was found to correspond with stance phase. This was true for walking with self selected speed, walking with faster and slower speeds, going up the stairs and going down the stairs;
2. Activities with the highest risk of edge contact were found to be all the locomotor activities and standing on two-one-two legs;
3. Edge contact incidence was registered only for one patient, with highest cup inclination angle and body weight across the patient cohort;
4. Exclusion of pelvic motions resulted in decrease in risk of edge contact for walking with self-selected speed and walking fast, during stance phase;
5. For standing on two-one-two legs the exclusion of pelvic motions from the simulation increased the risk of edge contact in two patients;
6. Risk of edge contact for locomotor activities for HIP98 patients was found to be comparable to the results for proximity angles under *Paul Cycle* conditions. However, for the rest of the activities, the risk of edge contact throughout the activity cycle did not resemble proximity angles under *Paul Cycle* conditions;
7. The location of the potential damage along the rim was found to be at the superior part of the rim for all the locomotor activities, standing and *Paul Cycle*. For rising from the chair, sitting down on the chair and bending knees the location of the potential rim damage was established to be at the inferior-posterior part of the cup.

3.6.2 Discussion on the findings

Current pre-clinical testing studies mainly focus on the effects of surgical cup orientation and head-cup separation. These tests include ISO 14242-4:2014, modified ISO 14242-4:2018, loading and motion conditions which take into account standardised walking gait cycle. The ISO standard, developed in the year 2002, was derived from earlier tests which in some cases used *Paul Cycle* (Paul, 1966) as discussed by Ali et al. (2016). The effect of daily activities on the success of THR is not investigated under ISO 14242-4:2014. Hua et al. (2016) investigated the effects of daily activities using the same database as in current study, HIP98 (Bergmann, 2008). In the study by Hua et al. (2016) the occurrence and duration of edge contact for variable activities and cup orientation angles were assessed in computational parametric tests. The study showed that for some activities the THR are more at risk of edge contact than others. However, the Hua et al. (2016) study focus was only on the averaged patient's joint contact force inputs. The pelvic motions and patient variability were studied. The aim of the present study was to investigate into the risk of edge contact occurrence for four available patients in isolation, addressing the variability between both patients and activities.

This chapter was split into three sub-studies which highlighted the variation between patients, activities and a comparison with *in vitro* testing. The sub-studies included evaluation of risk of edge contact across patients and activities, the effects of pelvic motions on contact location between THR bearings and comparison of proximity tool outputs from HIP98 patients, to *Paul Cycle* outputs.

Edge contact is known to be caused by sub-optimal alignment of the total hip replacement components (Hua et al., 2016; Underwood et al., 2012). As discussed in many studies the combination of inclination and anteversion contribute to the success of THR *in vivo* (Lewinnek et al., 1978; McLawhorn et al., 2015; Lazennec et al., 2017). The current study found highest edge contact risk for patient with highest cup inclination, 59°, and mean, across the patients, cup anteversion of 18°. For this patient the theoretical contact area was found to be outside the generalised cup rim for most of the stance phase. Even though the cup

orientation was outside "safe zones", for dislocation, established by Lewinnek et al. (1978), the patient demographics (Table A.1) information shows that this patient had the highest body weight which might also contribute to the increased risk of edge contact.

Variability between patients seen for contact force magnitudes was also reflected by the proximity angle outputs across the patients and activities. The greater variability in joint contact forces was seen for non-locomotor activities such as rising up from the chair, sitting down on the chair and bending knees. The results for proximity angles also suggested that in those activities variation between patients is higher. Interestingly, the variation between trials for each patient and activity was also higher in non-locomotor activities, compared to walking and stair activities. This suggests that the actual pre-clinical and research analysis of component performance and success *in vivo*, might have to not only account for patient and activity variability but also inpatient activity performance variability. Potentially, the effects of inpatient variation during the cycle can be assessed by varying the load amplitudes during the pre-clinical test. Some research exists which confirms the effect of joint contact force variation on component damage during edge loading conditions. O'Dwyer Lancaster-Jones (2017) showed that the change in swing phase load directly affects the separation between THR bearing components.

Standard *in vitro* test set-up could be adjusted to involve static pelvic orientation by adjusting cup orientation (Grammatopoulos et al., 2014). However, the dynamic pelvic orientation is not explicitly included pre-clinical tests. Current study shows that pelvic motions influence the risk of edge contact to different extent during gait and standing. Specifically, for patients with similar edge proximity angle profiles the exclusion of pelvic motions underestimates the risk of edge contact during high load region. This suggests that current biomechanical pre-clinical tests might not encompass the severity and occurrence of the THR damage.

Standard total hip replacement experimental simulation tests could be adjusted to assess the wear rates related to edge contact (Williams et al., 2003). However, as mentioned in Section 3.1 most *in vitro* tests are aimed at assessing change

in wear rates between variable component designs rather than assessing mechanical rim damage other than wear. This could include fatigue damage and rim cracking (Tower et al., 2007). In current study, outputs of the proximity tool for HIP98 patients were compared to *Paul Cycle*. Results of that sub-study suggest that proximity angle profiles produced under *Paul Cycle* conditions do not represent the *in vivo* dynamic joint organisation. Under surgical alignment within the "safe zones" the risk of edge contact was under-predicted for most patients. For patient with closest cup orientation to *Paul Cycle* maximum risk of edge contact was lower than for *Paul Cycle* conditions, during walking with self-selected speed.

Retrieval analysis can be challenging in terms of identification of component damage reasons (Nevelos et al., 1999). Potential location of the damage along the rim was predicted by *Paul Cycle* for locomotor activities. For non-locomotor activities the locations were not predicted well.

Even though for this study there was no incidence of edge contact for non-locomotor activities, except for standing, the variation between patients was high while version angles were all positive. During retrieval analysis or *in vivo* radiological analysis this damage can be mistaken for other failure types, which could influence the alignment choice for revision surgery or recommendations for other patients. Hence, outcomes of the proximity tool developed in the scope of this project and other similar tools (Langston et al., 2018) can not only evaluate the risk of damage but also aid in identification of the location of the damage with respect to component design, including dual mobility and lipped liners.

There are several limitations to this study, the most evident is the small number of patients, four, of which one patient showed more irregular activity patterns compared to other patients. More controlled patient selection would be beneficial to confirm or reject the findings observed. Therefore, it is recommended that for future studies patient number and selection criteria are improved. In terms of pelvic motions, HIP98 (Bergmann, 2008) does not contain separate pelvic internal-external rotation, which could potentially reveal the pelvic motion having most effect on the risk of edge contact. Finally, the relationship between supine and standing position was not known, hence cup orientation was assumed

not to change between the imaging reference system and laboratory coordinate system for the initial cup position within the tool. It was shown that pelvic orientation both changes and does not change cup orientation (Grammatopoulos et al., 2014; Inaba et al., 2016), again suggesting patient variation.

3.6.3 Summary

In scope of this study it was shown that risk of edge contact is higher for locomotor activities and standing, than for other studied activities. The exclusion of pelvic motions from locomotor activities and standing reduces the risk of edge contact for walking and stair gait. For standing on two-one-two legs, the exclusion of pelvic motions increased the risk of edge contact.

The variation in patient-specific gait biomechanics, daily activities and even variation between activity trials was shown to be high in terms of location of contact between total hip replacement bearings. The exclusion of pelvic motions from the simulation showed an underestimation of edge contact risk for three THR patients during walking. The maximum decrease in edge contact risk was shown to be 12° which is higher than variation in surgical cup alignment (Kano et al., 2010). It can be suggested that before attempting the development of new profiles and standards for pre-clinical testing this variation should be quantified. The comparison to one of the pre-clinical test profiles, *Paul Cycle*, showed that while under idealised component placement the aforementioned profile underestimates the risk of potential damage, it is not clear whether adjustment to component alignment and introduction of edge loading would encompass the worst case scenario seen *in vivo*. Therefore, future studies should focus on assessing data for large number of patients with aim to identify whether ISO14242-4:2018 could be enhanced by activity and patient-specific variation. Based on findings of this study it can be suggested that pre-clinical testing could be focused on the damage location assessment, beneficial to retrieval analysis, as potential damage location is variable between non-locomotor and locomotor activities.

Chapter 4

Analysis of unilateral total hip replacement patients' gait and motion profiles

4.1 Introduction

This chapter describes the analysis of patient-specific gait data processed using the developed proximity tool (Chapter 2). The work reported was performed in collaboration with Leeds Biomechanical Research Centre (LBRC). Following the findings in Chapter 3, the effect of pelvic motions on the risk of edge contact was investigated for a patient cohort with stricter selection criteria and larger sample size. The hypothesis of the current study was that the pelvic motions substantially affect the risk of edge contact in total hip replacement patients during walking. To evaluate the effect of pelvic motions the case where pelvic motions were included into the simulation was compared to case where pelvic motions were excluded. The main outputs of this study were the angles between acetabular cup pole and contact area centre, and angle between cup pole and contact area edge. The measurements were taken for stance phase of the walking cycle.

In addition to the analysis done for the main hypothesis, other sub-studies were performed. Firstly, the contribution of separate pelvic motions around anatomical axes and their pairs to the overall pelvic motion effect was investigated. Secondly, the role of static pelvic orientation in the location of contact between THR bearings was assessed. Here the static pelvic orientation is governed by individuals posture and bone alignment. Thirdly, each pelvic motion pattern in the patient group was compared to the risk of edge contact for same patients. This allowed to establish the possible indicators of increased edge contact. The same was done for patient-specific demographic characteristics within the stud-

ied group. Finally, the risk of edge contact between patients was investigated. The sub-studies contribute to the overall aim of the PhD project of establishing the effect of patient or population gait variation, in terms of rotations and forces in hip joint on the risk of edge contact.

4.2 Patients and Methods

The data used in this study was acquired from Leeds Biomechanical Research Centre for 20 THR patients. Ethical approval was obtained via the UK national NHS ethics (IRAS project ID 151079) system and all participants provided informed, written consent. Data included pelvic angles, derived from the raw motion marker data and hip-joint contact forces, derived from the raw force platform data. The bespoke proximity tool, that calculates centre and edge proximity angles was used. The data format description and tool development process is described and discussed in detail in chapter 2.

4.2.1 Patient demographics and selection

The sample size in biomechanical activity studies ranges from four (Bergmann et al., 2001) to above hundred (Bennett et al., 2017) patients. In the current study the sample size of ten was chosen at first to determine whether there is a clear trend in the effects of pelvic motions. Based on preliminary results, which showed some pattern, data for another ten patients was acquired for more in-depth analysis. In total, 20 unilateral total hip replacement patients were selected for this study, of which seven were females and thirteen were males. Patients were selected from a wider cohort of 137 THR patients (Lunn et al., 2019), with inclusion criteria of 1 to 5 years post THR surgery. For this study patients with walking speeds of one standard deviation above the average were selected, and identified as high-functioning based on their speed. According to Gimmon et al. (2015) and Crosbie et al. (1997) the higher the walking speed the more mobile the pelvis is. Therefore, it can be speculated that there is greater chance of pelvic motion influencing the contact mechanics of THR. The level walking at self-selected speed was chosen as it is one of the regular daily activities and is the standard activity investigated by biomechanical studies. In addition, results

for the study in chapter 3 showed that walking is one of the activities that puts THR at most risk of edge contact. The data was provided for three walking trials and one standing trial for each patient. Patient demographics is presented in Table 4.1.

Table 4.1: Patients demographics and walking speed.

Patient	Gender	Age at Implantation [years]	Operated Hip	Total Body Weight [kg]	Height [cm]	BMI	Speed [$\frac{m}{s}$]
001	Male	57	Left	93	171.5	31.53	1.28
002	Male	63	Right	86	179	26.73	1.27
026	Male	80	Left	77	178	24.26	1.28
073	Male	64	Left	85	178	26.96	1.36
075	Male	69	Left	80	166.5	28.8	1.35
084	Male	69	Left	86	178	27.14	1.43
093	Male	69	Right	78	172	26.32	1.66
114	Male	60	Right	76	177	24.40	1.47
116	Male	62	Right	112	182	33.91	1.32
118	Male	62	Right	116	180	35.83	1.26
120	Male	65	Left	78	173	25.99	1.38
131	Male	73	Right	87	176	27.99	1.32
151	Male	65	Right	93	176	29.95	1.35
025	Female	72	Right	68	177	21.83	1.36
042	Female	81	Right	81	167	29.17	1.44
050	Female	63	Right	68	163.5	25.45	1.43
052	Female	72	Right	73	172	24.57	1.30
086	Female	68	Right	75	159.5	29.53	1.27
094	Female	75	Right	77	158	30.67	1.34
148	Female	78	Right	58	156	23.88	1.38

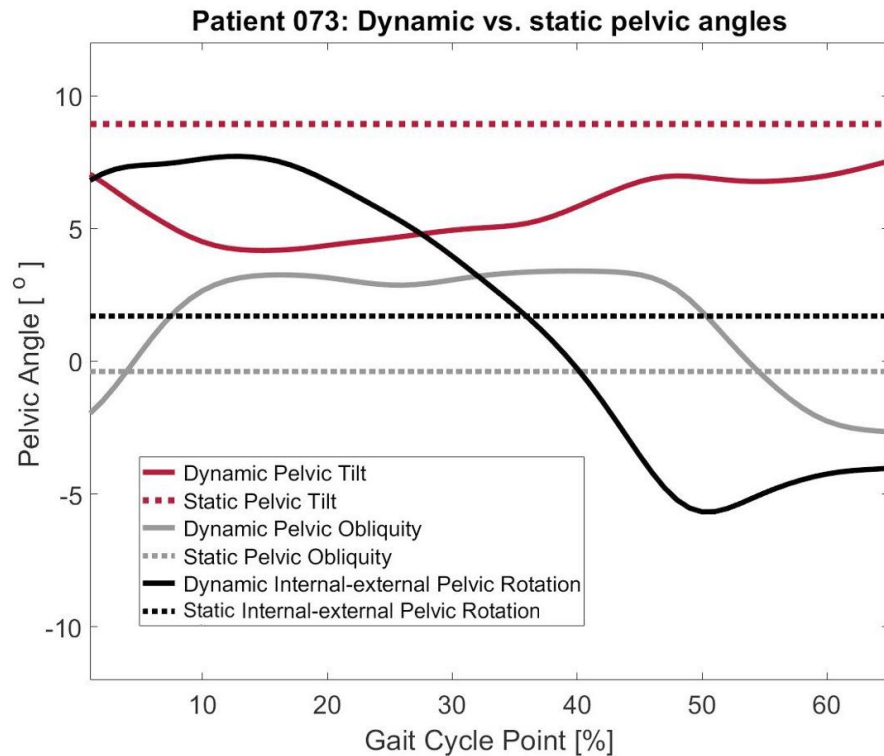
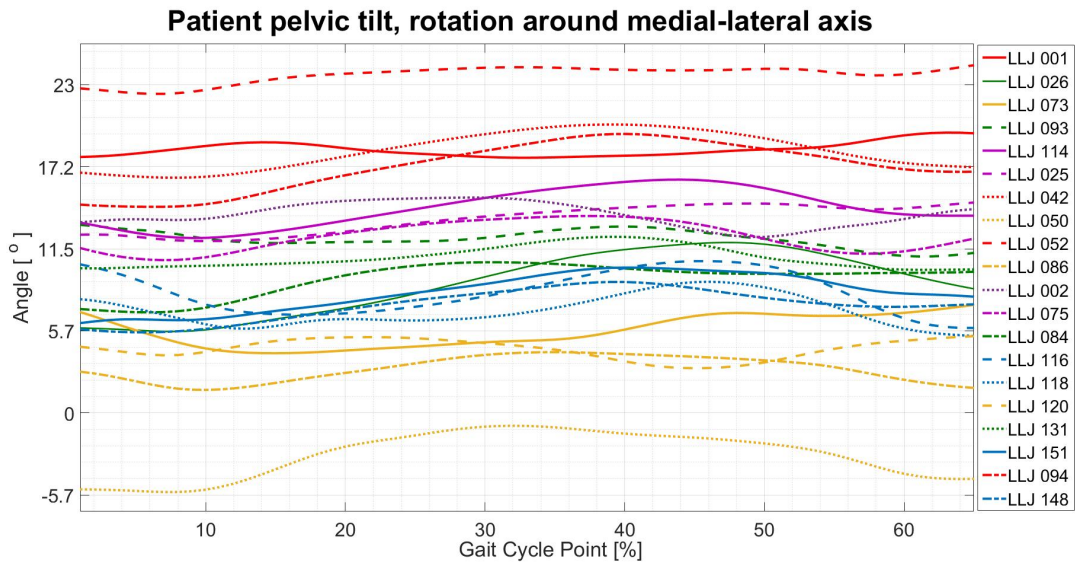
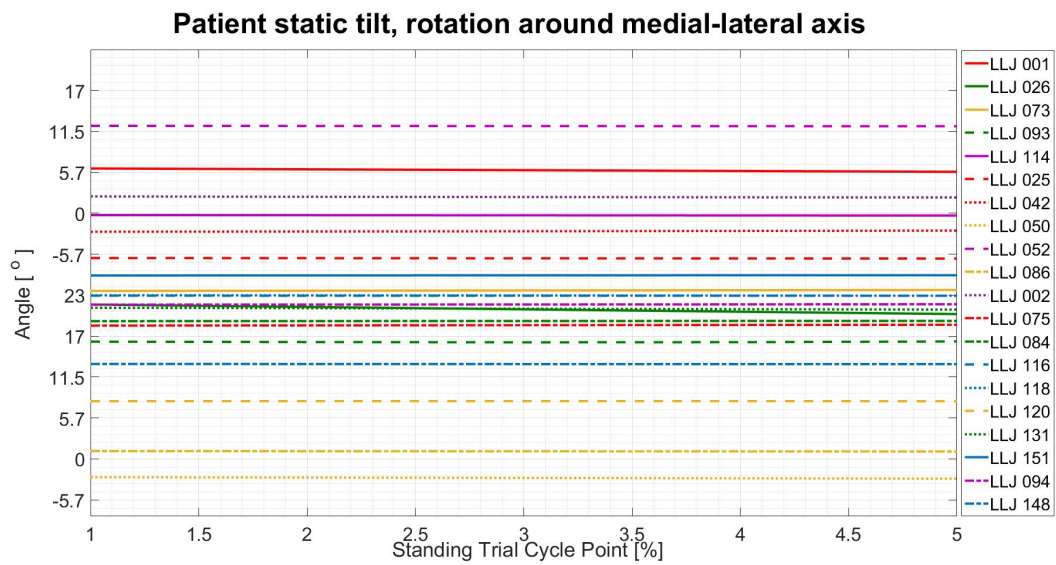


Figure 4.1: Patient 073 pelvic dynamic and static angles. Dynamic data measured through the stance phase for walking, and for five consecutive time-points for standing.

For each gait cycle point, the specific to patient hip-joint contact force vector components and three pelvic angles were provided. The joint contact force directions were specific to the operated leg. The contact force data included medial-lateral, anterior-posterior and superior-inferior force components. The pelvic angles included tilt, motion around medial-lateral axis; obliquity, motion around anterior posterior axis; and internal-external rotation, motion around superior-inferior axis. The three pelvic angles were used to apply the motions around the corresponding axes using the technique described in chapter 2, section 2.6.5. The data was provided in the laboratory coordinate system, which was assumed in current study to correspond with neutral pelvic coordinate system due to the absence of orientation information. This is the pelvic position in which the acetabular cup orientation is initially defined within the proximity tool. Due to the nature of the data capture method, only stance phase was considered. An example of pelvic static and dynamic angles for one patient, 073, for one trial are shown in Figure 4.1. As can be seen, the static angles do not fully represent the dynamic pelvic motions. Pelvic angles during one walking trial and standing trial for each individual are presented in Figures 4.2 - 4.4.

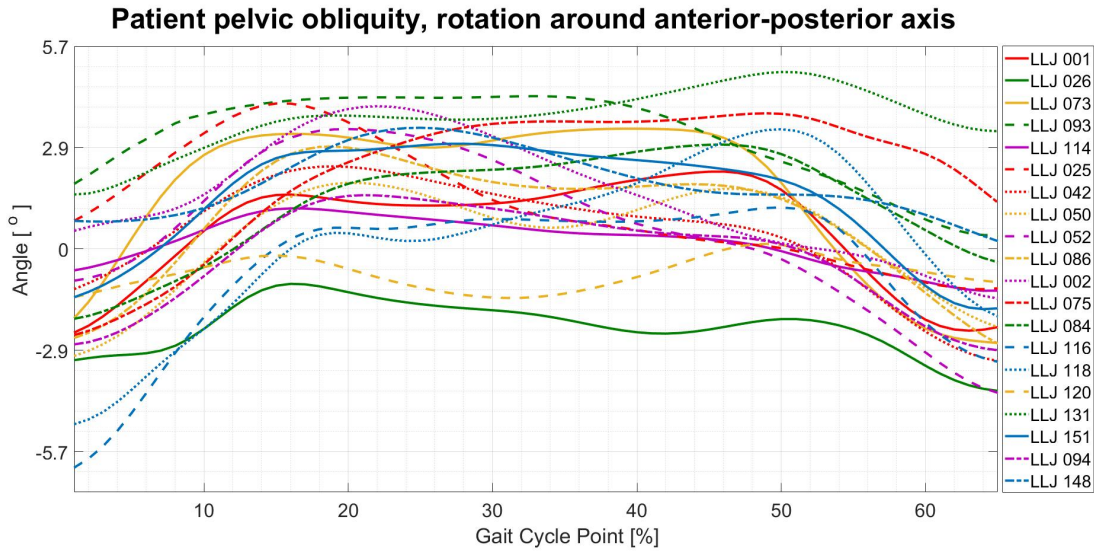


(a)

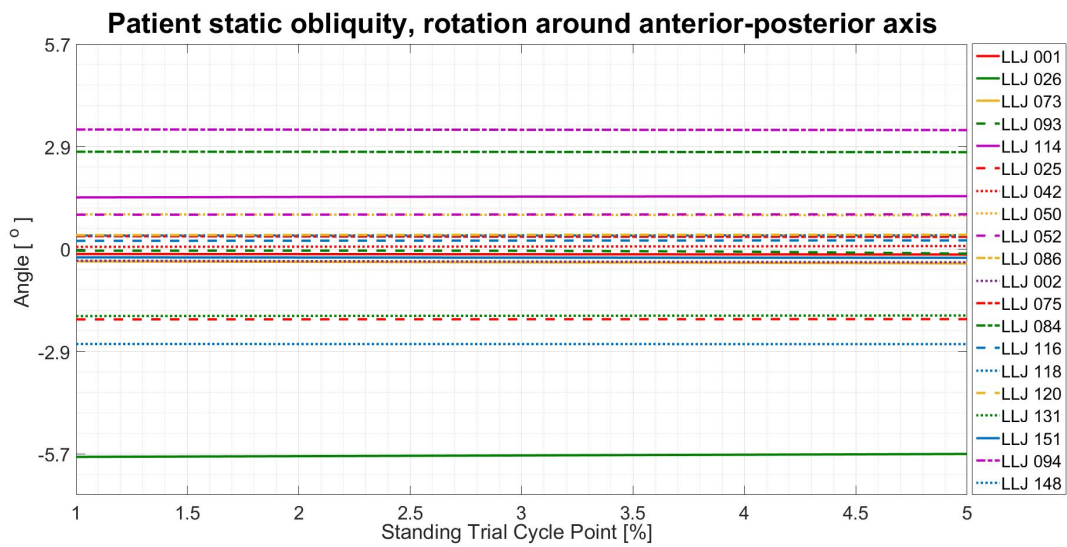


(b)

Figure 4.2: Patients pelvic dynamic walking (a) and static pelvic tilt (b). Dynamic tilt data for all 20 patients through the stance phase for walking and five consecutive cycle points for standing.

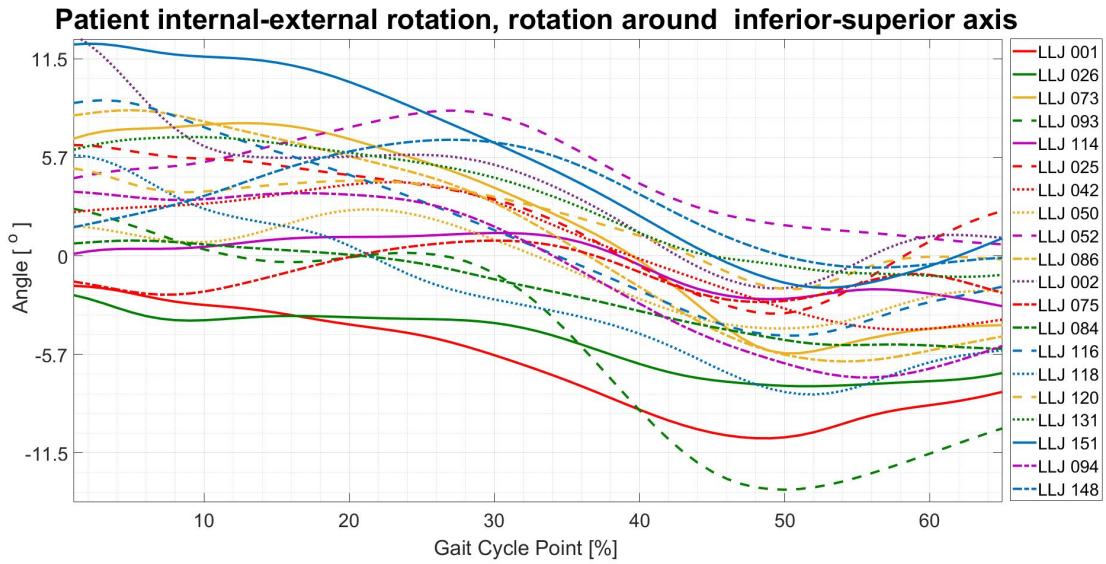


(a)

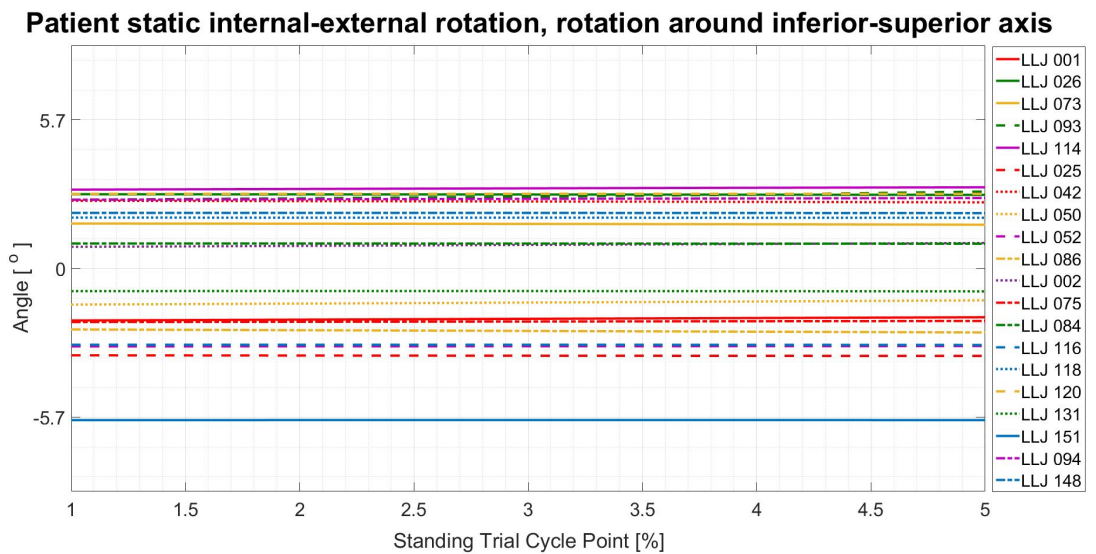


(b)

Figure 4.3: Patients pelvic dynamic walking (a) and static pelvic obliquity (b). Dynamic obliquity data for all 20 patients through the stance phase for walking and five consecutive cycle points for standing.



(a)



(b)

Figure 4.4: Patients pelvic dynamic walking (a) and static pelvic internal-external rotation (b). Dynamic tilt data for all 20 patients through the stance phase for walking and five consecutive cycle points for standing.

4.2.2 Study set-up and considerations

The same as in the previous study (Chapter 3), the centre proximity angle is defined as the angle from the centre of the contact to the cup pole. And edge proximity angles is defined as the angle from edge of contact to cup pole. The acetabular cup was assumed to have head-coverage of 180° , hence the proximity angle equal or above 90° would indicate an edge contact event. The acetabular cup was orientated in MATLAB global coordinate system at 45° inclination and 7° version. Therefore, there was an assumption that during the cup positioning the pelvic coordinate system is identical to MATLAB coordinate system, and imaging coordinate system. The identical cup inclination and version angles were used for each patient, to allow for comparison between patients, which is independent of static cup orientation.

4.2.3 Sub-studies description and analysis.

For each patient, nine proximity tool simulations were performed (Table 4.2). These were cases where the pelvic motions were excluded, all pelvic motions were included, one pelvic motion was included, pairs of pelvic motions were included and static pelvic orientation was excluded. The data analysis was separated into five sub-studies, which focused on different aspects of the output data. The proximity profiles generated and analysed in each study are presented in Table 4.2. The output data was split into two groups, representing proximity angles from heel-strike to mid-stance for region 1, and mid-stance to toe-off for region 2.

Table 4.2: Cases for each sub-study. The outputs were separated into, CP - centre proximity angle profiles, EP - edge proximity angles and none.

SUB-STUDY NUMBER	1	2	3	4	5
Pelvic Motions Excluded	CP	none	none	none	none
Pelvic Motions Included	CP	CP	CP	CP & EP	EP
Pelvic Tilt	none	CP	none	none	none
Pelvic Obliquity	none	CP	none	none	none
Pelvic Internal-External (IE) Rotation	none	CP	none	none	none
Pelvic Tilt & Obliquity	none	CP	none	none	none
Pelvic Obliquity & IE Rotation	none	CP	none	none	none
Pelvic IE Rotation & Tilt	none	CP	none	none	none
Pelvic Static Motions Excluded	none	none	CP	none	none

The effect of pelvic motions compared to simulations with no pelvic motions

The first sub-study was aimed at establishing the effect of pelvic motion exclusion from the proximity tool simulation. The two cases were considered for each patient, where all pelvic motions were included and all pelvic motions were excluded.

The focus was on the centre proximity angles as these show only the effect of pelvic motions, excluding the effect of joint contact force magnitude. To identify if the difference between two cases is substantial, two methods in conjunction were used. One was the confidence band overlap between the two, and second was the root mean square error (RMSE) between the two cases. The confidence band was defined as the area between centre proximity angles profiles generated for each of three walking trials. This was done for both pelvic motions included and excluded, hence the overlap could be visually observed if present. The RMSE method (Equation 4.1) was adopted from linear regression analysis technique, where the observed values are known results from real data, and expected values are the ones predicted by statistical model (derived from the data). The estimated values can also be viewed as the curve of best fit, hence the RMSE was the measure of prediction error. The closer RMSE value was to zero the more similar the observed result is to a predicted model (Myers et al., 2012). In this sub-study, the proximity angles when pelvic motions were included were expected values; and the proximity angles when pelvic motions were excluded were the observed values. The values which were above average RMSE were

counted as the ones affected by the exclusion of pelvic movement. These were further combined with the confidence band overlap analysis output.

$$RMSE = \sum_{i=1}^n \frac{(y_i - f(x_i))^2}{2} \quad (4.1)$$

Equation 4.1: root mean square error equation, where y_i is the observed value and x_i is the expected value.

The maximum centre proximity angles for two cases were evaluated. This was done for both stance phase regions. And the differences in maximum centre proximity angles were calculated between simulation with and without pelvic motions.

The contribution of each pelvic motion to the overall effect of inclusion of pelvic motions

In this sub-study the contribution of each individual pelvic motion, and paired pelvic motions to the overall pelvic motion effect was investigated. Hence the simulations for each patient were done for sagittal tilt, coronal obliquity, internal-external rotation and combination of sagittal tilt and coronal obliquity, sagittal tilt and internal-external rotation, coronal obliquity and internal-external rotation. The data was analysed for patients, for which the difference between pelvic motions included and excluded simulations was substantial. The first walking trial data was processed for each patient. Same as in previous section only the centre proximity angles were investigated. Each of the planar pelvic motions and pelvic motion pairs were compared to the case where all pelvic motions were included. In total there were six cases investigated, which were inclusion of tilt, obliquity, internal-external rotation, tilt and obliquity, obliquity and internal-external rotations, as well as tilt and external-internal rotations. The analysis was done both visually and using RMSE method described in previous sub-section. The lower the RMSE value the stronger the contribution to overall pelvic motions effect. The output for the case where all pelvic motions were included was taken as the expected data and output for the rest of the cases was taken as the

observed data.

The contribution of static pelvic orientation to the overall effect of inclusion of pelvic motions

The main aim of the third study was to investigate how much of the pelvic motion effect on the risk of edge contact is dominated by static pelvic orientation. For example, whether a large difference in proximity angle between pelvic motions included and pelvic motions excluded simulations can be predicted by applying the contact force profiles at standing tilt, obliquity and rotational position of the pelvis.

In the default analysis, the cup was placed in a neutral position before the application of pelvic motions and contact forces. For the current analysis the static angles of the pelvis were subtracted from the pelvic dynamic profiles. Figure 4.5a shows the example of raw pelvic static orientations shown by dotted lines, and dynamic shown by solid curves. Figure 4.5b shows modified dynamic pelvic profiles, which exclude static pelvic orientations. The two cases were compared in this study. First, where all pelvic motions were included and second, where all pelvic motions were included but with exclusion of static pelvic orientation (Figure 4.5b).

For the initial position in the proximity tool, the exclusion of static motions would be equivalent to a cup being positioned at 45° inclination and 7° version, while patient is standing. From biomechanical data collection perspective, this is the position from which patient starts walking. The schematic of the cup and pelvis position at the proximity tool initiation is show in Figure 4.6. On the left pelvis is in neutral position prior to the simulation and on the right the pelvis is in the standing position, the orientation of the cup between two pelvic orientations was the identical. Hence, for the case where static motions were excluded the initial cup orientation would not be in the same coordinate system, as in the other cases studied within this chapter. Only first trial was analysed for each patient in this sub-study. The visual data analysis was performed for this sub-study.

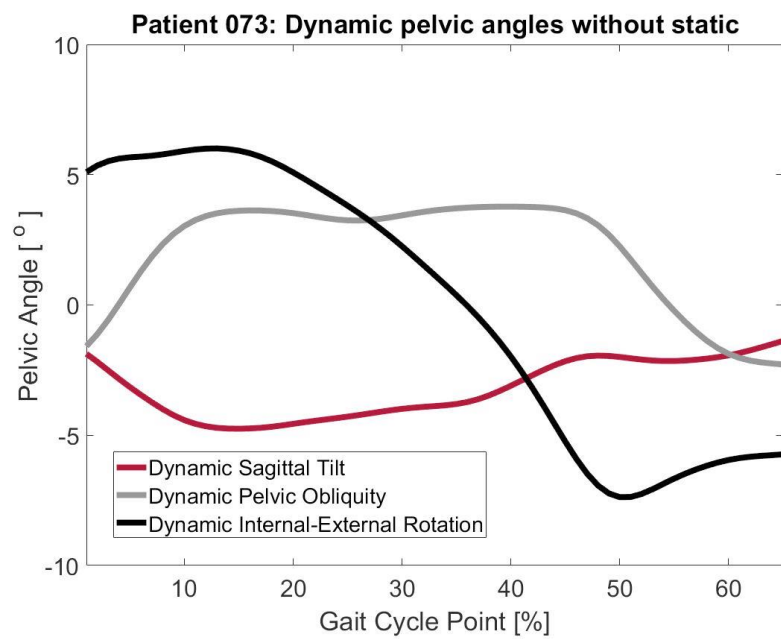
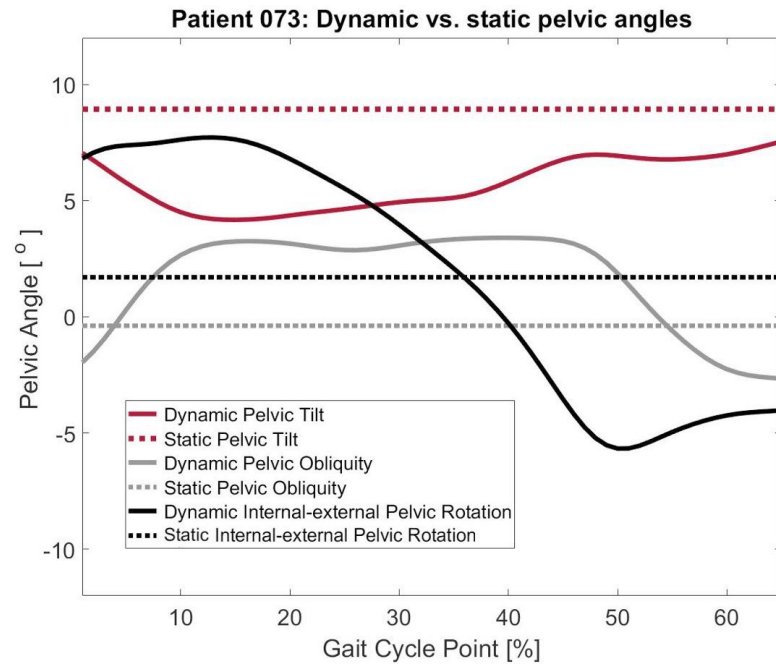


Figure 4.5: The example of static pelvic orientations, dynamic pelvic orientations and modified pelvic motion orientations for patient 073.

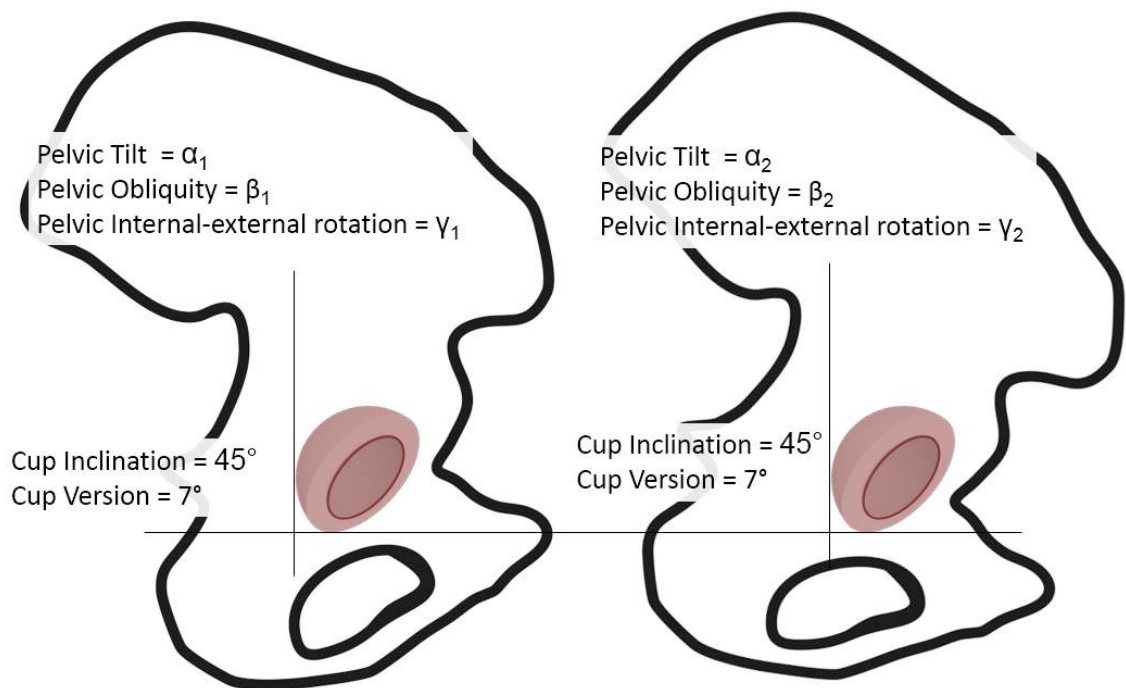


Figure 4.6: The schematics of the cup orientation within the pelvis for cases where patient-specific pelvic tilt was included (left) and excluded (excluded) from proximity tool simulations.

Centre proximity angle and patient-specific demographics and gait characteristics correlation

First, this sub-study was aimed to investigate if the centre proximity angles, for all pelvic motions included case, can be grouped for patients by their demographics characteristics outlined in Table 4.1. To achieve that, the patients were divided into two groups, the ones with risk of edge contact affected by pelvic motions and not affected. These groups were used to determine if the demographic characteristics divided into two groups for the same patients display any similar features.

Second, the pelvic motion profiles were analysed in terms of similarities for patients with similar pelvic motion effect. The possible correlation between the change in edge contact risk and pelvic motion pattern on the patient-specific basis was assessed. The RMSE values, pelvic motions were included versus excluded, were compared to average, maximum, minimum and range for each pelvic motion. This was done for region 1 and region 2 separately. Here the values for mid-stance and end of stance phase were estimated as averages across the patients.

The linear regression model was fitted to each case. The curve fitting tool available in MATLAB was used to identify coefficients of determination, R^2 and adjusted R^2 , and slope of the regression line. The R^2 is defined by Equation 4.2 and in the current study identifies the proportion of variation in RMSE values determined by the chosen pelvic motion variable. The proportion was established in the range from 0 to 1, the closer R^2 is to 1 the stronger was linear relationship (Myers et al., 2012).

$$R^2 = \frac{\sum_{i=1}^n (y_i - f(x_i))^2}{\sum_{i=1}^n (y_i - \bar{y})^2} \quad (4.2)$$

Equation 4.2: Coefficient of determination, where y_i is observed value, in this case RMSE for each patient, and $f(x_i)$ expected value by the regression model, in this case predicted RMSE from pelvic motion average, maximum, minimum or range. \bar{y} is the mean of RMSE values across the patients.

The adjusted R^2 values, explained by Equation 4.3, take into account the overall sample size. The negative adjusted R^2 suggests that the relationship is too complex to be described by the chosen regression model. The adjusted coefficient of determination was found for 95% confidence interval, due to it being a standard one used (Myers et al., 2012).

$$\bar{R}^2 = 1 - (1 - R^2) \frac{n - 1}{n - p - 1} \quad (4.3)$$

Equation 4.3: Adjusted coefficient of determination, \bar{R}^2 , where R^2 is explained in 4.2, n is sample size, in this case number of patients, and p is number of explanatory variables (independent variable), which for linear regression is equal to 1.

Finally, the slope of the regression line explained by Equation 4.4 indicated the direction of the relationship, positive for increasing regression line, negative for decreasing regression line and zero for constant regression line.

$$m = \frac{\Delta y}{\Delta x} \quad (4.4)$$

Equation 4.4: Slope of the regression line, where Δy is change in RMSE values and Δx is change in chosen pelvic motion variables.

The maximum edge proximity angles: stance regions comparison and location along the cup rim

The overall risk of edge contact for each patient was analysed using the results for edge proximity angles. This allowed the risk of edge contact to be established between two stance regions. This analysis included only the case where all three pelvic motions were included in the simulation. The maximum and average proximity angles for each region across all the 20 patients were compared. A visual comparison was done for this sub-study. In addition, a two sample paired t-test was used to determine the significance of the difference between two regions' maximum and average proximity angles. The analysis was performed using IBM SPSS software (IBM Corporation ® US).

Firstly, the normality of data distribution was determined using Shapiro-Wilk test. The skewness and kurtosis were checked, where skewness should not exceed 0.8 and kurtosis should not exceed 2 for the distribution to be normal. If these values were out of range, the outliers were removed. These were found using IBM SPSS built-in analysis for Interquartile Range (IQR) rule (Center, 2019). Secondly, if the normality was confirmed, a t-test was performed with a confidence interval of 95%, which meant if p-value was less than 0.05 then the variables were statistically different (Myers et al., 2012).

Finally, the clockwise location of the potential edge contact inflicted damage was established for both regions, using the add-on to the proximity tool described in chapter 2, section 2.6.7. The clockwise location from the reference vector was shown as negative angle, anti-clockwise from reference vector was shown as positive angle. The reference vector here is in the line of the version axis. Only maximum edge proximity angles were considered in this sub-study for both stance phase regions. The first quadrant was the region around the cup rim from 0° to 90° (anti-clockwise), second quadrant 0° to -90° (clockwise), third quadrant from -90° to -180° (clockwise) and fourth quadrant from 90° to 180° (anti-clockwise). Here the version axis was set as zero mark.





4.3 Results

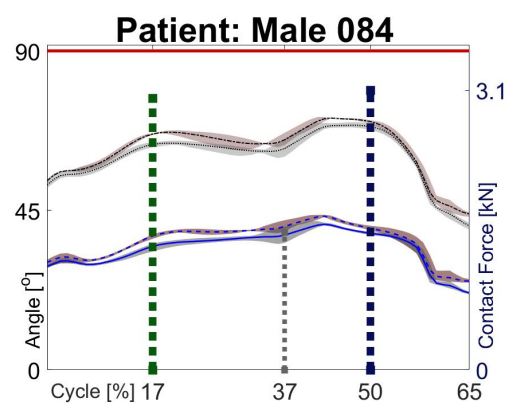
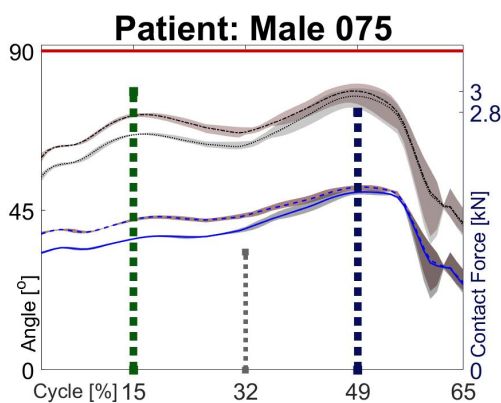
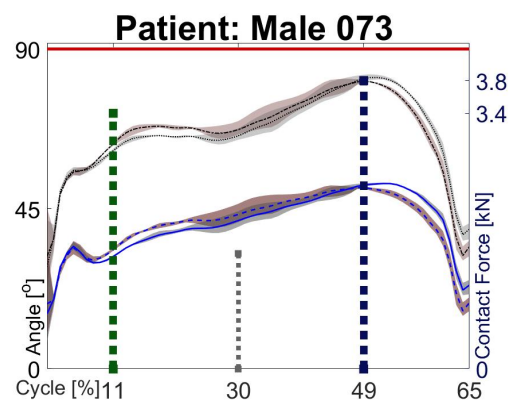
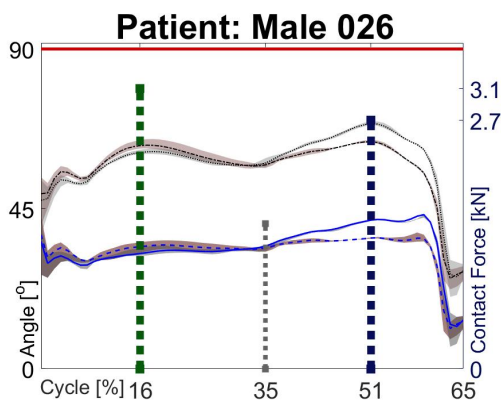
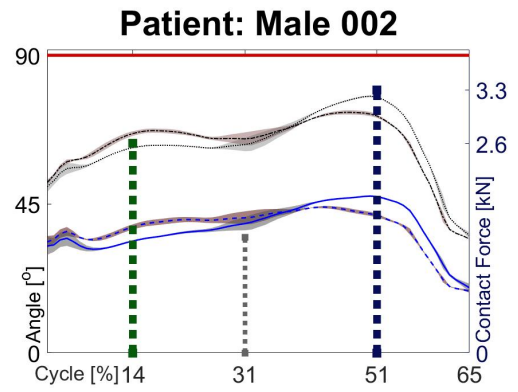
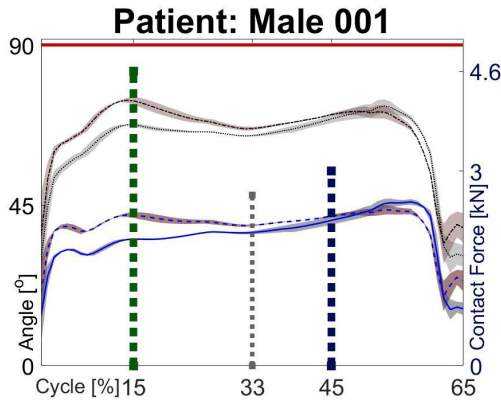
In total, walking profiles for 20 patients were analysed using the proximity tool. The centre proximity angles and edge proximity angles for each patient are reported in Figures 4.7 to 4.9. Figures show the results for cases where pelvic motions were included and where pelvic motions were excluded. These figures include the confidence band for each case, established from three walking trials. In addition, the incidents of resultant hip joint contact force peaks and mid-stance are added to each figure. Regions 1 and 2 were set from 0 to mid-stance and from mid-stance to end of the stance phase respectively.

From results graphs it can be seen that for some patients the inclusion of pelvic motion played a role of balancing the proximity angles between two gait cycle regions. The proximity angles for two load peaks were compared for simulation where pelvic motions were included and excluded. The results showed that the difference between load peaks angle was greater for simulations where pelvic motions were excluded, which can be clearly seen for patient 114. For this patient change between difference in the load peaks' proximity angles, was the greatest between simulations. The change was recorded to be 8° , where the differences between two load peaks proximity angles were 14° for pelvic motions excluded and 6° for pelvic motions included.

Proximity Results Legend :

-  Acetabular cup rim representation for head-coverage of 1.57 radians (90°)
-  Peak contact force during *region 1*
-  Peak contact force during *mid-stance*
-  Peak contact force during *region 2*

-  Pelvic motions excluded, centre proximity angle and edge proximity angle confidence bands
-  Pelvic motions included, centre proximity angle and edge proximity angle confidence band
-  Average for centre proximity angles included and excluded
-  Average for edge proximity angles included and excluded



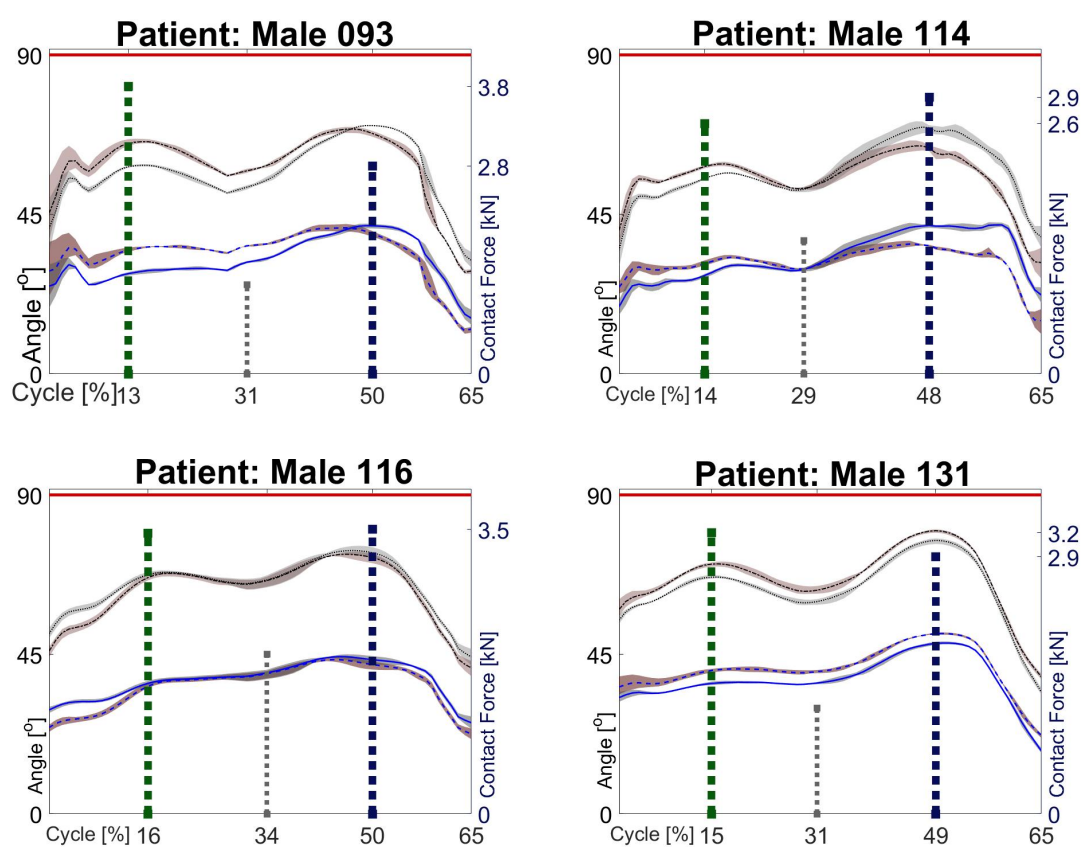


Figure 4.7: Results for centre and edge proximity angles visualised with the confidence bands for patients who's edge contact risk was not affected by pelvic motion inclusion. The peak contact, for region 1 and region 2 and mid-stance force instances are marked by hashed lines the values displayed on right yaxis.

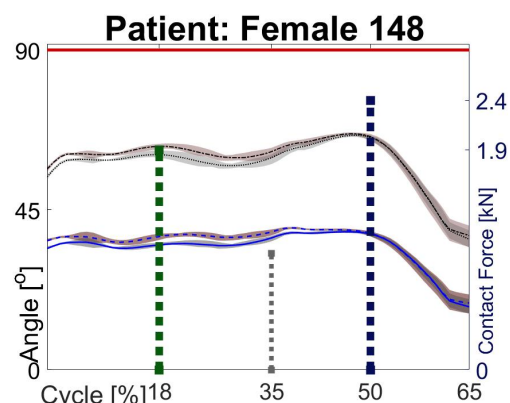
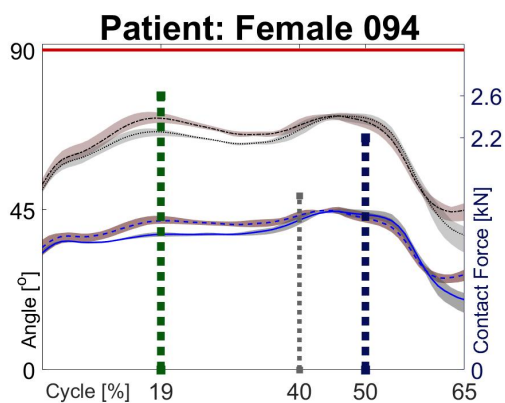
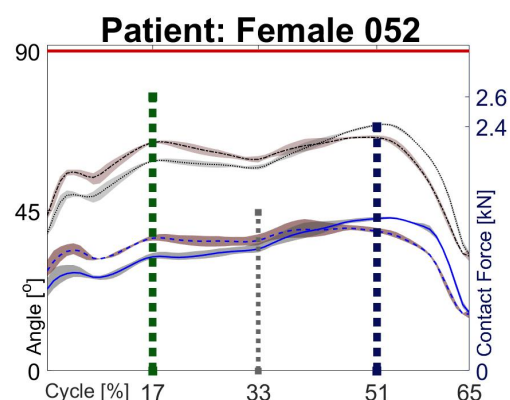
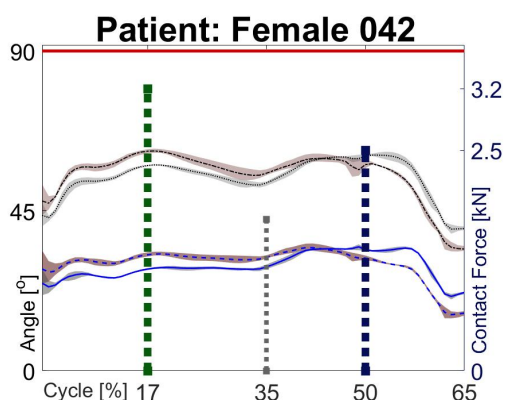
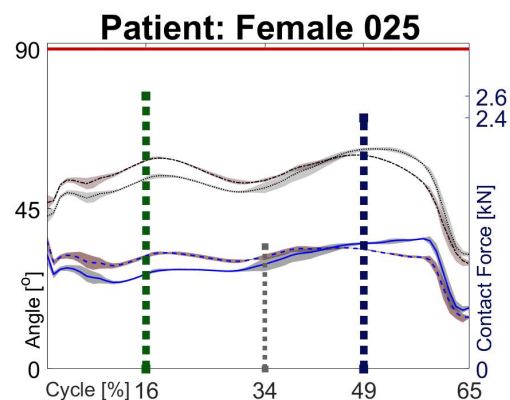
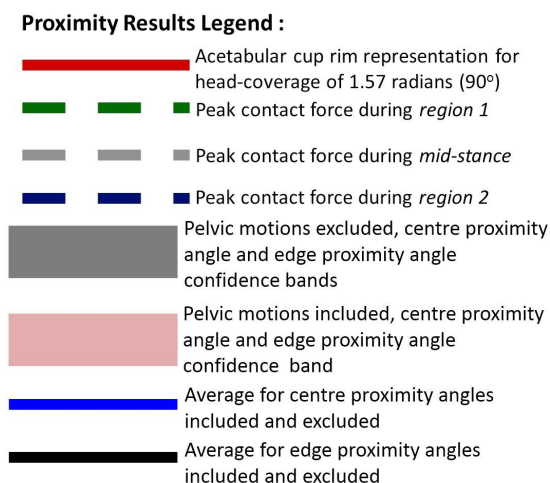


Figure 4.8: Results for centre and edge proximity angles visualised with the confidence bands for female patients who's edge contact risk was affected by pelvic motion inclusion. The peak contact, for region 1 and region 2 and mid-stance force instances are marked by hashed lines the values displayed on right axis.

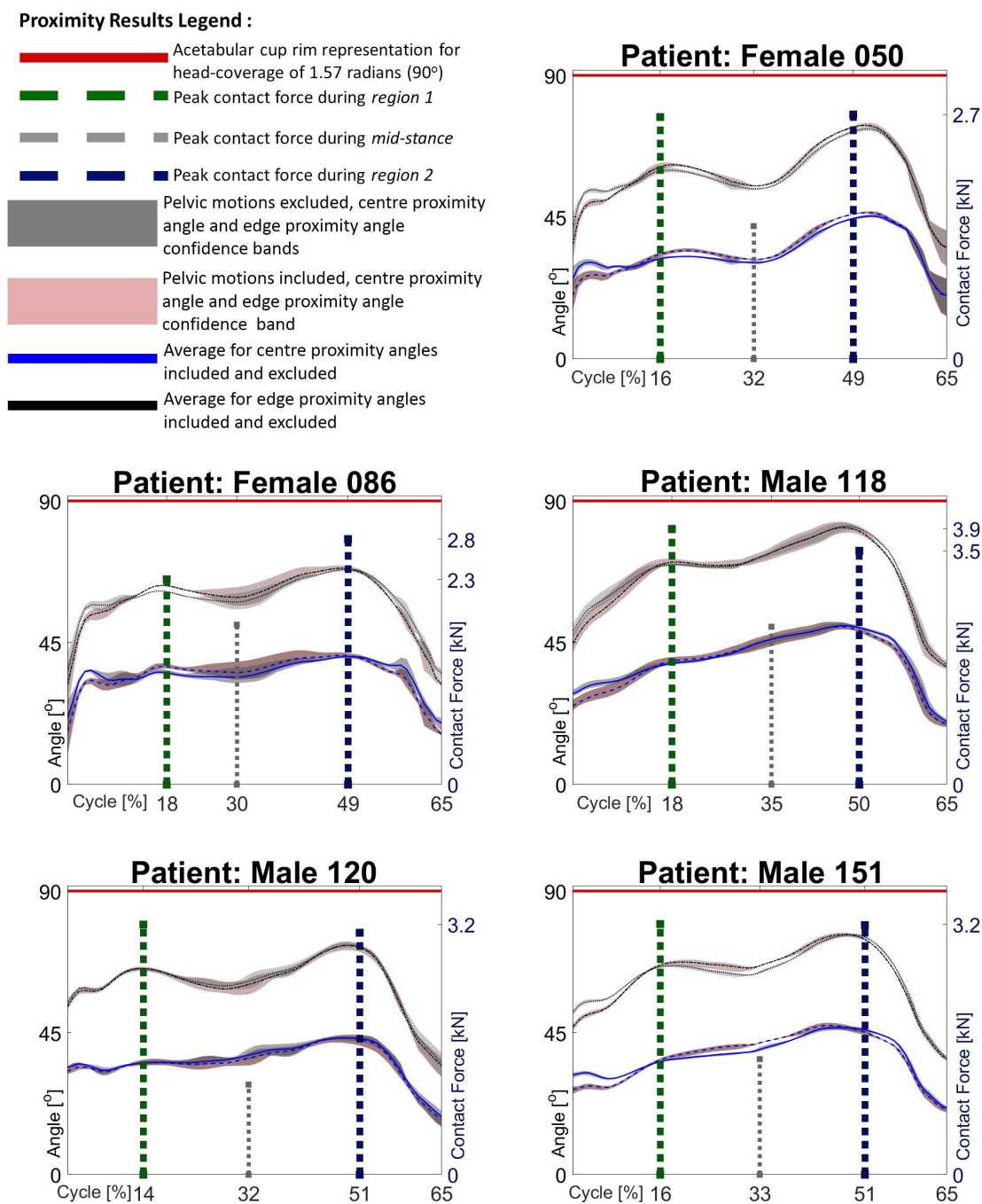


Figure 4.9: Results for centre and edge proximity angles visualised with the confidence bands for male patients who's edge contact risk was affected by pelvic motion inclusion. The peak contact, for region 1 and region 2 and mid-stance force instances are marked by hashed lines the values displayed on right axis.

4.3.1 The effect of pelvic motions compared to simulations with no pelvic motion inclusion

Overall for 15 patients out of 20, a substantial change was identified between the cases where pelvic motions were included and excluded. The graphical results

for male and female patients are presented in 4.7 and 4.8 respectively. For these patients the risk of edge contact was determined to be affected by pelvic motion exclusion. These patients were 001, 026, 073, 093, 114, 025, 042, 052, 002, 075, 084, 116, 131, 094, 148. For patients 026, 75, 148 the difference was seen in one region only. Figure 4.9 shows graphical results for the other five patients whose edge contact risk was not affected by pelvic motion exclusion.

Table 4.3: RMSE values and pelvic motions included versus excluded. The bold values are for above the average RMSE, the underlined values are substantial difference including confidence bands.

Patients	Region 1 [°]	Region 2 [°]
001	<u>6.2</u>	<u>2.9</u>
026	1.2	<u>4.6</u>
073	<u>1.8</u>	<u>3.0</u>
093	<u>5.9</u>	<u>4.0</u>
114	<u>2.7</u>	<u>5.3</u>
025	<u>3.7</u>	<u>2.7</u>
042	<u>4.3</u>	<u>3.1</u>
050	2.0	1.0
052	<u>4.7</u>	<u>4.5</u>
086	2.4	2.2
002	<u>4.0</u>	<u>4.3</u>
075	<u>4.6</u>	1.8
084	<u>2.9</u>	<u>2.3</u>
116	<u>2.6</u>	<u>2.1</u>
118	2.0	1.2
120	1.1	1.5
131	<u>2.8</u>	<u>2.6</u>
151	2.3	1.2
094	<u>2.6</u>	1.7
148	<u>2.6</u>	0.9

The RMSE values measured between cases where pelvic motions were included and cases where pelvic motions were excluded were summarised in Table 4.3. The values which were above the average RMSE values are highlighted in bold. Underlined values show patients for which the effect of pelvic motion exclusion was established to be substantial based on both confidence band overlap and above average RMSE values. For patients whose RSME were above average but confidence band overlap did not occur for substantial period, the effect of pelvic motion exclusion was also considered substantial.

Results of the analysis show that in region 1, for 14 out of 20 patients the exclusion of pelvic motions affected the risk of edge contact substantially, decreasing the centre proximity angles. Maximum RMSE value of 6.9° was seen for patient 093. Across all patients the maximum difference in proximity angles between pelvic motions included case and excluded case, was seen for patient 001 of 8.1° at gait cycle point 2%. During region 2, data for 12 out of 20 patients showed that the effect of pelvic motions was substantial. The exclusion of pelvic motions increased the risk of edge contact for 11 patients, and decreased the risk for one patient, namely 131. Maximum RMSE value of 5.3° was seen for patient 114. Maximum proximity angle difference of 8.2° at gait cycle point 61% between two cases was seen for patient 052.

4.3.2 The contribution of each pelvic motion to the overall effect of pelvic motions

In this section each separate pelvic motion and their pairs were assessed in terms of their role in overall pelvic motion inclusion effect on the risk of edge contact. Hence, RMSE values were measured between the case where all pelvic motions were included and other cases studied (Table 4.3). For the first stance phase region, region 1, the data was analysed for 14 patients and for second stance phase region, region 2, the data was analysed for 12 patients (Table 4.3). This was done for patients whose proximity angles were affected by pelvic motions exclusion described in previous section.

Figure 4.10 shows the centre proximity angles for patient 052 for all introduced cases in this sub-study (Table 4.2). For this individual, it can be seen that for the majority of region 1 pelvic tilt is the closest to the case where all three pelvic motions were included. RMSE value between the case where all pelvic motions are included and the case where only pelvic tilt is included was 1.7° . For region 2, starting at gait cycle point 33%, the main contributor seems to be the combination of tilt and obliquity. The lowest RMSE value for this region was found for tilt and obliquity motion combination (RMSE = 0.6°) which confirms the observation. Table 4.4 lists the major contributor to all pelvic motions included scenario, either one motion or two motion combination, for 15 studied patients.

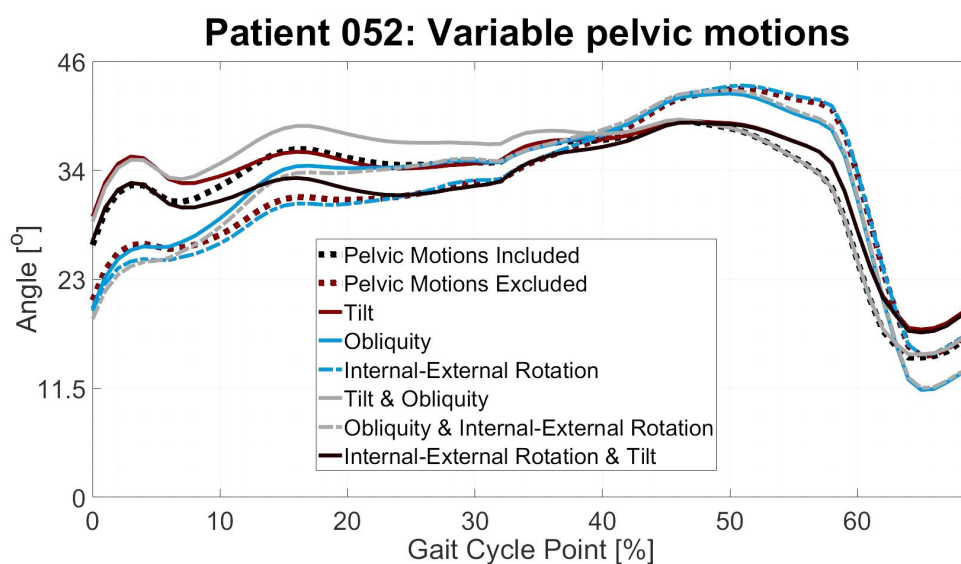


Figure 4.10: Patient 052 centre proximity angles, separate motions and motion pairs.

In total it was found that, during region 1 for two out of 14 patients the main contributing motion was pelvic tilt, for one patient out of the same patient group the main contributing motion was obliquity. For five out of 14 patients the main contributor was a combination of two pelvic motions, obliquity and tilt. However, for highest number of patients, six, there were no main contributors.

During region 2 for four out of 12 patients there was no clear contributor to the overall effect of pelvic motions. However, for the majority of patients, eight, for this region, the main contributor was the combination of pelvic tilt and obliquity.

Table 4.4: Pelvic motion or combination, that contributes to overall pelvic motion effect for each patient. T - Tilt; O - Obliquity; IE - Internal-external rotation; & - combination of two motions; × - no difference between pelvic motions included and excluded.

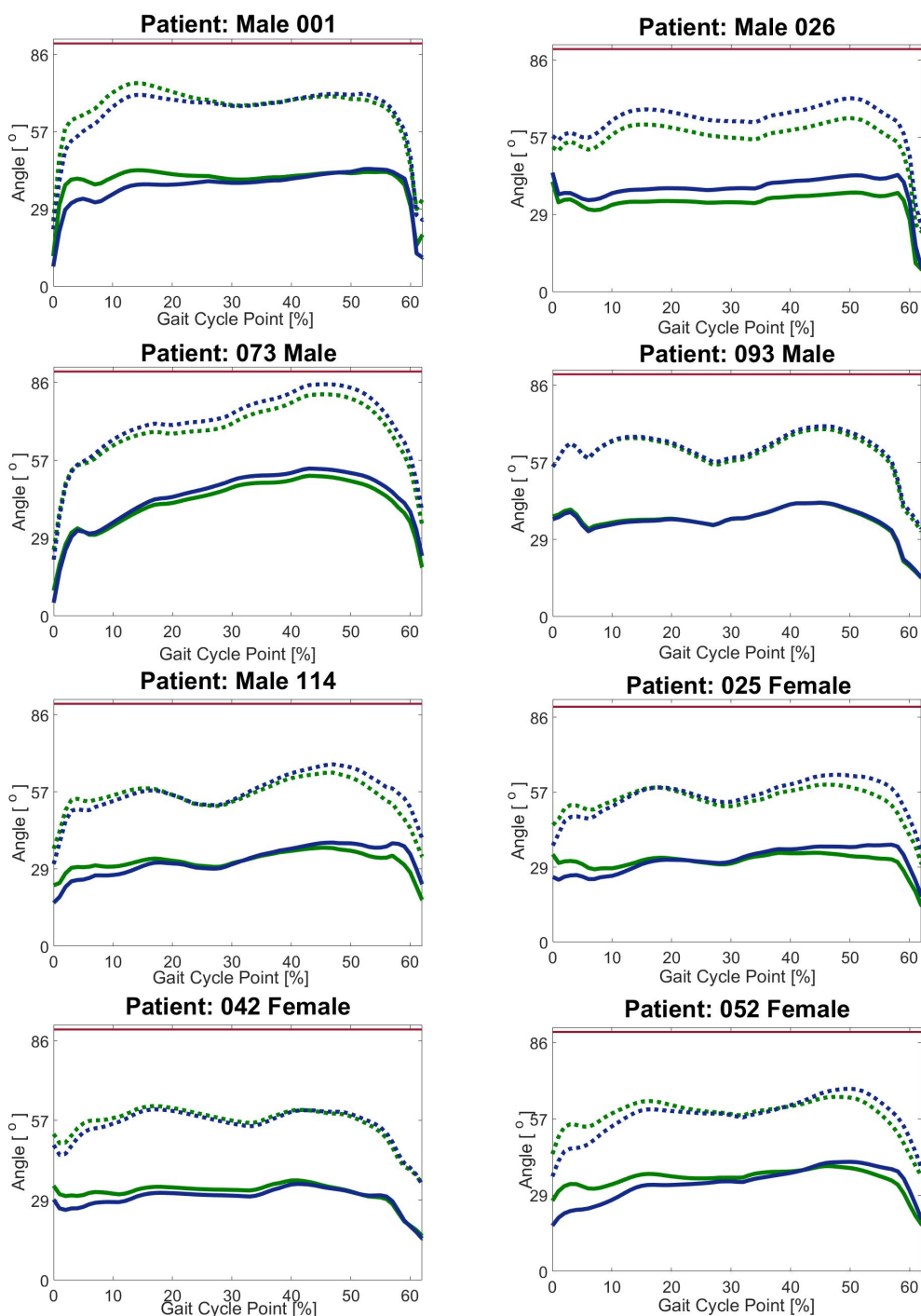
Patients	Region 1 [°]	Region 2 [°]
001	T & O, T & IE	T & O, T & IE, O & IE
026	×	T & O
073	O, O & IE	T & O
093	T & O	T & O, O & IE
114	T & O	T & O, O & IE
025	T, O	T & O
042	T	T & O
052	T	T & O
002	T & O	T & O
075	T & O	×
084	T & O	O, T & O, O & IE
116	O & IE	T & O
131	O	T & O
094	T & O, T & IE	×
148	T, O, O & IE	×

4.3.3 The contribution of static pelvic orientation to the overall effect of inclusion of pelvic motions

The data analysed in this sub-section was only for patients, whose centre proximity angles changed substantially with exclusion of pelvic motions. For the first stance phase region, region 1, the data was analysed for 14 patients and for the second stance phase region, region 2, the data was analysed for 12 patients (Table 4.3).

The simulations excluding pelvic static motions were also performed to see the difference in the centre proximity angles. Figure 4.11 shows the output for cases where pelvic motions were included and static excluded. This was done for patients whose centre proximity angles were identified to have been affected by dynamic pelvic motion exclusion. The exclusion of static pelvic orientation, for region 1 in three out of 14 patients, overestimated the centre proximity angles by maximum of 5°. However, for 11 out of 14 patients the exclusion of static orientation underestimated the proximity angle, with maximum difference of 10°. Only for one patient the exclusion of static pelvic orientation resulted in the same proximity results as without the exclusion. For the region 2, for nine out of

12 patients the exclusion of static pelvic orientation resulted in overestimation of centre proximity angles. For one patient the centre proximity angles were underestimated, and for two out of 12 patients the exclusion of static pelvic orientation did not affect the proximity angles.



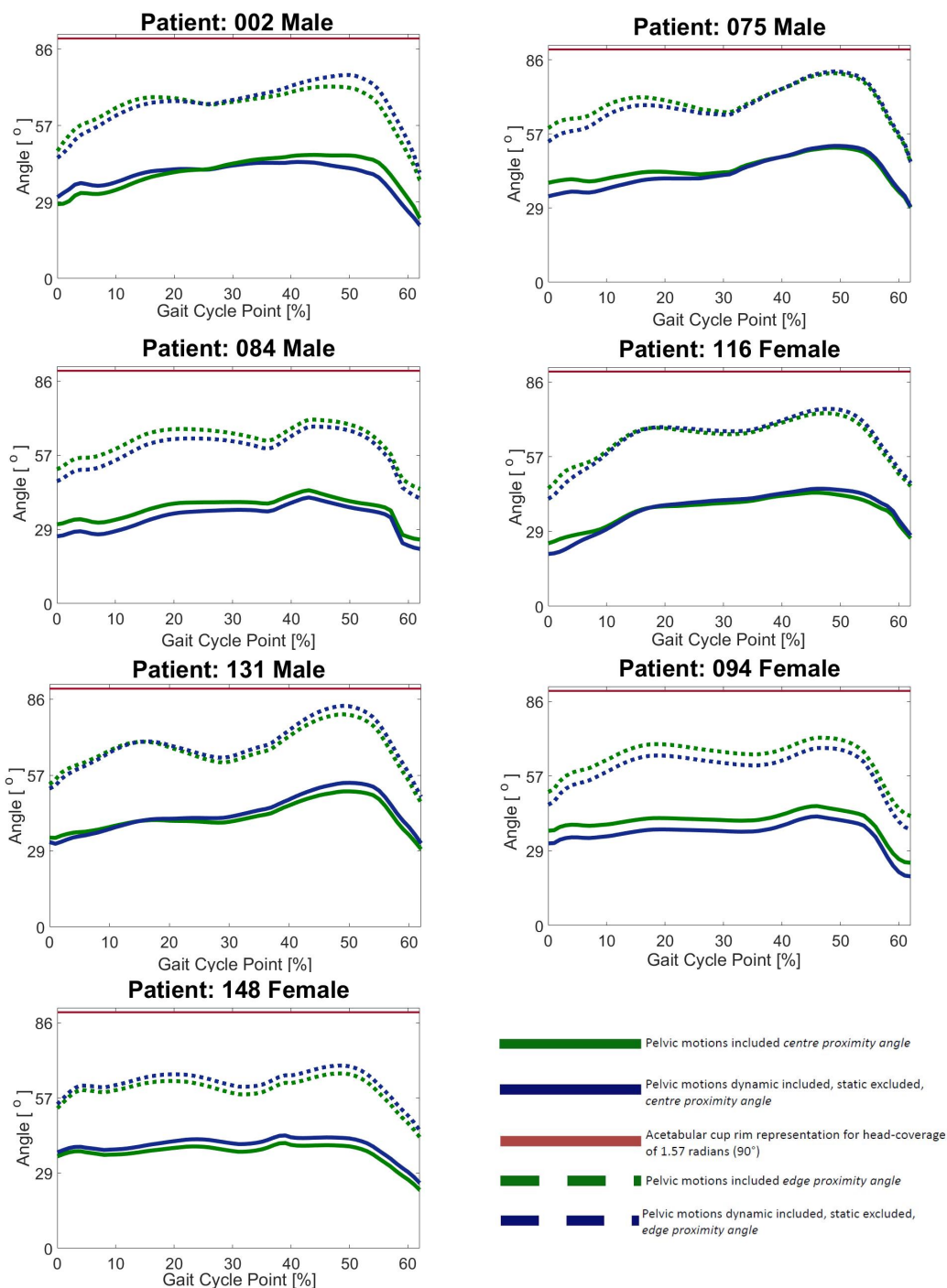


Figure 4.11: Results for pelvic motions included, excluded and pelvic dynamic motions included (static excluded)

4.3.4 Centre proximity angle and patient-specific demographics and gait characteristics correlation

The difference in pelvic profiles for patients whose centre proximity angles were affected by pelvic motion exclusion and for those whose centre proximity angles were not affected by pelvic motion exclusion, was analysed. For the region 1 of the stance phase the pelvic anterior tilt was mostly higher for the patients whose proximity angles were different between pelvic motions included and excluded. On the other hand, for the patients whose proximity angles did not differ between pelvic motions included and excluded the anterior tilt was lower than the average across all the patient set and for one patient, 050, the tilt was posterior. Table 4.5 shows linear regression analysis for RMSE values for each patient, between the cases where pelvic motions were included and excluded, versus the maximum, minimum, range and mean of the tilt values for each patient. Results for pelvic sagittal tilt show that the stronger correlation of RMSE values is with minimum, maximum and mean pelvic sagittal tilt, where the relationship is in the positive direction. The detailed graphs for RMSE and pelvic tilt regression analysis are shown in Appendix BA.1 for region 1.

Table 4.5: Linear regression analysis results between RMSE values and pelvic sagittal tilt maximum, minimum, range and mean. Positive slope direction - positive linear correlation, negative slope direction - negative linear correlation, negative adjusted R^2 - correlation is too complex to be described by linear regression, R^2 - the closer to 1 the stronger the correlation.

Sagittal Tilt				
Region 1	Max	Min	Range	Mean
Slope Dir	+	+	-	+
Adjusted R^2 Dir	+	+	+	+
R^2 Value	0.4	0.5	0.2	0.5
Region 2	Max	Min	Range	Mean
Slope Dir	+	+	-	+
Adjusted R^2 Dir	+	+	+	+
R^2 Value	0.3	0.3	0.01	0.3

Similar pattern was seen for region 1 obliquity angles, where the obliquity motion angles were higher for patients with different proximity angles between pelvic motions included and excluded. For only two patients, 086 and 151, whose proximity angles were similar between pelvic motions included and excluded, the obliquity angles were higher than average. Table 4.6 show the linear regression analysis for RMSE values for each patient, between the cases where pelvic motions were included and excluded, versus the maximum, minimum, range and mean of the tilt values for each patient. Similar to pelvic sagittal tilt, the stronger correlation of RMSE values is with maximum and mean pelvic coronal obliquity, where the relationship is in the positive direction. However, the linear correlation, R^2 values, is not as strong as for pelvic tilt. The detailed graphs for RMSE and pelvic obliquity regression analysis are shown in Appendix BA.3 for region 1.

Table 4.6: The linear regression analysis results between RMSE values and pelvic coronal obliquity maximum, minimum, range and mean. The positive slope direction - positive linear correlation, negative slope direction - negative linear correlation, negative adjusted R^2 - correlation is too complex to be described by linear regression, R^2 - the closer to 1 the stronger the correlation.

Coronal Obliquity				
Region 1	Max	Min	Range	Mean
Slope Dir	+	+	-	+
Adjusted R^2 Dir	+	+	+	+
R^2 Value	0.2	0.1	0.0001	0.3
Region 2	Max	Min	Range	Mean
Slope Dir	-	-	-	-
Adjusted R^2 Dir	+	-	-	+
R^2 Value	0.06	0.002	0.1	0.02

No apparent pattern was identified for internal-external rotations in region 1, which is reflected by small R^2 values and negative direction of adjusted R^2 (Table 4.7, Figure A.5).

For region 2 of stance phase anterior tilt was mostly higher for the patients whose proximity angles output varied substantially between pelvic motions included and excluded. However, for two out of eight patients, 094 and 075,

whose proximity angles output was not affected by pelvic motions tilt was above average across patients. Same as for stance region 1 for patient 050 the pelvic tilt was posterior. Table 4.5, Region 2, shows the linear regression analysis for RMSE values for each patient, between the cases where pelvic motions were included and excluded, versus the maximum, minimum, range and mean of the tilt values for each patient. Results for pelvic sagittal tilt show that the stronger correlation of RMSE values is with minimum, maximum and mean pelvic sagittal tilt, where relationship is in the positive direction. This is identical to region 1, but the correlation is not as strong. The detailed graphs for RMSE and pelvic tilt regression analysis are shown in Appendix BA.2 for region 2.

For other motions no apparent pattern was found. For each motion, range of minimum and maximum angles was also analysed but no pattern was found. The detailed correlation graphs are presented in the appendices for obliquity and internal-external rotation for second region (Figures A.4 and A.6).

Table 4.7: The linear regression analysis results between RMSE values and pelvic internal-external rotation maximum, minimum, range and mean. The positive slope direction - positive linear correlation, negative slope direction - negative linear correlation, negative adjusted R^2 - correlation is too complex to be described by linear regression, R^2 - the closer to 1 the stronger the correlation.

Internal-External Rotation				
Region 1	Max	Min	Range	Mean
Slope Dir	-	-	+	-
Adjusted R^2 Dir	-	+	-	+
R^2 Value	0.04	0.03	0.002	0.07
Region 2	Max	Min	Range	Mean
Slope Dir	-	-	+	-
Adjusted R^2 Dir	-	-	-	-
R^2 Value	0.01	0.2	0.005	0.02

The demographics parameters in Table 4.1 were listed next to RMSE values and no visual correlation between any of the demographics parameter and effect of pelvic motion on proximity angles was found.

4.3.5 Maximum edge proximity angles: stance regions comparison and location along the cup rim.

In addition to the analysis of pelvic motions effect, the overall risk of edge contact was analysed. In this section only the proximity angles for the case where all three pelvic motions were included were considered as they represent the *in vivo* scenario closer than pelvic motions excluded simulations. Figure 4.12 shows that the contact area proximity reached up to 81.5° where 90° is the rim of the cup. The average edge proximity angles for the regions reach up to 68° as shown in Figure 4.13.

Both the maximum edge proximity regions had normal distribution based on Shapiro-Wilk test, skewness and kurtosis. The Shapiro-Wilk test showed $p > 0.05$ for maximum edge proximity angles for region one and two, and their difference. This meant that there was no statistically significant difference between these values and normal distribution. No outliers were detected and skewness and kurtosis were within the normality range. Average edge proximity values for both regions were also found to be normally distributed ($p > 0.05$). However, the difference between two regions had skewness and kurtosis determinants which exceeded the normality. One outlier was removed from the data. The repeated Shapiro-Wilk test for difference between regions one and two showed the $p > 0.05$, skewness of < 0.8 and kurtosis < 2 , confirming no significant difference to normal distribution.

The paired sample t-test for maximum and average edge proximity angles for two regions was performed. The results show that the maximum edge proximity angle were statistically significant between region 1 and region 2 ($p = 0.00007$). However, the average edge proximity angles were found not to be statistically significant between two regions ($p = 0.543$).

For all pelvic motions included case, for four out of 20 patients, region 1 displayed highest risk of edge, and for 16 out of 20 patients region 2 displayed highest risk of edge 4.12.

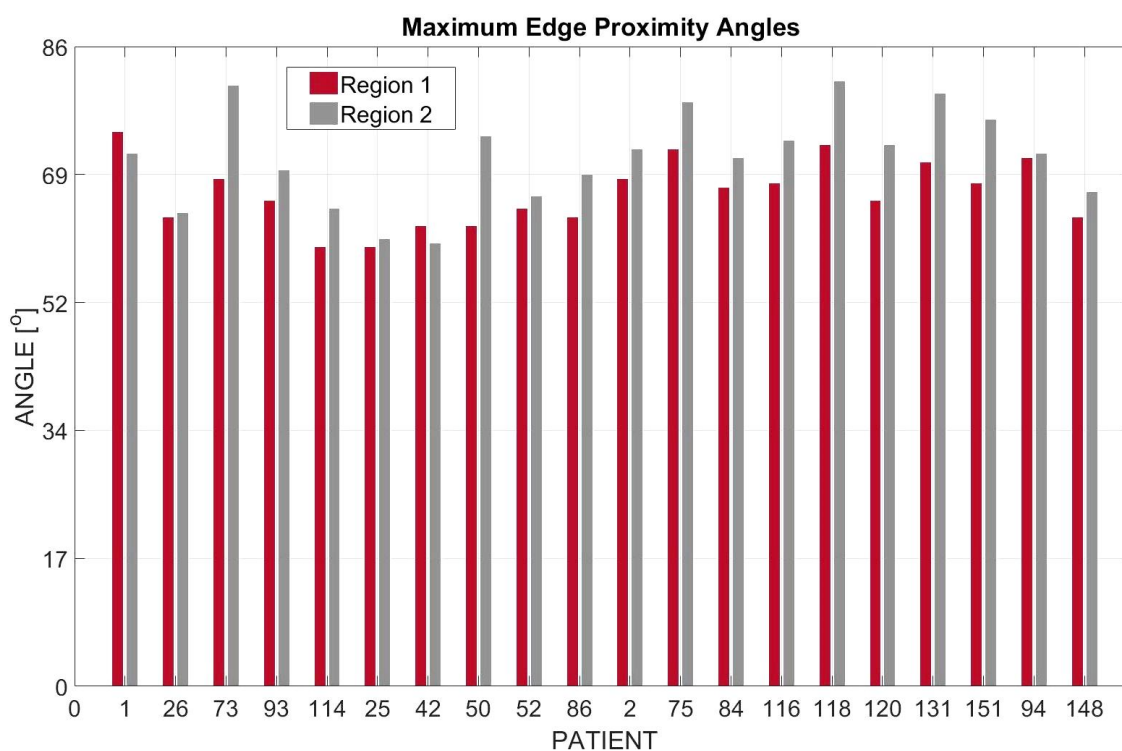


Figure 4.12: Maximum edge proximity angles for two regions during stance phase for the *in vivo* condition, pelvic motions included. Region 1 for heel-strike to mid-stance, and region 2 for mid-stance to toe-off. The edge proximity angles include both the effects of pelvic motions as well as the contact force.

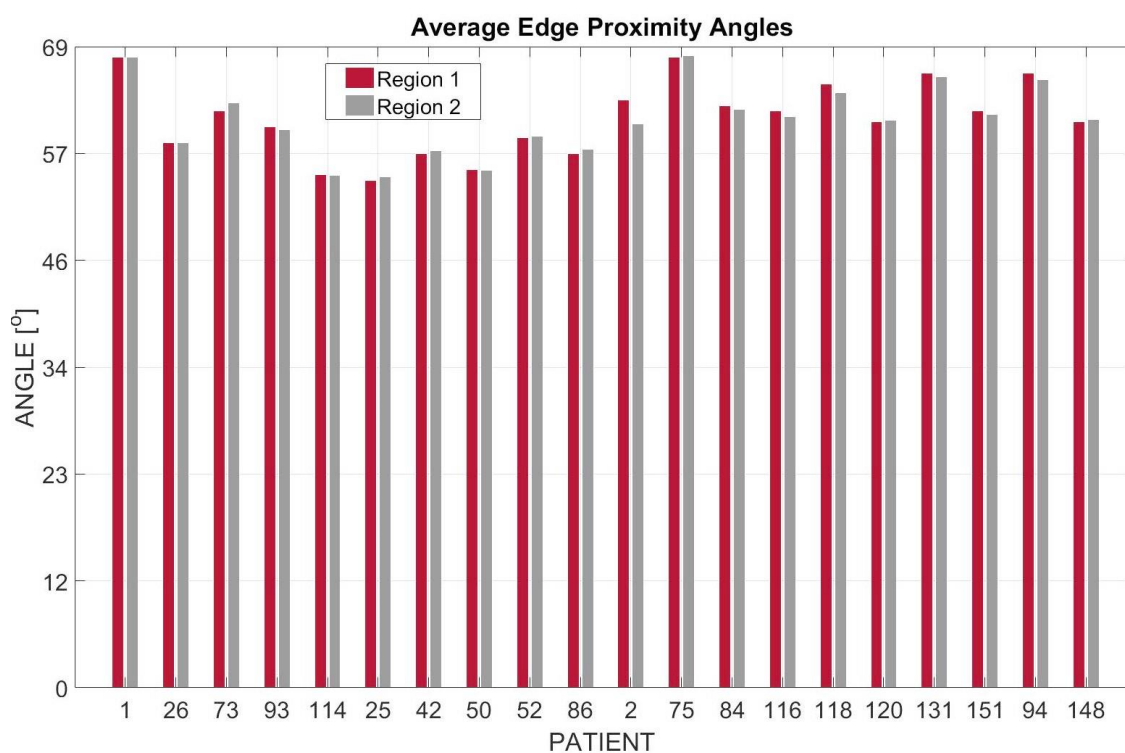


Figure 4.13: Average edge proximity angles for two regions during stance phase for the *in vivo* condition, pelvic motions included. Region 1 for heel-strike to mid-stance, and region 2 for mid-stance to toe-off. The edge proximity angles include both the effects of pelvic motions as well as the contact force.

The instance of the highest proximity angles was analysed in respect to highest force, also shown in Figures 4.7 to 4.9. For region 1, for most of the patients, 13 out of 20, the maximum edge proximity angles occurred after maximum force within five gait cycle points. For three patients the highest edge proximity angle also occurred after maximum force but beyond five gait cycle points. For three out of 20 patients the instance of the highest edge proximity angle corresponded to the maximum force instance. And for one patient, the highest edge proximity angle occurred much later than maximum contact force, beyond fifteen gait cycle points.

For region 2, for most of the patients, 13 out of 20, the highest edge proximity angles occurred before maximum force within five gait cycle points. For two patients the highest edge proximity angle occurred also after maximum force but beyond five gait cycle points. For three out of 20 patients the instance of highest edge proximity angle corresponded to the maximum force instance. For two patients the instance of the highest edge proximity angle occurred before the maximum contact force and beyond five gait cycle points.

The results suggest there is no distinct difference in the magnitudes of the edge proximity angles between patients whose risk of edge contact was affected by inclusion of pelvic motion and whose was not.

Additionally, it was found that for patients with body weight above the average, the edge proximity angles were also above the average. The average body weight was 82.3kg and there were 8 patients with body weight above that. The average edge proximity angle for region 1 was 67° and for region 2 it was 71°. During the stance region 1, for 10 out of 12 patients with weight lower than average, the edge proximity angles were also below the average. And during region 2, same was observe for 8 out of 12 patients. No other trends were found between edge proximity angles and patient demographics.

Table 4.8 shows the results for the analysis of the potential edge contact damage for all 20 patients based on the maximum edge proximity angles (4.12). These results suggest that the damage to the cup is most likely to occur at the superior

part, illustrated in Figure 2.21

Table 4.8: Potential of edge contact clock-wise orientation along the rim. The quadrants are normalised for the left THR side as shown in Figure 2.21. (I) superior-anterior and (II) superior-posterior quadrants.

Patients	Region 1 Angle	Region 2 Angle	Region 1 Quad	Region 2 Quad
1	-42	-15	I	I
26	-29	-3	I	I
73	-8	-17	I	I
93	44	0.7	I	I
114	22	-12	I	II
25	31	7	I	I
42	35	22	I	I
50	-1	-30	II	II
52	37	12	I	I
86	-0.9	-16	II	II
2	32	-6	I	II
75	-37	-0.7	I	I
84	-31	-10	I	I
116	8	-7	I	II
118	-10	-15	II	II
120	-48	-10	I	I
131	29	-5	I	II
131	29	-5	I	II
151	18	-7	I	II
94	35	14	I	I

Figure 2.21 (Chapter 2) shows the four quadrants of potential damage. The quadrants I and IV are representative of posterior damage, and quadrants II and III are representative of the anterior damage. Therefore, for region 1, the damage was mostly, 17 out of 20, superior-posterior. For region 2 the damage was more even between superior-anterior and superior-posterior with nine out 20 and 11 out of 20 respectively.

4.4 Conclusions and summary

4.4.1 Main findings

Main findings and observations of the current study are listed below:

1. For 15 out of 20 patients the proximity angles were identified to be substantially affected by addition of pelvic motions into the proximity tool simulation. The maximum difference between pelvic motions included and excluded maximum proximity angles reached 8° ;
2. For affected patients the inclusion of pelvic motions decreased the difference in maximum proximity angles between two load peaks during stance phase. The change in that difference reached 8° ;
3. During the stance region from heel-strike to mid-stance in 14 out of 20 patients the inclusion of pelvic motions increased the risk of edge contact. During stance region from mid-stance to toe-off in 12 out of 20 patients the inclusion of pelvic motions decreased the risk of edge contact;
4. Pelvic motions that contribute to the overall effect of pelvic motion inclusion were identified to be pelvic tilt and obliquity in most cases. However, some cases of internal-external rotation contribution were also recorded;
5. Exclusion of static pelvic orientation did not result in zero pelvic motion effect during walking. This was expected from the differences between raw data for static and dynamic pelvic angles. Hence, the static position of the pelvis during standing does not represent the contact location during walking;
6. From the previous point (5) it can be concluded that the alignment of the cup within the pelvis in its functional orientation did not consistently decrease the risk of edge contact, over the alignment in the pelvic system;
7. Effect of pelvic motions was not dependent on any demographic factor in the selected patient cohort;
8. With the increase in pelvic tilt and obliquity the effect of pelvic motions on proximity angles also increases;
9. For the current orientation, force vector direction and motion combination the edge contact was not recorded. Moreover, the proximity angles magnitudes were found not to be dependent on the degree of pelvic motion effect. The maximum edge proximity angles were found to be significantly

lower ($p = 0.000$) for the first peak in comparison to the second peak. The average proximity angles were found not be significantly different ($p = 0.9$);

10. Potential location of the damage around the acetabular cup rim was found to be superior during stance phase, with deviations to anterior and posterior direction.

4.4.2 Discussion on the findings

Influence of patient-specific gait features with respect to the THR contact mechanics performance is not fully understood. The studies on metal-on-metal hip replacements have shown the importance of head coverage and force vector direction (Underwood et al., 2012) and shown that the distance from contact patch edge to the rim of the cup (CPEr) was significantly lower for the implants with signs of edge wear, suggesting that the cup orientation and design influences the risk of edge contact. In recent study by Langston et al. (2018) the influence of pelvic sagittal tilt and lumbar flexion during stand-to-sit motion on risk of THR dislocation using three static CT scans was investigated. The study revealed that the patients at most risk had limited lumbar mobility as well as pelvic tilt in posterior direction. In fact, study by Tezuka et al. (2018) confirms that the Lewinnek "safe zone" (Lewinnek et al., 1978) based on anterior-posterior standing radiography does not always result in cup being orientated safely. This was shown using radiographs taken in the stated position. The current study aimed to investigate the effect of patient-specific gait features from a dynamic perspective and their influence on the risk of edge contact, which in worst case scenario leads to dislocation. To fulfil the aim of the study the dynamic activity was chosen to be walking.

The primarily objective of the study was to investigate the role of pelvic motions on the large cohort, as a study described in Chapter 3 has shown that pelvic motion can influence the risk of edge contact. The secondary objective was to investigate the variation of the risk of edge contact between patients when pelvic motions were included in the simulation. The inclusion of pelvic motion represents more *in vivo*-like conditions.

Results of the current study show that the addition of pelvic motions influenced the output for proximity angles substantially for most of the patients, increasing the risk of edge contact in the first stance region and decreasing it in the second stance region. Hence, the pelvic motion plays an almost balancing and stabilisation role in contact location, lowering the difference in centre proximity angles between first load peak and second load peak substantially 4.7-4.9. This synergy of pelvis and femur is coherent with basic biomechanics principle of postural balance control, where the extensor muscles at the joints during non-pathological gait prevent the vertical collapse of the body. This is also called support synergy and is one of the mechanisms of central neural system (CNS) balance control (Winter, 1995). From this it can be theorised that even though there might be some gait feature similarities between patients, other gait features might be the result of patient-specific gait adaptations based on lifestyle and age-related changes. In addition it can be speculated that for the patient group with higher instability, usually elderly patients, those gait features could be even more variable and show no obvious trend, as to achieve postural balance there might be variable muscle activation. Hence, for the pre-clinical medical device testing it might be more reasonable to derive a profile which does not replicate the ones seen *in vivo* but generate the same contact force vector deviations.

Recent studies by Langston et al. (2018) and Roettges et al. (2018) both focused on the role of pelvic sagittal tilt effect on the outcomes of the THR. These studies take the stand-to-sit activity as the one covering the functional range of pelvic orientation, where the tilt has the larger range of motion compared to other pelvic motions. Based on the findings of those studies authors recommend that the pelvic sagittal tilt is a measure to be considered during the acetabular cup positioning. Langston et al. (2018) recommends to use the patient-specific approach and consider different acetabular positions for patients with posterior and anterior tilt. While stand-to-sit activity provides sufficient range of motion for pelvic tilt, there are no studies that looked at the effect of all three motions in the activities where there is no clear dominant pelvic motion. The findings of the current study suggest that for high-functioning patients during walking pelvic tilt affects the risk of edge contact in the first region of stance phase which is coherent with the assumption of the study by Langston et al. (2018). In

addition authors (Langston et al., 2018) found that anterior tilt retroverts the acetabular cup hence, the cup should be positioned with higher anteversion. This is also coherent with the current study as all the patients whose proximity angles were affected by pelvic tilt had an anterior tilt which caused a higher risk of edge contact during first region of the stance phase. However, for the second region of the stance phase the risk was decreased even though the tilt remained anterior. The findings of the current study suggest that obliquity also plays a role specifically in the second region of the stance phase on the location of contact during walking. The additional correlation analysis between the change in proximity angles with addition of pelvic motions showed that most of the patients with substantial pelvic motion effect, had the high anterior tilt and obliquity with larger deviation from baseline.

The effect of static pelvic tilt on the proximity angles was investigated. Based on the findings it can be suggested that stationary position does not fully represent dynamic scenario in terms of proximity to the rim, which is again coherent with finding by Langston et al. (2018) that the functional position of the acetabular cup changes during activity. The case where pelvic static tilt was excluded from simulation represents cup orientation based on the standing anterior-posterior radiography scan. For the first stance region this exclusion resulted in decrease in the risk of edge contact and for the second increase in the risk. This adds to finding by Tezuka et al. (2018) that Lewinnek "safe zones" (Lewinnek et al., 1978) defined for static standing acetabular cup orientation do not fully represent the *in vivo* functional cup orientation.

Results of this study shown that the variation in edge proximity angles reach up to 25°, which suggests that the optimum cup position for one patient might be catastrophic for patient with different anatomy and kinematics. The study by Underwood et al. (2012) looked at different component designs but same force vector magnitude and direction. The results of that study suggest that the low clearance in THR increase the risk of edge contact which was verified by explant analysis, hence the risk can be predicted by CPER which is the millimetre equivalent to the proximity angle measured in current study.

Maximum edge proximity angle of 81° observed in this study was well below the cup rim threshold. However, any adjustment to cup orientation, either due to surgical positioning accuracy tolerance, which can reach up to 10° (Kano et al., 2010) or cup *in vivo* migration, which was shown to reach up to 4° for inclination angle (Tian et al., 2018) could result in edge contact. Additionally difference in implant design, such as introduction of fillets and chamfers, can also alter the edge proximity angles as shown by Underwood et al. (2012).

Some studies reported the failure of the acetabular component in the superior region. This is most likely due to fatigue damage (Tower et al., 2007; Hill et al., 2016). Current study shows that during walking all of the contact happens in the superior region hence, it can be speculated that up-right locomotion activities such as walking, stairs ascend and descend cause the catastrophic failures of such types.

4.4.3 Limitations and future work

Current study investigates only high-functioning patients with good mobility. However, the effect of the gait features on the low mobility patients with possible poorer balance control were not covered in this study. The sample size for this study is limited compared to other biomechanics and positioning studies (Langston et al., 2018; Beaulieu et al., 2010). Hence, it is possible that some trends and patterns were missed out in the analysis.

Even though, the damage during stance phase due to edge contact would be more severe based on the higher loads, the role of pelvic motions during swing phase would provide an insight into edge loading damage (Al-Hajjar et al., 2013). However, the data gathering method currently does not provide reliable force vector data as the contact force is estimated through inverse mechanics. For the low forces which are typical for swing phase, small inaccuracies could result in totally different proximity angle output.

In current study only walking cycle was investigated. Other activities such as stand-to-sit, stair ascend/descent might also reveal a high risk of edge contact as seen in Langston et al. (2018) and Chapter 3, where potential damage location,

or in worst case dislocation direction, in relation to the rim might vary to walking. This could be used as a guide for surgeons on making more patient-specific positioning decisions. For example, less active patients might perform more sit-to-stand tasks, dictating positioning of lipped liner.

Finally, missing cup orientation data and imaging of the standing pelvic position conversion information does not allow for patient-specificity. Hence, this study focused more on the parametric testing using patient-specific gait biomechanics data. Limitations of the tool used in this chapter are detailed in Chapter 2 discussion section.

4.5 Summary

Investigation of the effect of pelvic motions on the risk of edge contact for 20 high-functioning patients was performed in the current study. Based on the results of the proximity tool and statistical analysis it can be concluded that:

1. Developed tool, described in Chapter 2, offers a fast processing of conventional biomechanical data which results are comparable to other clinical studies. In addition to static analysis it also offers a dynamic activity analysis which was shown to differ from static output.
2. Statistical methods were investigated in this chapter, which confirmed and facilitated visual observations. These can be further used in the analysis of larger data sets and be a valuable addition to the proximity tool.
3. Results suggested that consideration of the pelvic motion or functional orientation is crucial for prediction of total hip replacement performance *in vivo*.
4. Pre-clinical testing should take into account the actions of the whole body including CNS and muscle activity, rather than just recorded femoral and pelvic motions to accurately predict performance of implant *in vivo*.

Chapter 5

Techniques for pelvic dynamic orientation analysis using video-fluoroscopy : a case study.

5.1 Introduction

The effect of pelvic static orientation on the functional THR acetabular cup orientation is the subject of many studies, which focus on preoperative planning. In a study by Blondel et al. (2009), data for 50 THR patients was assessed in terms of preoperative and postoperative pelvic orientation. The study found that pelvic orientation while the patient was in a neutral standing position, was not significantly altered by total hip replacement surgery. In contrast, results for a similar study by Lazennec et al. (2017) suggests that the pelvic sagittal tilt varies significantly between preoperative and postoperative measurements. The study found that average pelvic sagittal tilt across 66 patients changed from anterior to posterior post-surgery. In the same study, the excessive change in pelvic tilt has been shown to significantly alter acetabular cup orientation angles to outside Lewinnek et al. (1978) "safe zones" for dislocation (Lazennec et al., 2017; Lembeck et al., 2005). Recent studies have also addressed the change in pelvic sagittal tilt during supine position, standing and sitting down positions. It was reported in study by Pierrepont et al. (2017) that for components which were within the "safe zones" (Lewinnek et al., 1978) during supine position, the pelvic orientation while standing and sitting results in re-orientation of component outside the "safe zones".

The role of pelvic sagittal tilt during daily activity cycle on the acetabular cup orientation has not been established yet. According to findings in Chapter 4 of this thesis, the pelvic sagittal tilt during walking is not always represented by sagittal tilt in neutral position. To determine bone and THR component organi-

sation during motion, tools such as video-fluoroscopy and EOS (EOS imaging®, Paris, France) are used (Sections 1.3.1 and 1.6, Chapter 1). These methods are based on taking multiple *in vivo* bone-organisation scans throughout the activity (D'Isidoro et al., 2017; Westberry et al., 2018). This allows to assess the acetabular cup orientation angles during motion. In addition video-fluoroscopy and EOS techniques avoid errors related to skin marker placement seen in conventional biomechanical studies when recording patient kinematic data.

The aim of the current study was to investigate potential use of bi-plane video-fluoroscopy in assessing the effect of pelvic dynamic orientation on the functional acetabular position.

The dual video-fluoroscopy technique is based on two mobile fluoroscopes positioned orthogonally to each other. The patient-specific pelvic and femoral three-dimensional geometries are acquired from CT scans, which are then manually aligned to dual-fluoroscopy images for each activity cycle point (Tsai et al., 2013).

Within the scope of the current study, the pelvic sagittal tilt and THR acetabular cup inclinations were measured for one THR patient during two activities, walking and stand-to-sit, and in the supine position. Video-fluoroscopy data was available through the collaboration with Centre of Orthopaedic Biomechanics (COB), University of Denver. For the activities the data was provided from video-fluoroscopy scans and for supine position from the CT scans.

5.2 Measurement method development

5.2.1 Input data and processing

Video-fluoroscopy and supporting data was available one total hip replacement patient, for both femur and pelvis. Here both pelvic and femoral geometry data represents bone structures and associated THR component, stem for femur and cup for pelvis. Ethical approval was obtained via University of Denver ethics IRB system (IRB approval ID 552844-10) and all participants provided informed,

written consent. The acetabular component's nominal radius was equal to 16mm. The femoral geometry was used during method development stage for verification. Video-fluoroscopy data was provided for walking with self-selected speed on a treadmill and performing a stand-to-sit activity. The additional three-dimensional surface geometry was provided for the pelvis and femur while the patient was in the supine position. The bone geometry in supine position was derived from CT scans by the COB group.

There were three files associated with each activity for pelvis and femur. The data is listed in Table 5.1. The *.TIFF stack files were provided for construction of surface geometry files (*.STL) for both pelvis and femur. The two types of transformation files (1) and (2) for each bone were available. Transformation files (1) was used to re-orientate pelvic and femur throughout the activity. The transformation files (1) were derived from video-fluoroscopy scans for each time-point during the activity. The use of transformation files allows to save storage space, as one video-fluoroscopy geometry file *.STL is on average 65MB for one activity time-point, and transformation file *.XLS is on average 0.04MB for whole activity cycle. The second transformation (2) file type was used to convert the geometry orientations throughout the activity from video-fluoroscopy imaging system to laboratory space coordinate system. The transformation files were compiled at COB using XROMM AutoScoper (Copyright © 2011, Brown University) (Myers et al., 2017).

The data for supine position was provided as a three-dimensional surface geometry which was constructed at COB from pelvic supine CT scan using ScanIP software (© 2019 Simpleware Inc.). Table 5.1 lists the formats of aforementioned data pre-processed by COB (Myers et al., 2017).

Coordinate system of the joint geometry for the activities that was used for further data processing was laboratory space coordinate system. For supine position the coordinate system varied from laboratory one, and was defined by the CT scanner. The transformation information from CT to laboratory coordinate space was not available.

Both transformation files (1) and (2) consisted of linear transformation matrices encompassing rotations and translations. Equation 5.1 shows the format of single transformation matrix, M_T , where $r_{11}...r_n$ are the combined rotations around three principal axes, or axes of the global coordinate system which take format of $\begin{vmatrix} 1 & 0 & 0 \\ 0 & 1 & 0 \\ 0 & 0 & 1 \end{vmatrix}$ commonly denoted in literature as x, y and z respectively (Weisstein, 2018d). The translations in three-dimensional space are represented by t_1, t_2, t_3 .

Table 5.1: Pre-processed data provided by COB, including format and application. VF for video-fluoroscopy.

File	Format	Application
Pelvis VF	*.TIFF	Bone 3D Geometry
Femur VF	*.TIFF	Bone 3D Geometry
Transformation (1)	*.XLS	Motions during Activity
Transformation (2)	*.XLS	Coordinate System Change
Pelvis CT	*.STL	Bone 3D Geometry (supine)

$$M_T = \begin{vmatrix} r_{11} & r_{12} & r_{13} & t_1 \\ r_{21} & r_{22} & r_{23} & t_2 \\ r_{31} & r_{32} & r_{33} & t_3 \\ 0 & 0 & 0 & 1 \end{vmatrix} \quad (5.1)$$

MATLAB (©The MathWorks, Inc., US) was used within this study for preliminary algorithm development and as execution software. For dynamic activities the point cloud array had to be generated for activity time-point, which would represent the dynamic orientations of bone structures during the activity. The necessary steps, prior to using video-fluoroscopy data for measurements are listed below:

1. Create *.STL files for pelvis and femur from video-fluoroscopy images (*.TIFF).
2. Convert *.STL files into point clouds (PCs) representing pelvis and femur.
3. Apply motions (re-orientate) to the pelvis and femur PCs.
4. Write separate PC array for each activity time-point and each bone structure.

5. Change the coordinate system of every PC to match the laboratory coordinate system.

The *.TIFF stack files were used to create *.STL surface geometry files for both pelvis and femur according to the standard operating procedures provided by the Centre of Orthopaedic Biomechanics. To create the *.STL files, the plug-in, "3D viewer", within ImageJ (Rueden et al., 2017) software was used.

Then, the *.STL files for pelvis and femur were converted to point clouds, PC_p and PC_f respectively within MATLAB. This was done through built-in function "pointCloud". First, transformation (1) files were used to orientate PC_p and PC_f throughout the activity. The locations of PC_p and PC_f at every activity time-point were compiled into a three-dimensional arrays within MATLAB PC_{p3} and PC_{f3} , for pelvis and femur respectively. Second, transformation (2) files were used to change the coordinate system of PC_{p3} and PC_{f3} , to the laboratory coordinate system.

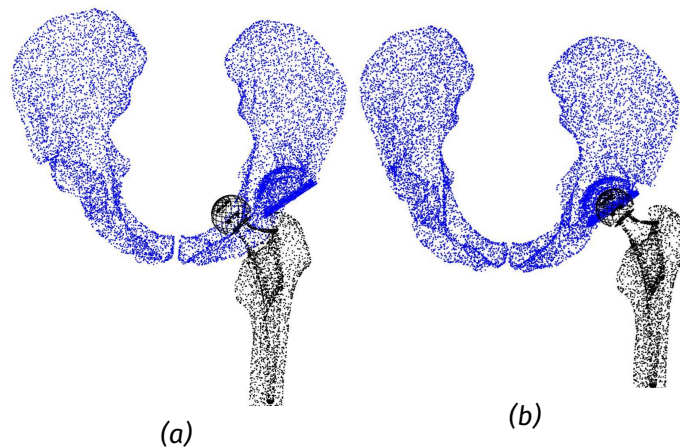


Figure 5.1: Algorithm check for dynamic pelvic orientation. When acetabular cup and femoral head don't align the algorithm is not working, when acetabular cup and femoral head align the algorithm is working properly.

The data for the femur was used to check whether the transformation matrices were applied correctly. Hence, if the centre of the femoral head and acetabular cup were aligned then the transformations were applied correctly. The example of this check is shown in Figure 5.1, where centres did not align in Figure 5.1a and did align in Figure 5.1b. After the algorithm for dynamic pelvic orientation

was checked, the pelvic sagittal tilt and acetabular cup inclination measurement were taken as described in following sections.

The CT scan for pelvis was already in *.STL format, and did not require re-orientation. This file was directly converted to point cloud using MATLAB "point-Cloud" function.

5.2.2 Reference systems and relevant considerations

The pelvic tilt and cup inclination measurements were also made using MATLAB environment, hence the specific global coordinate system was defined. The directions of global coordinate system axes corresponded to $\begin{bmatrix} 1 & 0 & 0 \\ 0 & 1 & 0 \\ 0 & 0 & 1 \end{bmatrix}$ which were named ML_G (medial-lateral), AP_G (anterior-posterior) and SI_G (superior-anterior) axes.

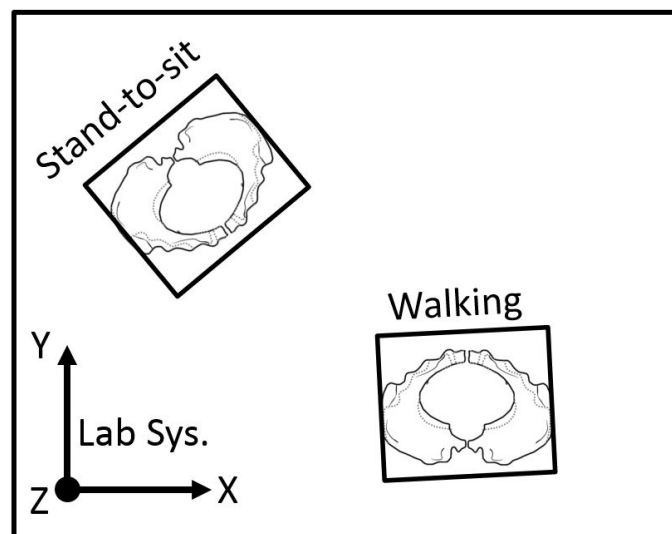


Figure 5.2: The schematic of laboratory space taken parallel to the ceiling. The schematic shows the comparison in patient's pelvis orientation during walking and stand-to-sit activity, as well as in relation to the laboratory coordinate system "Lab Sys."

A set of assumptions was made based on the data availability. The data for both walking and stand-to-sit was taken in the same laboratory space, as shown in Figure 5.2. However, for each activity the patient's location changed to allow for capturing the THR motions, without restricting the view for video-fluoroscopy equipment. From the Figure 5.2 it can be seen that the starting orientation of the

pelvis in the laboratory coordinate system for walking differs from sitting down. No additional data for setting-up the neutral position was available. Therefore, an assumption was made that transverse plane of the laboratory coordinate system, otherwise ceiling, was the global transverse plane for walking and sitting down. The global transverse plane was defined by ML_G and AP_G axes. Furthermore, reference coordinate system was available for supine data and the assumption was made that the transverse plane of global coordinate system is orthogonal to transverse plane of the supine CT image. This assumption is similar in concept to other imaging studies, where image reference planes or axes for two different measurement methods are orthogonal. In study by Pierrepont et al. (2016a) the two orthogonal axes were used, vertical and horizontal, for lateral standing radiograph and supine CT.

Construction of reference systems

Aside from global coordinate system, the coordinate system and planes related to pelvis were constructed to aid in measurements. The local coordinate system of the pelvis was defined by axis ML_L , AP_L and SI_L as seen in Figure 5.4. There were also three planes constructed which were pelvic transverse plane, pelvic sagittal plane and pelvic coronal plane. The construction of these reference geometries is discussed further in this sub-section. These were constructed for supine and activity data analysis, using the same method.

The necessary reference points for the construction of coordinate systems, axes and supporting geometries were manually selected from the surface geometry. For activity data this was done for the initial point cloud, PC_p , and the indices of these reference points were recorded to be used during activity PC_{p3} analysis. The indices method was used throughout the study to avoid manual reference point selection where possible. For supine position the reference points were only required to be selected once.

The pelvic transverse plane defined within current study was consistent with other studies performed by the Centre of Orthopaedic Biomechanics group. This was done according to International Society of Biomechanics (ISB) guidelines

(Wu et al., 2002). The pelvic transverse plane was defined by three points, or landmarks on the pelvis, which were right and left anterior iliac spines (ASIS) most prominent points, and mid-point between right and left posterior iliac spines (PSIS) most prominent points, as shown in Figure 5.3. For pelvic local coordinate system, the origin was set at the THR joint centre. The medial-lateral axis of the pelvis, ML_L , was the line parallel to the ASIS pointing laterally from the origin. The anterior-posterior axis of the pelvis, AP_L , was orthogonal to ML_L and parallel to pelvic plane pointing anteriorly. The superior-inferior axis, SI_L , was perpendicular to both ML_L and AP_L (Figure 5.4).

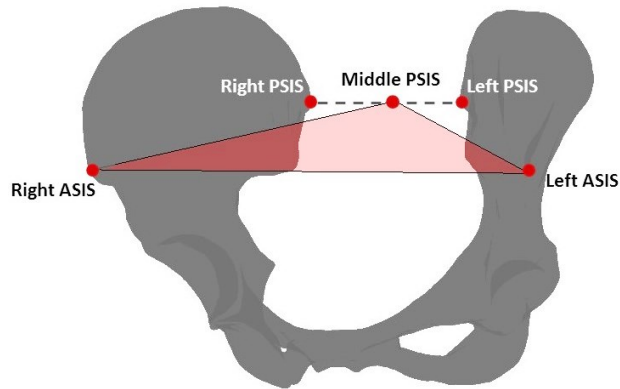


Figure 5.3: Pelvic plane definition according to Grood and Suntay (Wu et al., 2002), defined by PSIS mid-point and two ASIS landmarks.

The additional plane, coronal pelvic plane, was constructed to aid in the measurements. This plane was defined by two ASIS landmarks and was perpendicular to the global transverse plane, which was defined by normal $\begin{vmatrix} 0 & 0 & 1 \end{vmatrix}$ as seen in Figure 5.5. This plane represents the two-dimensional image (scan) taken parallel to coronal plane of the patient and allows for comparison of cup orientations between different activities. Mathematically, the pelvic coronal plane was presented by its normal, n_c , and a point on a plane, which was chosen to be a middle point between two ASIS. The normal was found as the cross product (Equation 5.2) of its directional vectors, which were normal to global transverse plane, n_G and vector between left and right ASIS landmarks, v_{asis}^{\rightarrow} .

$$n_c = \frac{n_G \times v_{asis}^{\rightarrow}}{|n_G| |v_{asis}^{\rightarrow}|} \quad (5.2)$$

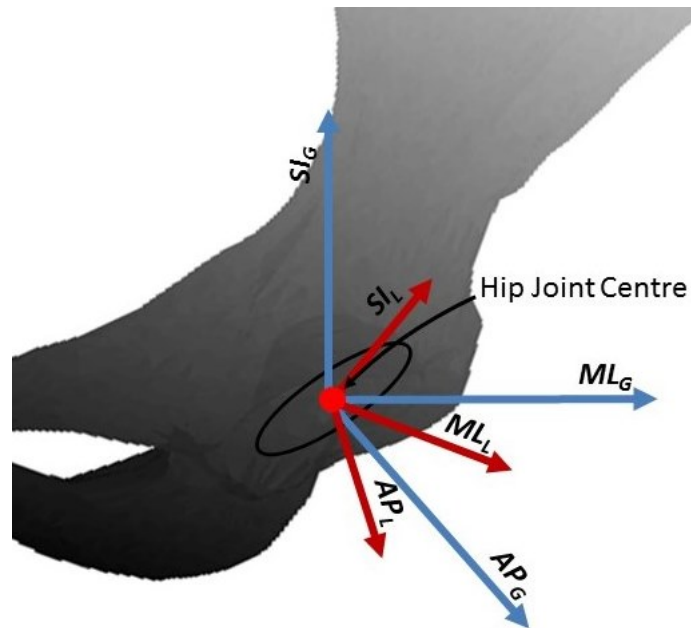


Figure 5.4: Definition of local pelvic coordinate system (Wu et al., 2002) in red, and global coordinate system in blue, where AP is anterior-posterior, ML - medial-lateral and SI - superior-inferior axes.

Finally, the pelvic sagittal plane was defined, which was orthogonal to the global transverse plane and pelvic coronal plane. The plane is presented in Figure 5.6. This plane represents the imaging of the pelvis from plane orthogonal to v_{asis}^{\rightarrow} and was defined by its normal, n_s and hip joint centre point. The n_s , was found using the same method as for pelvic coronal plane (Equation 5.2), selecting the directional vectors to be the normal to global transverse plane, n_G , and normal to pelvic coronal plane, n_C .

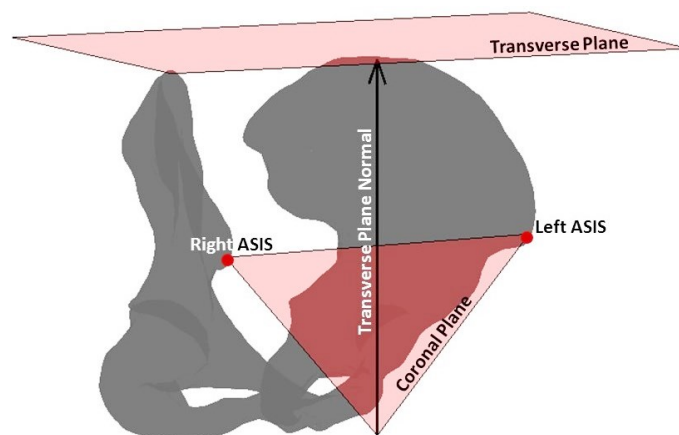


Figure 5.5: The pelvic coronal plane defined by ASIS landmarks and global transverse plane orthogonal to pelvic coronal plane.

5.2.3 Measurement definition and methods

Pelvic tilt and acetabular inclination were measured for each activity time-point, and for the supine position. The acetabular cup and hip joint centres were assumed to match.

The sagittal tilt angle was measured between SI_G axis and axis projected onto sagittal plane SI_L , namely SI_{LP} . The SI_L was projected using Equation 5.3, where n_s is normal to sagittal plane. The tilt angle, θ_s , was found using Equation 5.4.

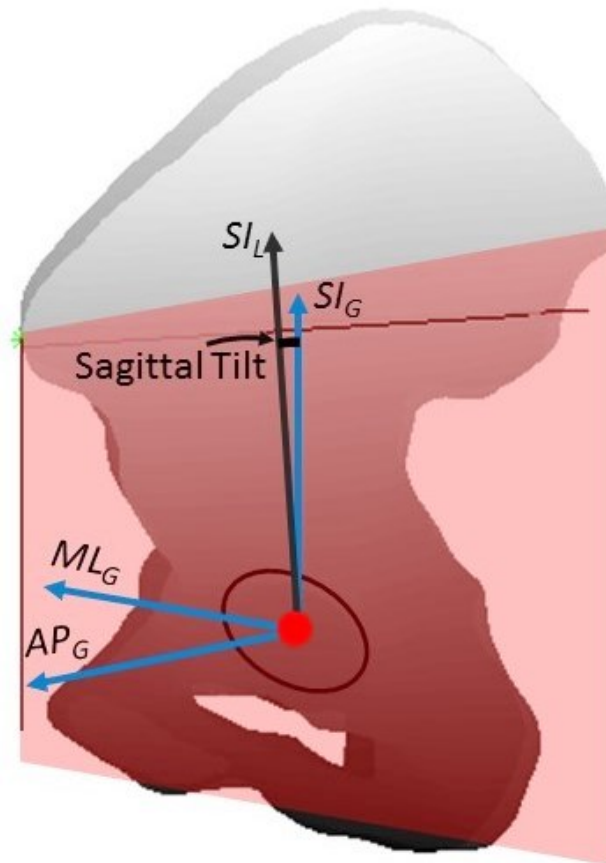


Figure 5.6: View from pelvic sagittal plane, for sagittal tilt measurement, where local SI_L axis is in black and global axes are in blue. From this view SI_{LP} is coincident with SI_L .

$$SI_{LP} = SI_L - \frac{SI_L \cdot n_s}{|n_s|^2} n_s \quad (5.3)$$

$$\theta_s = \cos^{-1} \left(\frac{\vec{SI}_{LP} \cdot \vec{SI}_G}{|\vec{SI}_{LP}| |\vec{SI}_G|} \right) \quad (5.4)$$

The inclination of the acetabular cup was measured from the coronal plane. Firstly, two points around the cup rim were selected, namely x_1 and x_2 . These were selected manually from the point cloud geometry defining pelvic motion orientations during activity's first time-point. For further time-points the indices of those points were used. Then, points were generated for a circle, that represented the acetabular rim, with radius of 16mm using parametric equation of a circle as in Equation 5.5. Here, \vec{v}_c are coordinates of each point of the circle. Here o is the hip joint centre, r is selected radius, a_1 and a_2 are the orthogonal vectors to the circle plane and γ is the angular distance parameter. Orthogonal vectors a_1 and a_2 were unit vectors with origin at the cup centre with direction defined by a randomly selected points x_1 and x_2 around the cup rim.

$$\vec{v}_c(\gamma) = o + r(a_1 \cos \gamma \hat{i} + a_2 \sin \gamma \hat{j}), \quad 0 \leq \gamma \leq 2\pi \quad (5.5)$$

The \vec{v}_c and o were projected onto pelvic coronal plane according to the Equation 5.6, where P was the point to be projected, n_c was normal to pelvic coronal plane and P_P was the projected point. Then inclination vector, \vec{v}_i , was defined based on the projected point, P_P , in the coronal plane connecting the hip joint centre and the furthest from it projected rim point. The inclination angle, θ_i , was defined as the angle between the vector connecting two ASIS landmarks, \vec{v}_{asis} , and \vec{v}_i shown in Figure 5.7 and found through Equation 5.7.

$$\vec{P}_P = P - \frac{P \cdot n_c}{|n_c|^2} n_c \quad (5.6)$$

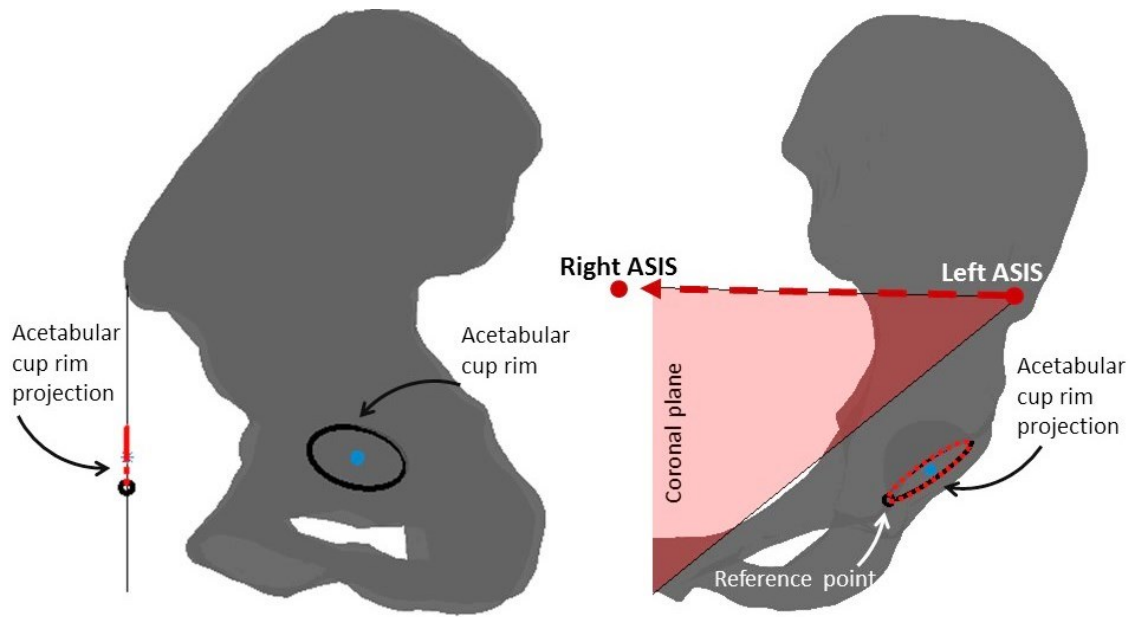


Figure 5.7: The pelvic coronal plane for projection of the acetabular cup rim, side view on the left and frontal view on the right.

$$\theta_i = \cos^{-1} \left(\frac{\vec{v}_i \cdot \vec{v}_{asis}}{|\vec{v}_{asis}| |\vec{v}_i|} \right) \quad (5.7)$$

5.3 Case Study Results

Results of this study suggest that two activities and supine position display different pelvic tilt and acetabular inclination angles. The results for all three activities are shown in Figures 5.8 and 5.9 for pelvic sagittal tilt and cup inclination angles respectively. For walking, the average pelvic tilt angle was 19.4° and the range was 4.5° , from 17.5° to 22° . For stand-to-sit activity, average pelvic tilt angle was 5° and the range was 5° , from 2.6° to 7.6° . Finally, for supine position, pelvic tilt was equal to 15.5° which falls between two dynamic activities presented in this study.

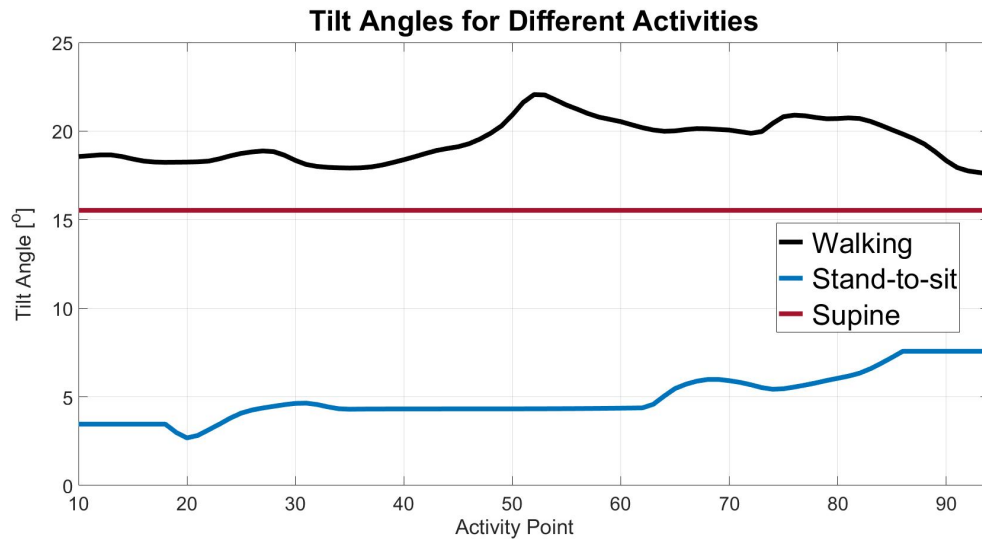


Figure 5.8: The results for the sagittal pelvic tilt angles measured in pelvic sagittal plane, where blue, red and black lines represent stand-to-sit, supine and walking respectively.

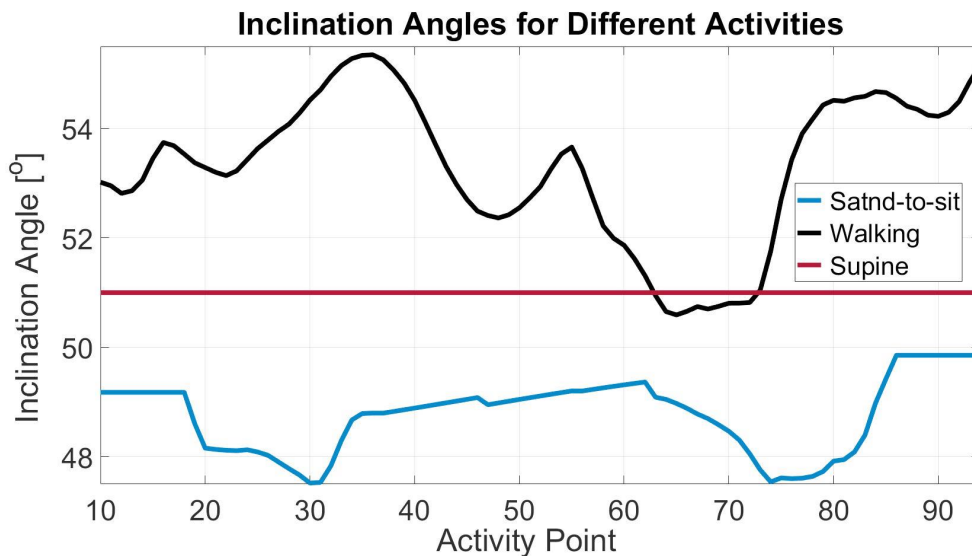


Figure 5.9: The results for the inclination angles measured in pelvic coronal plane, where blue, red and black lines represent stand-to-sit, supine and walking respectively.

For walking the average inclination angle was 53° and the range was 4.8° , from 50.6° to 55.3° . For stand-to-sit movement cup inclination angle was 48.8° and the range was 2.3° , from 47.5° to 49.8° . Finally, for supine position pelvic tilt was

equal to 50° which falls between two dynamic activities presented in this study, and therefore follows the pattern seen for pelvic tilt.

5.4 Discussion

The study by Pierrepont et al. (2017) showed that pelvic tilt during supine body position does not represent the functional pelvic tilt during standing and sitting positions. Authors suggest that functional change in pelvic sagittal tilt of more than 13° from supine to other positions in both anterior and posterior directions. This put THR acetabular component in unfavourable anteversion position leading to dislocation (Lembeck et al., 2005). The results of the current study suggest that, for studied patient, the supine position does not cover the functional orientation of the acetabular cup during two common daily activities. The pelvic sagittal orientation and cup inclination in supine position fall between the dynamic orientations of two activities. For the patient, the change in tilt between supine position and stand-to-sit activity was up to 12.3° posteriorly and between supine position and walking was up to 6.6° anteriorly.

The limitation of this study's method is manual landmark point selection, hence there is some uncertainty in the results. If using this methods to assess other patients, the uncertainty must be quantified. For example, multiple trials of landmark selection can be performed, with possibility of multiple users. Additionally, the automatic selection of pelvic landmarks was considered, the possible solution can be principal axis and second moment of inertia approach commonly used for computational purposes in solid body re-orientation (Bourg, 2002). The method would require anatomically correct point cloud distribution, matching bone and implant density.

The limitation in terms of study's results is the unavailability of information on the relationship between variable coordinate systems. To overcome this limitation, neutral position, which can be standing, just before the start of the activity should be performed from the activity start point. Hence, the neutral position can be matched when processing the data.

The results for the dynamic activity data, such as shown in this study, could be used to define the "safe zones" for acetabular cup orientation. However, as pointed out by Lazennec et al. (2017) the acetabular cup orientation "safe zones" do not represent the cup orientations during standing. These can be re-assessed using preoperative three-dimensional imaging assessment techniques such as EOS imaging (Copyright© 2009 EOS imaging), (Lazennec et al., 2017). "Safe zones" defined by Lewinnek et al. (1978) and McLawhorn et al. (2015) were not based on functional measurement, but rather on correlation between dislocation rate and postoperative cup orientations. This might ignore some cup orientations which can cause dislocation might not be encompassed within those zones. To add, "safe zone" approach does not consider other types of failure, as well as pelvic orientations in all three anatomical or radiological planes, which were shown to alter the location of contact between THR bearings in Chapter 3 and 4 of this thesis. Computational systems like OPS™ (© 2019 Corin, UK) are being developed, allowing determination of the optimum cup position in terms of dislocation during sit-to-stand and stand-to-sit activities. This system performs analysis on patient-specific basis but only considers pelvic orientations in sagittal plane. Hence, future studies, prior to the development of any clinical assistance tools, should assess the contribution of other pelvic motions, as well as focus on other failure modes such as impingement, edge contact and edge loading.

In conclusion, video-fluoroscopy allows three-dimensional *in vivo* bone orientation determination throughout the activity which was not possible to achieve from either conventional biomechanical activity methods or static imaging techniques. In terms of THR success video-fluoroscopy can be used to identify activities that cause most unfavourable acetabular cup orientations. This would be even more valuable if combined with force platform data for the same patient. Finally, video-fluoroscopy can be used to further enhance the knowledge (Chapter 4) on the pelvic motions that contribute to the contact location between total hip replacement bearings.

Chapter 6

Final discussion and conclusions

This chapter focus is an overview of work described within the current thesis. The first section lists the key findings and associated achievements, followed by a thorough discussion. The current chapter also considers challenges and limitations of the project as a whole, consequently exploring the potential future work.

The aim of this work was to assess patient-specific gait characteristics role in the success of THRs. This was done from an edge contact point of view, which is a recognised contributor to implant failure. The mechanical issues potentially caused by edge contact include liner dissociation, rim cracking and high-wear (Tower et al., 2007; Gray et al., 2012). However, these occurrences are not fully understood and documented from the *in vivo* perspective. Both rim cracking and liner dissociation can be caused by other mechanisms such as impingement and edge loading.

The approach taken in this work was the simplification of the solution, with the aim of evaluating larger sets of patient biomechanical data. The need for patient-specific edge contact evaluation was explored from multiple perspectives, namely pre-clinical testing, *in vivo* component orientation and retrieval analysis. Aside from the main aim, the work also addressed the challenges of linking multiple disciplines within orthopaedic field such as biomechanical gait analysis, imaging, *in vitro* testing and *in silico* modelling. This topic is relevant to the wider orthopaedic research community and will be discussed within this chapter.

6.1 Main findings and achievements

1. An analytical computational tool was developed in this project, which allowed for biomechanical activity data processing from risk of edge contact perspective. The developed tool was capable of processing data for one patient, one activity and one pelvic motion case in less than one minute. This allowed for rapid data processing throughout this project, highlighting the potential use on much larger datasets.
2. In contrast to similar tools developed to assess the influence of cup orientation on the rim loading (Underwood et al., 2012), the proximity tool allowed for processing of the whole activity cycle and with the addition of pelvic motion.
3. A total of 242 parametric test cases were successfully generated within this project using the aforementioned tool. Sixty two of which were generated for instrumented implant data, which included cases for pelvic motions included and excluded, nine activities and four patients. The rest of the outputs were generated during conventional biomechanical activity data analysis. This included variable pelvic motion scenarios as well as pelvic motions excluded. The cases were performed using walking profiles collected for 20 THR patients.
4. For the first patient set, HIP98 instrumented implant cohort, the activities of highest edge contact risk were found to be forward locomotion and standing. In other words, activities during which the contact force vector direction is predominantly superior.
5. For three out of four patients, the exclusion of pelvic motions from the gait profiles resulted in decreased risk of edge contact during stance phase.
6. In addition to pelvic motion assessment, patient-specific proximity tool outputs were compared to ideal generic *in vitro* conditions. This revealed potential underestimation of edge contact risk by ideal *in vitro* conditions. However, the potential damage location along the rim was consistent between *in vitro* conditions and patient-specific profiles. The exceptions were bending knees, sitting on the chair and rising from the chair.

7. Larger cohort study, LBRC gait data, revealed that for 75% of the patients, exclusion of pelvic motions from the simulation did substantially affect the contact location between total hip replacement bearings during stance phase of the gait cycle. This study was performed for a high-functioning group. However, the increase or decrease was dependent on the region of stance phase. The maximum change between simulations where pelvic motions were included and where pelvic motions were excluded reached 8°.
8. For the LBRC cohort study the difference in edge contact risk between first and second region of stance phase was assessed. The results showed that the exclusion of pelvic motions increased that difference. This suggests that pelvic motions play a balancing role in the contact location between the femoral head and acetabular cup.
9. Importantly, the LBRC cohort study showed that pelvic tilt (in the sagittal plane) and obliquity (in the coronal plane) both contribute to the overall effect of pelvic motion on the location of contact between total hip replacement bearings. In addition to that finding, it was also found that patient-specific static pelvic orientation does not fully represent the functional dynamic pelvic orientation throughout the activity. Therefore, contact location cannot be accurately predicted just by inclusion of patient-specific static pelvic orientation.
10. Effect of static and dynamic pelvic motion on the functional cup orientation was also assessed in a dual video-fluoroscopy study. Techniques for static and dynamic cup and pelvic orientation measurements were successfully implemented using available information.
11. In a dual video-fluoroscopy study the pelvic tilt and acetabular cup inclination were measured for walking, sitting down and supine positions. This study showed that supine cup and pelvic orientation does not represent the functional orientation during two common daily activities.
12. Throughout this PhD work, techniques for incorporating variable research methods in one study were explored and successfully implemented in relation to risk of edge contact and *in vivo* THR component orientation.

6.2 Discussion on the findings and achievements

6.2.1 Effect of patient-specific gait features

As outlined in literature review of this thesis,(Chapter 1), the function of the hip is governed by many processes of the human body, ranging from motions of the anatomical structures forming the joint to vascular supply around it. The focus of this project was assessment of biomechanical activity influence on the success of total hip replacement, particularly from an edge contact perspective. The activity features affecting the dynamic cup alignment and contact location within THR bearings include motions of femur and pelvis, as well as joint contact force direction and magnitude. The importance of the synergy between femur and pelvis in overall function of the hip is well-recognised within the orthopaedic field. In early clinical studies, such as by Bohannon et al. (1985), on patients' hip functionality, the awareness of synergy between the femur and pelvis was drawn in order to successfully evaluate and treat patients with thigh, pelvis, lower spine disorders. To date, biomechanical activity studies do not exclude that synergy. However, in the early studies on total hip replacement bearing performance the role of pelvic motions was simplified (Dowson and Jobbins, 1988). The typical testing profile consisted of the angular motions of the femur and joint contact force magnitude, where direction of this force was vertical in relation to testing reference system. Currently, a variation of that profile is widely used and is known as ISO 14242-4:2018, where the synergy of femur and pelvis is not explicitly stated. Dowson and Jobbins (1988) suggested a revision of the testing profile as it does not encompass the full *in vivo* joint organisation. The need for the revision of those profiles is only beginning to be addressed, while it is still unclear on the most efficient techniques for THR bearing performance evaluation from a patient-specific perspective.

The work presented in this thesis confirms the importance of the pelvifemoral synergy, specifically on the risk of edge contact in THR patients. For the larger number of patients within two biomechanical activity cohorts, presented in Chapters 3 and 4, the exclusion of pelvic motions substantially altered the extent of the risk of edge contact, as well as the regions where the risk of edge contact

is the highest.

The exclusion of pelvic movement had different effects for the four HIP98 patients with instrumented hip implants, versus the 20 LBRC high functioning patients. For the HIP98 patient cohort (Chapter 3) the exclusion of pelvic motions resulted in decreased risk of edge contact during the stance phase region where the highest contact forces were found. In contrast, for patients in the larger cohort, LBRC data (Chapter 4), the effect of edge contact varied between first and second half of the stance phase. In the first half of the stance phase, from heel-strike to mid-stance the risk of edge contact decreased with exclusion of pelvic motions. The opposite was observed for second half of the stance phase, from mid-stance to toe-off, where exclusion of pelvic motions increased the risk of edge contact. Variability between two studies can be attributed to very different patient demographics and selection criteria. The first cohort from a HIP98 dataset (Bergmann, 2008) was small, only four patients, with one patient experiencing difficulties in performing some of the activities (Bergmann et al., 2001). The second cohort, LBRC data, was larger and selected from even larger cohort of approximately 137 patients under strict criteria of unilateral THR with highest normal walking speeds (Lunn et al., 2019). The self-selected walking speed for the first cohort was much lower, $1.08 \frac{m}{s}$, than the second cohort, $1.36 \frac{m}{s}$. Study on 137 patients, 20 of which were used in Chapter 4, De Pieri et al. (2019), showed that it was the patient's functional outcome that was one of the determinants for the contact force direction and magnitude along with patients' BMI. It can be speculated that patient's walking speed also affects the range and pattern of pelvic motions hence the differences between the two studied cohorts in this project. This pattern was also shown in a review paper by Lewis et al. (2017).

In terms of pre-clinical testing profiles, the HIP98 cohort was compared to the *Paul Cycle* (*in vitro* testing protocol), (Dowson and Jobbins, 1988). It was found that *Paul Cycle* does not represent the *in vivo*-like conditions. Firstly, due to the high interpatient variability of LBRC and HIP98 outputs. Secondly, due to the subject selection differences between *Paul Cycle*, which were healthy and young volunteers, and LBRC and HIP98 subjects, which were THR patients. Hence, these pre-clinical testing profiles, and derived from them ISO 14242-4:2018, as such are

not representative of biomechanical profiles seen for THR patients. The load and motion profiles for patients with hip joint disease, deviate from normal mainly as a reaction to pain and discomfort. After being treated with THR patients continue with those adaptations as a habit. In addition, to those there are also adaptations post-surgery imposed by soft-tissue disruption (Beaulieu et al., 2010). From a device pre-clinical testing perspective, adjusting the cup inclination and version angle might be enough to mechanically test the patient-specific effects of edge contact on the performance of THR in terms of materials and geometry (Williams et al., 2003). THR mechanical performance would depend on the duration of edge contact or other failure contributors. As shown in a study by Hua et al. (2016), the duration of edge contact was variable between the activities and for averaged HIP98 patients was highest during normal walking and elevated cup orientation angles. This suggests that pre-clinical test might encompass damage provoked by edge contact by varying cup orientation angle.

The testing of each implant bearing design under ISO conditions is costly in terms of materials and time. Hence, pre-clinical testing of each patient's profile is impractical and even impossible either through cup orientation variation or adjustment of motion and loading profiles (Al-Hajjar et al., 2013). The *in vitro* testing machinery functionality constrain, such as range of motion, also imposes limitations on patient-specific testing. Pre-clinical testing should achieve wear and damage patterns that can potentially occur *in vivo*, rather than focus directly on interpatient variability. The analysis of data from biomechanical studies for the improvement of pre-clinical testing must be performed with this in mind. Therefore, the pre-clinical testing standard development process should encompass the loads and motions and characteristic component alignments seen *in vivo*, as well as the prevalence of those aspects.

6.2.2 Patient-specific functional cup orientation

The evaluation of functional cup angles is the subject of many studies, and has mostly been linked to static pelvic tilt. One of the first studies to include dynamic pelvic tilt, in the sagittal plane, was by Pierrepont et al. (2017), where functional cup orientation and sagittal pelvic tilt were measured for supine,

seated and standing positions. The study used the conjunction of anterior-posterior radiographs for standing and sitting, and CT scans for the supine position. It was found that pelvic sagittal tilt varied significantly between all three aforementioned body positions, altering the functional cup orientation. The study also found that the functional cup orientations, inclination and version, for studied patients were outside the Lewinnek "safe zone", while cup orientations in supine position were within that zone (Pierrepont et al., 2017).

Moreover, during sitting down and standing cup orientations were completely different for the same patient (Pierrepont et al., 2017). Studies performed in Chapters 4 and 5 of this thesis, addressed the dynamic pelvic motion during walking in relation to cup functional orientation. The dual video-fluoroscopy case study described in Chapter 5 can be compared to a study by Pierrepont et al. (2017), which shows that the pelvic sagittal tilt and cup inclination angles during walking and dynamic sitting down motion are variable from the supine position. It is not clear whether a standing position represents walking in terms of functional pelvic sagittal tilt and cup inclination. However, study LBRC cohort study (Chapter 4), revealed that pelvic effect on the contact location between the THR bearings was not always dominated by static pelvic orientation. It can be assumed that pelvic motion changes the cup's functional orientation between standing and walking. In addition, pelvic sagittal tilt was found not to be the only pelvic motion which influences the contact location between THR bearing. The second contributing motion of the pelvis was found to be obliquity in the coronal plane, which is not as well-studied as the sagittal pelvic tilt. It was shown by Zhou et al. (2012) that there is a potential need for excessive pelvic obliquity compensation when positioning the acetabular component. This was clear from post-surgical imaging scans where cup orientation angles did not always correspond to the ones planned pre-operatively.

Apart from pelvic dynamic cup alignment, the components can migrate from the original position while *in vivo*. The migration of the cup can be provoked by edge contact. This usually occurs in the early days after THR surgery and leads to cup loosening after rehabilitation period (Krismer et al., 1996). The asymptomatic edge contact can technically persist for years before dramatic failure, that could

also contribute to gradual cup migration. In a study by Tian et al. (2017) it was found that the liners migrated within 10 years by up to 4° in terms of inclination angle. Whether or not this change would cause failure, would depend on the original cup position and patient-specific characteristics, such as gait or weight loss.

While the functional orientation of the cup is an important measure in risk of edge contact, it is not the sole contributor. This was explicitly shown in a LBRC study (Chapter 4) within this project, as even when pelvic motions were excluded and cup had the same orientation for all the patients, the risk of edge contact was variable between patients. There was no patient-characteristic found that directly influences this variability, but for the eight patients with the highest body weight the risk of edge contact was higher than average across the patients. The HIP98 study (Chapter 3), actually showed that for patient with steepest cup the risk of edge contact was highest from all the other patients. However, the weight of the patient also was the highest. Findings of both studies suggest that risk of edge contact is multi-factorial. Hence, the "safe zones" require the consideration of patient-specific characteristics, as well as device-specific considerations as shown by Underwood et al. (2012).

6.2.3 Importance of inpatient and interpatient variation in THR success prediction

There are multiple methods for the evaluation and prediction of variable failure causes within the THR, including *in vitro*, *in silico* and *ex vivo* analysis, as well as *in vivo* imaging. The idea behind developing tools and mathematical algorithms within this project originated from techniques such as *in vitro* simulator tests and finite element analysis techniques being time-consuming while providing variable mechanical performance measurement. Simplified solutions were explored within this project which do not provide as detailed mechanical assessment of the THR, but give broader overview of the *in vivo* organisation of the joint. This allows processing of a large number of patients and identifying the biomechanical activities and patient-specific features which put THR at most risk of edge contact.

The important aspect highlighted by the use of the developed techniques was substantial variation between the patients, cohorts, activities and variation between trials for same patient and activity. This suggests that the rehabilitation and monitoring techniques should remain large focus of the orthopaedic studies. Early detection of the failure mechanism could eliminate further complications. Melvin et al. (2014) states that caution should be taken prior to the development of the new devices, because interpatient variability, discussed in previous section, as well as inpatient variability are not taken into account by current pre-clinical testing.

6.3 Challenges, limitations and future work

A central challenge of this project was data interpretation from different sources and disciplines, while *in silico* studies mostly use standardised mathematical notions such as rotation direction, the biomechanical gait studies which are more clinically focused use specialised notions for rotations. Similarly, the definitions of the coordinate and reference systems in biomechanical studies can be unreported, which makes it impossible to set-up a mathematical model using data from those studies. Open-source databases or collaborations are the only possible method, at the moment, in linking variable orthopaedic research fields.

The supplementary data, which could be used to enhance the studies was often missing. The limitation of this work is the assumptions about cup alignment, in terms of its position within the pelvis and associated alignment of the pelvis within the global coordinate system. This limitation is linked to a challenge of gathering a complete set of patient-specific data for all of the subjects in a study. In order to calculate the edge proximity in a fully subject-specific manner it is necessary to know the alignment of the cup in the pelvic coordinate system and have a measure of the pelvic orientation at one point in the activity cycle for both imaging and motion analysis. The first activity point could potentially be the neutral static standing position. In this position, the current technology allows for both the two dimensional radiographs to be taken and the biomechanical activity data to be captured. This way the motion marker location and force vector

direction can be correlated with the radiographical cup and pelvis alignment.

The verification of the tool was performed for each algorithm of the proximity tool. However, the absence of some *in vitro* or imaging validation study was another limitation of this project, which could form separate research project. The potential validation techniques from *in vitro* perspective might include contact area measurement between two bearings surfaces as in Groves et al. (2017). The system will have to be adjusted and the use of experimental equipment such as robotic arms might be more versatile than joint simulators, specifically for this purpose (Herrmann et al., 2015).

The work presented in Chapters 3 and 4, HIP98 and LBRC data, only focused on concentric conditions, which are not representative for all patients. The combination or enhancement of the proximity tool with edge loading methods could show totally different results. Dual video-fluoroscopy studies performed simultaneously with conventional gait analysis, could provide detailed *in vivo* analysis of patients biomechanics and component orientation (Dennis et al., 2003; Myers et al., 2017).

The future work regarding this thesis is recommended to be the analysis of further 137 patients from the LBRC dataset, which will provide enough data for more sophisticated statistical analysis than presented in Chapter 4. Statistical methods such as principal component analysis (Linley et al., 2010), would allow for finding the characteristic patterns that cannot be identified with other means. With broad patient database the statistical information generated from tool's output can be further used in pre-operative planning, eliminating the need for processing every single patient and at the same time advising on the best component positioning.

Moreover, there is a possibility in using the proximity tool to manage THR performance postoperatively. For more active patients with larger ROM's and wider range of daily activities which are not accounted by pre-clinical device assessment the use of the proximity tool can highlight potential risks (Anderson and Madigan, 2014).

Finally, the tool can be successfully used to predict locations within the cup that are mostly subjected to force action. For a commercially available products this might hint to the device optimisation strategies, while for the custom-made implants this could protect the device from future failure, similar to the OPS™ (Pierrepont et al., 2016a), by understanding the range of cup positions during patient's activity.

6.4 Final conclusion

The project described in this thesis focused on the development of novel methods for *in vivo* THR success evaluation. A bespoke computational tool was developed to allow for processing of the large patient activity datasets in terms of contact location between THR bearings. The developed tool allowed estimation of the possible sources of variation in the risk of edge contact beyond the THR component design. The work presented in this thesis illustrates the importance of dynamic pelvic orientation consideration when assessing the potential success of THR *in vivo*. In conclusion, it is important to recognise that human body functionality is highly variable and cannot be described as one would describe a man-made machine. And the possibility of eliminating all the failures associated with THR is not realistic, but effort should be made to minimise the effects associated with those failures on patients well-being.

References

- Abdulkarim, A., Ellanti, P., Motterlini, N., Fahey, T., and O'Byrne, J. M. (2013). Cemented versus uncemented fixation in total hip replacement: a systematic review and meta-analysis of randomized controlled trials. *Orthopedic reviews* 5.1.
- Abu-Amer, Y., Darwech, I., and Clohisy, J. C. (2007). Aseptic loosening of total joint replacements: mechanisms underlying osteolysis and potential therapies. *Arthritis research & therapy* 9.1, S6.
- Affatato, S, Traina, F, Mazzega-Fabbro, C, Sergo, V., and Viceconti, M (2009). Is ceramic-on-ceramic squeaking phenomenon reproducible in vitro? A long-term simulator study under severe conditions. *Journal of Biomedical Materials Research Part B: Applied Biomaterials* 91.1, pp. 264–271.
- Al-Hajjar, M., Fisher, J., Tipper, J. L., Williams, S., and Jennings, L. M. (2013). Wear of 36-mm BIOLOX delta ceramic-on-ceramic bearing in total hip replacements under edge loading conditions. *Proceedings of the Institution of Mechanical Engineers, Part H: Journal of Engineering in Medicine* 227.5, pp. 535–542.
- Ali, M, Al-Hajjar, M, Jennings, L., and Fisher, J (2017). WEAR AND DEFORMATION OF METAL-ON-POLYETHYLENE HIP REPLACEMENTS UNDER EDGE LOADING CONDITIONS DUE TO VARIATIONS IN SURGICAL POSITIONING. *Bone Joint J* 99.SUPP 3, pp. 12–12.
- Ali, M., Al-Hajjar, M., Partridge, S., Williams, S., Fisher, J., and Jennings, L. M. (2016). Influence of hip joint simulator design and mechanics on the wear and creep of metal-on-polyethylene bearings. *Proceedings of the Institution of Mechanical Engineers, Part H: Journal of Engineering in Medicine* 230.5, pp. 389–397.
- Anderson, D. E. and Madigan, M. L. (2013). Effects of age-related differences in femoral loading and bone mineral density on strains in the proximal femur during controlled walking. *Journal of applied biomechanics* 29.5, pp. 505–516.
- Anderson, D. E. and Madigan, M. L. (2014). Healthy older adults have insufficient hip range of motion and plantar flexor strength to walk like healthy young adults. *Journal of biomechanics* 47.5, pp. 1104–1109.
- Aqil, A., Wiik, A., Zanotto, M., Manning, V., Masjedi, M., and Cobb, J. P. (2016). The effect of hip arthroplasty on osteoarthritic gait: a blinded, prospective and controlled gait study at fast walking speeds. *The Journal of arthroplasty* 31.10, pp. 2337–2341.

- Ashby, M. F. and Jones, D. R. H. (2012). *Engineering materials 1: an introduction to properties, applications and design*. Vol. 1. Elsevier.
- Balakrishnan, A., Schemitsch, E. H., Pearce, D., and McKee, M. D. (2003). Distinguishing transient osteoporosis of the hip from avascular necrosis. *Canadian journal of surgery* 46.3, p. 187.
- Banks, S., Banks, A., Klos, T., and Cook, F. (1997). "A simple fluoroscopy based technique for assessing 3D knee kinematics before, during, and after surgery". *CVRMed-MRCAS'97*. Springer, pp. 639–643.
- Barbour, P., Stone, M., and Fisher, J (1999). A hip joint simulator study using simplified loading and motion cycles generating physiological wear paths and rates. *Proceedings of the Institution of Mechanical Engineers, Part H: Journal of Engineering in Medicine* 213.6, pp. 455–467.
- Barrett, W. P., Turner, S. E., and Leopold, J. P. (2013). Prospective randomized study of direct anterior vs postero-lateral approach for total hip arthroplasty. *The Journal of arthroplasty* 28.9, pp. 1634–1638.
- Bartel, D., Burstein, A., Toda, M., and Edwards, D. (1985). The effect of conformity and plastic thickness on contact stresses in metal-backed plastic implants. *Journal of Biomechanical Engineering* 107.3, pp. 193–199.
- Beaulieu, M. L., Lamontagne, M., and Beaulé, P. E. (2010). Lower limb biomechanics during gait do not return to normal following total hip arthroplasty. 32.2, pp. 269 –273. ISSN: 0966-6362. DOI: <http://dx.doi.org/10.1016/j.gaitpost.2010.05.007>. URL: <http://www.sciencedirect.com/science/article/pii/S0966636210001311>.
- Bennett, D, Humphreys, L, O'brien, S, Kelly, C, Orr, J., and Beverland, D. (2008). Gait kinematics of age-stratified hip replacement patients—a large scale, long-term follow-up study. *Gait & posture* 28.2, pp. 194–200.
- Bennett, D., Ryan, P., O'Brien, S., and Beverland, D. E. (2017). Gait kinetics of total hip replacement patients—A large scale, long-term follow-up study. *Gait & posture* 53, pp. 173–178.
- Bergmann G. (ed.), C. U. B. (2008). *OrthoLoad*. URL: <http://orthoload.com/>.
- Bergmann, G, Deuretzbacher, G, Heller, M, Graichen, F, Rohlmann, A, Strauss, J, and Duda, G. (2001). Hip contact forces and gait patterns from routine activities. *Journal of Biomechanics* 34.7, pp. 859 –871. ISSN: 0021-9290.
- Berry, D. J. (2014). Utility of modular implants in primary total hip arthroplasty. *The Journal of arthroplasty* 29.4, pp. 657–658.
- Bhushan, B. (2000). *Modern tribology handbook, two volume set*. CRC press.

REFERENCES

- Blondel, B, Parratte, S, Tropiano, P, Pauly, V, Aubaniac, J.-M., and Argenson, J.-N. (2009). Pelvic tilt measurement before and after total hip arthroplasty. *Orthopaedics & Traumatology: Surgery & Research* 95.8, pp. 568–572.
- Blumenfeld, T. J., Glaser, D. A., Bargar, W. L., Langston, G. D., Mahfouz, M. R., and Komistek, R. D. (2011). In vivo assessment of total hip femoral head separation from the acetabular cup during 4 common daily activities. *Orthopedics* 34.6, e127–e132.
- Bobman, J. T., Danoff, J. R., Babatunde, O. M., Zhu, K., Peyser, K., Geller, J. A., Gorroochurn, P., and Macaulay, W. (2016). Total hip arthroplasty functional outcomes are independent of acetabular component orientation when a polyethylene liner is used. *The Journal of arthroplasty* 31.4, pp. 830–834.
- Bohannon, R. W., Gajdosik, R. L., and LeVeau, B. F. (1985). Relationship of pelvic and thigh motions during unilateral and bilateral hip flexion. *Physical Therapy* 65.10, pp. 1501–1504.
- Bourg, D. M. (2002). *Physics for game developers*. " O'Reilly Media, Inc."
- Brockett, C., Williams, S., Jin, Z., Isaac, G., and Fisher, J. (2007). Friction of total hip replacements with different bearings and loading conditions. *Journal of Biomedical Materials Research Part B: Applied Biomaterials: An Official Journal of The Society for Biomaterials, The Japanese Society for Biomaterials, and The Australian Society for Biomaterials and the Korean Society for Biomaterials* 81.2, pp. 508–515.
- Buckwalter, J., Einhorn, T., Simon, S., and Orthopaedic Surgeons, A. A. of (2000). *Orthopaedic Basic Science: Biology and Biomechanics of the Musculoskeletal System*. Orthopaedic Basic Science: Biology and Biomechanics of the Musculoskeletal System v. 1. American Academy of Orthopaedic Surgeons. ISBN: 9780892031771. URL: <https://books.google.co.uk/books?id=e8NsAAAAMAAJ>.
- Budinski, K. G. (2013). *Friction, wear, and erosion atlas*. CRC Press.
- Buechel, F. F. and Pappas, M. J. (2011). *Principles of human joint replacement: design and clinical application*. Springer.
- Byrne, D. P., Mulhall, K. J., and Baker, J. F. (2010). Anatomy & biomechanics of the hip. *The open sports medicine Journal* 4.1.
- Callaghan, J. J., Rosenberg, A. G., and Rubash, H. E. (2007a). *The adult hip*. Vol. 1. Lippincott Williams & Wilkins.
- Callaghan, J. J., Rosenberg, A. G., and Rubash, H. E. (2007b). *The adult hip*. Vol. 2. Lippincott Williams & Wilkins.
- Callanan, M. C., Jarrett, B., Bragdon, C. R., Zurakowski, D., Rubash, H. E., Freiberg, A. A., and Malchau, H. (2011). The John Charnley Award: risk factors for cup malpositioning: qual-

- ity improvement through a joint registry at a tertiary hospital. *Clinical Orthopaedics and Related Research*® 469.2, pp. 319–329.
- Caplan, N., Stewart, S., Kashyap, S., Banaszkiwicz, P., Gibson, A. S. C., Kader, D., and Ewen, A. (2014). The effect of total hip and hip resurfacing arthroplasty on vertical ground reaction force and impulse symmetry during a sit-to-stand task. *Clinical Biomechanics* 29.10, pp. 1164–1169.
- Carter, D., Vasu, R, and Harris, W. (1982). Stress distributions in the acetabular region—II. Effects of cement thickness and metal backing of the total hip acetabular component. *Journal of biomechanics* 15.3, pp. 165–170.
- Center, I. K. (2019). *BOX Subcommand (IGRAPH command)*. URL: [\url{https://www.ibm.com/support/knowledgecenter/en/SSLVMB_24.0.0/spss/base/syn_igraph_box.html}](https://www.ibm.com/support/knowledgecenter/en/SSLVMB_24.0.0/spss/base/syn_igraph_box.html) (visited on 08/30/2019).
- Cibulka, M. T. (2004). Determination and significance of femoral neck anteversion. *Physical therapy* 84.6, pp. 550–558.
- Cole, G., Nigg, B., Ronsky, J., and Yeadon, M. (1993). Application of the joint coordinate system to three-dimensional joint attitude and movement representation: a standardization proposal. *Journal of biomechanical engineering* 115.4A, pp. 344–349.
- Conway, J. and Smith, D. (2003). *On Quaternions and Octonions*. Ak Peters Series. Taylor & Francis. ISBN: 9781568811345. URL: https://books.google.co.uk/books?id=E_HCwwxMbFMC.
- Crawford, R. W. and Murray, D. W. (1997). Total hip replacement: indications for surgery and risk factors for failure. *Annals of the Rheumatic Diseases* 56.8, pp. 455–457. ISSN: 0003-4967. DOI: 10.1136/ard.56.8.455. eprint: <https://ard.bmj.com/content/56/8/455.full.pdf>. URL: <https://ard.bmj.com/content/56/8/455>.
- Crosbie, J., Vachalathiti, R., and Smith, R. (1997). Patterns of spinal motion during walking. *Gait & Posture* 5.1, pp. 6–12.
- Damm, P., Dymke, J., Ackermann, R., Bender, A., Graichen, F., Halder, A., Beier, A., and Bergmann, G. (2013). Friction in total hip joint prosthesis measured in vivo during walking. *PloS one* 8.11, e78373.
- De Pieri, E., Lunn, D. E., Chapman, G. J., Rasmussen, K. P., Ferguson, S. J., and Redmond, A. C. (2019). Patient Characteristics Affect Hip Contact Forces during Gait. *Osteoarthritis and cartilage*.
- Dennis, D. A., Komistek, R. D., and Mahfouz, M. R. (2003). In vivo fluoroscopic analysis of fixed-bearing total knee replacements. *Clinical Orthopaedics and Related Research (1976-2007)* 410, pp. 114–130.

- Dennis, D. A., Komistek, R. D., Northcut, E. J., Ochoa, J. A., and Ritchie, A. (2001). "In vivo" determination of hip joint separation and the forces generated due to impact loading conditions. *Journal of biomechanics* 34.5, pp. 623–629.
- Di Puccio, F. and Mattei, L. (2015). Biotribology of artificial hip joints. *World journal of orthopedics* 6.1, p. 77.
- D'Isidoro, F., Eschle, P., Zumbrunn, T., Sommer, C., Scheidegger, S., and Ferguson, S. J. (2017). Determining 3D kinematics of the hip using video fluoroscopy: guidelines for balancing radiation dose and registration accuracy. *The Journal of arthroplasty* 32.10, pp. 3213–3218.
- Dora, C, Houweling, M, Koch, P, and Sierra, R. (2007). Iliopsoas impingement after total hip replacement: the results of non-operative management, tenotomy or acetabular revision. *The Journal of bone and joint surgery. British volume* 89.8, pp. 1031–1035.
- Dowson, D and Jobbins, B (1988). Design and development of a versatile hip joint simulator and a preliminary assessment of wear and creep in Charnley total replacement hip joints. *Engineering in Medicine* 17.3, pp. 111–117.
- Esposito, C, Roques, A, Tuke, M, Walter, W, and Walsh, W (2012a). "BIOLOX FORTE VERSUS BIOLOX DELTA STRIPE WEAR: 2 YEARS RESULTS". *Orthopaedic Proceedings*. Vol. 94. SUPP_XLI. The British Editorial Society of Bone & Joint Surgery, pp. 143–143.
- Esposito, C., Walter, W., Roques, A, Tuke, M., Zicat, B., Walsh, W., and Walter, W. (2012b). Wear in alumina-on-alumina ceramic total hip replacements: a retrieval analysis of edge loading. *The Journal of bone and joint surgery. British volume* 94.7, pp. 901–907.
- Ewen, A. M., Stewart, S., Gibson, A. S. C., Kashyap, S. N., and Caplan, N. (2012). Post-operative gait analysis in total hip replacement patients—a review of current literature and meta-analysis. *Gait & posture* 36.1, pp. 1–6.
- Fagan, M. J. a. (1992). *Finite Element Analysis Theory and Practice*. Vol. 1. Harlow UK Pearson Education.
- Fischer-Cripps, A. C., Gloyna, E. F., and Hart, W. H. (2000). *Introduction to contact mechanics*. Vol. 221. Springer.
- Fisher, J (2011). Bioengineering reasons for the failure of metal-on-metal hip prostheses: an engineer's perspective. *The Journal of bone and joint surgery. British volume* 93.8, pp. 1001–1004.
- Forczek, W. and Staszkiwicz, R. (2012). An evaluation of symmetry in the lower limb joints during the able-bodied gait of women and men. *Journal of human kinetics* 35.1, pp. 47–57.

REFERENCES

- Foucher, K. C. and Freels, S. (2015). Preoperative factors associated with postoperative gait kinematics and kinetics after total hip arthroplasty. *Osteoarthritis and cartilage* 23.10, pp. 1685–1694.
- Gilbert, J. L., Buckley, C. A., and Jacobs, J. J. (1993). In vivo corrosion of modular hip prosthesis components in mixed and similar metal combinations. The effect of crevice, stress, motion, and alloy coupling. *Journal of biomedical materials research* 27.12, pp. 1533–1544.
- Gimmon, Y., Riemer, R., Rashed, H., Shapiro, A., Debi, R., Kurz, I., and Melzer, I. (2015). Age-related differences in pelvic and trunk motion and gait adaptability at different walking speeds. *Journal of electromyography and kinesiology* 25.5, pp. 791–799.
- Grammatopoulos, G, Pandit, H., Da Assunção, R, McLardy-Smith, P, De Smet, K., Gill, H., and Murray, D. (2014). The relationship between operative and radiographic acetabular component orientation: which factors influence resultant cup orientation? *The bone & joint journal* 96.10, pp. 1290–1297.
- Gray, C. F., Moore, R. E., and Lee, G.-C. (2012). Spontaneous dissociation of offset, face-changing polyethylene liners from the acetabular shell: a report of four cases. *JBJS* 94.9, pp. 841–845.
- Grood, E. S. and Suntay, W. J. (1983). A joint coordinate system for the clinical description of three-dimensional motions: application to the knee. *Journal of biomechanical engineering* 105.2, pp. 136–144.
- Groves, D, Vasiljeva, K, Al-Hajjar, M, Fisher, J, and Williams, S (2017). “CONTACT AREA IN METAL-ON-POLYETHYLENE AND CERAMIC-ON-POLYETHYLENE TOTAL HIP REPLACEMENTS”. *Orthopaedic Proceedings*. Vol. 99. SUPP_3. The British Editorial Society of Bone & Joint Surgery, pp. 149–149.
- Hamill, J. and Knutzen, K. M. (2006). *Biomechanical basis of human movement*. Lippincott Williams & Wilkins.
- Harris, W. H. (1995). The problem is osteolysis. *Clinical orthopaedics and related research* 311, pp. 46–53.
- Herrmann, S., Kluess, D., Kaehler, M., Grawe, R., Rachholz, R., Souffrant, R., Zierath, J., Bader, R., and Woernle, C. (2015). A novel approach for dynamic testing of total hip dislocation under physiological conditions. *PLoS one* 10.12, e0145798.
- Hertz, H (1896). Über die berührung fester elastischer Körper (On the contact of rigid elastic solids) In: *Miscellaneous Papers. Jones and Schott, London*.
- Hill, D. S., Patel, K., and Herlekar, D. (2016). Early catastrophic failure of a PINNACLE MARATHON® polyethylene acetabular liner: a report of a malpositioned PINNACLE

- DUOFIX HA® acetabular shell resulting in point loading and accelerated wear. *Hip International* 26.6, pp. 52–55.
- Hodge, W., Andriacchi, T., and Galante, J. (1991). A relationship between stem orientation and function following total hip arthroplasty. *The Journal of arthroplasty* 6.3, pp. 229–235.
- Hoehn, K. and Marieb, E. N. (2007). *Human anatomy & physiology*. Benjamin Cummings.
- Horstmann, T., Listringhaus, R., Haase, G.-B., Grau, S., and Mündermann, A. (2013). Changes in gait patterns and muscle activity following total hip arthroplasty: a six-month follow-up. *Clinical Biomechanics* 28.7, pp. 762–769.
- Hua, X., Li, J., Jin, Z., and Fisher, J. (2016). The contact mechanics and occurrence of edge loading in modular metal-on-polyethylene total hip replacement during daily activities. *Medical Engineering and Physics* 38.6, pp. 518–525. ISSN: 1350-4533.
- Hua, X., Li, J., Wang, L., Jin, Z., Wilcox, R., and Fisher, J. (2014). Contact mechanics of modular metal-on-polyethylene total hip replacement under adverse edge loading conditions. *Journal of biomechanics* 47.13, pp. 3303–3309.
- Hua, X., Wroblewski, B. M., Jin, Z., and Wang, L. (2012). The effect of cup inclination and wear on the contact mechanics and cement fixation for ultra high molecular weight polyethylene total hip replacements. *Medical engineering & physics* 34.3, pp. 318–325.
- Hurwitz, D., Hulet, C., Andriacchi, T., Rosenberg, A., and Galante, J. (1997). Gait compensations in patients with osteoarthritis of the hip and their relationship to pain and passive hip motion. *Journal of orthopaedic research* 15.4, pp. 629–635.
- Inaba, Y., Kobayashi, N., Suzuki, H., Ike, H., Kubota, S., and Saito, T. (2016). Preoperative planning for implant placement with consideration of pelvic tilt in total hip arthroplasty: postoperative efficacy evaluation. *BMC musculoskeletal disorders* 17.1, p. 280.
- Isacson, M. J., Bunn, K. J., and Incavo, S. J. (2015). Trochanteric impingement: is it a source of pain after THR? *Arthroplasty Today* 1.3, pp. 73–75.
- Jackson, T. J., Estess, A. A., and Adamson, G. J. (2016). Supine and standing AP pelvis radiographs in the evaluation of pincer femoroacetabular impingement. *Clinical Orthopaedics and Related Research*® 474.7, pp. 1692–1696.
- Jahani, F. (2017). “Modelling of Dynamic Edge Loading in Total Hip Replacements with ceramic on polyethylene Bearings”. PhD thesis. University of Leeds.
- Jain, S and Whitwell, G. (2016). Total hip replacement for elderly neck of femur fracture patients. *Orthopaedics and Trauma* 30.2, pp. 128–136.
- Jamali, A. A., Mladenov, K., Meyer, D. C., Martinez, A., Beck, M., Ganz, R., and Leunig, M. (2007). Anteroposterior pelvic radiographs to assess acetabular retroversion: High validity of the “cross-over-sign”. *Journal of orthopaedic research* 25.6, pp. 758–765.

- Jim, R (2008). Biomechanics in Clinic and Research: An Interactive teaching and Learning Course. *Churchill Livingstone Elsevier*.
- Jin, Z., Heng, S., Ng, H., and Auger, D. (1999). An axisymmetric contact model of ultra high molecular weight polyethylene cups against metallic femoral heads for artificial hip joint replacements. *Proceedings of the Institution of Mechanical Engineers, Part H: Journal of Engineering in Medicine* 213.4, pp. 317–327.
- Kadaba, M. P., Ramakrishnan, H., and Wootten, M. (1990). Measurement of lower extremity kinematics during level walking. *Journal of orthopaedic research* 8.3, pp. 383–392.
- Kanoh, T., Hasegawa, Y., Masui, T., Yamaguchi, J., Kawabe, K., and Ishiguro, N. (2010). Accurate acetabular component orientation after total hip arthroplasty using an acetabular alignment guide. *The Journal of arthroplasty* 25.1, pp. 81–86.
- Kaufman, K. R., Miller, L., and Sutherland, D. (1996). Gait asymmetry in patients with limb-length inequality. *Journal of Pediatric Orthopaedics* 16.2, pp. 144–150.
- Kelmanovich, D., Parks, M. L., Sinha, R., and Macaulay, W. (2003). Surgical approaches to total hip arthroplasty. *J South Orthop Assoc* 12.2, pp. 90–4.
- Kim, Y. (1987). Acetabular dysplasia and osteoarthritis developed by an eversion of the acetabular labrum. *Clinical orthopaedics and related research* 215, pp. 289–295.
- Komistek, R. D., Dennis, D. A., Ochoa, J. A., Haas, B. D., and Hammill, C. (2002). In vivo comparison of hip separation after metal-on-metal or metal-on-polyethylene total hip arthroplasty. *JBJS* 84.10, pp. 1836–1841.
- Korduba, L. A., Essner, A., Pivec, R., Lancin, P., Mont, M. A., Wang, A., and Delanois, R. E. (2014). Effect of acetabular cup abduction angle on wear of ultrahigh-molecular-weight polyethylene in hip simulator testing. *Am J Orthop* 43.10, p. 466.
- Korhonen, R. K., Koistinen, A., Konttinen, Y. T., Santavirta, S. S., and Lappalainen, R. (2005). The effect of geometry and abduction angle on the stresses in cemented UHMWPE acetabular cups—finite element simulations and experimental tests. *Biomedical engineering online* 4.1, p. 32.
- Krismer, M, Stöckl, B, Fischer, M, Bauer, R, Mayrhofer, P, and Ogon, M (1996). Early migration predicts late aseptic failure of hip sockets. *The Journal of bone and joint surgery. British volume* 78.3, pp. 422–426.
- Kumar, P., Sen, R., Aggarwal, S., and Jindal, K. (2019). Common hip conditions requiring primary total hip arthroplasty and comparison of their post-operative functional outcomes. *Journal of Clinical Orthopaedics and Trauma*.
- Kurtz, S., Dumbleton, J, Siskey, R., Wang, A, and Manley, M (2009). Trace concentrations of vitamin E protect radiation crosslinked UHMWPE from oxidative degradation. *Journal of Biomedical Materials Research Part A: An Official Journal of The Society for Bioma-*

REFERENCES

- terials, *The Japanese Society for Biomaterials, and The Australian Society for Biomaterials and the Korean Society for Biomaterials* 90.2, pp. 549–563.
- Kurtz, S. M. (2009). “UHMWPE biomaterials handbook: ultra high molecular weight polyethylene in total joint replacement and medical devices”. Academic Press. Chap. 5, pp. 43–55.
- Kurtz, S. M., Edidin, A. A., and Bartel, D. L. (1997). The role of backside polishing, cup angle, and polyethylene thickness on the contact stresses in metal-backed acetabular components. *Journal of biomechanics* 30.6, pp. 639–642.
- Kurtz, S. M., Kocagöz, S. B., Hanzlik, J. A., Underwood, R. J., Gilbert, J. L., MacDonald, D. W., Lee, G.-C., Mont, M. A., Kraay, M. J., Klein, G. R., et al. (2013). Do ceramic femoral heads reduce taper fretting corrosion in hip arthroplasty? A retrieval study. *Clinical Orthopaedics and Related Research*® 471.10, pp. 3270–3282.
- Langston, J, Pierrepont, J, Gu, Y, and Shimmin, A (2018). Risk factors for increased sagittal pelvic motion causing unfavourable orientation of the acetabular component in patients undergoing total hip arthroplasty. *Bone Joint J* 100.7, pp. 845–852.
- Lazennec, J. Y., Thauront, F., Robbins, C. B., and Pour, A. E. (2017). Acetabular and Femoral Anteversions in Standing Position are Outside the Proposed Safe After Total Hip Arthroplasty. *The Journal of arthroplasty* 32.11, pp. 3550–3556.
- Leigh, R. J., Osis, S. T., and Ferber, R. (2016). Kinematic gait patterns and their relationship to pain in mild-to-moderate hip osteoarthritis. *Clinical Biomechanics* 34, pp. 12–17.
- Leighton, R. D. (2006). A functional model to describe the action of the adductor muscles at the hip in the transverse plane. *Physiotherapy theory and practice* 22.5, pp. 251–262.
- Lembeck, B., Mueller, O., Reize, P., and Wuelker, N. (2005). Pelvic tilt makes acetabular cup navigation inaccurate. *Acta orthopaedica* 76.4, pp. 517–523.
- Lerner, Z. F. and Browning, R. C. (2016). Compressive and shear hip joint contact forces are affected by pediatric obesity during walking. *Journal of biomechanics* 49.9, pp. 1547–1553.
- Leslie, I. J., Williams, S., Isaac, G., Ingham, E., and Fisher, J. (2009). High cup angle and microseparation increase the wear of hip surface replacements. *Clinical Orthopaedics and Related Research*® 467.9, pp. 2259–2265.
- Lewinnek, G. E., Lewis, J., Tarr, R., Compere, C., and Zimmerman, J. (1978). Dislocations after total hip-replacement arthroplasties. *The Journal of bone and joint surgery. American volume* 60.2, pp. 217–220.
- Lewis, C. L., Laudicina, N. M., Khuu, A., and Loverro, K. L. (2017). The human pelvis: variation in structure and function during gait. *The Anatomical Record* 300.4, pp. 633–642.

REFERENCES

- Li, J., McWilliams, A. B., Jin, Z., Fisher, J., Stone, M. H., Redmond, A. C., and Stewart, T. D. (2015). Unilateral total hip replacement patients with symptomatic leg length inequality have abnormal hip biomechanics during walking. *Clinical Biomechanics* 30.5, pp. 513–519.
- Li, J., Redmond, A. C., Jin, Z., Fisher, J., Stone, M. H., and Stewart, T. D. (2014). Hip contact forces in asymptomatic total hip replacement patients differ from normal healthy individuals: Implications for preclinical testing. *Clinical Biomechanics* 29.7, pp. 747–751.
- Lim, S.-J., Ryu, H.-G., Eun, H.-J., Park, C.-W., Kwon, K.-B., and Park, Y.-S. (2018). Clinical outcomes and bearing-specific complications following fourth-generation alumina ceramic-on-ceramic total hip arthroplasty: a single-surgeon series of 749 hips at a minimum of 5-year follow-up. *The Journal of arthroplasty* 33.7, pp. 2182–2186.
- Linley, H. S., Sled, E. A., Culham, E. G., and Deluzio, K. J. (2010). A biomechanical analysis of trunk and pelvis motion during gait in subjects with knee osteoarthritis compared to control subjects. *Clinical Biomechanics* 25.10, pp. 1003–1010.
- Liu, F. and Fisher, J. (2017). Effect of an edge at cup rim on contact stress during micro-separation in ceramic-on-ceramic hip joints. *Tribology international* 113, pp. 323–329.
- Loizeau, J., Allard, P., Duhaime, M., and Landjerit, B. (1995). Bilateral gait patterns in subjects fitted with a total hip prosthesis. *Archives of physical medicine and rehabilitation* 76.6, pp. 552–557.
- Loudon, J. R. and Charnley, J. (1980). Subsidence of the femoral prosthesis in total hip replacement in relation to the design of the stem. *The Journal of bone and joint surgery. British volume* 62.4, pp. 450–453.
- Lunn, D. E., Chapman, G. J., and Redmond, A. C. (2019). Hip kinematics and kinetics in total hip replacement patients stratified by age and functional capacity. *Journal of Biomechanics*.
- Lusty, P., Tai, C., Sew-Hoy, R., Walter, W., Walter, W., and Zicat, B. (2007). Third-generation alumina-on-alumina ceramic bearings in cementless total hip arthroplasty. *JBJS* 89.12, pp. 2676–2683.
- Mabilleau, G., Kwon, Y.-M., Pandit, H., Murray, D. W., and Sabokbar, A. (2008). Metal-on-metal hip resurfacing arthroplasty: a review of periprosthetic biological reactions. *Acta orthopaedica* 79.6, pp. 734–747.
- Madsen, M. S., Ritter, M. A., Morris, H. H., Meding, J. B., Berend, M. E., Faris, P. M., and Vardaxis, V. G. (2004). The effect of total hip arthroplasty surgical approach on gait. *Journal of orthopaedic research* 22.1, pp. 44–50.

REFERENCES

- Mak, M., Jin, Z., Fisher, J., and Stewart, T. D. (2011). Influence of acetabular cup rim design on the contact stress during edge loading in ceramic-on-ceramic hip prostheses. *The Journal of arthroplasty* 26.1, pp. 131–136.
- Maratt, J. D., Esposito, C. I., McLawhorn, A. S., Jerabek, S. A., Padgett, D. E., and Mayman, D. J. (2015). Pelvic tilt in patients undergoing total hip arthroplasty: when does it matter? *The Journal of arthroplasty* 30.3, pp. 387–391.
- Marchetti, E., Krantz, N., Berton, C., Bocquet, D., Foulleron, N., Migaud, H., and Girard, J (2011). Component impingement in total hip arthroplasty: frequency and risk factors. A continuous retrieval analysis series of 416 cup. *Orthopaedics & Traumatology: Surgery & Research* 97.2, pp. 127–133.
- Marel, E., Walter, L., Solomon, M., Shimmin, A., and Pierrepont, J. (2016). Investigation of Patient-Specific Acetabular Cup Malorientation in Functional Positions in the Failing Total Hip Replacement. *Bone Joint J* 98.SUPP 3, pp. 20–20.
- McGrory, B., McGrory, C., Barbour, L., and Barbour, B (2010). Transient subluxation of the femoral head after total hip replacement. *The Journal of bone and joint surgery. British volume* 92.11, pp. 1522–1526.
- McLawhorn, A., Sculco, P., Weeks, K. D., Nam, D., and Mayman, D. (2015). Targeting a New Safe Zone: A Step in the Development of Patient-Specific Component Positioning for Total Hip Arthroplasty. *American journal of orthopedics (Belle Mead, NJ)* 44.6, pp. 270–276.
- Meek, R., Allan, D., McPhillips, G, Kerr, L, Howie, C., et al. (2008). Late dislocation after total hip arthroplasty. *Clinical medicine & research* 6.1, pp. 17–23.
- Melvin, J. S., Karthikeyan, T., Cope, R., and Fehring, T. K. (2014). Early failures in total hip arthroplasty—a changing paradigm. *The Journal of arthroplasty* 29.6, pp. 1285–1288.
- Miki, H., Sugano, N., Hagio, K., Nishii, T., Kawakami, H., Kakimoto, A., Nakamura, N., and Yoshikawa, H. (2004). Recovery of walking speed and symmetrical movement of the pelvis and lower extremity joints after unilateral THA. *Journal of biomechanics* 37.4, pp. 443–455.
- Morlock, M. M., Bishop, N., Zustin, J., Hahn, M., Rütther, W., and Amling, M. (2008). Modes of implant failure after hip resurfacing: morphological and wear analysis of 267 retrieval specimens. *JBS* 90, pp. 89–95.
- Murakami, Y, Ochi, M, Ikuta, Y, and Higashi, Y (1996). Permeation from the synovial fluid as nutritional pathway for the anterior cruciate ligament in rabbits. *Acta Physiologica Scandinavica* 158.2, pp. 181–187.
- Myers, C., Shelburne, K., Laz, P., Schmidt, W., Morrison, H., Yang, C., Kindsfater, K., and Rullkoetter, P. (2017). “In Vivo Total Hip Arthroplasty Kinematics during a Range of

- Dynamic Activities using Stereo Radiography". *ORS Annual Meeting Paper*. Vol. 0114. The Orthopaedic Research Society.
- Myers, R., Myers, S., Walpole, R., and Ye, K (2012). *Probability & Statistics for Engineers and Scientists, Ninth Edition*. Pearson.
- Nantel, J., Termoz, N., Vendittoli, P.-A., Lavigne, M., and Prince, F. (2009). Gait patterns after total hip arthroplasty and surface replacement arthroplasty. *Archives of physical medicine and rehabilitation* 90.3, pp. 463–469.
- National Joint Registry UK (2018). *15th Annual Report 2018*, pp. 1–220. URL: <http://www.njrreports.org.uk/s>.
- Nevelos, J., Ingham, E, Doyle, C, Fisher, J, and Nevelos, A. (1999). Analysis of retrieved alumina ceramic components from Mittelmeier total hip prostheses. *Biomaterials* 20.19, pp. 1833–1840.
- Nordin, M. and Frankel, V. H. (2001). *Basic biomechanics of the musculoskeletal system*. Lippincott Williams & Wilkins.
- Northcut, E., Komistek, R., Dennis, D., Ochoa, J., and Ritchie, A (1998). In vivo determination of normal, constrained and unconstrained THA kinematics. *Journal of Biomechanics* 1001.31, p. 54.
- O'Brien, S. (2014). Femoral offset in total hip replacement: A study of anatomical offset in the Northern Ireland population. *International Journal of Orthopaedic and Trauma Nursing* 18.3, pp. 162–169.
- O'Dwyer Lancaster-Jones, O. G. (2017). "The Effect of Variations in Component Positioning and Swing Phase Load on the Occurrence and Severity of Edge Loading and Wear in Hip Joint Replacements". PhD thesis. University of Leeds.
- Paoloni, M., Di Sante, L., Dimaggio, M., Bernetti, A., Mangone, M., Di Renzo, S., and Santilli, V. (2012). Kinematic and kinetic modifications in walking pattern of hip osteoarthritis patients induced by intra-articular injections of hyaluronic acid. *Clinical Biomechanics* 27.7, pp. 661–665.
- Paul, J. (1966). *Biomechanics. The biomechanics of the hip-joint and its clinical relevance*.
- Peng, Y., Arauz, P., An, S., and Kwon, Y.-M. (2019). Computational modeling of polyethylene wear in total hip arthroplasty using patient-specific kinematics-coupled finite element analysis. *Tribology International* 129, pp. 162–166.
- Pentlow, A. K. and Heal, J. S. (2012). Subsidence of collarless uncemented femoral stems in total hips replacements performed for trauma. *Injury* 43.6, pp. 882–885.
- Perron, M., Malouin, F., Moffet, H., and McFadyen, B. J. (2000). Three-dimensional gait analysis in women with a total hip arthroplasty. *Clinical Biomechanics* 15.7, pp. 504–515.

REFERENCES

- Pierrepont, J, Hawdon, G, Miles, B., Connor, B. O., Baré, J, Walter, L., Marel, E, Solomon, M, McMahon, S, and Shimmin, A. (2017). Variation in functional pelvic tilt in patients undergoing total hip arthroplasty. *The bone & joint journal* 99.2, pp. 184–191.
- Pierrepont, J, Walter, L, Miles, B, Marel, E, Baré, J, Solomon, M, McMahon, S, and Shimmin, A (2016a). “Pelvic tilt in the standing, supine and seated positions”. *Orthopaedic Proceedings*. Vol. 98. SUPP_9. The British Editorial Society of Bone & Joint Surgery, pp. 30–30.
- Pierrepont, J. W., Stambouzou, C. Z., Miles, B. P., O’Connor, P. B., Walter, L., Ellis, A., Molnar, R., Baré, J. V., Solomon, M., McMahon, S., et al. (2016b). Patient specific component alignment in total hip arthroplasty. *Reconstructive Review* 6.4.
- Ranawat, A. S. and Kelly, B. T. (2005). Anatomy of the hip: open and arthroscopic structure and function. *Operative Techniques in Orthopaedics* 15.3, pp. 160–174.
- Robertson, D. G. E. (2009). Vicon Workstation Quick Reference Guide. *Biomechanics Laboratory, School of Human Kinetics: University of Ottawa*.
- Roettges, P. S., Hannallah, J. R., Smith, J. L., and Ruth, J. T. (2018). Predictability of Pelvic Tilt During Total Hip Arthroplasty Using a Traction Table. *The Journal of arthroplasty*.
- Rueden, C. T., Schindelin, J., Hiner, M. C., DeZonia, B. E., Walter, A. E., Arena, E. T., and Eliceiri, K. W. (2017). ImageJ2: ImageJ for the next generation of scientific image data. *BMC bioinformatics* 18.1, p. 529.
- Sado, N., Yoshioka, S., and Fukashiro, S. (2017). A non-orthogonal joint coordinate system for the calculation of anatomically practical joint torque power in three-dimensional hip joint motion. *International Journal of Sport and Health Science*, p. 201712.
- Saikia, K., Bhuyan, S., and Rongphar, R (2008). Anthropometric study of the hip joint in Northeastern region population with computed tomography scan. *Indian Journal of Orthopaedics* 42.3, p. 260.
- Sariali, E., Stewart, T., Jin, Z., and Fisher, J. (2010). In vitro investigation of friction under edge-loading conditions for ceramic-on-ceramic total hip prosthesis. *Journal of Orthopaedic Research* 28.8, pp. 979–985.
- Schache, A. G., Blanch, P. D., and Murphy, A. T. (2000). Relation of anterior pelvic tilt during running to clinical and kinematic measures of hip extension. *British journal of sports medicine* 34.4, pp. 279–283.
- Schroder, D. T., Kelly, N. H., Wright, T. M., and Parks, M. L. (2011). Retrieved highly crosslinked UHMWPE acetabular liners have similar wear damage as conventional UHMWPE. *Clinical Orthopaedics and Related Research*® 469.2, pp. 387–394.

REFERENCES

- Seagrave, K. G., Troelsen, A., Malchau, H., Husted, H., and Gromov, K. (2017). Acetabular cup position and risk of dislocation in primary total hip arthroplasty: A systematic review of the literature. *Acta orthopaedica* 88.1, pp. 10–17.
- Smith, L. K., Lelas, J. L., and Kerrigan, D. C. (2002). Gender differences in pelvic motions and center of mass displacement during walking: stereotypes quantified. *Journal of women's health & gender-based medicine* 11.5, pp. 453–458.
- Smith, S. S. (2000). Measurement of neuromuscular performance capacities. *The biomedical engineering handbook 2nd ed* 2.
- Stewart, T. D., Tipper, J. L., Insley, G., Streicher, R. M., Ingham, E., and Fisher, J. (2003). Long-term wear of ceramic matrix composite materials for hip prostheses under severe swing phase microseparation. *Journal of Biomedical Materials Research Part B: Applied Biomaterials: An Official Journal of The Society for Biomaterials, The Japanese Society for Biomaterials, and The Australian Society for Biomaterials and the Korean Society for Biomaterials* 66.2, pp. 567–573.
- Sutherland, D. H. and Hagy, J. L. (1972). Measurement of gait movements from motion picture film. *JBJS* 54.4, pp. 787–797.
- Swaminathan, V. and Gilbert, J. L. (2012). Fretting corrosion of CoCrMo and Ti6Al4V interfaces. *Biomaterials* 33.22, pp. 5487–5503.
- Tangsataporn, S., Safir, O. A., Vincent, A. D., Abdelbary, H., Gross, A. E., and Kuzyk, P. R. (2015). Risk factors for subsidence of a modular tapered femoral stem used for revision total hip arthroplasty. *The Journal of arthroplasty* 30.6, pp. 1030–1034.
- Tezuka, T., Heckmann, N. D., Bodner, R. J., and Dorr, L. D. (2018). Functional Safe Zone Is Superior to the Lewinnek Safe Zone for Total Hip Arthroplasty: Why the Lewinnek Safe Zone Is Not Always Predictive of Stability. *The Journal of arthroplasty*.
- Tian, J.-l., Sun, L., Hu, R.-y., Han, W., and Tian, X.-b. (2017). Correlation of Cup Inclination Angle with Liner Wear for Metal-on-polyethylene in Hip Primary Arthroplasty. *Orthopaedic Surgery*.
- Tian, J., Sun, L., Hu, R., Han, W., and Tian, X. (2018). Long-term Results of Primary Hip Arthroplasty with Cup Inclination Angle Bigger than Fifty Degrees. *Journal of clinical orthopaedics and trauma* 9.2, pp. 133–136.
- Tönnis, D. (2012). *Congenital dysplasia and dislocation of the hip in children and adults*. Springer Science & Business Media.
- Tower, S. S., Currier, J. H., Currier, B. H., Lyford, K. A., Van Citters, D. W., and Mayor, M. B. (2007). Rim cracking of the cross-linked longevity polyethylene acetabular liner after total hip arthroplasty. *JBJS* 89.10, pp. 2212–2217.

REFERENCES

- Tsai, T.-Y., Dimitriou, D., Li, J.-S., Nam, K. W., Li, G., and Kwon, Y.-M. (2015). Asymmetric hip kinematics during gait in patients with unilateral total hip arthroplasty: In vivo 3-dimensional motion analysis. *Journal of Biomechanics* 48.4, pp. 555–559.
- Tsai, T.-Y., Li, J.-S., Wang, S., Lin, H., Malchau, H., Li, G., Rubash, H., and Kwon, Y.-M. (2013). A novel dual fluoroscopic imaging method for determination of THA kinematics: in-vitro and in-vivo study. *Journal of biomechanics* 46.7, pp. 1300–1304.
- Underwood, R. J., Zografos, A., Sayles, R. S., Hart, A., and Cann, P. (2012). Edge loading in metal-on-metal hips: low clearance is a new risk factor. *Proceedings of the Institution of Mechanical Engineers, Part H: Journal of Engineering in Medicine* 226.3, pp. 217–226.
- Van Rietbergen, B, Huiskes, R, Eckstein, F, and R uegsegger, P (2003). Trabecular bone tissue strains in the healthy and osteoporotic human femur. *Journal of Bone and Mineral Research* 18.10, pp. 1781–1788.
- Vogt, L, Brettmann, K, Pfeifer, K, and Banzer, W (2003). Walking patterns of hip arthroplasty patients: some observations on the medio-lateral excursions of the trunk. *Disability and rehabilitation* 25.7, pp. 309–317.
- Weisstein, E. W. (2018a). *Circular Segment*. URL: [\url{http://mathworld.wolfram.com/CircularSegment.html}](http://mathworld.wolfram.com/CircularSegment.html) (visited on 06/06/2018).
- Weisstein, E. W. (2018b). *Direction Cosine*. URL: [\url{http://mathworld.wolfram.com/DirectionCosine.html}](http://mathworld.wolfram.com/DirectionCosine.html) (visited on 06/06/2018).
- Weisstein, E. W. (2018c). *Dot Product*. URL: [\url{http://mathworld.wolfram.com/DotProduct.html}](http://mathworld.wolfram.com/DotProduct.html) (visited on 06/06/2018).
- Weisstein, E. W. (2018d). *Rotation Matrix*. URL: [\url{http://mathworld.wolfram.com/RotationMatrix.html}](http://mathworld.wolfram.com/RotationMatrix.html) (visited on 01/30/2019).
- Weisstein, E. W. (2018e). *Spherical Cap*. URL: [\url{http://mathworld.wolfram.com/SphericalCap.html}](http://mathworld.wolfram.com/SphericalCap.html) (visited on 06/06/2018).
- Werner, B. C. and Brown, T. E. (2012). Instability after total hip arthroplasty. *World journal of orthopedics* 3.8, p. 122.
- Westberry, D. E., Wack, L. I., Davis, R. B., and Hardin, J. W. (2018). Femoral anteversion assessment: Comparison of physical examination, gait analysis, and EOS biplanar radiography. *Gait & posture* 62, pp. 285–290.
- Westerhoff, P, Graichen, F, Bender, A, Rohlmann, A, and Bergmann, G (2009). An instrumented implant for in vivo measurement of contact forces and contact moments in the shoulder joint. *Medical Engineering & Physics* 31.2, pp. 207–213.
- Williams, S, Butterfield, M, Stewart, T, Ingham, E, Stone, M, and Fisher, J (2003). Wear and deformation of ceramic-on-polyethylene total hip replacements with joint laxity and

- swing phase microseparation. *Proceedings of the Institution of Mechanical Engineers, Part H: Journal of Engineering in Medicine* 217.2, pp. 147–153.
- Williams, S., Leslie, I., Isaac, G., Jin, Z., Ingham, E., and Fisher, J. (2008). Tribology and wear of metal-on-metal hip prostheses: influence of cup angle and head position. *JBJS* 90, pp. 111–117.
- Winter, D. A. (1995). Human balance and posture control during standing and walking. *Gait & posture* 3.4, pp. 193–214.
- Wu, G., Siegler, S., Allard, P., Kirtley, C., Leardini, A., Rosenbaum, D., Whittle, M., D’Lima, D., Cristofolini, L., Witte, H., et al. (2002). ISB recommendation on definitions of joint coordinate system of various joints for the reporting of human joint motion—part I: ankle, hip, and spine. *Journal of biomechanics* 35.4, pp. 543–548.
- Yan, X., Li, H., Li, A. R., and Zhang, H. (2017). Wearable IMU-based real-time motion warning system for construction workers’ musculoskeletal disorders prevention. *Automation in Construction* 74, pp. 2–11.
- Yan, Y., Neville, A, and Dowson, D (2006). Biotribocorrosion—an appraisal of the time dependence of wear and corrosion interactions: II. Surface analysis. *Journal of Physics D: applied physics* 39.15, p. 3206.
- Yun, A., Koli, E. N., Moreland, J., Iorio, R., Tilzey, J. F., Mesko, J. W., Lee, G.-C., and Froimson, M. (2016). Polyethylene liner dissociation is a complication of the DePuy pinnacle cup: a report of 23 cases. *Clinical Orthopaedics and Related Research*® 474.2, pp. 441–446.
- Zeng, P., Inkson, B. J., Rainforth, W. M., and Stewart, T (2008). “3D surface reconstruction and FIB microscopy of worn alumina hip prostheses”. *Journal of Physics: Conference Series*. Vol. 126. 1. IOP Publishing, p. 012044.
- Zhou, X., Wang, Q., Zhang, X., Chen, Y., Shen, H., and Jiang, Y. (2012). Effect of pelvic obliquity on the orientation of the acetabular component in total hip arthroplasty. *The Journal of arthroplasty* 27.2, pp. 299–304.
- Zienkiewicz, O. C., Taylor, R. L., and Zhu, J. Z. (2005). *The finite element method: its basis and fundamentals*. Elsevier.

APPENDICES

Appendix A

APPENDICES

Table A.1: Reference table developed for HIP98 cup orientation in proximity tool. The values between Rotation for Version Angle and Inclination Angle, are two-dimensional Version Angles measured in transverse plane of the proximity tool. Further details in chapter 3 and section 3.2.2.

Degrees °	Inclination Angle																				
	40	41	42	43	44	45	46	47	48	49	50	51	52	53	54	55	56	57	58	59	60
7	10.8	10.6	10.4	10.2	10.0	9.9	9.7	9.5	9.4	9.2	9.1	9.0	8.9	8.7	8.6	8.5	8.4	8.3	8.2	8.2	8.1
7.5	11.6	11.4	11.1	10.9	10.7	10.6	10.4	10.2	10.0	9.9	9.8	9.6	9.5	9.4	9.2	9.1	9.0	8.9	8.8	8.7	8.6
8	12.3	12.1	11.9	11.6	11.4	11.2	11.1	10.9	10.7	10.6	10.4	10.3	10.1	10.0	9.9	9.7	9.6	9.5	9.4	9.3	9.2
8.5	13.1	12.8	12.6	12.4	12.1	11.9	11.7	11.6	11.4	11.2	11.0	10.9	10.7	10.6	10.5	10.3	10.2	10.1	10.0	9.9	9.8
9	13.8	13.6	13.3	13.1	12.8	12.6	12.4	12.2	12.0	11.9	11.7	11.5	11.4	11.2	11.1	10.9	10.8	10.7	10.6	10.5	10.4
9.5	14.6	14.3	14.0	13.8	13.5	13.3	13.1	12.9	12.7	12.5	12.3	12.2	12.0	11.8	11.7	11.5	11.4	11.3	11.2	11.0	10.9
10	15.3	15.1	14.8	14.5	14.2	14.0	13.8	13.6	13.3	13.2	13.0	12.8	12.6	12.5	12.3	12.2	12.0	11.9	11.7	11.6	11.5
10.5	16.1	15.8	15.5	15.2	14.9	14.7	14.4	14.2	14.0	13.8	13.6	13.4	13.2	13.1	12.9	12.8	12.6	12.5	12.3	12.2	12.1
11	16.8	16.5	16.2	15.9	15.6	15.4	15.1	14.9	14.7	14.4	14.2	14.0	13.9	13.7	13.5	13.4	13.2	13.1	12.9	12.8	12.7
11.5	17.6	17.2	16.9	16.6	16.3	16.1	15.8	15.6	15.3	15.1	14.9	14.7	14.5	14.3	14.1	14.0	13.8	13.6	13.5	13.4	13.2
12	18.3	18.0	17.6	17.3	17.0	16.7	16.5	16.2	16.0	15.7	15.5	15.3	15.1	14.9	14.7	14.6	14.4	14.2	14.1	13.9	13.8
12.5	19.0	18.7	18.3	18.0	17.7	17.4	17.1	16.9	16.6	16.4	16.1	15.9	15.7	15.5	15.3	15.1	15.0	14.8	14.6	14.5	14.4
13	19.8	19.4	19.0	18.7	18.4	18.1	17.8	17.5	17.3	17.0	16.8	16.6	16.3	16.1	15.9	15.7	15.6	15.4	15.2	15.1	14.9
13.5	20.5	20.1	19.7	19.4	19.1	18.8	18.5	18.2	17.9	17.7	17.4	17.2	16.9	16.7	16.5	16.3	16.1	16.0	15.8	15.7	15.5
14	21.2	20.8	20.4	20.1	19.7	19.4	19.1	18.8	18.5	18.3	18.0	17.8	17.6	17.3	17.1	16.9	16.7	16.6	16.4	16.2	16.1
14.5	21.9	21.5	21.1	20.8	20.4	20.1	19.8	19.5	19.2	18.9	18.7	18.4	18.2	17.9	17.7	17.5	17.3	17.1	17.0	16.8	16.6
15	22.6	22.2	21.8	21.5	21.1	20.8	20.4	20.1	19.8	19.6	19.3	19.0	18.8	18.6	18.3	18.1	17.9	17.7	17.5	17.4	17.2
15.5	23.3	22.9	22.5	22.1	21.8	21.4	21.1	20.8	20.5	20.2	19.9	19.6	19.4	19.2	18.9	18.7	18.5	18.3	18.1	17.9	17.8
16	24.0	23.6	23.2	22.8	22.4	22.1	21.7	21.4	21.1	20.8	20.5	20.3	20.0	19.8	19.5	19.3	19.1	18.9	18.7	18.5	18.3
16.5	24.7	24.3	23.9	23.5	23.1	22.7	22.4	22.1	21.7	21.4	21.1	20.9	20.6	20.4	20.1	19.9	19.7	19.5	19.3	19.1	18.9
17	25.4	25.0	24.6	24.2	23.8	23.4	23.0	22.7	22.4	22.1	21.8	21.5	21.2	21.0	20.7	20.5	20.2	20.0	19.8	19.6	19.4
17.5	26.1	25.7	25.2	24.8	24.4	24.0	23.7	23.3	23.0	22.7	22.4	22.1	21.8	21.5	21.3	21.1	20.8	20.6	20.4	20.2	20.0
18	26.8	26.4	25.9	25.5	25.1	24.7	24.3	24.0	23.6	23.3	23.0	22.7	22.4	22.1	21.9	21.6	21.4	21.2	21.0	20.8	20.6
18.5	27.5	27.0	26.6	26.1	25.7	25.3	24.9	24.6	24.2	23.9	23.6	23.3	23.0	22.7	22.5	22.2	22.0	21.8	21.5	21.3	21.1
19	28.2	27.7	27.2	26.8	26.4	26.0	25.6	25.2	24.9	24.5	24.2	23.9	23.6	23.3	23.1	22.8	22.6	22.3	22.1	21.9	21.7
19.5	28.8	28.4	27.9	27.4	27.0	26.6	26.2	25.8	25.5	25.1	24.8	24.5	24.2	23.9	23.6	23.4	23.1	22.9	22.7	22.5	22.2
20	29.5	29.0	28.5	28.1	27.7	27.2	26.8	26.5	26.1	25.8	25.4	25.1	24.8	24.5	24.2	24.0	23.7	23.5	23.2	23.0	22.8

Rotation for Version Angle

APPENDICES

Appendix B

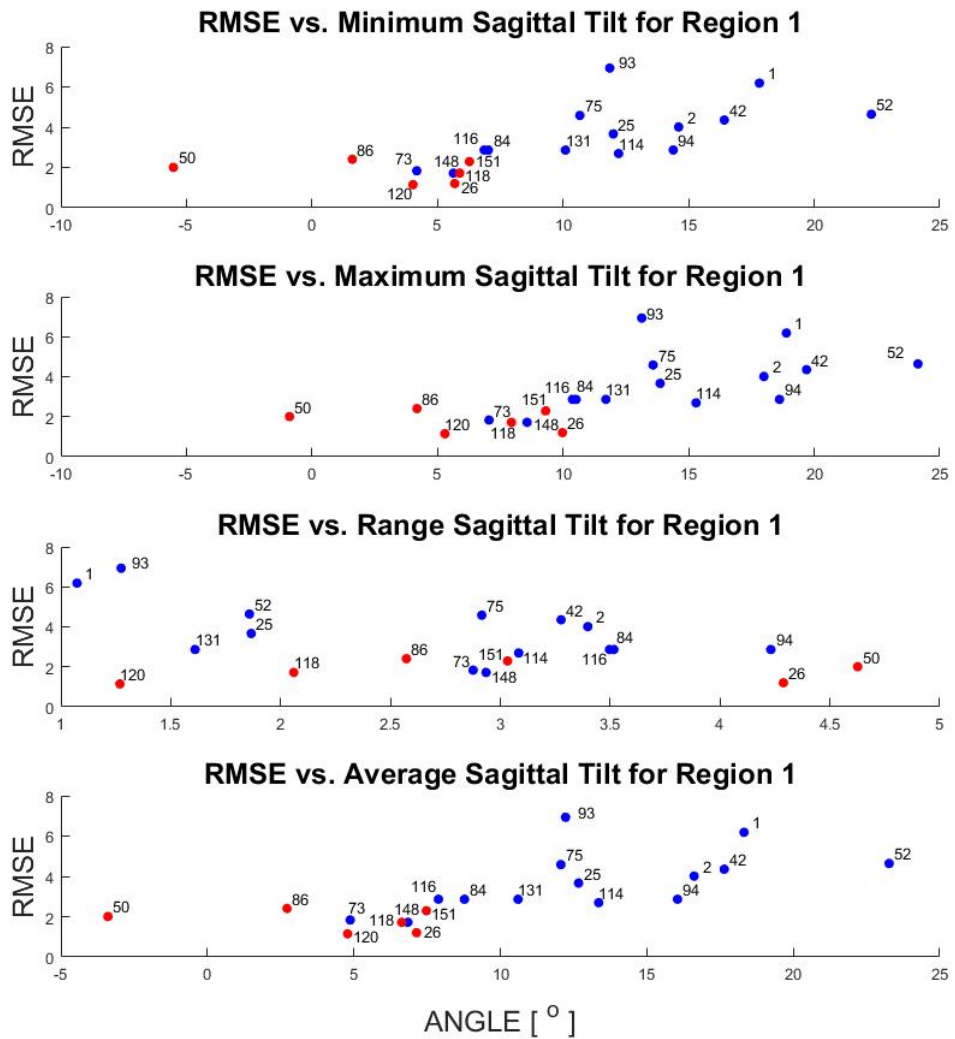


Figure A.1: RMSE [$^{\circ}$] values, between pelvic motions included and excluded, versus pelvic sagittal tilt, for region 1. Red for patients whose proximity angles were not affected by the exclusion of pelvic motions, blue for patients whose proximity angles were affected by the exclusion of pelvic motions.

APPENDICES

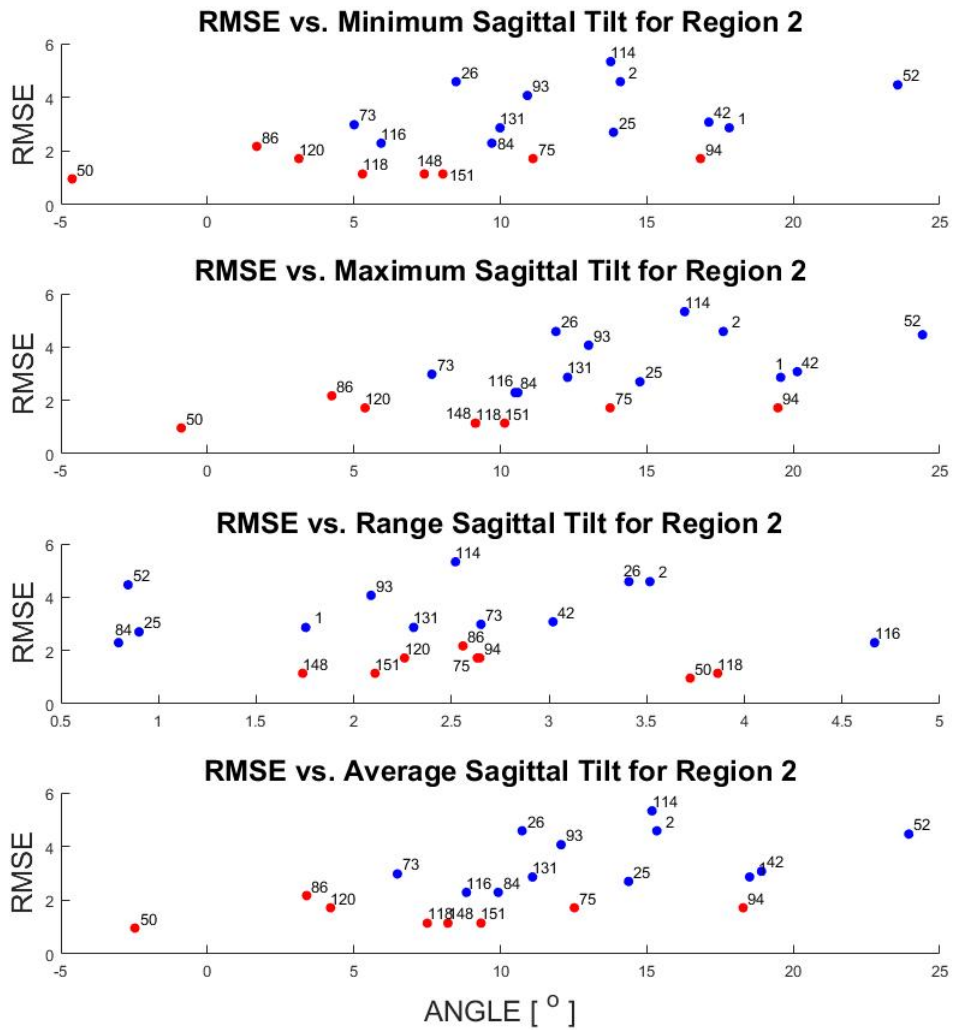


Figure A.2: RMSE [$^{\circ}$] values, between pelvic motions included and excluded, versus pelvic sagittal tilt, for region 2. Red for patients whose proximity angles were not affected by the exclusion of pelvic motions, blue for patients whose proximity angles were affected by the exclusion of pelvic motions.

APPENDICES

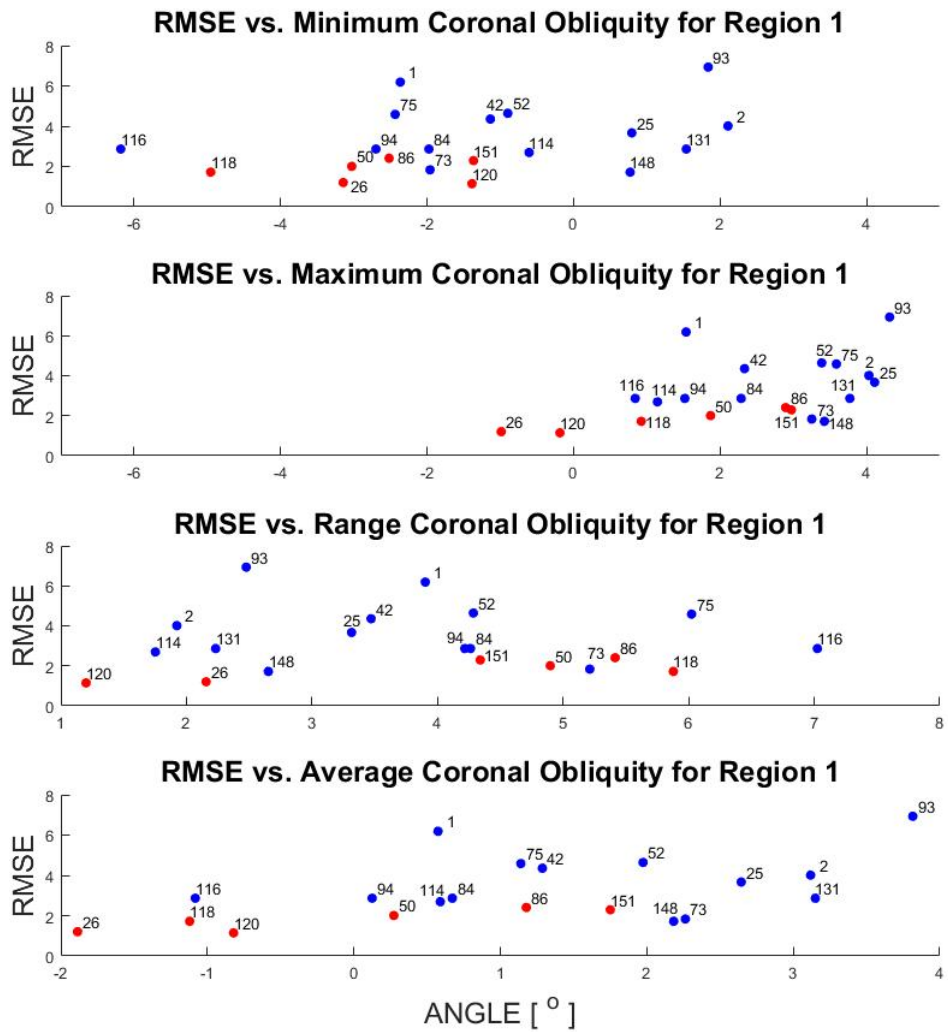


Figure A.3: RMSE [$^{\circ}$] values, between pelvic motions included and excluded, versus pelvic coronal obliquity, for region 1. Red for patients whose proximity angles were not affected by the exclusion of pelvic motions, blue for patients whose proximity angles were affected by the exclusion of pelvic motions.

APPENDICES

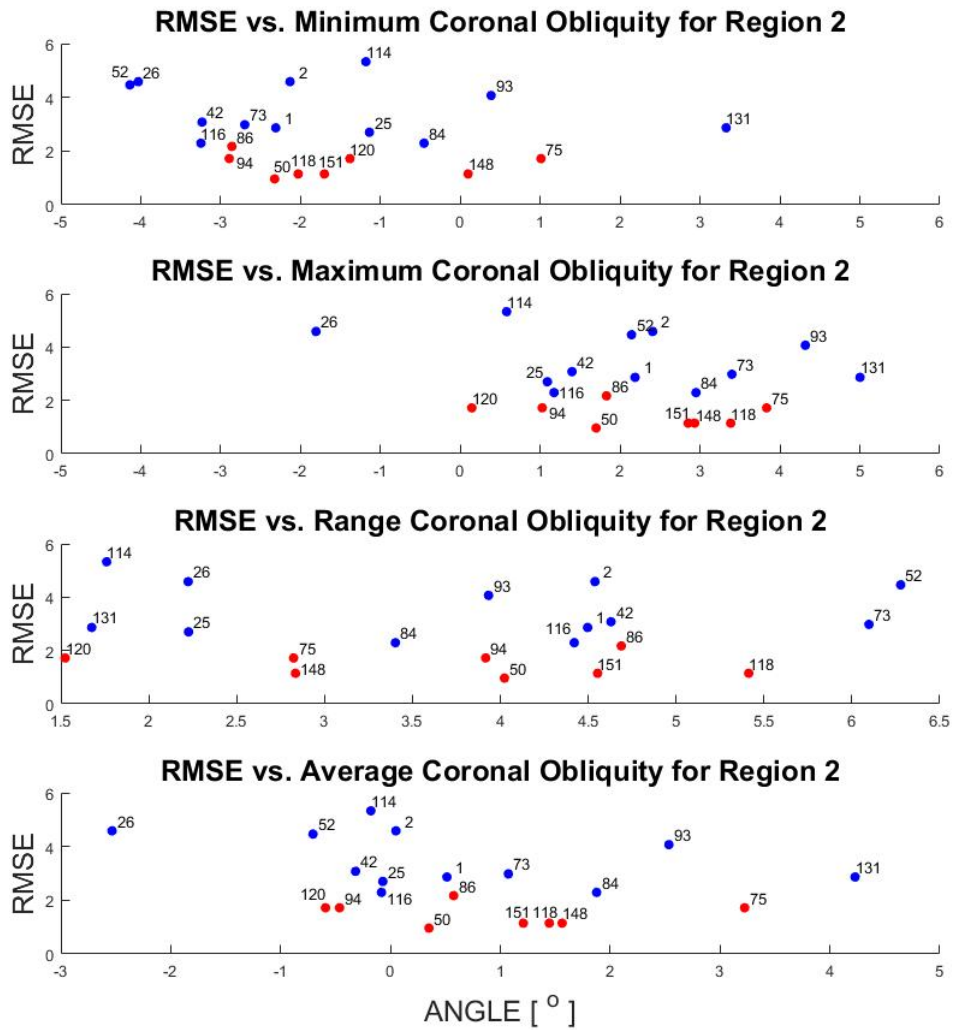


Figure A.4: RMSE [°] values, between pelvic motions included and excluded, versus pelvic coronal obliquity, for region 2. Red for patients whose proximity angles were not affected by the exclusion of pelvic motions, blue for patients whose proximity angles were affected by the exclusion of pelvic motions.

APPENDICES

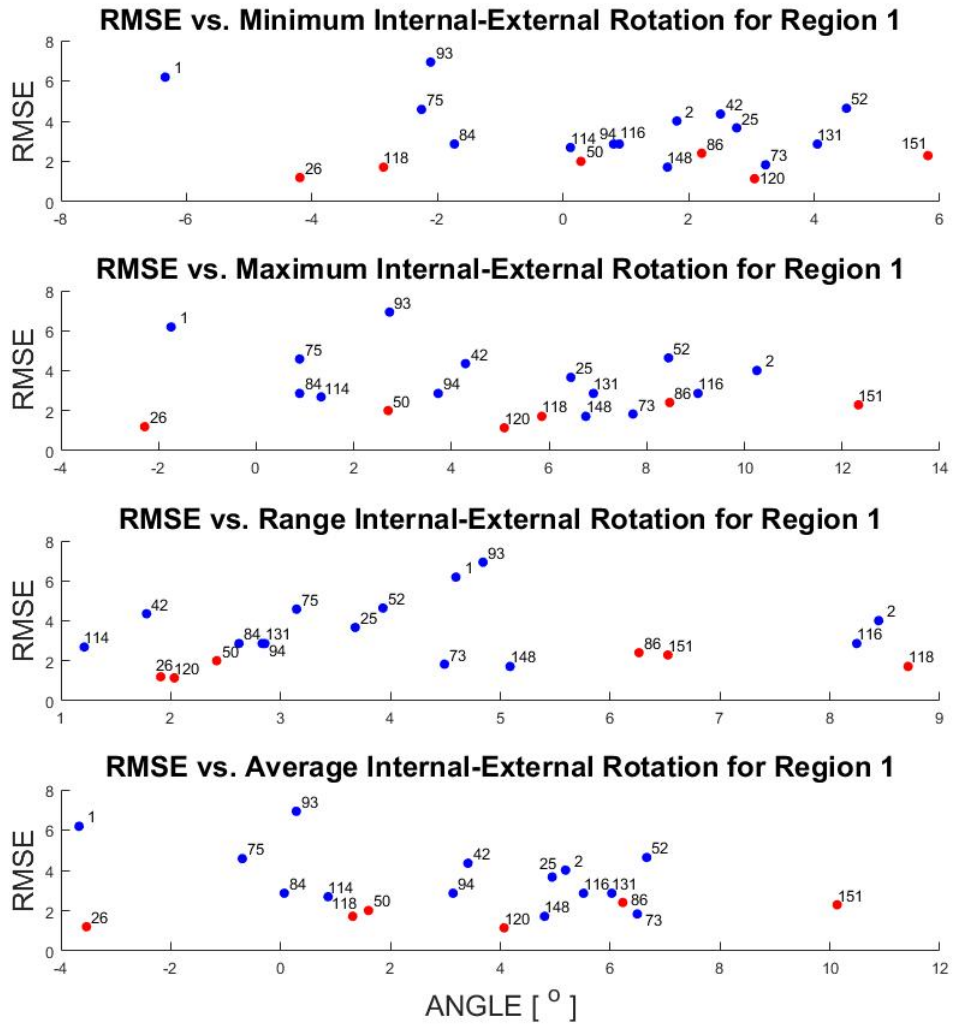


Figure A.5: RMSE [$^{\circ}$] values, between pelvic motions included and excluded, versus pelvic internal-external rotation, for region 1. Red for patients whose proximity angles were not affected by the exclusion of pelvic motions, blue for patients whose proximity angles were affected by the exclusion of pelvic motions.

APPENDICES

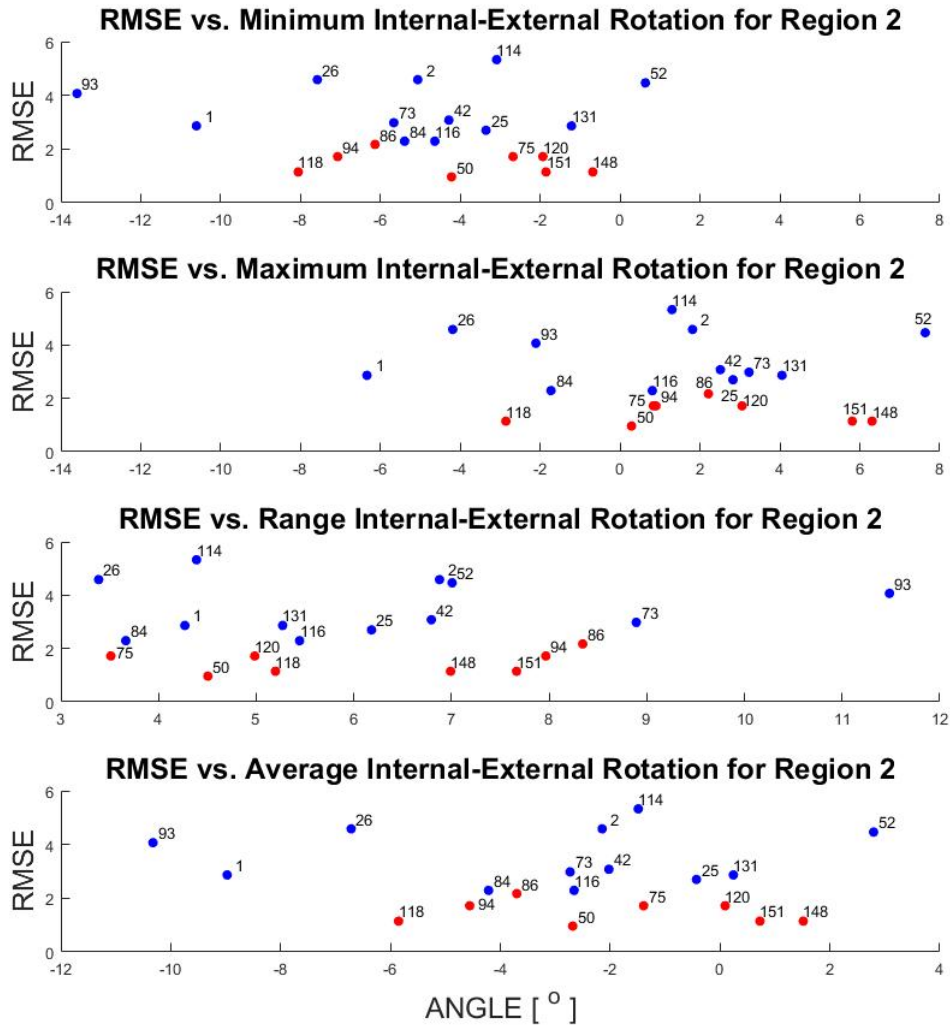


Figure A.6: RMSE [°] values, between pelvic motions included and excluded, versus pelvic internal-external rotation, for region 2. Red for patients whose proximity angles were not affected by the exclusion of pelvic motions, blue for patients whose proximity angles were affected by the exclusion of pelvic motions.